University of Oxford

Department of Engineering Science

Comprehensive and dynamic prognostic modelling for spontaneous subarachnoid haemorrhage



Yiming Luo

Hertford College

Supervisors: **Prof. Stephen J. Payne**

Prof. Alison Noble

A thesis submitted for the degree of

Doctor of Philosophy

Trinity Term 2024

Acknowledgement

This Dphil thesis represents not only just the culmination of three and a half years of journey, but also the collection of support, encouragement, enlightenment, and love from many incredible individuals in this beautiful world.

First and foremost, my heartfelt gratitude goes to my supervisor, Prof. Stephen Payne. Your continuous support along this journey has always been encouraging and inspiring me to move forward bravely. Your guidance provided enlightenment whenever I felt aimless, and you introduced me to excellent researchers who inspired and influenced my work profoundly. Your belief in my abilities has always been a source of motivation. I would also like to extend my deepest gratitude to Prof. Alison Noble. Your meticulous checks on my progression kept everything on track, ensuring that I remained on the right path. Your valuable feedback and encouragement enriched my Dphil journey in countless ways.

To my colleagues and friends at Institute of Biomedical Engineering in University of Oxford, your support, collaboration, and friendship are invaluable for me. Prof. Lionel Tarassenko, and Prof. Timothy Denison, your expertise and constructive suggestions during ToS and CoS inspired me to think deeper, focusing on the clinical significance of my research, contributing to the improvement of this thesis. I would also express my sincere thanks to my colleagues Wahbi El-Bouri, Tamas Jozsa, Yun-Kai Lee, Yun Bing, Wei Wei, Selena Milanovic, Minh Tran, Chun-Ting Lau, Yahya Almuallem, Jiayu Wang, Yidan Xue, Michael Newsome, Jeffrey Howman, Hyunhong Min, Natali Van Zijl, Ali Daher, Xi Chen, Zheng Tong, and Yufan Wang, your companion along this DPhil journey is always appreciated.

Words cannot express the depth of gratitude to my family. To my parents, your unconditional love, sacrifice and belief in me have provided the foundation of my perseverance. Your toughest shoulders and back have carried me through the most challenging times. To my sisters, Echo Luo, Le Xiong, Fangfang Xu, Yuanyuan Xu, Beibei Xu, Xinran Li, Guanai Pan, Guanzhao Pan, your unwavering support and love have always been my bedrock. I also wish to honour the memory of my grandfathers, who have passed away during my Dphil studies. I will never forget the cherished times when you rode me on your tricycle to McDonald's in my childhood and when I secretly made special flower tea made from petals collected in your garden. These simple joys and your nurturing love have left an indelible mark on my heart and shaped who I am today. Finally, to my love, Sixuan, you make me feel complete.

A special thanks to my friends who pursued their PhDs alongside me. Yuan He, Moy Zhang, Yixuan He, Wenxing Duan, Ying Lu, Yalei Fu, Ziyun Liang, your camaraderie and shared experiences have been a source of strength and motivation. The late-night study sessions, mutual encouragement, and understanding have been invaluable.

Abstract

Spontaneous subarachnoid haemorrhage (SAH) is a critical condition characterised by sudden bleeding into the subarachnoid space, primarily due to ruptured cerebral aneurysms.. This life-threatening emergency necessitates prompt medical intervention due to its high mortality rate and severe functional outcomes. Given its complex and acute nature, along with the potential for rapid deterioration, comprehensive and continuous monitoring of disease progression is essential.

Accurate, timely and comprehensive prognostication is vital for optimising patient outcomes due to its ability to capture the evolving disease progression and personalised prognostic profiles of patients. This enables healthcare providers to identify the risks of complications and unfavourable clinical outcomes for early interventions, as well as facilitate personalised post-SAH management and patient care.

Traditional prognostic tools, such as the Hunt and Hess scale, and WFNS grading system, lack the capability to comprehensively and dynamically monitor disease progression and predict outcomes based on continuously updated clinical data. There is a need for prognostic modelling techniques that integrate comprehensive real-time data for accurate prognostications. Additionally, the impact of intermediate events, such as complications and neurosurgeries, on disease progression has been poorly investigated. Modeling these state transitions is crucial for comprehensive prognostication.

This study proposes a comprehensive prognostic framework and develops personalised dynamic prognostic models for SAH patients. We have examined the prognostic values of various baseline, such as demographic factors, and dynamic covariates, such as repeated neurological assessments, haematological biomarkers, and vital sign indices. By integrating these dynamic factors into our models, we have constructed comprehensive and dynamic prognostic profiles, thereby improving personalised disease progression modeling and post-SAH management. Additionally, we have proposed a multi-state prognostic framework, allowing for the incorporation of intermediate events to assess their impact on disease progression and outcomes.

Our novel framework combines dynamic and static prognostic factors to provide real-time, personalised prognostication. It evaluates the impact of various factors on disease progression and patient outcomes. Additionally, we have proposed synthetic ABP modeling and artefact rejection to enhance physiological monitoring for SAH management and dynamic representations of cardiovascular status. Studies in this thesis jointly contribute to a comprehensive and dynamic approach to prognostication, potentially enhancing critical care management and personalised post-SAH patient care.

List of Abbreviations

ABP: Arterial Blood Pressure

AKI: Acute Kidney Injury

AFT: Accelerated Failure Time

ASA: American Stroke Association

AVM: Arteriovenous Malformation

ARDS: Acute Respiratory Distress Syndrome

AUC: Area Under the Curve

BCI: Bicaudate Index

BMI: Body Mass Index

BNP: Brain Natriuretic Peptide

BP: Blood Pressure

CI: Confidence Interval

CK-MB: Creatine Kinase-MB

CPP: Cerebral Perfusion Pressure

CSF: Cerebrospinal Fluid

CT: Computed Tomography

CTA: Computed Tomography Angiography

CV: Coefficient of Variation

DCI: Delayed Cerebral Ischaemia

DSA: Digital Subtraction Angiography

EBM: Evidence-Based Medicine

ECG: Electrocardiogram

EEG: Electroencephalography

EMG: Electromyography

ESRD: End-Stage Renal Disease

EVD: External Ventricular Drain

FLAIR: Fluid-Attenuated Inversion Recovery

GCS: Glasgow Coma Scale

GOS: Glasgow Outcome Scale

HR: Hazard Ratio

HRT: Hormone Replacement Therapy

HHT: Hereditary Haemorrhagic Telangiectasia

ICP: Intracranial Pressure

ICU: Intensive Care Unit

IVH: Intraventricular Haemorrhage

JVD: Jugular Venous Distention

LDH: Lactate Dehydrogenase

LP: Lumbar Puncture

LSTM: Long Short-Term Memory

LVH: Left Ventricular Hypertrophy

MAP: Mean Arterial Pressure

MCA: Middle Cerebral Artery

mRS: Modified Rankin Scale

MRI: Magnetic Resonance Imaging

NMR: Nuclear Magnetic Resonance

NSM: Neurogenic Stunned Myocardium

OR: Odds Ratio

PTCA: Percutaneous Transluminal Coronary Angioplasty

PPA: Phenylpropanolamine

PPV: Pulse Pressure Variability

QTc: Corrected QT Interval

RBCI: Relative Bicaudate Index

RBCs: Red Blood Cells

RNN: Recurrent Neural Network

RR: Relative Risk

SAH: Subarachnoid Haemorrhage

SBP: Systolic Blood Pressure

SBPV: Systolic Blood Pressure Variability

SNR: Signal-to-Noise Ratio

TCD: Transcranial Doppler

TMPG: Trans-Mural Pressure Gradient

VAS: Visual Analogue Scale

VPS: Ventriculoperitoneal Shunt

Contents

Acknowledgement ..... **I**
Abstract ..... **II**
List of Abbreviations ..... **III**
Chapter 1 Physiological and medical background of SAH **1**
1.1 Structure of the brain 1
1.1.1 Anatomy and physiology of cerebral vasculature 2
1.1.2 Anatomy and physiology of meninges 3
1.2 Subarachnoid haemorrhage (SAH) 4
1.2.1 Traumatic SAH 4
1.2.2 Spontaneous SAH 6
1.3 Epidemiology of spontaneous SAH 8
1.3.1 Incidence, prevalence and fatality 8
1.3.2 Risk factors of spontaneous SAH 9
1.4 Diagnosis of spontaneous SAH 10
1.4.1 Computed tomography (CT) and CT angiography (CTA) 10
1.4.2 Lumbar puncture (LP) 11
1.4.3 Magnetic resonance imaging (MRI) 12
1.4.4 Digital subtraction angiography (DSA) 13
1.4.5 Discussions on diagnosis methods 15
1.5 Complications after spontaneous SAH 16
1.5.1 Re-bleeding 17
1.5.2 Vasospasm and delayed cerebral ischaemia (DCI) 18
1.5.3 Hydrocephalus 21
1.5.4 Other complications 24
1.6 Treatment of spontaneous SAH 26
1.6.1 Stabilisation 26
1.6.2 Neurosurgical intervention 27
1.6.3 Rehabilitation 27
1.7 Summary 28

Chapter 2 Understanding prognosis of spontaneous SAH **37**
2.1 Evolution of prognosis 37
2.1.1 From experience-based to evidence-based prognosis 37
2.1.2 From generalised to individualised prognosis 39
2.1.3 From static to dynamic prognosis 40
2.2 Methodologies for prognosis 43
2.2.1 Statistical tools for continuous outcomes 43
2.2.2 Statistical tools for binary outcomes 45
2.2.3 Statistical tools for time-to-event outcomes 47
2.2.4 Asssessing the performance of prognostication 54
2.3 Spontaneous SAH prognosis studies 56
2.3.1 Prognosis research topics in spontaneous SAH 56

2.3.2 Mortality 57
2.3.3 Poor neurological outcomes measured by neurological grades 63
2.3.4 Re-bleeding 68
2.3.5 Vasospasm and DCI 70
2.3.6 Hydrocephalus 73
2.3.7 Other complications 75
2.4 Datasets of this thesis 76
2.5 Summary and discussion 81

Chapter 3 Personalised dynamic survival prediction with vital sign indices in SAH patients 90
3.1 Feature extraction from ABP and ECG measurements 90
3.1.1 Prognostic features in ABP and ECG measurements 90
3.1.2 Annotation of waveforms for feature extraction 93
3.2 Dynamic prognostic modelling with vital sign indices 96
3.2.1 Introduction 96
3.2.2 Patient population and clinical characteristics 99
3.2.3 Dynamic predictor extraction 100
3.2.4 Statistical explanations 102
3.3 Results 105
3.3.1 Joint analysis of vital sign indices and baseline covariates 105
3.3.2 Dynamic survival prediction and assessment 106
3.4 Discussion 108

Chapter 4 Synthetic ABP modeling and artefact rejection within digital twin for SAH management 114
4.1 Common artefacts and their rejection in ABP waveforms 115
4.1.1 Common artefacts in ABP measurements 115
4.1.2 Artefact detection and rejection in ABP measurements 123
4.1.3 Discussion on proposed methods for ABP artefact rejection 128
4.2 Arterial blood pressure modelling 129
4.2.1 The morphology of arterial blood pressure waveform 129
4.2.2 Piece-wise parametric ABP model 132
4.2.3 Assessing the fitting performance of ABP models 134
4.2.4 Personalised synthetic ABP generation 137
4.3 Applications with digital twins in SAH management 140
4.4 Summary and discussion 141

Chapter 5 Neurological intervention transition model for dynamic prediction of good outcome in spontaneous SAH 146
5.1 Introduction 146
5.2 Methods 148
5.2.1 Data Collection and Visualisation 148
5.2.2 Prognostic modelling 151

5.3 Results 154
5.3.1 Simultaneous analysis on longitudinal and survival data 154
5.4 Discussion 158

Chapter 6 Incorporating pharmacological effects into prognostic models for SAH disease progress 163
6.1 Medication protocols for SAH recovery 164
6.2 Analysis on pharmacological effects on SAH recovery 165
6.2.1 Data description and methods 165
6.2.2 Effects of medications for complication prevention and management on SAH prognosis 166
6.2.3 Effects of medication for pain relief and control on SAH prognosis 172
6.2.4 Effects of medication for intracranial and blood pressure control on SAH prognosis 175
6.3 Summary and discussion 176

Chapter 7 Multi-state dynamic prognostic modelling for spontaneous SAH 182
7.1 Introduction 182
7.2 SAH prognostic framework 184
7.2.1 Key elements in statistical framework 184
7.2.2 Longitudinal sub-model 191
7.2.3 Survival sub-model 191
7.2.4 State-transition sub-model 193
7.2.5 Parameter estimation 194
7.3 Simulation and analysis 198
7.3.1 Dataset and simulation 198
7.3.2 Survival analysis on baseline covariates 200
7.3.3 Longitudinal process and dynamic prognosis 202
7.3.4 Individualised state-transition prediction 204
7.4 Discussion, limitations and future work 210
7.4.1 Discussion on multi-state prognostic framework for SAH 210
7.4.2 Limitations and future work 211
7.4.3 Summary 213

Chapter 8 Conclusion and future outlook 217
8.1 Conclusion of this thesis 217
8.2 Future outlook 219
8.2.1 Potential improvements in chapters 219
8.2.2 Future research directions 220

Chapter 1 Physiological and medical background of SAH

To place our study on the dynamic prognosis of spontaneous subarachnoid haemorrhage (SAH) in context, this chapter offers a comprehensive overview of the physiological and medical background of SAH, especially spontaneous SAH. This chapter begins with reviewing some knowledge of cerebral structure relevant to our study, particularly anatomy and physiology of cerebral vasculature and meninges. Then differences between traumatic and spontaneous SAH and their respective characteristics will be discussed regarding their epidemiology, pathophysiology, clinical manifestation, diagnosis, prognosis, and treatment. The reasons for emphasising spontaneous SAH are discussed, followed by detailed sections on its epidemiology, diagnosis, complications, and treatment.

1.1 Structure of the brain

The human brain is an extraordinarily complex organ that is responsible for controlling and coordinating all body functions. It is composed of billions of neurons that communicate with each other to allow humans to think, feel, move, and perceive their environment. The brain can be divided into three main parts: the cerebrum, the cerebellum, and the brainstem, with its major structures illustrated in Figure 1.1.

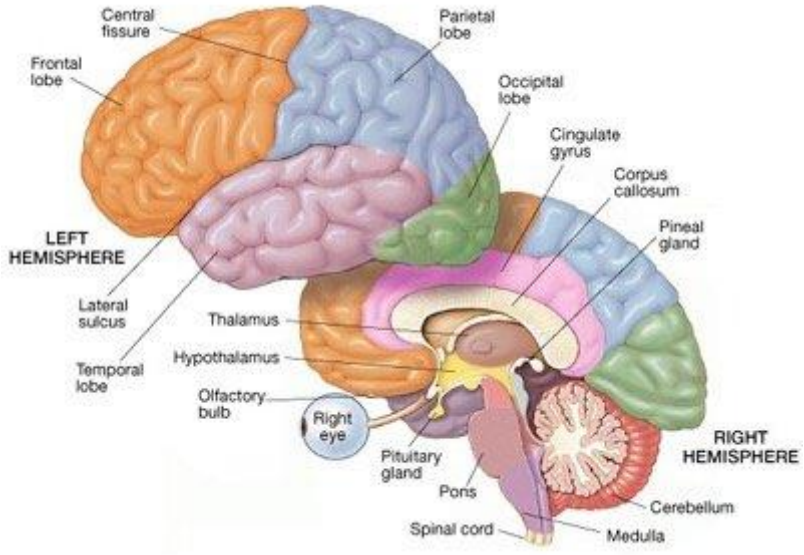


Figure 1.1 Major structures of the human brain (Publicly available in [1])

The cerebrum is the largest part of the brain, responsible for conscious thought, memory, language, perception, and voluntary movement. It is divided into two hemispheres, left and right, with each hemisphere further divided into four lobes: the frontal lobe, parietal lobe, temporal lobe, and occipital lobe. Each lobe controls specific functions.

Located beneath the cerebrum, the cerebellum is responsible for coordinating movement, balance, and posture. It is divided into three parts: the cerebrocerebellum, the spinocerebellum, and the vestibulocerebellum. The brainstem, which connects the cerebrum to the spinal cord and cerebellum, regulates basic life-support functions such as breathing, heart rate, and blood pressure. It is composed of three sections, listed in descending order: the midbrain, pons, and medulla oblongata. To better understand SAH, particularly spontaneous SAH, the following section covers the cerebral vasculature and meninges, focusing on their definition and pathophysiology.

1.1.1 Anatomy and physiology of cerebral vasculature

The cerebral vasculature is a complex network of blood vessels that supplies the brain with essential oxygen and nutrients. Given the brain's high metabolic rate, it requires a continuous and adequate supply of oxygen and glucose to maintain normal functions. The cerebral vasculature is composed of three main types of blood vessels: arteries, veins, and capillaries. Arteries carry oxygen-rich blood to the brain, while veins carry oxygen-poor blood away. Capillaries, the smallest blood vessels within the brain, are responsible for the transportation of oxygen and nutrients to brain cells and the removal of waste products.

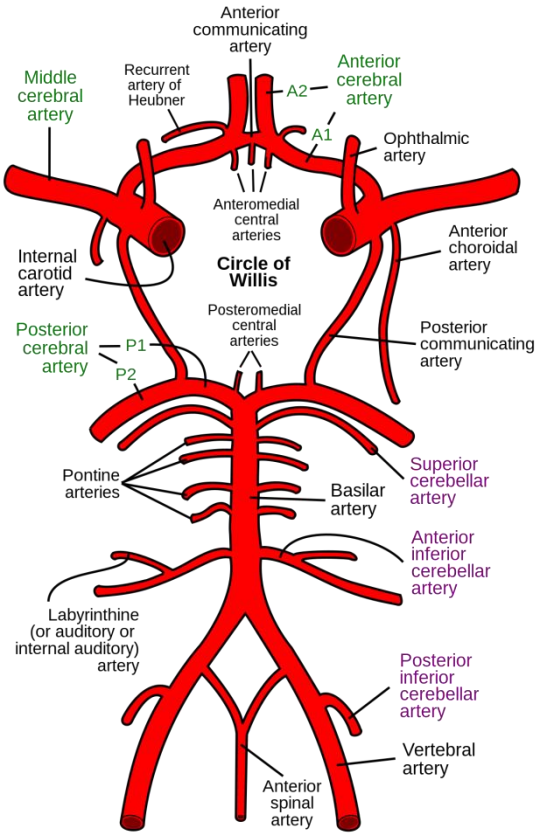


Figure 1.2 Anatomy of cerebral vasculature (Publicly available in [2])

This network can be divided into two main systems: the anterior circulation and the posterior circulation. The anterior circulation encompasses the territory of the internal carotid, middle, and anterior cerebral arteries, supplying the frontal and temporal lobes. The posterior circulation includes the territory of the vertebral, basilar, cerebellar, and posterior cerebral arteries, supplying the occipital lobe and the brainstem. For clearer understanding and visualisation, the primary cerebral arteries are illustrated in Figure 1.2.

Disruptions in the cerebral vasculature can lead to serious conditions such as strokes, cerebral aneurysms, and cerebral haemorrhages. Understanding the anatomy and physiology of the cerebral vasculature is crucial for comprehending these conditions, particularly subarachnoid hemorrhages.

1.1.2 Anatomy and physiology of meninges

The meninges are the three layers of protective membranes surrounding the brain and spinal cord, which are the dura mater, arachnoid mater, and pia mater, as illustrated in Figure 1.3.

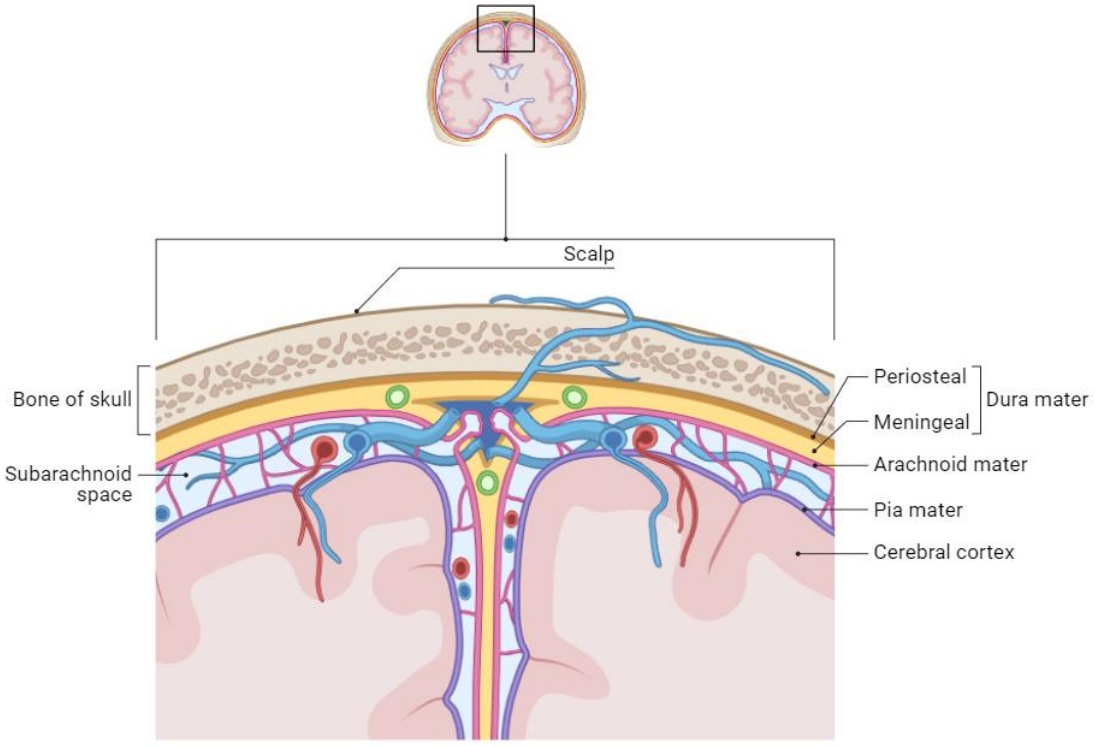


Figure 1.3 Anatomy of meninges (Produced in BioRender[1])

- **Dura mater**: The dura mater is the outermost layer, composed of tough, fibrous connective tissue, forming a protective barrier around the brain and spinal cord.

[1] BioRender (www.biorender.com): a scientific image and illustration software

- **Arachnoid mater**: The arachnoid mater is the middle layer and is a thin, web-like membrane that lies between the dura mater and the pia mater.
- **Pia mater**: The pia mater is the innermost layer and is a thin, delicate membrane that closely adheres to the surface of the brain and spinal cord.

Between the arachnoid mater and the pia mater is the subarachnoid space, also known as the leptomeningeal space. This space is filled with cerebrospinal fluid (CSF), which is produced in the ventricles of the brain. CSF circulates around the brain and spinal cord, providing nutrients, removing waste products, and acting as a cushion against physical trauma. The meninges are involved in the production, circulation, and absorption of CSF into the bloodstream. The primary function of the meninges is to protect the brain and spinal cord from physical trauma and injury, with CSF providing an additional layer of cushioning to prevent damage.

1.2 Subarachnoid haemorrhage (SAH)

Subarachnoid haemorrhage (SAH) refers to bleeding into the subarachnoid space, the area between the arachnoid mater and the pia mater, as illustrated in Figure 1.3. This condition is life-threatening and often presents with symptoms such as a sudden and severe headache, vomiting, fever, and decreased level of consciousness. Aneurysmal SAH affects up to 9 people per 100,000 annually, with a mortality rate ranging from 30% to 45%. Additionally, approximately 20% of aneurysmal SAH survivors are left dependent on assistance for daily activities. [3]

SAH can arise from either traumatic head injury or spontaneous causes. Traumatic SAH occurs due to head trauma, whereas spontaneous SAH arises without an external injury. Spontaneous SAH is often caused by the rupture of a cerebral aneurysm, but there are other causes including non-aneurysmal perimesencephalic haemorrhage and vascular disorders like cerebral arteriovenous malformations (AVM).

Although traumatic and spontaneous SAH share some pathological similarities, they differ in their epidemiology, pathophysiology, clinical manifestations, diagnosis, prognosis, and treatment. These distinctions are crucial for understanding and managing the condition effectively. In this section, we will explore and compare these two types of SAH across several aspects to highlight their differences and implications for patient care.

1.2.1 Traumatic SAH

Trauma is the leading cause of SAH, making it the most prevalent form of intracranial hemorrhage following traumatic events. Reports indicate that 26%-53% of all trauma cases may develop traumatic SAH. This type of SAH is commonly observed after head traumas, such as those sustained in vehicle accidents or serious falls, and it occurs in about 35% of traumatic brain injuries. Pathological causes of traumatic SAH include arterial dissection, direct damage to small veins and arteries, rupture due to a

sudden increase in intravascular pressure, and direct extravasation from blood resulting from an adjacent cerebral contusion. This extravasation can lead to the rupture of cortical veins, the pia mater, and basilar arteries. The primary mechanism behind these ruptures is believed to be the direct impact or movement of the head, which generates shearing, stretching, and compressive forces. [4]

Traumatic SAH often co-exists with other types of brain injuries, such as cerebral contusions or subdural haematomas, as a concomitant manifestation of brain trauma. The subarachnoid bleeding in traumatic SAH tends to be relatively minor, appearing as spotted or diffuse with well-defined regions of haemorrhage. Typically, the bleeding is located over the convexity of the brain, in areas of contusion, rather than around the circle of Willis or in the posterior fossa. [5]

Radiographic features of traumatic SAH are generally identified using computed tomography (CT) scans performed shortly after the head trauma, often within minutes or hours of the injury. These scans usually detect small amounts of blood, often filling only a few sulci, and sometimes reveal adjacent cerebral contusions. Additionally, small amounts of blood may be visible in the interpeduncular fossa or within the occipital horns of the lateral ventricles.

Patients with traumatic SAH generally experience a shorter disease course and may lack significant clinical manifestations, making timely diagnosis and appropriate treatment crucial to reduce mortality and disability. For diagnosing traumatic SAH, after obtaining a thorough medical history and performing physical examinations suggestive of SAH, non-contrast CT scans of the brain are typically used to confirm the presence and location of haemorrhage. This imaging helps determine whether the SAH is traumatic or spontaneous by identifying the blood in the subarachnoid space.

Additional diagnostic technologies, such as magnetic resonance imaging (MRI), digital subtraction angiography (DSA), and lumbar puncture (LP), can also be employed to diagnose both traumatic and spontaneous SAH. These methods provide detailed images and information about the vascular structures and cerebrospinal fluid, which are vital for comprehensive assessment and management of the condition. These diagnostic techniques will be discussed in detail in Section 1.3.

The treatment of traumatic SAH focuses on stabilising patients' condition and preventing complications. Initial management includes ensuring a clear airway, maintaining blood pressure and flow, and optimising cerebral oxygenation. In advanced ICU settings, additional measures such as intracranial pressure (ICP) monitoring, brain tissue oxygen tension monitoring, transcranial Doppler ultrasonography (TCD), and haemodynamic support are utilised to maintain stable cerebral perfusion pressure (CPP) and prevent secondary brain injury.

If complications like electrolyte disturbances, vasospasm, or hydrocephalus are detected, targeted treatments are employed. For instance, electrolyte imbalances are

corrected with appropriate therapy, vasospasm is treated with medications or interventional procedures, and hydrocephalus may require drainage or surgery. These comprehensive strategies aim to stabilise the patient, prevent further complications, and promote recovery. Detailed management of specific complications will be discussed in Section 1.5

Generally, patients with traumatic SAH have better prognoses and recover more quickly compared to those with spontaneous SAH, often requiring only conservative treatments. The prognosis of traumatic SAH depends on the cause and neurological condition of the patient. Specifically, the severity of traumatic SAH, classified using the modified Fisher scale, is a significant predictor of outcomes. This scale helps assess the extent of bleeding and predict the likelihood of complications, thereby guiding treatment decisions and prognostication. [4]

1.2.2 Spontaneous SAH

Spontaneous SAH is the third most common type of stroke, accounting for 2%-7% of all stroke cases. [6] Most spontaneous SAH cases are caused by ruptured cerebral aneurysms, which are responsible for approximately 85% of these instances. Cerebral aneurysms, typically located in the Circle of Willis and its branches, cause the enlargement and weakening of arterial walls. Over time, the wall of an aneurysm can become unstable and undergo morphological changes, eventually leading to rupture at an unpredictable time. In aneurysmal SAH, blood accumulation is typically centred around the aneurysm's location, primarily in the basal cisterns, and frequently extends into the suprasellar cistern, sylvian fissures, and interhemispheric fissure.

Approximately 15%-20% of spontaneous SAH cases are not caused by the rupture of intracranial aneurysms. These non-aneurysmal SAH cases can be attributed to a variety of causes. About half of these are due to perimesencephalic SAH, where the bleeding is confined to the cisterns surrounding the brainstem and suprasellar cistern, predominantly in the interpeduncular cistern. [7]

The remaining non-aneurysmal SAH cases are termed non-perimesencephalic SAH, based on the distribution of the haemorrhage. Non-perimesencephalic haemorrhage is diffuse, primarily occurs in locations like the sylvian cisterns, interhemispheric cisterns, or convexity, and can result from various vascular disorders, including cerebral arteriovenous malformations, dural arteriovenous fistulas, spinal tumors, intracranial neoplasms, or infarctions. Generally, non-aneurysmal SAH patients typically experience more favourable clinical outcomes than those with aneurysm-related SAH. [8]

Spontaneous SAH is initially confirmed by CT and/or LP, differentiated from traumatic SAH by the absence of trauma history and the specific location of the blood. For spontaneous SAH cases, DSA is considered the gold standard to identify intracranial sources of bleeding, particularly aneurysms that might not be visible on

CT or MRI scans. DSA can be repeated if the initial angiography is negative but clinical suspicion for an aneurysm remains high. Both aneurysmal and non-aneurysmal SAH can be confirmed through DSA findings. [8]

For aneurysmal SAH, it is recommended to repair the ruptured aneurysm as soon as possible. Clinical intervention primarily involves two methods: surgical clipping and endovascular coiling, which may also include the use of other devices. Symptomatic treatment for non-aneurysmal SAH includes sedation, analgesia, and antifibrinolytic therapy to prevent re-bleeding and vasospasm.

As spontaneous SAH, predominately aneurysmal SAH, is a high-risk condition that requires urgent medical intervention. Accurate prognosis is crucial for predicting complications and clinical outcomes, guiding treatment decisions, and improving patient management. Various predictors have been investigated for their prognostic value in assessing complications and clinical outcomes. These predictors encompass patient demographics, admission status, underlying conditions, radiographic findings, causes of SAH, indices from physiological monitoring, and other relevant factors. Chapter 3 will explore these predictors, their associations with complications, survival outcomes, and other clinical outcomes, as well as the underlying mechanisms, with their incorporation into prognostic models to be covered in later chapters.

In the following sections of this chapter and subsequent chapters in this thesis, we will primarily focus on spontaneous SAH, particularly aneurysmal SAH. Prognostic research is more feasible and crucial in spontaneous SAH compared to traumatic SAH for several reasons.

Firstly, spontaneous SAH, often caused by ruptured aneurysms, carries a higher risk of mortality and complications, making accurate prognosis essential for guiding treatment and improving outcomes. Additionally, while traumatic SAH is more common, it often occurs with other injuries, such as contusions and fractures, complicating the assessment specific impact of a prognostic factor on prognosis. In contrast, spontaneous SAH is typically an isolated event, making it easier to analyse the influence of prognostic factors on patient outcomes. Finally, spontaneous SAH generally involves a prolonged disease course and poorer prognosis, underscoring the value of developing dynamic and accurate prognostic models to capture the influence of each factor and enhance patient management.

In this context, developing a prognostic model for spontaneous SAH to predict dynamic survival probabilities and the likelihood of complications is both urgently needed in clinical practice and feasible. This feasibility is due to the availability of various fixed-time and dynamic predictors that accurately reflect the evolving medical conditions of non-traumatic SAH patients. Moreover, the critical importance of effective critical care management highlights the necessity for such a prognostic model to improve patient outcomes.

1.3 Epidemiology of spontaneous SAH

1.3.1 Incidence, prevalence and fatality

Previous studies have shown that the incidence of spontaneous SAH depends on several factors, including region, gender, age, and race. The annual incidence of spontaneous SAH in the United Kingdom is 7.9 (*95% CI: 6.2-9.9*) cases per 100,000 population, based on a multi-ethnic population study in London. [9] A systematic review in 2007 reported that the annual incidences of spontaneous SAH were 4.2 (*95% CI: 3.1-5.7*) in South and Central America, 19.7 (*95% CI: 18.1-21.3*) in Finland, 22.7 (*95% CI: 21.9-23.5*) in Japan, and 9.1 (*95% CI: 8.8-9.5*) in other regions of the world. [10] Regional differences were also reported in another stroke study by the World Health Organization (WHO), which found that the annual incidence of spontaneous SAH varies from 2.0 (*95% CI: 1.6-2.4*) in Beijing, China, to 22.5 (*95% CI: 20.9-24.1*) in Finland per 100,000 population. [11]

Regarding gender differences in spontaneous SAH incidence, women are more likely to suffer from aneurysmal SAH, with an incidence approximately 1.24 times higher than that of men. Studies suggest that these gender differences may be related to hormone levels. The risk of aneurysmal SAH is higher among postmenopausal women who report active use of hormone replacement therapy (HRT) compared to those who do not use HRT. [12] The incidence of spontaneous SAH is also age-dependent, with most aneurysmal SAH cases occurring in the fifth and sixth decades of life, although younger children and older adults can also be affected. [13] When controlling for age and gender, the incidence of non-traumatic SAH is greater in black patients (15.4 per 100,000 population annually) compared to non-Hispanic white patients (9.9 per 100,000 population annually) and other races ($p<0.001$). [14]

Among all cerebrovascular disease patients in the United States, approximately 5% are affected by SAH, with the prevalence of aneurysmal SAH being 80 per 100,000 population. After treatment for aneurysmal SAH, the annual prevalence of new aneurysms is about 1% to 2%, with patients who have multiple aneurysms on their radiographic findings being more likely to develop new aneurysms. [15] For patients with a family history of aneurysms, the prevalence can reach up to 9.5%. [16]

Regarding the fatality of spontaneous SAH, about 15% of patients die before arriving at the hospital; among those who reach the hospital, 25% die within the first 24 hours, and a total of 50% die within 6 months. [17] The WHO MONICA stroke study reported that 1,404 of 3,368 SAH cases died within 28 days, accounting for 41.7% of all included cases. Of these 1,404 fatal cases, 37% died within 24 hours, 60% within 48 hours, and 75% within one week. Mortality rates are higher for SAH patients over 60 compared to those under 60 within 24 hours, 1 day, and 30 days. [11] The in-hospital fatality of SAH has decreased over time, from 30% (*1979-1983*) to 20% (*2004-2008*), which can be attributed to advances in neurological intensive care, neurovascular imaging, and neurointervention. [9][18] For haemorrhages caused by

arteriovenous malformations (AVM), including SAH, the annual disability and fatality rates are 1.7% and 1.0%, respectively. [19]

1.3.2 Risk factors of spontaneous SAH

Risk factors for spontaneous SAH can be discussed from three aspects: the risk factors for aneurysms, cerebral arteriovenous malformations (AVMs), and SAH itself. The risk factors for aneurysms can be further categorised into three perspectives: the risk factors for the development of aneurysms, the risk factors for morphological changes in aneurysms, and the risk factors for the rupture of aneurysms. Some of these risk factors are non-intervenable, including age, gender, cerebral AVM, multiple aneurysms, and a family history of aneurysms and SAH. In a magnetic resonance angiography (MRA) study involving 8,680 patients, which included 380 patients with a family history of aneurysms and 8,300 patients without, the prevalence of aneurysms was 10.5% among those with a family history, compared to 6.8% for those without. [20]

Intervenable risk factors for aneurysms include smoking, alcohol consumption, hypertension, hypolipidemia, drug abuse, and HRT. For example, tobacco use is an independent risk factor for the development and enlargement of aneurysms. Abuse of cocaine and phenylpropanolamine (PPA) has also been shown to contribute to the development and rupture of aneurysms. [21][22]

The risk factors for cerebral AVMs can be considered in terms of their development and rupture. The risk of developing AVMs includes gender and family history, with cerebral AVMs being more common in males and those with a family history of AVMs. However, it is unclear whether family history is a genetic factor. Moreover, hereditary haemorrhagic telangiectasia (HHT) is an inheritable medical condition that increases the risk of cerebral AVMs. [23] The factors believed to increase the risk of haemorrhage in AVM patients include a history of prior bleeding, small AVM size, deep venous drainage, and higher feeding artery pressures. However, the relative importance of these risk factors is still uncertain. [24]

The main independent factors that increase the risk of spontaneous SAH are smoking, alcohol abuse, and hypertension. Multiple cohort and case-control studies have revealed that smoking is the most significant independent risk factor for spontaneous SAH, with 40% of non-traumatic SAH cases attributed to smoking. In Europe and North America, the smoking rate among patients affected by SAH (45%-75%) is significantly higher than that of the general population (20%-35%). Alcohol abuse is another important risk factor for spontaneous SAH, independent of smoking, age, and hypertension, as shown in both cohort and case-control studies. [25-29]

Compared to cigarette smoking and alcohol abuse, hypertension is a less significant risk factor, with the prevalence of hypertension in SAH patients only slightly higher

than that in the general population. While relevant case-control studies have demonstrated that hypertension is not a significant risk factor for SAH when controlling for age, gender, alcohol, and smoking, a systematic review of cohort and case-control studies has indicated that hypertension remains a valuable risk factor for spontaneous SAH. [28]

1.4 Diagnosis of spontaneous SAH

In Section 1.2, the diagnosis of both traumatic and spontaneous SAH was briefly discussed. This section will delve into the diagnosis of spontaneous SAH, examining various technical modalities, their applicable conditions, sensitivity, specificity, and key considerations for their use in clinical practice.

1.4.1 Computed tomography (CT) and computed tomography angiography (CTA)

A CT scan utilises a series of rotating X-rays taken from different angles around the body, along with a row of detectors, to create cross-sectional images of internal tissues. These images are processed on a computer using algorithms for tomographic reconstruction. When clinicians suspect SAH based on medical history, examination, and symptoms, a non-contrast CT is usually the first diagnostic tool employed.

Non-contrast CT allows for rapid, cost-effective, accurate, and less hazardous detection of blood in the subarachnoid space. It is also valuable for differential diagnosis, helping to exclude other pathologies such as other types of intracranial haemorrhage, malignancy, and abscess. Subarachnoid blood is most visible at the onset of bleeding, but as red blood cell (RBC) degradation progresses, the blood in the subarachnoid space becomes more difficult to detect. If the initial CT scan is negative but SAH is still suspected, a LP is necessary to confirm the diagnosis.

Computed tomography angiography (CTA) builds upon CT technology to create detailed images of blood vessels and surrounding tissues in various body regions. For patients with a negative non-contrast CT scan of the brain, CTA is a viable option for evaluating SAH. However, physicians must weigh the benefits against the potential risks of CTA, such as infection or injury at the injection site, before making a decision.

The sensitivity of a non-contrast CT scan for detecting the presence of SAH depends on the amount of haemorrhage and the time elapsed since the initial onset. A prospective cohort study has shown that the overall sensitivity of CT for SAH is 92.9% (*95% CI: 89.0%-95.5%*) and the specificity is 100% (*95% CI: 99.9%-100.0%*). However, the sensitivity of CT decreases with time from the onset of SAH. A conservative statistical analysis indicates that a non-contrast CT performed within 6 hours of headache onset has a sensitivity of 98.7% (*95% CI: 97.1%-99.4%*). This sensitivity drops to 93% within 24 hours of onset, 80% at 3 days, and 50% at 1 week. [30][31]

After performing a non-contrast CT scan on patients, the diagnosis of SAH is based on the distribution of blood in the CT slices. The diagnosis is confirmed if hyperdense material, appearing as a lighter shade of grey, is seen filling the subarachnoid space. In cases of spontaneous SAH, this hyperdensity is most commonly observed around the Circle of Willis or in the Sylvian fissure. Radiographic findings in CT slices also help identify the sources of bleeding, thereby determining the sub-types of spontaneous SAH. Figure 1.4 illustrates the presence of SAH, showing hyperdense blood in the Sylvian fissures and basal cisterns, which are common locations for blood accumulation in cases where an aneurysm has ruptured.

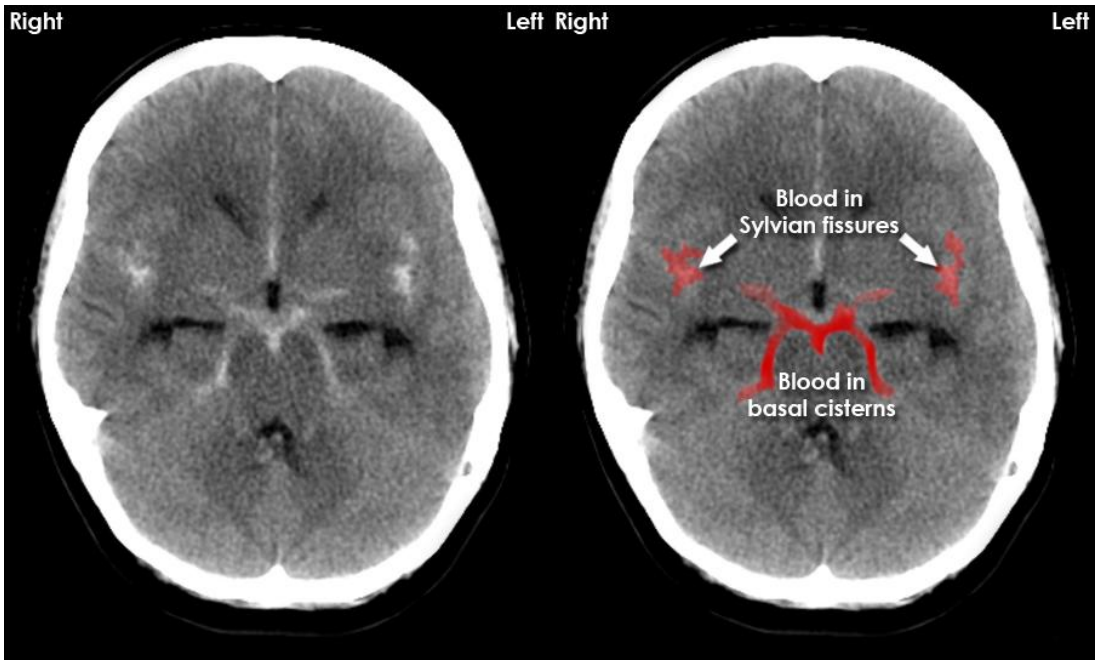


Figure 1.4 CT scan illustrating aneurysmal SAH (Publicly available in [32])

SAHs can be classified into four levels of severity using the Fisher scale (grades 1-4) or five levels of severity using the modified Fisher scale (grades 0-4). These classifications are based on the amount of haemorrhage in the subarachnoid space, whether the blood is diffused or localised, and the presence of intraventricular haemorrhage (IVH). Both the Fisher scale and the modified Fisher scale are valuable tools for categorising SAH patients by severity, guiding medical resource allocation, and predicting the risk of mortality and vasospasm.

1.4.2 Lumbar puncture (LP)

LP is a medical procedure where a needle is inserted into the spinal canal, primarily for the collection of cerebrospinal fluid for diagnostic and therapeutic purposes. It should be noted that a puncture should not be performed if there is inflammation in the local skin, soft tissue, or bones. Additionally, the procedure is contraindicated in the presence of signs of brain herniation or critical medical conditions such as shock, symptoms of spinal cord compression, or spinal cord dysfunction. Following a lumbar

puncture, patient health management should focus on preventing headache, infection, and brain herniation.

LP is traditionally recommended if the CT scan is negative and is currently considered the gold standard for SAH diagnosis, as it can detect small amounts of blood and xanthochromia in the spinal fluid. [33] However, the routine performance of LP after a negative CT scan remains debated. One argument against its routine use is the high accuracy of modern CT scanners. When a CT scan is performed within 6 hours of symptom onset, the sensitivity is between 97% and 100%, resulting in a very low probability of a false negative.

Although CT scans conducted after 6 hours from the onset of haemorrhage are less sensitive, the prevalence of SAH also decreases over time. Among patients receiving a CT scan after 6 hours of symptom onset, only 0.8% (*95% CI: 0.5%-1.3%)* are ultimately diagnosed with SAH. Additionally, the sensitivity and specificity of LP for SAH diagnosis depend on the biomarkers used, such as xanthochromia and red blood cells (RBCs), and the thresholds set for these biomarkers. No combination of biomarkers and thresholds can achieve both sensitivity and specificity greater than 90%. [34]

A common issue during LP is a traumatic tap, where the needle inadvertently enters an epidural vein. Traumatic taps occur in 10% to 30% of patients and can reduce the interpretability of LP results. Additionally, the procedure is painful for most patients, and post-LP headaches occur in 4% to 10% of cases. Despite being traditionally referred to as a standard step following a negative CT scan, the routine use of LP is debated. Therefore, although LP is often considered after a negative CT scan, physicians use clinical judgement to determine whether or not it is necessary. [34]

1.4.3 Magnetic resonance imaging (MRI)

MRI, a medical application of nuclear magnetic resonance (NMR), is used in radiology to produce images that reveal the anatomy of organs in the human body. For the diagnosis of SAH, MRI is sensitive to subarachnoid blood, which appears as hyperintensity (an area of high intensity) in fluid-attenuated inversion recovery (FLAIR) sequences, and which can be visualised well within the first 12 hours after symptom onset. [35]

Conventional T1-weighted and T2-weighted MRI scans are less sensitive to SAH and require longer scan times than CT, making them unsuitable for SAH detection. Studies have shown that gradient echo T2* and FLAIR sequences can effectively detect SAH. Gradient echo T2* is the most sensitive sequence, with sensitivities of 94% and 100% in the acute and sub-acute phases, respectively. Although the sensitivity of FLAIR sequences is lower than that of gradient echo T2*, it remains satisfactory for SAH detection, with sensitivities of 81% and 87% in the acute and

sub-acute phases, respectively. [36]

As discussed above, combining CT and LP in the presence of a negative CT scan achieves high sensitivity and specificity for diagnosing SAH in the acute phase. However, in the sub-acute phase, the sensitivity of this combination reduces to 75%. In such cases, MRI methods like gradient echo T2* and FLAIR can effectively supplement the radiographic findings of CT. Additionally, the combination of FLAIR and gradient echo T2* sequences has proven valuable in detecting SAH, especially in late-presenting or atypical cases, during more extensive MR investigations, and when CT and LP results are contradictory. [36]

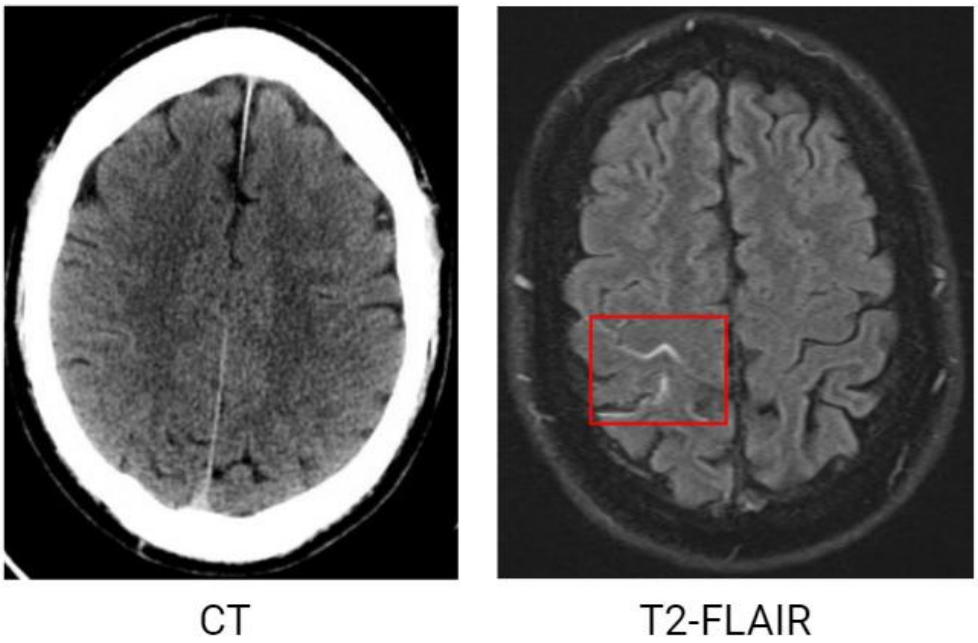


Figure 1.5 CT and T2-FLAIR images 5 days after SAH (Produced in BioRender)

As shown in Figure 1.5, in the sub-acute phase post-SAH (day 5), CT images may appear negative, while MRI images with T2-FLAIR sequences show an abnormal signal within the right parietal sulci, as highlighted. Compared to CT scans, MRI is free of ionising radiation, robust against artefacts from bone, and provides detailed anatomical images of soft tissues and organs. Despite these advantages, MRI has several drawbacks that reduce its availability and popularity. MRI takes longer to perform, is more expensive, and is more sensitive to patient motion compared to CT. Additionally, patients with implantable medical devices, such as cardiac pacemakers or defibrillators, are often advised against undergoing MRI scans due to safety concerns. [37]

1.4.4 Digital subtraction angiography (DSA)

Digital subtraction angiography (DSA) is a widely used fluoroscopic technique in interventional radiology for imaging blood vessels. This method digitally removes

radiopaque structures, such as bones, to provide a clear view of the blood vessels. DSA is considered the gold standard for diagnosing and evaluating vascular abnormalities. Even when lesions are detected through MRI or CT and surgery is indicated, a catheter study is often performed at many medical centres. In the investigation of spontaneous SAH, DSA with three-dimensional reconstruction is regarded as the gold standard due to its high sensitivity of 99% for diagnosing blood vessel lesions causing SAH. Because of its high sensitivity and the importance of identifying a treatable cause for SAH, DSA is frequently performed on patients who present with SAH and have negative results from CTA. [38]

DSA provides real-time assessment of blood flow in the source vessel, revealing any collateral supply and the viability of the donor's inflow artery. DSA can detect aneurysms that are not visible through ultrasonography, CTA, or MRI and offers the added benefit of enabling simultaneous treatment. [39] Figure 1.6 illustrates the roles of non-contrast CT, and two-dimensional and three-dimensional DSA in detecting spontaneous SAH, particularly aneurysmal SAH. [40]

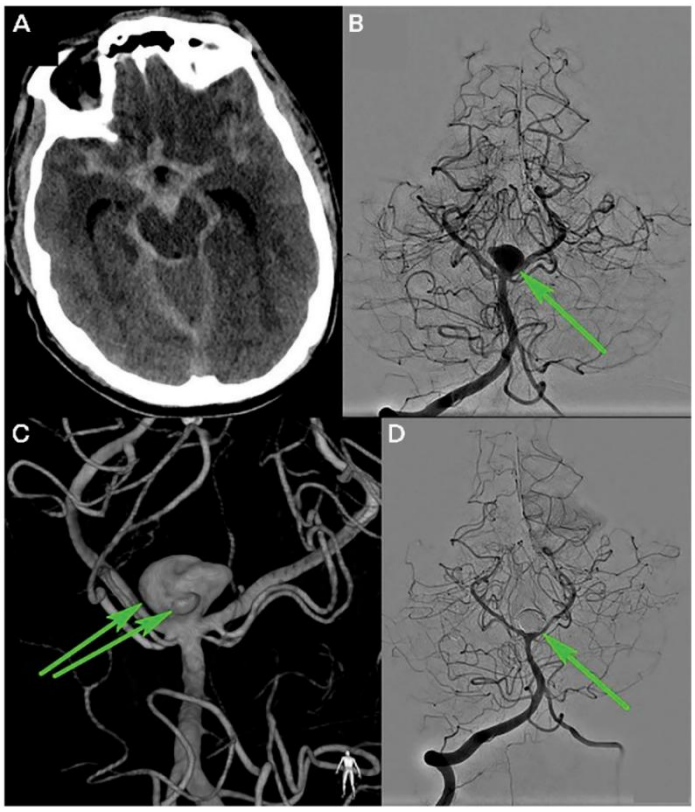


Figure 1.6 Non-contrast head CT (A) showing acute subarachnoid haemorrhage, and two-dimensional (B) and three-dimensional (C) four-vessel angiogram showing a large top of the basilar artery aneurysm with an irregular shape (B, C, arrows). Two-dimensional angiogram after coiling shows embolization of the aneurysm (D, arrow) [40]

Non-contrast head CT, typically the initial exam, highlights suspected SAH regions as

bright white areas, providing a rapid initial diagnosis. Two-dimensional and three-dimensional four-vessel DSA can precisely identify the sources of bleeding, such as ruptured aneurysms or AVMs, detailing their location, shape, and size as key prognostic factors. DSA can also evaluate the rehabilitation of cerebral blood vessels post-treatment. As shown in Figure 1.6 (B and D), two-dimensional DSA demonstrates the removal of an aneurysm following coiling.

However, DSA is an invasive procedure that can result in various side effects and complications. Prolonged DSA increases the risk of both neurological and wound-related complications. Cancer patients should be cautious of the risk of cerebral infarction, while individuals on anticoagulants or those who regularly consume alcohol should be aware of the possibility of angiographic-site haematomas. [41]

1.4.5 Discussions on diagnosis methods

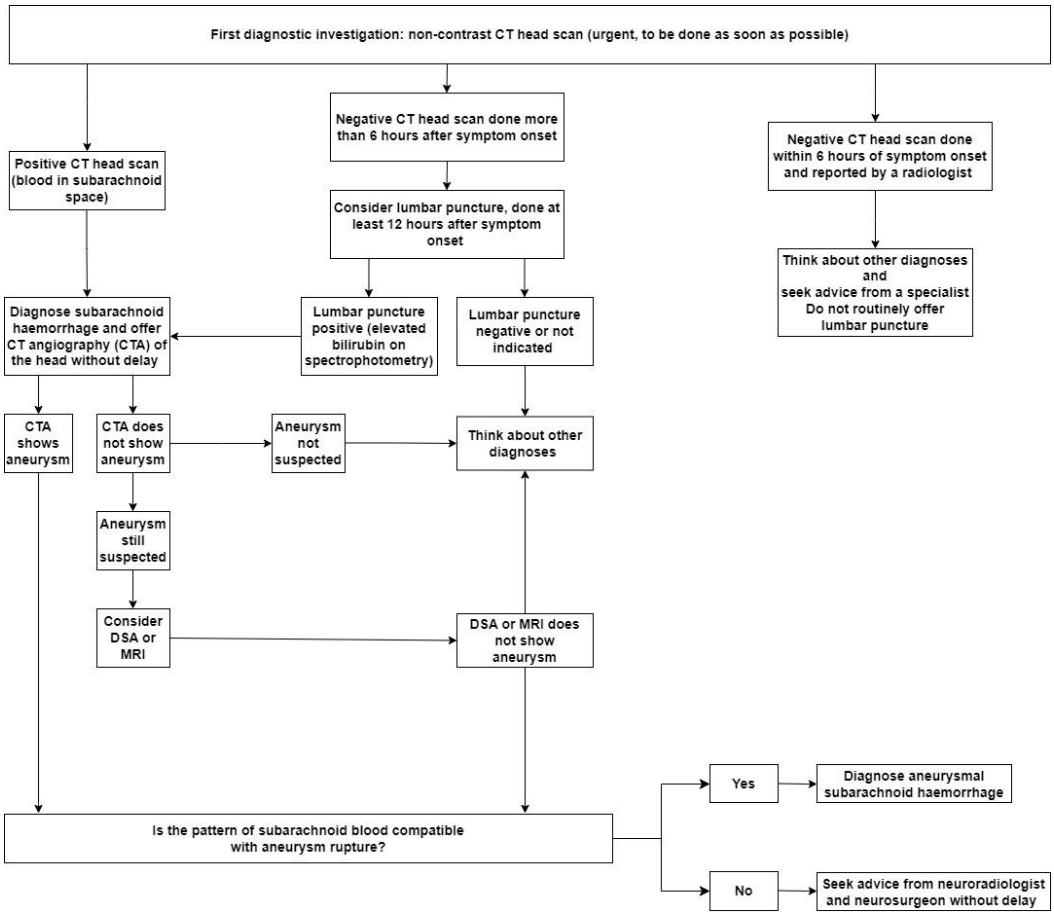


Figure 1.7 Diagram of use of diagnosis methods in aneurysmal SAH

Figure 1.7 presents the decision flow diagram for diagnosing aneurysmal SAH as suggested by NICE's guidelines on subarachnoid haemorrhage caused by a ruptured aneurysm. [42] After symptom onset, a non-contrast CT head scan is the first diagnostic investigation to be performed. If blood is present in the subarachnoid space, CTA should be performed for further evaluation. LP should not be routinely offered

after a negative CT scan, especially if the scan is conducted more than 6 hours after symptom onset, as discussed previously.

If SAH is confirmed by an initial positive CT head scan or by a negative CT head scan with a positive LP, further investigations, including CTA, DSA, and MRI, should be employed to identify the source of bleeding. If aneurysms cannot be detected using CTA, DSA, and MRI as suggested by NICE's guidelines, non-aneurysmal causes, such as non-aneurysmal perimesencephalic haemorrhage or other vascular disorders like AVMs, should be considered and investigated using the radiographic findings from CTA, DSA, and MRI.

In conclusion, the diagnosis of spontaneous SAH, once trauma has been excluded as a potential source of bleeding, involves two main steps: the detection of subarachnoid blood and the identification of its source. Non-contrast CT and LP are crucial for the initial detection of subarachnoid blood, while CTA, DSA, and MRI are primarily used to identify the source of the bleeding. The diagnostic process progresses from rapid, easy-to-perform, and cost-effective tests such as non-contrast CT to more detailed and complex investigations like DSA. The radiographic findings from these diagnostic methods not only have significant diagnostic value but also play a crucial role in the prognosis of the disease, which will be discussed later in this thesis.

1.5 Complications after spontaneous SAH

The complications of spontaneous SAH depend on the severity of the aneurysmal condition or other neurological deficits, significantly impacting both survival and functional outcomes. The occurrence of post-SAH complications follows distinct temporal patterns. Based on the time elapsed since the onset of haemorrhage, SAH can be categorised into three phases: the acute phase (0 to 3 days), the sub-acute phase (3 to 14 days), and the chronic phase (more than 14 days). [43]

Each phase is associated with specific complications. For example, the acute phase is characterised by suddenly increased intracranial pressure and the risk of re-bleeding, the sub-acute phase by vasospasm and DCI, and the chronic phase by long-term neurocognitive deficits. It should be noted that the definitions of these phases may vary across studies, e.g., some studies defining the sub-acute phase as ranging from 5 to 20 days, or 8 to 10 days post-SAH. [44][45]

Besides the timing of occurrence, these complications can also be characterised by their risk factors and effects on survival and functional outcomes. In this section, we will review common complications following spontaneous SAH, focusing on their aetiology, patterns of occurrence, risk factors, impacts on survival and functional outcomes, as well as corresponding diagnosis, treatment, and prevention methods.

1.5.1 Re-bleeding

Re-bleeding is the most severe early complication of SAH that occurs when a brain aneurysm ruptures again after initially sealing itself. Re-bleeding after an initial SAH is a devastating neurological event with high mortality and morbidity rates. This complication is most common within the first 6 hours following the initial bleed. The reported incidence of re-bleeding is up to 15% within the first 24 hours, and the associated fatality rate can reach 70%. [46]

Promptly securing the ruptured aneurysm through clipping or coiling can significantly reduce the likelihood of re-bleeding. Some risk factors for re-bleeding are non-modifiable, making it challenging to eliminate this complication entirely. It is worth noting that patients with non-aneurysmal SAH do not carry the same risk of re-bleeding in the initial years following the haemorrhage. [47]

Regarding the pathophysiology of re-bleeding, several theories have been proposed based on experimental studies, with the change in trans-mural pressure gradient (TMPG) theory being considered the most significant. The TMPG of an aneurysm is determined by subtracting the pressure outside the aneurysm (intracranial pressure, ICP) from the pressure inside the aneurysm (mean arterial pressure, MAP), i.e., TMPG = MAP - ICP. A sudden increase in arterial pressure or decrease in ICP results in an increase in TMPG, potentially causing an aneurysm to rupture. To prevent re-bleeding, it is crucial to maintain a balance between the pressure inside the aneurysm and the external pressure on the arterial wall. This balance is vital in reducing the risk of aneurysm rupture. [48]

The diagnosis of re-bleeding is established through the presence of new clinical symptoms and changes in radiological findings. Symptoms can range from a mild headache to a coma, often involving a sudden intensification of headache accompanied by a decline in the Glasgow Coma Scale (GCS) score. In some cases, there may be a loss of consciousness following a seizure or the emergence of new neurological deficits. Brain CT scans are essential for all patients presenting with new neurological symptoms and should be compared to the initial CT scan to confirm re-bleeding. Diagnosing re-bleeding can be challenging if it occurs before the initial CT scan or a thorough assessment by emergency physicians. [49]

Identifying the factors that increase the risk of re-bleeding after SAH, particularly aneurysmal SAH, is crucial for determining the optimal surgical approach and improving patient outcomes. These key risk factors can be categorised into the following groups: demographics, clinical findings on admission, radiographic findings, medical conditions and indices, and other risk factors.

Age increases the risk of re-bleeding and poor outcomes, with a re-bleeding rate of 16.4% in patients over 70, compared to a rate of 4.5% in the youngest age group. [63] The re-bleeding rate is strongly correlated with poor Hunt-Hess grades, which

describe the clinical severity of SAH. Studies have shown a higher incidence of re-bleeding in patients with poor Hunt-Hess grades (IV-V) compared to those with good Hunt-Hess grades (I-III). [50]

Radiographic risk factors include the amount of subarachnoid blood on the initial non-contrast head CT, the size, location, and number of aneurysms, and DSA findings within 6 hours. The likelihood of re-bleeding during DSA performed within 6 hours of the initial injury is estimated to be 3.3%, possibly due to a sudden increase in pressure inside the atria caused by the injection of contrast material. [51][52] Medical conditions such as a sentinel headache preceding SAH and high blood pressure (systolic blood pressure higher than 160 mmHg) also increase the risk. The fragile fibrin clot formed over a ruptured aneurysm during the early stages of a subarachnoid haemorrhage is likely to rupture with a significant increase in transmural pressure, resulting in re-bleeding. [53]

Prevention strategies target these risk factors correspondingly, including securing aneurysms, controlling blood pressure, and using antifibrinolytic medications. To prevent re-bleeding, the early removal of the aneurysm within 72 hours is the preferred treatment, as recommended by the American Stroke Association (ASA) and the European Stroke Organisation (ESO). [52][54] Additionally, early securing of a ruptured aneurysm within the first 24 hours is associated with improved clinical outcomes. [55] According to the 2012 AHA/ASA guidelines for preventing re-bleeding of aneurysmal SAH, blood pressure should be controlled to balance the risk of re-bleeding with maintaining adequate cerebral perfusion pressure (CPP), the pressure gradient driving blood flow to the brain. It is reasonable to keep systolic blood pressure (SBP) below 160 mmHg. [54] For patients at high risk of re-bleeding, who missed early aneurysm securing, short-course therapy with tranexamic acid or aminocaproic acid is recommended if there are no contraindications. [56]

1.5.2 Vasospasm and delayed cerebral ischaemia (DCI)

Cerebral vasospasm, the narrowing of the cerebral arteries, is a common complication that occurs in up to 70% of patients who have suffered from SAH. This condition can be detected through radiographic and ultrasound imaging. While some patients may experience cerebral vasospasm within 24 hours of the initial onset, it typically begins 3 to 4 days after the aneurysm rupture. The occurrence of vasospasm peaks 7 to 10 days after the onset of SAH and usually resolves spontaneously after 21 days. The cause of vasospasm is attributed to the accumulation of blood products in the subarachnoid and perivascular spaces. Oxyhaemoglobin contributes to vasospasm through several mechanisms, including direct constriction of blood vessels, release of metabolites and endothelin from arterial walls, reduction of nitric oxide-dependent vasodilation, damage to perivascular nerves, and an increase in free radical production. [57]

DCI is one of the most severe post-SAH complications in patients who have survived SAH, affecting about one-third of these patients. It typically occurs 4 to 10 days after the initial bleed and is characterised by symptoms such as aphasia, hemiparalysis, or a decline in consciousness. While DCI can sometimes be reversible, it can also progress to cerebral infarction, resulting in severe neurological deficits or even mortality. Cerebral ischaemia and neurological deficits are commonly associated with vasospasm, though DCI and vasospasm can occur independently. Some patients with aneurysmal SAH may develop DCI despite moderate vasospasm, while others with significant blood vessel narrowing on an angiogram may not exhibit any symptoms. [58] Patients with non-aneurysmal SAH experience significantly fewer instances of DCI and vasospasm compared to those with aneurysmal SAH. [8]

Various imaging methods are utilised to identify cerebral vasospasm following SAH caused by a ruptured aneurysm. Currently, the most commonly used method for detecting asymptomatic spasms like vasospasm is transcranial Doppler (TCD), which serves both diagnostic and continuous monitoring purposes. [59] Due to the potential for neurological deterioration caused by vasospasm and DCI, close neurological monitoring of SAH patients is crucial for early diagnosis and treatment. The early detection of vasospasm and DCI in aneurysmal SAH patients involves three main components: clinical, radiological, and physiological monitoring:

- **Clinical monitoring**: Clinical monitoring involves frequent neurological examinations to detect changes in the patient's condition.
- **Radiological monitoring**: Radiological monitoring utilises various imaging modalities such as DSA, CTA, and MRI to diagnose, locate, and assess the severity of vasospasm and DCI.
- **Physiological monitoring**: Physiological monitoring includes methods like TCD, electroencephalography (EEG), and brain tissue oxygen monitoring, which monitor physiological indices for early detection and diagnosis of vasospasm.

In physiological monitoring, for example, assuming continuous blood flow, vasospasm narrows the diameter of vessels and increases blood flow velocity. Very high blood flow velocity in the middle cerebral arteries (>200 cm/s) reliably indicates the presence of clinically significant cerebral vasospasm. [60]

The mechanisms and pathophysiology of cerebral vasospasm and delayed cerebral ischaemia (DCI) are complicated and remain to be investigated. Figure 1.8 illustrates possible mechanisms of vasospasm and DCI in aneurysmal SAH, highlighting key aspects of their pathophysiology. Vasospasm leads to the narrowing of cerebral arteries, which limits blood flow to brain tissue. This reduction in blood flow results in decreased oxygen and nutrient delivery, directly causing cerebral ischaemia.

Additionally, the inflammatory response triggered by blood in the subarachnoid space releases cytokines and other inflammatory mediators, which exacerbate vasoconstriction and further intensify vasospasm. [61] Oxidative stress is another

critical factor in the pathophysiology of vasospasm. Free radicals generated from the breakdown of blood products damage endothelial cells and smooth muscle cells in cerebral arteries, worsening vasospasm and contributing to further ischaemia. [62]

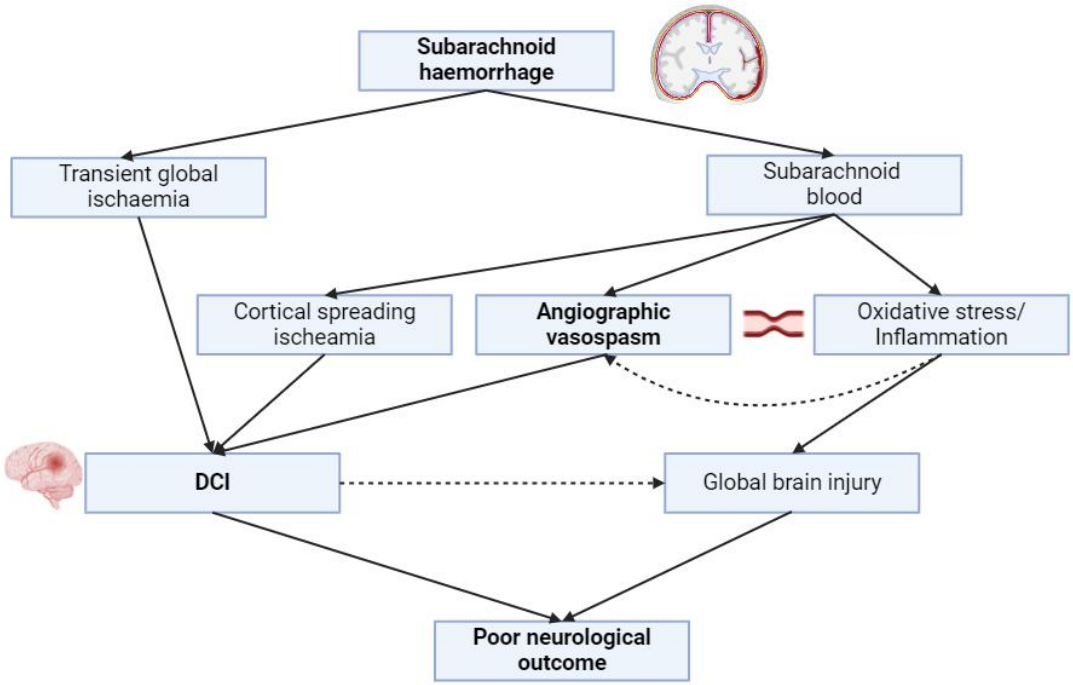


Figure 1.8 Possible mechanisms of vasospasm and DCI in aneurysmal SAH (Produced in BioRender)

To better understand the mechanisms and pathophysiology of cerebral vasospasm and DCI, it is crucial to identify their potential risk factors. Various predictors have been investigated for their potential correlation with cerebral vasospasm, including age, gender, hypertension, diabetes, and anomalies in physiological monitoring. These factors will be presented in detail in Chapter 3, highlighting how they contribute to the risk and severity of cerebral vasospasm and DCI.

Although prevention strategies against the occurrences of cerebral vasospasm and DCI have been extensively investigated over the past few decades, the results have been unsatisfactory and only limited treatment options are available to reduce the risks of vasospasm and DCI. [57] These prevention methods include pharmacological intervention, e.g., nimodipine, fludrocortisone, vasopressors such as norepinephrine, dopamine, and phenylephrine, and surgical intervention, e.g., endovascular therapy and mechanical dilatation.

Pharmacological interventions for preventing DCI and vasospasm primarily focus on optimising blood pressure, perfusion pressure, and maintaining electrolyte equilibrium in patients with SAH. Nimodipine, a dihydropyridine L-type calcium channel blocker, is recommended as a first-line treatment for preventing cerebral vasospasm following

aneurysmal SAH and reducing the risk of ischaemic events, although its mechanisms are not entirely understood [63][64]. Maintaining euvolemia and normal serum sodium levels with isotonic crystalloid solutions is advised to prevent DCI. Fludrocortisone, administered at 0.2mg to 0.4mg per day, has been shown to reduce hyponatraemia and consequently DCI [65].

Induced hypertension is an effective method for reversing neurological symptoms of DCI, with vasopressors considered the first-line therapy for blood pressure augmentation. Vasopressors such as noradrenaline, dopamine, and phenylephrine significantly enhance cerebral blood flow and oxygenation, leading to notable neurological improvement in approximately 70% of SAH patients [63].

Endovascular intervention is recommended when DCI is refractory to optimisation of blood flow or for SAH patients with multiple comorbidities that might experience complications from medical therapy, such as heart attack, heart failure, or fluid overload. Endovascular therapy can be performed using mechanical dilation, such as percutaneous transluminal coronary angioplasty (PTCA), or through intra-arterial infusion of vasodilators. PTCA is also used to dilate spastic proximal vessels, boasting a high success rate of over 90% if performed within 2 hours of neurological deterioration. However, it may need to be repeated due to recurrence of arterial vasospasm. Mechanical dilation can induce serious complications, such as cerebral artery rupture, thrombosis, embolism, and arterial dissection, occurring in up to 5% of patients. [65]

1.5.3 Hydrocephalus

Hydrocephalus, defined as “an active distention of the ventricular system of the brain resulting from an inadequate passage of cerebrospinal fluid (CSF) from its point of production within cerebral ventricles to its point of absorption into systemic circulation,” is a serious neurological complication affecting a significant proportion of individuals with SAH. This condition can lead to substantial neurological deterioration, prolonged hospital stays, and an increased risk of mortality. Symptoms of hydrocephalus include nausea, headache, blurred vision, and difficulty with movement. Therefore, early detection and treatment of hydrocephalus are crucial for improving patient outcomes.

Hydrocephalus may occur in different phases following the initial onset of SAH. Acute hydrocephalus, which develops within the first 72 hours after a haemorrhage, affects approximately 20% of patients. Sub-acute hydrocephalus, occurring between the 4th and 14th day after the haemorrhage, affects 2-3% of patients. Chronic hydrocephalus, developing two weeks or more after the initial haemorrhage, impacts 10-20% of patients. Despite these occurrences, the aetiology of post-SAH hydrocephalus remains not entirely understood [63].

The diagnosis of hydrocephalus can be challenging due to the wide range of symptoms associated with post-SAH, which are common in many SAH patients. Therefore, relying solely on symptoms for diagnosing post-SAH hydrocephalus is infeasible. The primary diagnostic tool is radiographic investigation, particularly CT scans. Based on CT scans, the bicaudate index (BCI) and the relative bicaudate index (RBCI) are calculated to guide diagnostic decisions. The BCI is defined as the ratio of the distance between the caudate nuclei to the width of the brain at the same level, as illustrated in Figure 1.9.

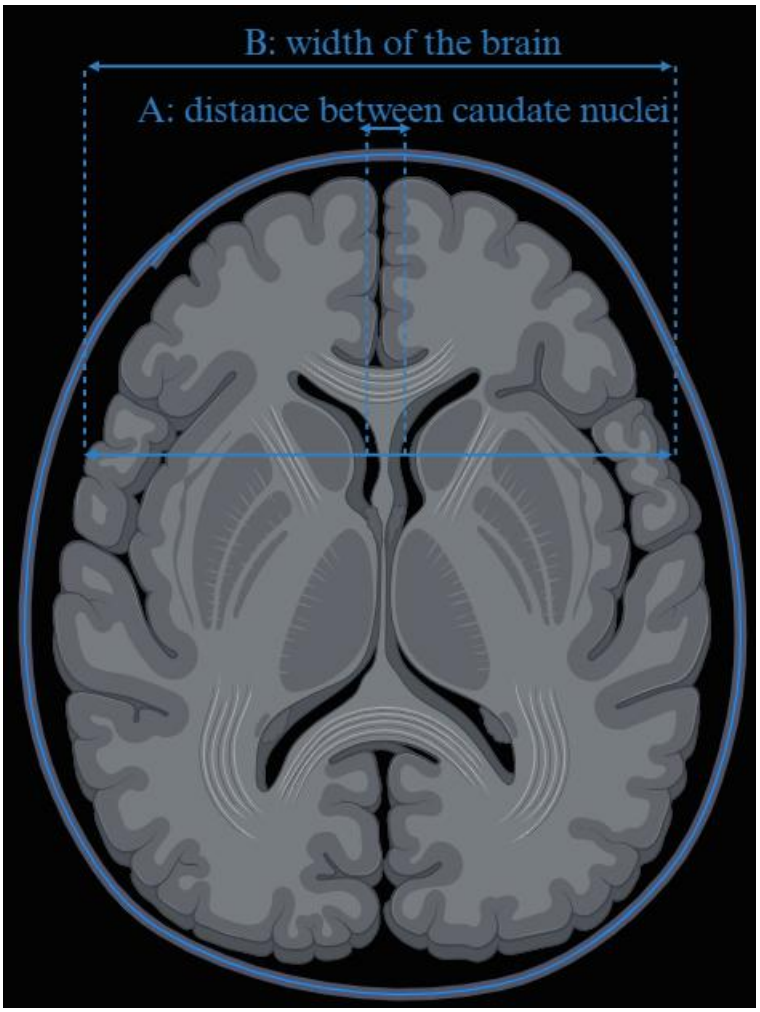


Figure 1.9 CT of brain to demonstrate how to calculate BCI: A is the distance between caudate nuclei, while B is the width of brain at same level (produced in BioRender)

The RBCI is the BCI divided by the upper limit of the normal ratio for a given age group, which increases with age. The upper limits (95% confidence value) for different age groups are: 0.16 for <30 years, 0.18 for 30-49 years, 0.19 for 50-59 years, 0.21 for 60-79 years, and 0.25 for >80 years. An RBCI greater than 1 suggests a high likelihood of hydrocephalus and supports the diagnosis. [66] Additionally, MRI can provide more detailed information about the dynamics of CSF, aiding in the determination of the diagnosis, cause, and pathophysiology of hydrocephalus.

However, use of MRI comes at the expense of higher costs, longer procedure times, and the potential need for sedation [67]

Treatment options for hydrocephalus include the insertion of an external ventricular drain (EVD), a ventriculoperitoneal shunt (VPS), and a lumbar drain. The choice of treatment depends on the patient's medical condition and the physician's judgment. EVD insertion is commonly used for acute hydrocephalus, regardless of its cause, and is associated with rapid neurological improvement. Despite the simplicity and popularity of EVDs, they can result in serious complications, such as infection and bleeding. The reported bleeding rate can reach up to 41%, and infection rates range between 3% to 32%. To mitigate these risks, the use of antimicrobial-impregnated catheters is recommended. [68].

Approximately 25% of patients with aneurysmal SAH who cannot be weaned off an EVD may require cerebrospinal fluid diversion to treat hydrocephalus. Even after successful weaning and EVD removal, some patients may develop delayed hydrocephalus, which can manifest up to six months after discharge. This condition typically requires treatment with a ventriculoperitoneal shunt (VPS), which can lead to complications such as infection, shunt malfunction, pseudocyst formation, and bowel perforation [69].

To reduce the risk of complications, such as bleeding caused by frequent replacement of EVD, a lumbar drain can be used. It is considered safer and simpler, resulting in prolonged extracorporeal CSF drainage with fewer side effects compared to EVD. This approach increases the likelihood of arachnoid recovery and the resumption of CSF reabsorption, potentially preventing the need for a VPS. However, lumbar drains should be avoided in coagulopathic patients and those with obstructive hydrocephalus, supratentorial mass, or intraparenchymal haematoma [70].

For minimally invasive treatment of hydrocephalus, the eShunt system has been developed to avoid the need for invasive surgery. In the eShunt system, neurosurgeons drain cerebrospinal fluid using a catheter inserted through a small puncture hole in the leg, reaching the brain via the venous system instead of navigating through the brain tissue. This novel treatment method is still undergoing clinical trials and is not yet widely employed, but it has the potential to significantly improve patient outcomes and substantially decrease the overall cost of surgical treatment. [71]

Timely prediction of hydrocephalus is crucial for reducing parenchymal damage following SAH. Independent risk factors for the development of hydrocephalus include poor clinical examination results, such as high Hunt and Hess scores, advanced age, aneurysm location, and the occurrence of re-bleeding. [63] Identifying these risk factors early can facilitate timely intervention to improve patient outcomes. Additionally, perimesencephalic non-aneurysmal SAH patients have been reported to

have a lower incidence of hydrocephalus compared to those with aneurysmal SAH, indicating a variation in risk based on the type of SAH. [71]

1.5.4 Other complications

The major complications of re-bleeding, vasospasm, DCI, and hydrocephalus significantly impact patient outcomes, leading to high rates of morbidity and mortality. Besides these, other complications of SAH can be categorised into neurological and non-neurological complications. Neurological complications include seizures and cognitive deficits, while non-neurological complications affect various systems or organs, such as cardiac, pulmonary, and renal complications, electrolyte disturbances, and haematologic abnormalities. These additional complications further complicate the clinical management of SAH patients and negatively affect their overall prognosis.

Seizures are clinically rare, occurring in only 1% to 7% of patients suffering from SAH, often representing occurrences of re-bleeding from unsecured aneurysms. These seizures typically manifest early, before any medical intervention, and can rapidly resolve after treatment. However, seizure-like abnormal movements occur in 26% of aneurysmal SAH patients, though it remains unclear whether these are true seizures or just post-ictal posturing. Risk factors associated with seizures after aneurysmal SAH include advanced age, aneurysms located in the middle cerebral artery, poor neurological grade, and thick subarachnoid clots. Optimal treatments and medications for post-SAH seizures are still under debate due to a lack of randomised clinical trials. [63] However, the Neurocritical Care Society (NCS) recommends a short course, but not routine use, of anticonvulsant prophylaxis, as well as continuous EEG monitoring in SAH patients with poor neurological grades [72].

Cardiac complications, including mild myocardial injury, neurogenic stunned myocardium (NSM), and arrhythmias, occur in approximately 50% of patients suffering from aneurysmal SAH. These cardiac complications can manifest through changes in biomarkers and physiological indices. For example, serum troponin levels are significant predictors of cardiac complications, such as left ventricular dysfunction, and should be closely monitored, especially in patients with a history of cardiovascular disease. Decreased left ventricular contractility and regional wall motion abnormalities indicate NSM. Arrhythmias, typically manifesting as ECG changes like ST segment and T wave alterations, are commonly seen in patients with severe neurological insults. These markers of cardiac damage are associated with increased mortality, DCI, and poor neurological outcomes [73].

Renal complications have been reported to occur in 0.8% to 7% of patients with SAH. The severity of acute renal failure is classified based on changes in serum creatinine and urine output, as proposed by the Acute Dialysis Quality Initiative (ADQI) group. The ADQI classifies renal failure into three risk classes with increasing severity: risk, injury, and failure, along with two outcome classes: loss and end-stage renal disease

(ESRD) [74].

Renal complications, particularly acute kidney injury (AKI), can arise from various factors, such as reduced blood flow to the kidneys due to hypotension, exposure to contrast agents during diagnostic tests, or the use of nephrotoxic medications. These complications are associated with increased morbidity and mortality, as well as poor neurological outcomes. AKI encompasses a spectrum of conditions from mild to severe, with reported incidence rates ranging from 2% to 67%, depending on the definition and severity criteria used. To manage renal complications after SAH, it is essential to closely monitor kidney function, maintain adequate hydration, and avoid nephrotoxic medications. In severe cases of AKI, renal replacement therapy, such as dialysis, may be necessary. Early detection and management of post-SAH renal complications can help improve outcomes and reduce the risk of long-term kidney damage [75].

Pulmonary complications are common in patients with aneurysmal SAH and are associated with higher risks of mortality, vasospasm, poor neurological outcomes, and longer hospital stays [76]. Some of the pulmonary complications that can occur after SAH include acute respiratory distress syndrome (ARDS), pneumonia, pulmonary embolism, atelectasis, and pleural effusion, typically peaking around day 7 after the initial haemorrhage. ARDS is the most frequent complication, with risk factors including age and the severity of the initial haemorrhage. Prevention and management strategies for these pulmonary complications may involve early mobilization, respiratory therapy, appropriate use of antibiotics, and prophylaxis for venous thromboembolism [77].

Patients with aneurysmal SAH often suffer from electrolyte disturbances, which can impact their prognosis. These disturbances include hyponatraemia (low sodium levels), hypernatraemia (high sodium levels), hypokalaemia (low potassium levels), hypocalcaemia (low calcium levels), and hypomagnesaemia (low magnesium levels). Among these, hyponatraemia is the most frequently observed electrolyte disturbance in patients with aneurysmal SAH. The specific treatment for electrolyte imbalances depends on the type and severity of the disturbance. Generally, the primary goal of management is to correct and maintain electrolyte levels within normal ranges. This may involve the administration of intravenous fluids and/or electrolyte replacement therapy [63].

Various haematological abnormalities are common in SAH patients, including anaemia (low red cell count), thrombocytopenia (low platelet count), and coagulopathy, a disorder affecting blood clotting. These haematological issues are associated with an increased risk of DCI, higher mortality rates, and poor neurological outcomes. Managing these abnormalities typically involves close monitoring of blood counts and clotting parameters, along with the administration of blood products such as red blood cells, platelets, and fresh frozen plasma as needed. [63]

Patients with spontaneous SAH can experience numerous complications, such as cerebral oedema, fever, and infections. Those patients with SAH caused by ruptured aneurysms are at a higher risk of developing complications compared to non-aneurysmal SAH patients. The complications following spontaneous SAH, along with their categories and subcategories, are listed in Figure 1.10.

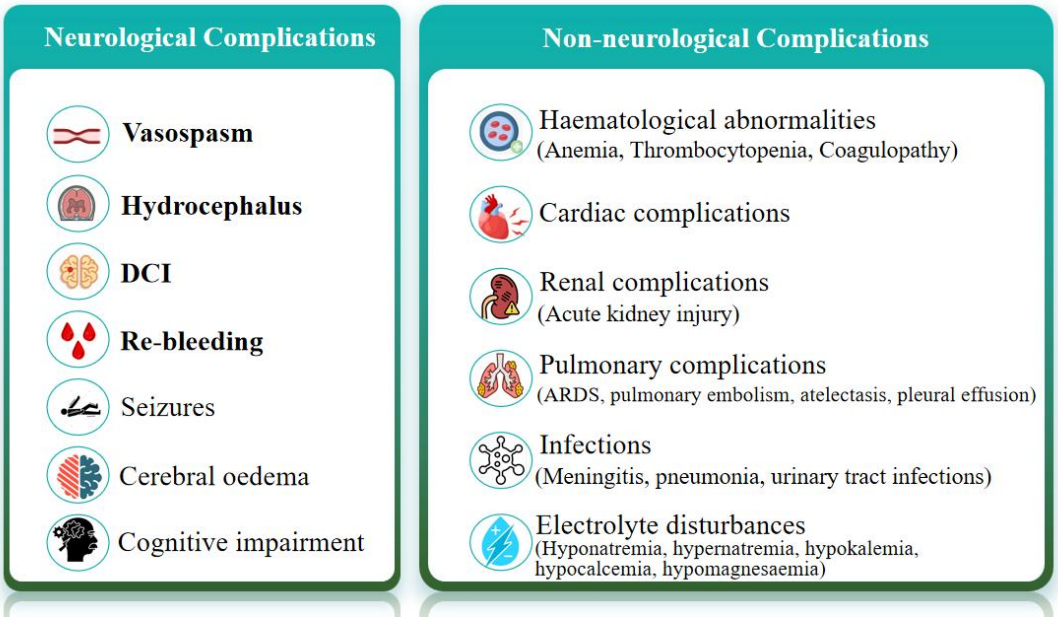


Figure 1.10 Complications after spontaneous SAH with major complications highlighted in bold.

1.6 Treatment of spontaneous SAH

In the previous sections of this chapter, we discussed treatment options for common complications. This section focuses on the treatment of spontaneous SAH, covering the stages from initial stabilisation and diagnosis to aneurysm repair, prevention of potential complications, and rehabilitation. Procedures for diagnosis and prevention of complications have been detailed previously and will not be repeated here. It is important to note that the treatment choices and procedures differ for aneurysmal SAH and non-aneurysmal SAH.

1.6.1 Stabilisation

The first step in stabilisation is to ensure a clear airway for adequate breathing. If needed, oxygen therapy can be used to improve oxygenation. Patients with spontaneous SAH are also at risk of developing hypotension and shock, which can be life-threatening. Haemodynamic support may be initiated to maintain adequate blood pressure and perfusion to vital organs. In addition to managing blood pressure and airway, pain management is crucial, primarily for controlling headaches and

postoperative craniotomy pain. For pain relief, opioids are often used despite their side effects, such as vomiting, haemodynamic instability, and respiratory depression [78].

1.6.2 Neurosurgical intervention

After spontaneous SAH has been diagnosed, whether from aneurysmal or non-aneurysmal causes, neurosurgical intervention may be necessary for some patients to treat the sources of bleeding, such as aneurysms or AVMs. One surgical procedure for treating aneurysms is clipping, where a small clip is placed across the base of the aneurysm, effectively separating it from the parent artery.

Coiling is a more recent treatment method for intracranial aneurysms. In this procedure, a small catheter is inserted into an artery in the groin and threaded up to the aneurysm. Tiny coils are then inserted through the catheter into the aneurysm, causing it to clot, a process known as embolisation, thereby preventing further bleeding [79]. When comparing these two techniques, the occlusion rate is a valuable parameter. A retrospective single-centre study involving 92 patients with middle cerebral artery (MCA) aneurysms reported a complete occlusion rate of 96.3% after clipping and 78.9% after coiling [80]. Despite the higher occlusion rate and long-term effectiveness of clipping, coiling is preferred for its minimally invasive nature, shorter hospital stays, and suitability for patients who are at higher surgical risk due to advanced age or comorbidities.

The treatment of non-aneurysmal SAH is complex and necessitates a thorough evaluation by clinicians with knowledge of various cerebrovascular diseases. The decision to perform a neurosurgical intervention depends on the individual patient's condition, the underlying cause of the SAH, and the location of the bleeding. For AVMs, endovascular embolisation is a commonly used minimally invasive procedure. In this approach, a catheter is inserted into the artery feeding the AVM, and a substance is injected to block off the blood flow to the AVM. [81] Additionally, in cases where there is excess CSF causing increased intracranial pressure, a shunt may be placed to drain the fluid, thereby reducing pressure in the brain.

1.6.3 Rehabilitation

Rehabilitation is an important aspect of treating spontaneous SAH, targeted at maximising the patient's recovery and enhancing their quality of life. The rehabilitation process typically begins during the acute phase of SAH and may extend for several weeks or even months after the initial event. Common rehabilitation interventions for spontaneous SAH include physical, occupational, and speech therapies, as well as cognitive rehabilitation and psychological support.

Physical therapy helps patients regain strength, mobility, and balance through

exercises designed to strengthen muscles, improve coordination, and increase endurance. Occupational therapy assists patients in regaining their ability to perform daily activities such as dressing and eating. Speech therapy addresses difficulties in speaking, swallowing, or understanding language, with exercises tailored to improve these skills. [82]

Cognitive rehabilitation is a critical component of SAH recovery, aimed at restoring cognitive functions such as memory, attention, and executive function. Recovery times vary across different cognitive domains, with verbal memory often requiring the longest period to recover. [83] Psychological support is also important for SAH patients, who frequently experience emotional and psychological changes following the event. Psychological interventions have been found to effectively reduce symptoms of anxiety and depression and improve overall survival rates for SAH patients. These comprehensive rehabilitation strategies are designed to help patients achieve the best possible outcomes and improve their overall well-being. [84]

1.7 Summary

This chapter discusses various aspects of spontaneous SAH. It begins by providing essential background knowledge of the human brain to facilitate understanding. SAH is categorised into traumatic and spontaneous types, with the latter further divided into aneurysmal and non-aneurysmal sub-types. The epidemiology of spontaneous SAH is examined, detailing its incidence, prevalence, fatality rates, and associated risk factors. Following this, the chapter reviews different diagnostic modalities for spontaneous SAH with illustrations, including CT/CTA, LP, MRI, and DSA, discussing the suitability of each method. The chapter also presents the diagram of recommended uses of diagnosis methods.

Next, the chapter delves into the complications of spontaneous SAH, highlighting four major complications: re-bleeding, vasospasm, DCI, and hydrocephalus. It also covers other neurological and non-neurological complications, including cardiac, pulmonary, and renal complications, electrolyte disturbances, and haematologic abnormalities. Finally, the chapter covers various treatment procedures, ranging from initial stabilisation and neurosurgical interventions to rehabilitation, which are aimed at maximising recovery and improving patient outcomes.

Reference for chapter 1

[1] Organes - Système Nerveux Central (cerveau) (2017) Laurine Moreau Illustratrice & Graphiste Available at: http://laurinemoreau.com/ressource-images/systeme-nerveux-central-cerveau-organes (Accessed: 24 May 2023).

[2] Cerebral arteries (2023) Wikipedia. Available at: https://en.wikipedia.org/wiki/Cerebral_arteries (Accessed: 24 May 2023).

[3] Maagaard, M., Karlsson, W.K., Ovesen, C., Gluud, C. and Jakobsen, J.C., 2021. Interventions for altering blood pressure in people with acute subarachnoid haemorrhage. Cochrane Database of Systematic Reviews, (11).

[4] Modi, N.J., Agrawal, M. and Sinha, V.D., 2016. Post-traumatic subarachnoid hemorrhage: A review. Neurology India, 64(Suppl 1), pp.S8-S13.

[5] Durango-Espinosa, Y., Moscote-Salazar, L., Keni, R., Deora, H. and Agrawal, A., 2019. The puzzle of spontaneous versus traumatic subarachnoid hemorrhage. Apollo Medicine, 16(3), pp.141-141.

[6] Maher, M., Schweizer, T.A. and Macdonald, R.L., 2020. Treatment of spontaneous subarachnoid hemorrhage: guidelines and gaps. Stroke, 51(4), pp.1326-1332.

[7] Van Gijn, J., Kerr, R.S. and Rinkel, G.J., 2007. Subarachnoid haemorrhage. The Lancet, 369(9558), pp.306-318.

[8] Konczalla, J., Platz, J., Schuss, P., Vatter, H., Seifert, V. and Güresir, E., 2014. Non-aneurysmal non-traumatic subarachnoid hemorrhage: patient characteristics, clinical outcome and prognostic factors based on a single-center experience in 125 patients. BMC neurology, 14(1), pp.1-8.

[9] Wolfe, C.D.A., Rudd, A.G., Howard, R., Coshall, C., Stewart, J., Lawrence, E., Hajat, C. and Hillen, T., 2002. Incidence and case fatality rates of stroke subtypes in a multiethnic population: the South London Stroke Register. Journal of Neurology, Neurosurgery & Psychiatry, 72(2), pp.211-216.

[10] de Rooij, N.K., Linn, F.H., van der Plas, J.A., Algra, A. and Rinkel, G.J., 2007. Incidence of subarachnoid haemorrhage: a systematic review with emphasis on region, age, gender and time trends. Journal of Neurology, Neurosurgery & Psychiatry, 78(12), pp.1365-1372.

[11] Ingall, T., Asplund, K., Mähönen, M. and Bonita, R., 2000. A multinational comparison of subarachnoid hemorrhage epidemiology in the WHO MONICA stroke study. Stroke, 31(5), pp.1054-1061.

[12] Qureshi, A.I., Malik, A.A., Saeed, O., Defillo, A., Sherr, G.T. and Suri, M.F.K., 2016. Hormone replacement therapy and the risk of subarachnoid hemorrhage in postmenopausal women. Journal of neurosurgery, 124(1), pp.45-50.

[13] Singer, R.J., Ogilvy, C.S., Rordorf, G., Biller, J. and Dashe, F., 2013. Aneurysmal subarachnoid hemorrhage: Epidemiology, risk factors, and pathogenesis. U: UpToDate, Post TW ur. UpToDate [Internet]. Waltham, MA: UpToDate.

[14] Xia, C., Hoffman, H., Anikpezie, N., Philip, K., Wee, C., Choudhry, R., Albright, K.C., Masoud, H., Beutler, T., Schmidt, E. and Gould, G., 2023. Trends in the Incidence of Spontaneous Subarachnoid Hemorrhages in the United States, 2007–2017. Neurology, 100(2), pp.e123-e132.

[15] Neurology Branch of Chinese Medical Association, Cerebrovascular Disease Group of Neurology Branch of Chinese Medical Association. Guidelines for Diagnosis and Treatment of Subarachnoid Hemorrhage in China 2015 [J]. Chinese Journal of Neurology, 2016,49 (3): 182-191. DOI: 10.3760/cma.j.issn.1006-7876.2016.03.003

[16] Steiner, T., Juvela, S., Unterberg, A., Jung, C., Forsting, M. and Rinkel, G., 2013. European Stroke Organization guidelines for the management of intracranial aneurysms and subarachnoid haemorrhage. Cerebrovascular diseases, 35(2), pp.93-112.

[17] Spontaneous subarachnoid hemorrhage (2023) Relias Media | Online Continuing Medical Education | Relias Media - Continuing Medical Education Publishing. Available at: https://www.reliasmedia.com/articles/spontaneous-subarachnoid-hemorrhage (Accessed: January 24, 2023).

[18] Mackey, J., Khoury, J.C., Alwell, K., Moomaw, C.J., Kissela, B.M., Flaherty, M.L., Adeoye, O., Woo, D., Ferioli, S., La Rosa, F.D.L.R. and Martini, S., 2016. Stable incidence but declining case-fatality rates of subarachnoid hemorrhage in a population. Neurology, 87(21), pp.2192-2197.

[19] Farhat, H.I., 2011. Cerebral arteriovenous malformations. Disease-a-Month, 57(10), pp.625-637.

[20] Kojima, M., Nagasawa, S., Lee, Y.E., Takeichi, Y., Tsuda, E. and Mabuchi, N., 1998. Asymptomatic familial cerebral aneurysms. Neurosurgery, 43(4), pp.776-781.

[21] Chang, T.R., Kowalski, R.G., Caserta, F., Carhuapoma, J.R., Tamargo, R.J. and Naval, N.S., 2013. Impact of acute cocaine use on aneurysmal subarachnoid hemorrhage. Stroke, 44(7), pp.1825-1829.

[22] Broderick, J.P., Viscoli, C.M., Brott, T., Kernan, W.N., Brass, L.M., Feldmann, E., Morgenstern, L.B., Wilterdink, J.L. and Horwitz, R.I., 2003. Major risk factors for aneurysmal subarachnoid hemorrhage in the young are modifiable. Stroke, 34(6), pp.1375-1381.

[23] Brain AVM (arteriovenous malformation) (2022) Mayo Clinic. Mayo Foundation for Medical Education and Research. Available at: https://www.mayoclinic.org/diseases-conditions/brain-avm/symptoms-causes/syc-20350260 (Accessed: January 25, 2023).

[24] Pollock, B.E., Flickinger, J.C., Lunsford, L.D., Bissonette, D.J. and Kondziolka, D., 1996. Factors that predict the bleeding risk of cerebral arteriovenous malformations. Stroke, 27(1), pp.1-6.

[25] Juvela, S., Hillbom, M., Numminen, H. and Koskinen, P., 1993. Cigarette smoking and alcohol consumption as risk factors for aneurysmal subarachnoid hemorrhage. Stroke, 24(5), pp.639-646.

[26] Longstreth Jr, W.T., Nelson, L.M., Koepsell, T.D. and Van Belle, G., 1992. Cigarette smoking, alcohol use, and subarachnoid hemorrhage. Stroke, 23(9), pp.1242-1249.

[27] Ruigrok, Y.M., Buskens, E. and Rinkel, G.J., 2001. Attributable risk of common and rare determinants of subarachnoid hemorrhage. Stroke, 32(5), pp.1173-1175.

[28] Feigin, V.L., Rinkel, G.J., Lawes, C.M., Algra, A., Bennett, D.A., van Gijn, J. and Anderson, C.S., 2005. Risk factors for subarachnoid hemorrhage: an updated systematic review of epidemiological studies. Stroke, 36(12), pp.2773-2780.

[29] Bonita, R., 1986. Cigarette smoking, hypertension and the risk of subarachnoid hemorrhage: a population-based case-control study. Stroke, 17(5), pp.831-835.

[30] Perry, J.J., Stiell, I.G., Sivilotti, M.L., Bullard, M.J., Émond, M., Symington, C., Sutherland, J., Worster, A., Hohl, C., Lee, J.S. and Eisenhauer, M.A., 2011. Sensitivity of computed tomography performed within six hours of onset of headache for diagnosis of subarachnoid haemorrhage: prospective cohort study. Bmj, 343.

[31] Tibor Becske, M.D. (2021) Subarachnoid hemorrhage workup, Approach Considerations, Computed Tomography, Lumbar Puncture. Medscape. Available at: https://emedicine.medscape.com/article/1164341-workup#:~:text=CT%20without%20contrast%20is%20the,and%2050%25%20at%201%20week. (Accessed: January 27, 2023).

[32] Dr Graham Lloyd-Jones BA MBBS MRCP FRCR - Consultant Radiologist - CT Brain Image Gallery, Welcome to Radiology Masterclass. Available at: https://www.radiologymasterclass.co.uk/gallery/ct_brain/ct_brain_images/subarachnoid_haemorrhage_sah_ct_brain#top_1st_img (Accessed: 08 July 2024).

[33] Boesiger, B.M. and Shiber, J.R., 2005. Subarachnoid hemorrhage diagnosis by computed tomography and lumbar puncture: are fifth generation CT scanners better at identifying subarachnoid hemorrhage?. The Journal of emergency medicine, 29(1), pp.23-27.

[34] Gottlieb, M. and Morgenstern, J., 2021. Lumbar Puncture Should Not Be Routinely Performed For Subarachnoid Hemorrhage After A Negative Head Ct. Annals of Emergency Medicine, 77(6), pp.643-645.

[35] Sohn, C.H., Baik, S.K., Lee, H.J., Lee, S.M., Kim, I.M., Yim, M.B., Hwang, J.S., Lauzon, M.L. and Sevick, R.J., 2005. MR imaging of hyperacute subarachnoid and intraventricular hemorrhage at 3T: a preliminary report of gradient echo T2*-weighted

sequences. American journal of neuroradiology, 26(3), pp.662-665.

[36] Mitchell, P., Wilkinson, I.D., Hoggard, N., Paley, M.N.J., Jellinek, D.A., Powell, T., Romanowski, C., Hodgson, T. and Griffiths, P.D., 2001. Detection of subarachnoid haemorrhage with magnetic resonance imaging. Journal of Neurology, Neurosurgery & Psychiatry, 70(2), pp.205-211.

[37] Bhuva, A.N., Feuchter, P., Hawkins, A., Cash, L., Boubertakh, R., Evanson, J., Schilling, R., Lowe, M., Moon, J.C. and Manisty, C.H., 2019. MRI for patients with cardiac implantable electronic devices: simplifying complexity with a 'one-stop'service model. BMJ quality & safety, 28(10), pp.853-858.

[38] Heit, J.J., Pastena, G.T., Nogueira, R.G., Yoo, A.J., Leslie-Mazwi, T.M., Hirsch, J.A. and Rabinov, J.D., 2016. Cerebral angiography for evaluation of patients with CT angiogram-negative subarachnoid hemorrhage: an 11-year experience. American Journal of Neuroradiology, 37(2), pp.297-304.

[39] Madhusudhan, K.S., Venkatesh, H.A., Gamanagatti, S., Garg, P. and Srivastava, D.N., 2016. Interventional radiology in the management of visceral artery pseudoaneurysms: a review of techniques and embolic materials. Korean journal of radiology, 17(3), pp.351-363.

[40] Muehlschlegel, S., 2018. Subarachnoid hemorrhage. Continuum: Lifelong Learning in Neurology, 24(6), pp.1623-1657.

[41] Nam, H.H., Jang, D.K. and Cho, B.R., 2022. Complications and risk factors after digital subtraction angiography: 1-year single-center study. Journal of Cerebrovascular and Endovascular Neurosurgery, 24(4), pp.335-340.

[42] Guideline NG228, N.I.C.E., 2022. Subarachnoid haemorrhage caused by a ruptured aneurysm: diagnosis and management. Methods.

[43] Zuerrer, M., Martin, E. and Boltshauser, E., 1991. MR imaging of intracranial hemorrhage in neonates and infants at 2.35 Tesla. Neuroradiology, 33, pp.223-229.

[44] Tanaka, A., Yoshinaga, S., Nakayama, Y. and Tomonaga, M., 1998. Cerebral blood flow and the response to acetazolamide during the acute, subacute, and chronic stages of aneurysmal subarachnoid hemorrhage. Neurologia medico-chirurgica, 38(10), pp.623-632.

[45] Fragata, I., Canto-Moreira, N. and Canhão, P., 2019. Ischemic lesions in acute and subacute perimesencephalic subarachnoid hemorrhage. American Journal of Roentgenology, 212(2), pp.418-424.

[46] de Oliveira Manoel, A.L., Goffi, A., Marotta, T.R., Schweizer, T.A., Abrahamson, S. and Macdonald, R.L., 2016. The critical care management of poor-grade subarachnoid haemorrhage. Critical care, 20, pp.1-19.

[47] Greebe, P. and Rinkel, G.J., 2007. Life expectancy after perimesencephalic subarachnoid hemorrhage. Stroke, 38(4), pp.1222-1224.

[48] Priebe, H.J., 2007. Aneurysmal subarachnoid haemorrhage and the anaesthetist. British journal of anaesthesia, 99(1), pp.102-118.

[49] Greenberg, S.M., Ziai, W.C., Cordonnier, C., Dowlatshahi, D., Francis, B., Goldstein, J.N., Hemphill III, J.C., Johnson, R., Keigher, K.M., Mack, W.J. and Mocco, J., 2022. 2022 guideline for the management of patients with spontaneous intracerebral hemorrhage: a guideline from the American Heart Association/American Stroke Association. Stroke, 53(7), pp.e282-e361.

[50] Lim, Y.C., Kim, C.H., Kim, Y.B., Joo, J.Y., Shin, Y.S. and Chung, J., 2015. Incidence and risk factors for rebleeding during cerebral angiography for ruptured intracranial aneurysms. Yonsei medical journal, 56(2), pp.403-409.

[51] SAMPEI, T., YASUI, N., MIZUNO, M., NAKAJIMA, S., ISHIKAWA, T., HADEISHI, H. and SUZUKI, A., 1990. Contrast Medium Extravasation During Cerebral Angiography for Ruptured Intracranial Aneurysm—Clinical Analysis of 26 Cases—. Neurologia medico-chirurgica, 30(13), pp.1011-1015.

[52] Steiner, T., Juvela, S., Unterberg, A., Jung, C., Forsting, M. and Rinkel, G., 2013. European Stroke Organization guidelines for the management of intracranial aneurysms and subarachnoid haemorrhage. Cerebrovascular diseases, 35(2), pp.93-112.

[53] Guo, L.M., Zhou, H.Y., Xu, J.W., Wang, Y., Qiu, Y.M. and Jiang, J.Y., 2011. Risk factors related to aneurysmal rebleeding. World neurosurgery, 76(3-4), pp.292-298.

[54] Connolly Jr, E.S., Rabinstein, A.A., Carhuapoma, J.R., Derdeyn, C.P., Dion, J., Higashida, R.T., Hoh, B.L., Kirkness, C.J., Naidech, A.M., Ogilvy, C.S. and Patel, A.B., 2012. Guidelines for the management of aneurysmal subarachnoid hemorrhage: a guideline for healthcare professionals from the American Heart Association/American Stroke Association. Stroke, 43(6), pp.1711-1737.

[55] Phillips, T.J., Dowling, R.J., Yan, B., Laidlaw, J.D. and Mitchell, P.J., 2011. Does treatment of ruptured intracranial aneurysms within 24 hours improve clinical outcome?. Stroke, 42(7), pp.1936-1945.

[56] Fonseca, A.C., Merwick, A., Dennis, M., Ferrari, J., Ferro, J.M., Kelly, P., Lal, A., Ois, A., Olivot, J.M. and Purroy, F., 2021. European Stroke Organisation (ESO) guidelines on management of transient ischaemic attack. European Stroke Journal, 6(2), pp.CLXIII-CLXXXVI.

[57] Psychogios, K., Tsivgoulis, G. and FESO, F., 2019. Subarachnoid hemorrhage, vasospasm, and delayed cerebral ischemia. Pract Neurol, 9, pp.37-41.

[58] Vergouwen, M.D., Vermeulen, M., van Gijn, J., Rinkel, G.J., Wijdicks, E.F., Muizelaar, J.P., Mendelow, A.D., Juvela, S., Yonas, H., Terbrugge, K.G. and Macdonald, R.L., 2010. Definition of delayed cerebral ischemia after aneurysmal subarachnoid hemorrhage as an outcome event in clinical trials and observational studies: proposal of a multidisciplinary research group. Stroke, 41(10), pp.2391-2395.

[59] Westermaier, T., Pham, M., Stetter, C., Willner, N., Solymosi, L., Ernestus, R.I., Vince, G.H. and Kunze, E., 2014. Value of transcranial Doppler, perfusion-CT and neurological evaluation to forecast secondary ischemia after aneurysmal SAH. Neurocritical care, 20, pp.406-412.

[60] Samagh, N., Bhagat, H. and Jangra, K., 2019. Monitoring cerebral vasospasm: How much can we rely on transcranial Doppler. Journal of anaesthesiology, clinical pharmacology, 35(1), p.12.

[61] Dumont, A.S., Dumont, R.J., Chow, M.M., Lin, C.L., Calisaneller, T., Ley, K.F., Kassell, N.F. and Lee, K.S., 2003. Cerebral vasospasm after subarachnoid hemorrhage: putative role of inflammation. Neurosurgery, 53(1), pp.123-135.

[62] Pyne-Geithman, G.J., Caudell, D.N., Prakash, P. and Clark, J.F., 2009. Glutathione peroxidase and subarachnoid hemorrhage: implications for the role of oxidative stress in cerebral vasospasm. Neurological research, 31(2), pp.195-199.

[63] Ganaw, A.E.A., Ahmed, S.M.G., Ehfeda, M. and Belkhair, S., 2022. Complications and Critical Care Management of Aneurysmal Subarachnoid Hemorrhage. Management of Subarachnoid Hemorrhage, pp.139-165.

[64] Woodford, H., Taylor, M., Eftekhar, B., Waugh, R. and Chaganti, J., 2022. Dual intra-arterial vasodilators in the management of post-aneurysmal subarachnoid haemorrhage vasospasm. Interdisciplinary Neurosurgery, 27, p.101442.

[65] Francoeur, C.L. and Mayer, S.A., 2016. Management of delayed cerebral ischemia after subarachnoid hemorrhage. Critical care, 20, pp.1-12.

[66] van Gijn, J., Hijdra, A., Wijdicks, E.F., Vermeulen, M. and van Crevel, H., 1985. Acute hydrocephalus after aneurysmal subarachnoid hemorrhage. Journal of neurosurgery, 63(3), pp.355-362.

[67] Kartal, M.G. and Algin, O., 2014. Evaluation of hydrocephalus and other cerebrospinal fluid disorders with MRI: An update. Insights into imaging, 5(4), pp.531-541.

[68] Chung, D.Y., Mayer, S.A. and Rordorf, G.A., 2018. External ventricular drains after subarachnoid hemorrhage: is less more?. Neurocritical care, 28, pp.157-161.

[69] Fried, H.I., Nathan, B.R., Rowe, A.S., Zabramski, J.M., Andaluz, N., Bhimraj, A., Guanci, M.M., Seder, D.B. and Singh, J.M., 2016. The insertion and management of external ventricular drains: an evidence-based consensus statement: a statement for healthcare professionals from the Neurocritical Care Society. Neurocritical care, 24, pp.61-81.

[70] Huttner, H.B., Nagel, S., Tognoni, E., Köhrmann, M., Jüttler, E., Orakcioglu, B., Schellinger, P.D., Schwab, S. and Bardutzky, J., 2007. Intracerebral hemorrhage with severe ventricular involvement: lumbar drainage for communicating hydrocephalus. Stroke, 38(1), pp.183-187.

[71] Hou, K. and Yu, J., 2022. Current status of perimesencephalic non-aneurysmal

subarachnoid hemorrhage. Frontiers in Neurology, 13.

[72] Diringer, M.N., Bleck, T.P., Claude Hemphill, J.I.I.I., Menon, D., Shutter, L., Vespa, P., Bruder, N., Connolly, E.S., Citerio, G., Gress, D. and Hänggi, D., 2011. Critical care management of patients following aneurysmal subarachnoid hemorrhage: recommendations from the Neurocritical Care Society's Multidisciplinary Consensus Conference. Neurocritical care, 15, pp.211-240.

[73] Behrouz, R., Sullebarger, J.T. and Malek, A.R., 2011. Cardiac manifestations of subarachnoid hemorrhage. Expert Review of Cardiovascular Therapy, 9(3), pp.303-307.

[74] Zacharia, B.E., Ducruet, A.F., Hickman, Z.L., Grobelny, B.T., Fernandez, L., Schmidt, J.M., Narula, R., Ko, L.N., Cohen, M.E., Mayer, S.A. and Connolly Jr, E.S., 2009. Renal dysfunction as an independent predictor of outcome after aneurysmal subarachnoid hemorrhage: a single-center cohort study. Stroke, 40(7), pp.2375-2381.

[75] Gupta, A., Pervez, H., & Sohail, M. R. 2017. Renal complications in patients with subarachnoid hemorrhage. Journal of the neurological sciences, 379, 43-48.

[76] Shrestha, G.S., 2017. Lung maladies following aneurysmal subarachnoid haemorrhage. Journal of Neuroanaesthesiology and Critical Care, 4(04), pp.S45-S48.

[77] Kramer, A. H., Gurka, M. J., Nathan, B., Dumont, A. S., Kassell, N. F., & Bleck, T. P. (2010). Pulmonary complications after subarachnoid hemorrhage: time course and predictors of poor clinical outcome. Neurocritical Care, 12(1), 25-31.

[78] Bernardini, G.L. and Brust, J.C., 2021. Pain Control in Aneurysmal Subarachnoid Hemorrhage Patients in the ICU: Can We Avoid Contributing to the Opioid Crisis?. Neurology, 96(19), pp.873-874.

[79] Raftopoulos, C., 2005. Is surgical clipping becoming underused?. Acta Neurochirurgica, 147, pp.117-124.

[80] Schwartz, C., Aster, H.C., Al-Schameri, R., Müller-Thies-Broussalis, E., Griessenauer, C.J. and Killer-Oberpfalzer, M., 2018. Microsurgical clipping and endovascular treatment of middle cerebral artery aneurysms in an interdisciplinary treatment concept: comparison of long-term results. Interventional Neuroradiology, 24(6), pp.608-614.

[81] Case, D., Kumpe, D., Cava, L., Neumann, R., White, A., Roark, C. and Seinfeld, J., 2017. Ruptured distal posterior inferior cerebellar artery (PICA) aneurysms associated with cerebellar arterial venous malformations (AVMs): a case series and review of the literature demonstrating the need for angiographic evaluation and feasibility of endovascular treatment. World neurosurgery, 97, pp.751-e7.

[82] Karic, T., Sorteberg, A., Haug Nordenmark, T., Becker, F. and Roe, C., 2015. Early rehabilitation in patients with acute aneurysmal subarachnoid hemorrhage. Disability and Rehabilitation, 37(16), pp.1446-1454.

[83] Haug, T., Sorteberg, A., Sorteberg, W., Lindegaard, K.F., Lundar, T. and Finset,

A., 2007. Cognitive outcome after aneurysmal subarachnoid hemorrhage: time course of recovery and relationship to clinical, radiological, and management parameters. Neurosurgery, 60(4), pp.649-657.

[84] Noble, A.J. and Schenk, T., 2014. Psychological distress after subarachnoid hemorrhage: Patient support groups can help us better detect it. Journal of the Neurological Sciences, 343(1-2), pp.125-131.

Chapter 2 Understanding prognosis in spontaneous SAH

Prognosis refers to the prediction of the likely course and outcomes of a disease. This includes estimating the chances of improvement, or deterioration, assessing the potential for developing complications, determining survival likelihood, and evaluating the expected quality of life. Prognostic predictions are made based on a comprehensive understanding of the diagnosed disease and individualised prognostic factors. These factors include medical conditions present at the time of admission, results from clinical examinations, and various physiological indices. Prognosis is a crucial component of clinical decision-making, alongside diagnosis and treatment.

Prognosis plays a crucial role in healthcare by assessing the risks of complications and poor outcomes, thus helping clinicians optimise treatment strategies for better disease management. For spontaneous SAH patients, accurate prognosis is particularly important due to the high rates of mortality and morbidity associated with this condition. In post-SAH management, early prognostication upon admission guides timely and effective interventions, while continuous dynamic prognostication during critical care management helps identify risks, prevent potential complications, and improve survival outcomes. Prognostic modelling, as a tool for prognosis, provides a structured method for prognostication by incorporating multiple covariates and ultilising sophisticated algorithms.

This chapter provides an in-depth review of advancements in prognostic modeling for spontaneous SAH, starting with an introduction to the concept of prognosis and its critical role in patient management. It traces the evolution of prognostic models from early experience-based approaches to modern evidence-based and dynamic models, highlighting key milestones and influential studies. The chapter then delves into the statistical tools and techniques essential for constructing prognostic models, evaluating each tool's applicability, strengths, and limitations.

The final section reviews prognostic factors associated with poor outcomes in SAH, focusing on the four major complications: re-bleeding, vasospasm and DCI, hydrocephalus, and other neurological and non-neurological complications. It also examines factors contributing to poor neurological outcomes and mortality, synthesising findings from significant studies. These factors potentially contribute to developing a comprehensive prognostic framework and model for SAH. Overall, this chapter lays the foundation for developing personalised and dynamic prognostic models, that aims to enhance predictive accuracy and improve post-SAH management.

2.1 Historical evolution of prognosis

2.1.1 From experience-based to evidence-based prognosis

The transition from experience-based to evidence-based prognosis represents a significant evolution in clinical practice. Traditionally, clinicians have relied on their past experiences with previous patients to predict the future outcomes of newly admitted patients. This method involves recalling symptoms and characteristics of initial patient states and matching them to outcomes observed in the past. Clinicians subjectively decide which features are indicative of specific outcomes, forming the basis of their prognostic decisions. For example, in ancient Greece, Hippocrates emphasised observing patterns in symptoms like fever and sweats to predict disease outcomes.

The development of randomised controlled trials (RCTs) and the rise of evidence-based medicine (EBM) are crucial milestones for the transition to evidence-based prognosis. Modern RCTs, proposed by Austin Bradford Hill in the 1940s, offer a rigorous method for assessing the effects of treatments. RCTs, together with other epidemiological studies, have also been instrumental in identifying and quantifying the influences of prognostic factors on outcomes.

The emergence of EBM in the late 20th century significantly advanced the field of evidence-based prognosis. EBM emphasises integrating individual clinical expertise with the best available external evidence from systematic research. This approach provides a comprehensive understanding of how various prognostic factors influence outcomes. [1] Additionally, EBM includes grading scales to assess the quality of evidence, thereby determining the reliability of prognostic factors in predicting specific outcomes within prognosis studies.

Historically, the prognosis of SAH relied on clinical experience and subjective judgment. For example, in the early 20th century, clinicians noted that older patients often had poor outcomes. This empirical observation would lead to a general prognosis that such patients were at high risk of mortality, as detailed in early medical literature. [2] In contrast, complementary evidence-based prognosis for SAH relies on prospective and retrospective cohort studies to analyse the effects of various factors on patient outcomes. Studies have shown that factors such as age, severity of the initial hemorrhage, and pre-existing comorbidities significantly influence outcomes. For instance, patients over the age of 60 have a higher mortality risk compared to younger patients ($p=0.0257$, $HR=1.399$). [3] With this evidence, prognosis can be made statistically to predict the expected outcomes of patients, e.g., the expected likelihood of survival within a month, with confidence intervals.

Evidence-based prognosis refers to using scientific evidence from research studies and clinical trials to make predictions about a patient's prognosis, whereas experience-based prognosis relies on the clinician's own experience and intuition. Evidence-based prognosis offers advantages over experience-based prognosis mainly in terms of objectivity, accuracy, consistency, and transparency, since evidence-based

prognosis relies on objective scientific evidence, uses large amounts of data from multiple sources, and provides consistent predictions across different clinicians and settings. While on the contrary, experience-based prognosis can be influenced by personal biases and beliefs, leading to inaccuracies and inconsistencies in the quality of care, and may lack transparency in the clinician's reasoning and judgment.

2.1.2 From generalised to personalised prognosis

Generalised prognosis refers to the expected outcome or course of a medical condition or disease for a large group of people sharing similar characteristics, such as age, gender, and medical history, based on statistical data and research studies. It provides information about the overall likelihood of recovery, recurrence, or complications for this group of patients. Generalised prognosis typically focuses on the effect of single prognostic factors within the group, which limits its ability to accurately and comprehensively predict outcomes for individuals who may have unique combinations of multiple influencing factors.

In the context of post-SAH management, the Hunt and Hess scale, proposed in 1960s, is commonly used to generally classify the severity of SAH based on patient's clinical findings. [3] According to the Hunt and Hess scale, a generalised prognosis can be made:

- **Grade *I* and *II*:** Alert and minimal symptoms, high likelihood with good recovery with appropriate treatment.
- **Grade *III* and *IV*:** More significant symptoms like confusion or neurological deficits, moderate to high risk of complications and poorer outcomes.
- **Grade *V*:** Coma or near coma state with severe neurological impairment, a very poor prognosis with high likelihood of severe disability or death.

While general prognostication using the Hunt and Hess scale stratifies patients by symptoms and associated risks, providing useful information for managing different risk groups, it does not account for individual variances within each group. These within-group variances can be attributed to various factors, including underlying health conditions, the presence of comorbidities, complications occurred during hospital, and genetic factors. Consequently, two patients classified under the same Hunt and Hess scale might have significantly different outcomes due to these individual prognostic factors. This limitation underscores the need for more personalised prognostic tools that can integrate a wider range of patient-specific prognostic data for more comprehensive prognostication and more accurate outcome predictions.

Several grading systems have been proposed to integrate a wider range of prognostic factors, thereby enhancing personalised prognosis. The World Federation of Neurological Surgeons (WFNS) grading system, proposed in 1988, enhances the personalised prognosis by integrating the Glasgow Coma Scale (GCS) score with the presence of focal neurological deficits. [4] The FRESH score, which stands for the

functional recovery after subarachnoid haemorrhage, represents a further advancement in personalised by incorporating a wider range of factors. This FRESH score incorporates initial severity of SAH, GCS score, demographic factors, radiological factors, pre-existing conditions, type and timing of neurological intervention. [5] By considering these diverse factors, the FRESH score offers more comprehensive assessment for personalised prognosis.

The progression from the Hunt and Hess scale to the WFNS grading system, and subsequently to the FRESH score, marks a significant evolution towards personalised prognosis in the management of SAH. This progression has been further enhanced by employing techniques such as multivariate prognostic modelling and machine learning in prognosis studies. Multivariate prognostic modelling determines the independent prognostic value of each factor while accounting for their confounding effects. Meanwhile, machine learning methods, including random forests, support vector machines, and neural networks, identify potential prognostic factors that traditional approaches might overlook.

Ensemble learning methods try to combine different types of input data, features, algorithms, and models to enhance comprehensiveness predictive performance in personalised prognosis compared to individual models. For example, ensemble techniques like random forests, boosting, bagging, hybrid RF/ET models can be employed to enhance prediction accuracy by integrating genomic, clinical, and proteomic data in cancer diagnosis and prognosis. These methods outperform individual classifiers in prediction performance, enabling a more personalised prognosis by integrating diverse datasets.

Personalised prognosis offers several advantages over generalised prognosis. It can improve accuracy by integrating multiple prognostic factors and diverse datasets, which can provide more accurate and comprehensive predictions. However, personalised prognosis also has some weaknesses. Its complex integration of data and advanced modelling techniques such as machine learning based models can be difficult to interpret in clinical practice. To improve the applicability of these methods, techniques for enhancing interpretability, such as local interpretable model-agnostic explanations (LIME), can be employed in medical settings. [7]

2.1.3 From static to dynamic prognosis

Static prognosis refers to one-time prediction of the likelihood of an outcome of a disease, performed at a specific time point, usually made early in the course of a disease such as the time point of admission. Dynamic prognosis, however, takes the changes of prognostic factors during the course of the disease into account so that the prediction can be updated and adjusted over time.

Cross-sectional studies are favoured in SAH prognosis research as they are effective

for identifying risk factors, and assessing the impact of various prognostic factors in SAH at a single point of time. Using Odds Ratios (OR), typically computed through logistic regression analysis, these studies estimate the odds of outcomes such as mortality based on the presence of specific prognostic factors. This approach provides a clear snapshot of the population's health status at admission, offering a one-time static prognosis. For instance, a cross-sectional study might examine the relationship between the development of hydrocephalus in SAH patients at admission and outcomes measured by the Glasgow Outcome Scale (GOS) three months post-SAH, finding that the presence of hydrocephalus is associated with significantly increased odds of poor clinical outcomes (*OR=1.78, 95%CI: 1.49-2.12*). [8]

Survival analysis and survival models, have been crucial in advancing dynamic prognosis by enabling more precise and individualised predictions of patient outcomes over time. These models are designed to analyse time-to-event data, accounting for the fact that not all patients may experience the event during the study period. The Cox proportional hazard model, introduced by Sir David Cox in 1972, has been foundation for dynamic prognosis. [9] Traditional Cox models, which typically incorporate static baseline covariates at admission, can provide outcome predictions over time by estimating the hazard ratio (HR) for each covariate.

The model's extension to include time-dependent covariates has further enhanced its capability, allowing for the incorporation of variables that change over time, thus providing a more accurate and evolving assessment of survival risks. However, the inclusion of time-dependent covariates in the Cox model also introduces potential violation of the proportional hazards assumption, potentially leading to biased estimates. [10] To address these limitations, joint modelling has been introduced to simultaneously analyse longitudinal data and time-to-event data. [11]

Joint modelling techniques, as a powerful statistical tool used to simultaneously analyse longitudinal data and time-to-event data, which are particularly useful in understanding the relationship between time-varying prognostic factors and the risks of event occurring. Joint modelling addresses the limitations of traditional Cox models with time-dependent covariates by accounting for measurement errors and the inherent correlation between longitudinal and survival processes.with shared random effects.

For example, in the context of cerebrovascular diseases, especially spontaneous SAH, joint models can effectively integrate dynamic prognostic factors, such as blood pressure and repeated neurological assessments, providing a more comprehensive and accurate prognostication. This prognostic modelling approach enhances the ability to capture the complex interactions between personalised prognostic factors and disease progression, leading to more comprehensive and personalised outcome predictions. However, prior to the studies conducted in this thesis, the application of joint modelling for SAH prognosis had not been explored.

Machine learning approaches can be utilised in dynamic prognosis due to their ability to handle complex and high-dimensional clinical data, continuously learning and adapting to new prognostic information as the disease progresses. One primary advantage of these methods is their capacity to manage sequential data and capture temporal dependencies. For instance, a recurrent neural network (RNN) with long short-term memory (LSTM) units is particularly adept at processing dynamically updated patient data and has been used to predict 90-day mortality in ICU patients [12]. Another significant benefit of machine learning in dynamic prognosis is its capability to extract useful prognostic features from high-dimensional longitudinal data, such as biomarkers. Techniques like functional principal component analysis (FPCA) can be employed to extract informative features from various lactate dehydrogenase (LDH) biomarkers, capturing over 99% of variability and enabling survival prediction in colorectal cancer patients [13].

Despite these merits from machine learning techniques, there are several limitations, requiring further improvements:

- **Interpretability and explainability:** The decision making processes of many machine learning models are not transparent and easily understood by clinicians. Lack of interpretability makes it challenging to understand how predictions are made, which can be important in clinical settings. Although approaches such as SHapley Additive exPlanations (SHAP) is employed to identify the dynamic contribution of each prognostic factor to model's predictions in dynamic prognosis. [12] While SHAP improves transparency and contributes to explaining the relative prognostic power of prognostic factors in predicting outcomes, machine learning models still cannot provide the same level of straightforward interpretation as statistical models.
- **Generalisation:** In the context of dynamic prognosis, machine learning models offer powerful tools for capturing complex, non-linear relationships and temporal dependencies in clinical data. While these machine learning models may offer advanced predictive capabilities, they may not generalise well compared to statistical models. An review article studying machine learning applications in medicine also highlights that while machine learning models can achieve accuracy, they often suffer from generalisation issues when deployed in different clinical environments, advocating for the use of simpler models to enhance interpretability and robustness. [14]

The evolution of prognosis in medicine reflects a journey from subjective, experience-based methods to objective, evidence-based approaches. This progression also includes a shift from generalised to personalised prognosis, incorporating a broader range of patient-specific factors, and from static to dynamic models, adapting to changes over time. These advancements have significantly improved the accuracy and reliability of prognostic predictions.

2.2 Methodologies for prognosis

Statistical methods are a crucial component of medical studies and form the foundation of prognosis research. They allow us to predict outcomes based on available prognostic data. In prognosis research, outcomes can be broadly classified into continuous outcomes (e.g., weight gain during pregnancy), binary outcomes (e.g., mortality six months after traumatic brain injury), and time-to-event outcomes (e.g., time to death following a breast cancer diagnosis). In this section, we will review fundamental statistical tools and advanced techniques for prognosis, discussing their mathematical principles, appropriate applications, and examples of their use in prognosis studies.

2.2.1 Statistical tools for continuous outcomes

Linear regression is a statistical method used to model the relationship between a dependent variable and one or more independent variables. When a single independent variable is involved, it is referred to as simple linear regression, while multiple linear regression involves two or more independent variables. The goal of linear regression is to determine the best-fitting line that allows for accurate predictions of the dependent variable based on the values of the independent variables.

Linear regression is widely applied in prognosis studies with continuous outcomes, such as the blood pressure of hypertension patients or the pain scale score one month after a hip replacement. These continuous outcomes often serve as clinical outcomes in some prognosis research. Linear regression can estimate various statistical measures, including the mean, median, standard deviation, and inter-quartile range of outcome values. It is particularly useful for estimating the mean and median outcomes for different sub-groups and for predicting the expected outcome change associated with a one-unit increase in a prognostic factor. In prognostic modelling studies, linear regression can predict expected outcome values for individuals based on their predictor variables.

Given a dataset that each individual is characterised by a set of k prognostic predictors measured a specific time point, e.g., on admission or at diagnosis, and one continuous outcome measured at a later time point, e.g., the end of follow-up period or one month after admission. Hence, a linear regression model for prognosis of a continuous outcome can be simply given by:

$$Y_i = \beta_0 + \beta_1 X_{1i} + \beta_2 X_{2i} + \beta_3 X_{3i} + \ldots + \beta_k X_{ki} + \varepsilon_i = \boldsymbol{X_i \beta} + \varepsilon_i \quad (2.1)$$

In this equation, Y_i denotes the continuous outcome of the i^{th} individual while X_{ki} is the value of the k^{th} predictor of that individual. For example, X_{1i} can be the age of this individual, which can take any forms, either numerical, e.g., 45-years old, categorical, e.g., 50 - 69 years, or binary, e.g., > 60 years. X_{2i}, for example, can be

the gender of this individual, 0 for males and 1 for females, conditions of smoking, alcohol use and so on. Additionally, β_0 is the intercept and ε_i is the residual term, which requires a distribution assumption to be made, e.g., normality assumption. Parameters in linear regression are estimated using maximum likelihood estimation (MLE), maximising the likelihood function, or least square estimation (LSE), minimising the sum of square residuals.

In prognostic factor research, $\widehat{\boldsymbol{\beta}}$, the estimated terms of $\boldsymbol{\beta}$, represent the change in mean outcome value, or mean difference, for a one-unit increase in the corresponding predictor, after adjusting for other factors. In prognostic model research, the primary interest lies in using the linear regression model to predict the continuous outcome of interest for new individuals based on their predictor values and the combination of estimated regression coefficients.

In joint modelling, longitudinal outcomes are a special type of continuous outcome where predictors and outcomes are measured simultaneously, and predictors can be time-dependent, including time itself as a predictor. For instance, in joint modelling of HIV/AIDS patient survival using survival data and longitudinal CD4 cell counts, the longitudinal outcome (CD4 cell count) is estimated using linear mixed-effect models, with predictors including visit time, sex and age. [15]

Compared to linear regression, which includes only fixed effects, linear mixed-effect models incorporate both random and fixed effects, allowing it to handle variability between individuals or groups and dependencies among observations.. Fixed effects are variables or factors assumed to have a constant, systematic impact on the dependent variable, remaining the same for all individuals or groups in the study. Common demographic variables like age and gender are often included as fixed effects in the longitudinal sub-model of joint modelling. In contrast, random effects are typically unobserved or unmeasured variables that contribute to the variability of the dependent variable. They are included in the model to account for the dependencies across observations, capturing variability between individuals or sub-groups, such as patient-specific intercepts and visit times. A linear mixed-effect model for estimating the longitudinal outcome in joint modelling can be expressed as:

$$\boldsymbol{Y_i = X_i\beta + Z_i b_i + \varepsilon_i} \ (\mathbf{2.2})$$

where $\boldsymbol{X_i\beta}$ and $\boldsymbol{Z_i b_i}$ are respectively fixed-effect and random-effect terms, while ε_i is the residual term.

So far, we have discussed basic techniques for continuous outcomes and longitudinal outcomes in joint modelling. Linear regression models and linear mixed-effect models, while useful for their simplicity and interpretability, are limited to handling linear relationships between predictors and continuous outcomes. The primary advantage of these models is their ability to provide straightforward insights into the effect of predictors on outcomes.

However, to account for non-linear relationships in the prognosis of continuous outcomes, various statistical methods are available, such as spline regression and polynomial regression. These non-linear methods offer the advantage of flexibility, allowing them to model more complex relationships between predictors and outcomes. Nonetheless, they also have weaknesses, such as increased complexity, lack of interpretability, and the potential for overfitting if not properly regularised.

2.2.2 Statistical tools for binary outcomes

Binary outcomes refer to the occurrence of specific events of interest within a defined time period, such as follow-up periods. An example of a binary outcome is whether mortality occurs in a group of patients suffering from spontaneous SAH, or whether hydrocephalus develops within the follow-up period. In prognosis research, the occurrence of binary outcomes within a particular time frame is expressed as average absolute risks, also known as cumulative incidence. This represents the percentage of patients in the cohort who experience a specific clinical outcome by the end of the time period. For instance, as discussed in the previous chapter, the WHO MONICA stroke study showed that 41.7% of patients with SAH died within 28 days. Therefore, the risk of death for this cohort, expressed as a percentage, is 41.7% within 28 days. [16]

Odds provide another way to measure the risk of binary outcomes, defined as the ratio of the number of individuals with the outcome to the number of individuals without the outcome within the time period of interest. For example, in the WHO MONICA stroke study, 1,404 out of 3,368 SAH cases resulted in death within 28 days, while the remaining 1,964 cases survived. This corresponds to odds of 1,404:1,964, or approximately 0.715 (roughly 5/7). Both risk and odds are crucial in prognostic factor research, where researchers investigate how various prognostic factors influence the risk and odds of the binary outcomes of interest.

In prognosis studies involving different sub-groups, three measures are often used to describe the associations between prognostic factors and binary outcomes: risk difference, risk ratio (RR), and odds ratio (OR). The risk difference is the absolute difference in the risk of a binary outcome between two groups, calculated by subtracting the absolute risk of the outcome in the control group from that in the experimental group. In prognostic factor research, the experimental group refers to individuals with specific prognostic factors or characteristics (e.g., age > 60, diabetes), while the control group consists of the remaining individuals in the cohort without these prognostic factors or characteristics.

The risk ratio (RR), is the ratio of the risk of an outcome in the experimental group to the risk in the control group. It represents the relative likelihood of developing the outcome in the experimental group compared to the control group. A RR greater than 1 indicates a higher risk in the experimental group, while a RR less than 1 indicates a

lower risk.

The odds ratio (OR) is used in prognosis to compare the odds of a binary outcome occurring in the experimental group to the odds of the outcome occurring in the control group. In prognosis research, the OR is often employed to assess the effectiveness of different treatments or the impact of various risk factors on a specific outcome. For example, it can be used to compare the odds of survival in non-traumatic SAH patients with high brain natriuretic peptide (BNP) levels to those without high BNP levels. In this case, the OR is calculated by dividing the odds of survival in the experimental group (patients with high BNP levels) by the odds of survival in the control group (patients without high BNP levels). [17]

Compared to the OR, risk differences and RR are often considered more intuitive measures. However, the OR is typically preferred in prognosis studies. Firstly, the OR is highly comparable, as it is widely used in clinical trials and other medical studies, facilitating comparisons across studies and enabling meta-analyses. Secondly, prognosis studies of binary outcomes frequently use logistic regression models for multivariable analysis, which naturally produce OR as the measure of association between predictors and the outcome. In these studies, ORs are the preferred measure of association because they are estimated for each prognostic factor after adjusting for the other included factors, thereby minimising potential confounding effects and providing a more accurate estimate of the true effect of the prognostic factor on the outcome. [18]

For a binary outcome, the response variable takes the value 1 when the outcome occurs within a specified period of time and 0 otherwise, following a Bernoulli distribution. Linear regression can produce predicted values outside the range of 0 and 1, making it unsuitable for binary outcomes. Therefore, the logistic regression model is often used to model binary outcomes, and it can be expressed as:

$$\boldsymbol{p_i = \frac{1}{1 + e^{-X_i\beta}}} \quad \boldsymbol{(2.3)}$$

where p_i denotes the probability of developing interested outcome for the i^{th} individual.

In logistic regression models, there are no residual terms as the use of the Bernoulli distribution inherently accounts for the differences between the observed binary outcomes and the predicted probabilities. The model is typically estimated using MLE. Each estimated coefficient $\widehat{\beta}$ quantifies the change in log odds for a one-unit increase in the corresponding prognostic predictor, such that $OR=e^{\widehat{\beta}}$. For instance, in a study examining the impact of comorbidities and smoking on outcomes in aneurysmal SAH, the OR for smoking's effect on achieving a good clinical outcome (mRS 0-2) is 0.21 after adjusting for other predictors such as hypertension. This indicates that smoking is associated with 79% lower odds of achieving a good clinical

outcome compared to the non-smoking group. [19]

The estimated coefficients in logistic regression models can be used to predict the probability of new individuals developing a specific binary outcome within a given time period, $\widehat{p}_i$. By using the values of the predictors for that individual and the estimated coefficients, the probability $\widehat{p}_i$ can be calculated through the following back-transformation:

$$\widehat{\boldsymbol{p}}_{\boldsymbol{i}} = \frac{\mathbf{1}}{\mathbf{1} + \boldsymbol{e}^{-\boldsymbol{X}_{\boldsymbol{i}}\widehat{\boldsymbol{\beta}}}} \ (\mathbf{2.4})$$

Additionally, other models, such as Poisson regression or binomial regression with a log link, are available and particularly useful when risk ratios (RRs) are desired. [20][21] Extending logistic regression to multinomial logistic regression, also known as softmax regression, allows for the modeling of outcomes with more than two categories.

2.2.3 Statistical tools for time-to-event outcomes

Unlike binary outcomes, time-to-event outcomes consider not only whether an event occurred but also when it occurred. In prognosis studies, some individuals may not complete the entire follow-up period, and others may not experience the outcome due to various reasons, such as withdrawing from the study for personal reasons or encountering competing risks, events that preclude the occurrence of the primary outcome. Consequently, time-to-event outcomes are more complex than binary outcomes and require careful specification before further discussion.

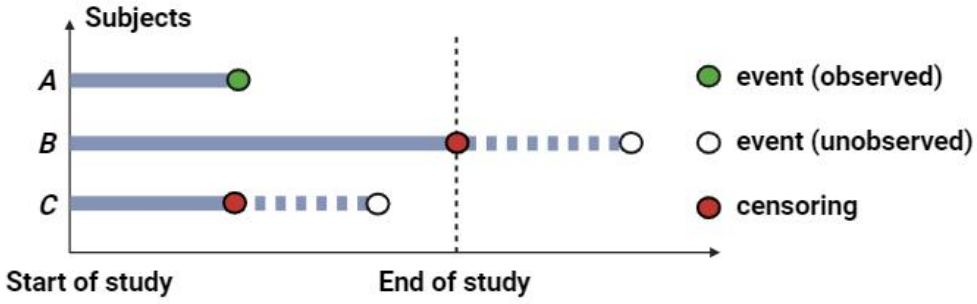


Figure 2.1: A visualisation for right censoring (Produced in BioRender)

An individual is considered to be right-censored if they are lost to follow-up, choose to withdraw from the study, experience another event that precludes the occurrence of the event of interest, or simply have not experienced the event by the end of the study. This is indicated by a red circles in Figure 2.1. In the figure, individual A experience the event before the end of the study, represented by full green circles, while individuals B and C do not experience the event before their censored time, indicated by full red circles. Individual B experiences the event after the study ends, while individual C might experience the event within the follow-up period, but it remains

unobserved due to an earlier censored time. Unlike right-censoring, left-censoring happens when the event of interest has occurred before the individual enters the study, which is uncommon in the context of spontaneous SAH prognosis. In the following chapters of this thesis, the focus will be limited to right-censoring in patients.

For time-to-event outcomes in prognosis research, the incidence rate is a important summary measure that describes how quickly an event occurs within a population. Unlike cumulative incidence, which is used for binary outcomes, the incidence rate is based on person-time and accounts for censoring and the length of the follow-up period. The incidence rate in prognosis is defined as the total number of observed events of interest occurring during the study period divided by the total person-time accumulated over all individuals during their follow-up time.

In prognosis research, the incidence rate can be used to determine the likelihood of developing the outcome of interest during the study period. Since the incidence rate often changes over the follow-up period, the overall incidence rate cannot indicate when the outcome is more likely to occur during the study. To model the incidence rate over time and determine, for example, whether the outcome is more likely to occur early or late in the study period, the hazard function $h(t)$ and cumulative hazard function $H(t)$ are employed. These functions provide a more detailed understanding of the timing and risk of the event throughout the study.

The hazard function, also known as the failure rate or hazard rate, is a fundamental concept in survival analysis. It measures the instantaneous rate of experiencing the outcome at a given time *t*, provided that the outcome has not yet occurred up to that point. Mathematically, the hazard function is defined as:

$$\boldsymbol{h(t) = \lim_{\Delta t \to 0} \frac{P(t \leq T < t + \Delta t | T \geq t)}{\Delta t}} \quad \boldsymbol{(2.5)}$$

The hazard function, $h(t)$, is defined as the limit of the conditional probability that an event will occur in the next infinitesimal time interval [*t, t*+ Δ *t*], given that the event has not occurred up to time *t*, divided by the length of the interval Δ *t*. Here, *T* represents the time of occurrence of the event.

The cumulative hazard function represents the accumulated risk of the event occurring over time. It describes the probability that the event of interest has occurred by a certain point in time and can be expressed as:

$$\boldsymbol{H(t) = \int_0^t h(s)\, ds} \quad \boldsymbol{(2.6)}$$

The survival function, also known as the survival curve, is more commonly used to communicate prognosis to health professionals and patients, compared to the hazard function and cumulative hazard function, which are more often used in statistical modeling. The survival function, *S(t)*, is related to and complements the cumulative hazard function. It can be obtained by taking the exponential of the negative

cumulative hazard function:

$$\boldsymbol{S(t) = P(T > t) = exp(-H(t))} \quad \boldsymbol{(2.7)}$$

Intuitively, the survival function represents the probability that an individual has not experienced the event of interest by time *t*. This is a decreasing function, as the probability of survival naturally decreases over time. The survival function, *S(t)*, can be estimated using the Kaplan-Meier method, a non-parametric technique for estimating survival probabilities in the presence of censored data. This method computes the Kaplan-Meier estimator, also known as the product limit estimator, which is a step function that decreases at each event time and remains constant between event times. [22]

The Kaplan-Meier curve is plotted by connecting the steps in the product limit estimator with a series of horizontal and vertical lines. The curve starts at 1.0, representing the probability of survival at time zero, and gradually decreases over time as more events occur. Abrupt changes or plateaus may appear if large numbers of subjects at risk are censored at specific time points. Figure 2.2 illustrates an example of a Kaplan-Meier curve, showing cumulative survival probabilities over time for high and low risk groups of patients with spontaneous intracerebral haemorrhage (ICH) without cerebral herniation at admission. The risk groups were determined by a risk score calculated based on a nomogram model. It indicates that the prognosis for high-risk patients is significantly worse than for low-risk patients over the study period. This difference is statistically significant, as demonstrated by the log-rank test ($p<0.0001$), a non-parametric hypothesis test based on the Kaplan-Meier estimator used to compare survival trends between two or more groups in the presence of censoring [23].

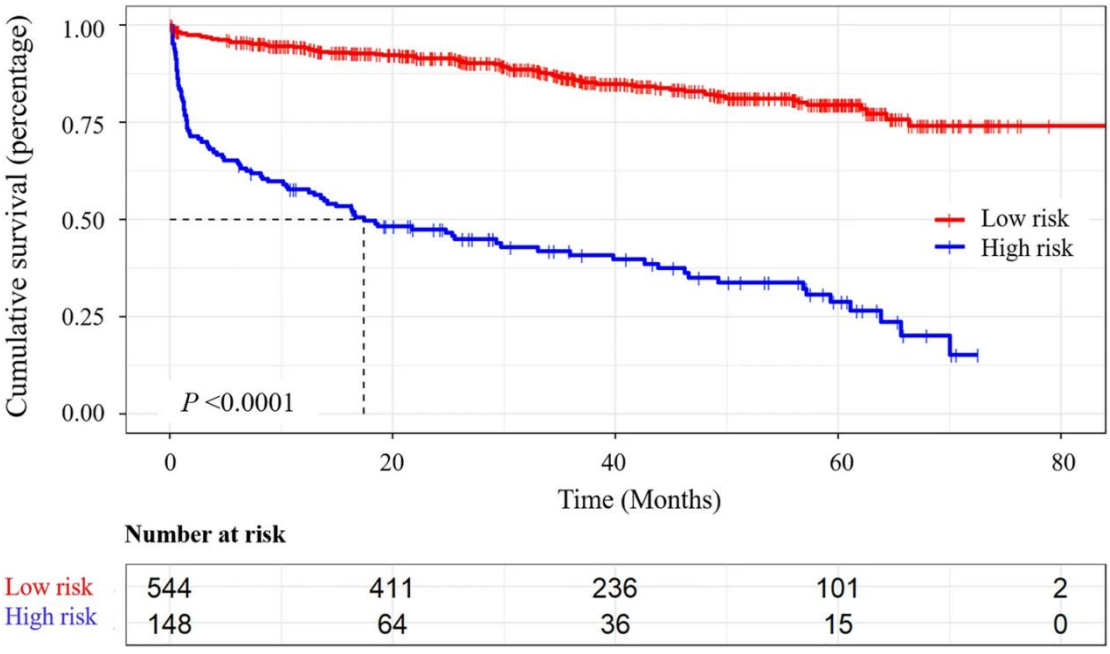


Figure 2.2: Kaplan–Meier survival curves comparing high and low risk groups for long-term survival in spontaneous ICH patients without cerebral herniation

at admission [23]

In addition to comparing the survival curves of patients with different medical conditions, such as melanoma versus non-melanoma cancer, Kaplan-Meier survival curves can also be used to visualise the effect of a prognostic factor. This is done by dividing the entire cohort into groups based on the values of the prognostic factor of interest. From the survival function $S(t)$, the corresponding probability that the outcome has occurred by time t, denoted as $F(t) = 1 - S(t)$, can be computed.

To quantitatively measure the relative risks between two groups differentiated by a prognostic factor of interest, the hazard ratio (HR) is often used. The HR is defined as the ratio of the hazard function, or hazard rate, in one group to the hazard rate in another group. A HR greater than 1 indicates a higher risk in one group compared to the other, while a HR less than 1 indicates a lower risk in one group compared to the other.

It is often assumed that the HR is proportional, meaning the HR between two groups remains constant throughout the follow-up period. This is known as the proportional hazards assumption. This assumption allows for the estimation of the effect of a prognostic predictor on the hazard rate while adjusting for other variables. However, if the proportional hazards assumption is violated, certain statistical models in survival analysis, such as the Cox proportional hazards model, may not provide accurate estimates of the hazard ratio. When this assumption is violated, alternative statistical methods must be used.

One such alternative is the accelerated failure time (AFT) model, which does not assume proportional hazards but instead models the survival time directly. [24] Another alternative is the use of joint modelling techniques, which allow for the incorporation of time-varying covariates and random effects. This method relaxes the proportional hazards assumption by accounting for the dynamic properties of longitudinal outcomes and their interaction with survival times. [25]

The Cox proportional hazards model, commonly known as the Cox model, is the most widely used model for survival analysis. It is a semi-parametric model, meaning it combines both parametric and non-parametric elements. The Cox model can be expressed by the following equation:

$$\boldsymbol{h_i(t) = h_0(t) exp(X_i \beta)} \ \boldsymbol{(2.8)}$$

where $h_0(\mathrm{t})$ is the baseline hazard function and represents the hazard when all of the predictors are equal to zero. As can be seen, the parametric component of the Cox model refers to the estimates of the regression coefficients for the predictor variables, which assumes a specific functional form for the hazard function, while the baseline hazard function is the non-parametric component of the Cox model. In the Cox model, the baseline hazard function is not explicitly specified and can take any arbitrary form

that satisfies the proportional hazards assumption. To simplify the modelling process, the forms of baseline hazard function are often assumed, e.g., exponential, Weibull, piecewise constant, Gompertz, log-normal, and log-logistic functions. [26-29]

In prognosis research for cerebrovascular diseases, particularly in cases of spontaneous SAH, certain predictors such as indices from physiological monitoring and repeated radiographic investigations can change over time. To accommodate these time-varying covariates, a time-dependent Cox model, also known as a Cox model with time-dependent covariates, can be utilised. This model allows the covariates to vary over time for each individual, rather than assuming they are fixed, providing a more accurate representation of the relationship between the covariates and the hazard rate. [30]

Time-dependent Cox models can be broadly categorised into two types: models with time-dependent covariates and models with time-dependent coefficients. In models with time-dependent covariates, the effect of covariates on the hazard of an event can vary over time because the values of the covariates change at different points within the study period. This approach allows for a more flexible and accurate representation of the relationship between covariates and the hazard, reflecting real-world scenarios where covariates such as physiological measures or treatment effects may fluctuate over time.

In contrast, models with time-dependent coefficients allow the coefficients themselves to change over time while keeping the covariates fixed. This means that the impact of a covariate on the hazard rate can evolve throughout the study period, accommodating scenarios where the influence of a covariate may increase, decrease, or change direction over time. The extended Cox model with time-dependent covariates and coefficients can be represented with the equations below:

$$\boldsymbol{h_i(t) = h_0(t) exp(\beta X_i(t))} \ \boldsymbol{(2.9)}$$

for extended Cox model with time-dependent covariates, and

$$\boldsymbol{h_i(t) = h_0(t) exp(\beta(t) X_i)} \ \boldsymbol{(2.10)}$$

for extended Cox model with time-dependent coefficients.

However, an extended Cox model with time-dependent covariates requires continuous, error-free measurements of all time-varying covariates to avoid biased estimates. [31] Unfortunately, this is not feasible for prognosis research in spontaneous SAH, where some predictors, such as radiographic findings, are measured intermittently and with measurement error. These errors can arise from various sources, including inconsistencies in measurement instruments and settings, environmental factors, and the fact that different individuals are measured at different times. In this context, joint modelling is optimal due to its ability to handle irregularly and imperfectly measured time-varying covariates effectively. [31]

The longitudinal process of joint modelling is composed of repeated measurements of

one or more longitudinal outcomes of each individual over the study period. These repeated measurements on the same individual, however, are expected to be positively correlated, e.g., two adjacent blood pressure measurements on the same individual are expected to be similar. In this situation, standard statistical tools, e.g., simple linear regression, with assumptions on independent observations are thus not applicable. An intuitive approach to handle this correlation is to assume each individual in the studied cohort has its own subject-specific mean response trajectory over time. Then the profile of the j^{th} longitudinal response for i^{th} individual can be described by:

$$\boldsymbol{y_i = X_i\beta + Z_i b_i + \varepsilon_i,} \quad \boldsymbol{\varepsilon_i \sim N(0, \sigma^2 I),} \quad \boldsymbol{b_i \sim N(0, D)} \ \ (\mathbf{2.11})$$

where β denotes the parameters for fixed effects and b_i denotes the parameters for random effects. The parameter for a fixed-effect covariate represents the average change in the corresponding longitudinal response when the covariate increases by one unit, while the parameter for a random effect can be interpreted as the deviation of a subset of regression parameters for a specific individual from those parameters of the whole cohort. The combination of parameters for fixed effects and random effects allows for the description of individual response trajectories, capturing both the average population trends and the individual-specific variations. [32]

In the context of longitudinal sub-models, $y_{ij}(t)$ can be used to denote the j^{th} longitudinal outcome for the i^{th} individual. However, this expression includes an error term, meaning the observed longitudinal outcome is contaminated with measurement error. The true value of the j^{th} longitudinal outcome for the i^{th} individual can be denoted as $m_i(t)$. Therefore, the expression of the j^{th} longitudinal outcome for the i^{th} individual at time *t* can be represented as follows:

$$\boldsymbol{y_{ij}(t) = x_{ij}^T(t)\beta_j + z_{ij}^T(t)b_{ij} + \varepsilon_{ij}(t) = m_{ij}(t) + \varepsilon_{ij}(t)} \ \ (\mathbf{2.12})$$

where $m_{ij}(t)$ is the true value of longitudinal outcome, not contaminated by measurement error.

To quantify the effect of true value of longitudinal outcomes $m_i(t)$ on the risk of true event outcome T_i^*, a common practice is to use a relative risk model for the survival process:

$$\boldsymbol{h_i(t|M_i(t), \omega_i) = h_0(t)exp(\gamma^T w_i + \alpha^T m_i(t))} \ \ (\mathbf{2.13})$$

where one or multiple longitudinal outcomes can be simultaneously included. In the expression, $M_i(t)$ denotes the history of true, error-free longitudinal outcomes up to time *t*. ω_i represents baseline covariates, which remain invariant during the study period, such as age, gender, and medical history. The vector γ corresponds to the coefficients for these baseline covariates, while α is the vector of coefficients for the longitudinal outcomes, which serve as time-varying covariates. As previously introduced, $h_0(\mathrm{t})$ is the baseline hazard function for modelling the survival process, which can be left unspecified.

AFT model, as an alternative to proportional hazard models does not assume constant

hazards in the survival data. [24] Unlike proportional hazards models, where the effects of covariates multiply the hazard by the exponential of the covariate multiplied by its corresponding parameter, the AFT model assumes that covariates accelerate or decelerate the occurrence of the event of interest. This model is parametric, assuming that the logarithm of survival time is a linear function of covariates. Thus, the effects of covariates are to accelerate or decelerate the event timing. The survival function for time t in the AFT model can be expressed as:

$$\boldsymbol{S_i(t) = P(T_i > t) = S_0(exp(X_i\beta)t)} \quad \mathbf{(2.14)}$$

where S_0 is the baseline survival function and β denotes the vector of regression coefficients.

Likewise, the hazard function of AFT model can be expressed by:

$$\boldsymbol{h_i(t) = exp(X_i\beta)h_0(exp(X_i\beta)t)} \quad \mathbf{(2.15)}$$

The term $exp(X_i\beta)$ is the acceleration factor of i^{th} individual which accelerates or decelerates the time to event of interest compared to when $X_i = 0$. It can be noticed that the effects of covariates act directly and multiplicatively on survival time. [24]

The acceleration factor in an AFT model allows for the investigation of how changes in covariate values influence the expected survival time relative to the baseline time scale. An acceleration factor greater than one indicates a deceleration in survival time, meaning the event occurs later, while an acceleration factor less than one signifies an acceleration, causing the event to occur sooner. This relationship between covariates and the time to the event can be expressed linearly by relating the covariates to the natural logarithm of the time to the event of interest. This relationship is given by the equation:

$$\boldsymbol{Y_i = lnT_i = -X_i\beta + \varepsilon} \quad \mathbf{(2.16)}$$

where the error term ϵ is independent of the covariates, and its distribution determines the distribution of the unmoderated time to event T_0. The distribution of T_0 then defines the specific type of AFT model. While the Cox model is a semi-parametric model that does not assume a specific distribution for the survival times, the AFT model is fully parametric, specifying the distribution of survival time by assuming a particular distribution for the error term ϵ. Common parametric distribution assumptions used in AFT models include the Weibull, exponential, log-normal, gamma, and log-logistic distributions. Each of these distributions provides a different shape and scale to the survival time, allowing for flexibility in modelling various types of survival data. [24]

In summary, time-to-event outcomes in prognosis research, particularly for conditions like spontaneous SAH, require sophisticated methods due to their complexity. Traditional models like the Cox proportional hazards model may not always provide accurate prognostication, especially when the proportional hazards assumption is violated. The AFT model offers an alternative by directly modelling survival time, accommodating varying event timings through acceleration factors. However, joint

modelling techniques provide a more comprehensive solution by integrating longitudinal data with survival outcomes, effectively handling time-varying covariates and random effects. This approach allows for a more comprehensive understanding of dynamic relationships between prognostic factors and event times, and offering more accurate and insightful analyses for prognosis research.

In sections 2.2.1 to 2.2.3, different types of outcomes in prognosis research and corresponding common statistical tools have been reviewed, summarised in Table 2.1.

Type of outcome in prognosis research	Common statistical tools
Continuous outcomes	Linear regression model, linear mixed-effect models, non-linear models such as spline regression and polynomial regression
Binary outcomes	Risk difference, risk ratio, odds ratio, logistic regression model, Poisson regression, binomial regression with a log link
More than two categories or ordinal outcomes	Multinomial logistic regression model (softmax regression model), ordinal regression model
Time-to-event outcomes	Kaplan-Meier estimators, Cox proportional hazards model, Accelerated Failure Time (AFT) models

Table 2.1: Different types of outcomes in prognosis research and corresponding common statistical tools

2.2.4 Assessing the performance of prognostication

After developing a prognostic model, regardless of the outcome type and statistical tools used, it is crucial to apply statistical measures to quantify its prognostic power. This allows for an accurate assessment of the model's accuracy, comparison between different models, and potential improvements to the model. To evaluate the overall performance of a prognostic model, various statistics of model fit can be adopted, depending on the type of outcome: continuous, binary/categorical, or time-to-event.

In the context of continuous outcomes, several statistical measures are utilised to assess the accuracy and effectiveness of prognostic models. One of the most common metrics is the coefficient of determination, denoted as R^2. This statistic is particularly useful in linear regression models as it quantifies the proportion of variance in the dependent variable that can be attributed to the independent variables included in the model. An R^2 value ranges from 0 to 1, where a value closer to 1 indicates a greater explanatory power of the model. A higher R^2 value means that the model explains a larger portion of the variability in the outcome variable, thus demonstrating stronger prognostic ability. Additionally, other measures such as the mean squared error (MSE) and its derivative, the root mean squared error (RMSE), are also important. MSE calculates the average squared differences between observed and predicted values, providing insight into the overall accuracy of the predictions, while RMSE translates this into the same units as the predicted values for easier interpretation.

When dealing with binary outcomes, various statistical measures are employed to assess the performance of prognostic models. One of the primary metrics is sensitivity, also known as the true positive rate, which measures the proportion of actual positives that are correctly identified by prognostication. Specificity, or the true negative rate, is complementary to sensitivity, which measures the proportion of actual negatives that are correctly identified. Together, these metrics provide a comprehensive view of a model's ability to distinguish between the two outcome states for binary outcomes.

Another crucial measure is the receiver operating characteristic (ROC) curve, which plots the true positive rate against the false positive rate at various threshold settings. The area under the curve (AUC) of the ROC provides a single value summarising the model's performance across all thresholds, with a value closer to 1 indicating better discriminatory ability, illustrated in Figure 2.3. Additionally, the Brier Score is used to measure the accuracy of probabilistic predictions, calculating the mean squared difference between predicted probabilities and actual outcomes.

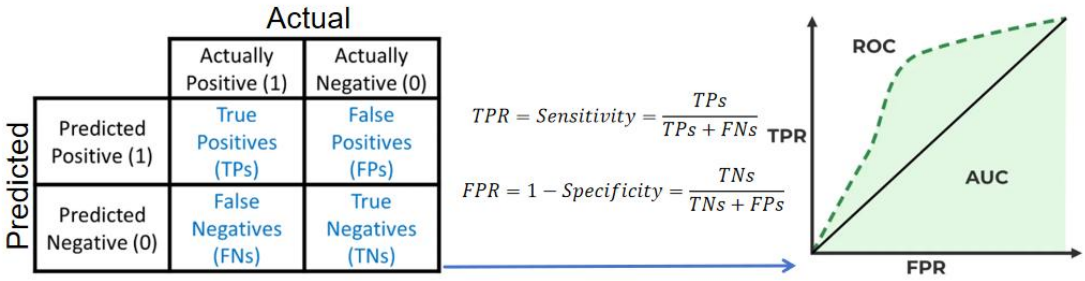


Figure 2.3: Visualisation of binary classification metrics

Time-dependent ROC curves and the Brier Score are commonly used tools for assessing the performance of prognostication in time-to-event outcomes. These two metrics provide comprehensive and dynamic insights into how well a model predicts the timing and occurrence of events. The time-dependent AUC quantifies the model's discriminative ability at specific time points, with higher AUC values indicating better performance. By evaluating the ROC curve at multiple time points, researchers can understand how well the model can distinguish between individuals' experiencing events across the entire study period. Similarly, the time-dependent Brier Score measures the accuracy of prognostication for time-to-event outcomes at various time points, incorporating adjustments for censored data. This metric measures the mean squared difference between predicted probabilities and actual outcomes over time, with lower scores indicating better model performance.

Beyond prediction performance, several other measures are critical for evaluating prognostic models in clinical settings, especially in the context of time-to-event outcomes:

- **Calibration:** Calibration assesses the agreement between predicted probabilities and actual outcomes in different percentiles (mostly deciles), usually via a calibration plot. Calibrating models brings benefits like better prediction accuracy, decreased uncertainty, and greater confidence in the model's predictive performance. [33]
- **Interpretability and explainability:** Clinical interpretability measures the degree that healthcare providers can easily understand and apply the model's predictions, while explainability focuses on explaining the predictions made. Simpler models with clear explanations are favoured in clinical practice, ensuring accountability, transparency, and confidence.
- **Reproducibility:** Reproducibility ensures that a prognostic model performs consistently well across different datasets and settings, with external validation to confirm its generalisability.

2.3 Spontaneous SAH prognosis studies

In this section, we will delve into the prognosis research concerning spontaneous SAH. Initially, we will provide an overview of various prognosis studies on spontaneous SAH, categorised by different prognosis types under the PROGRESS framework and various outcome types. Following this, we will review previous literature focusing on specific outcomes, such as mortality, poor neurological outcomes assessed by neurological scales, and related complications.

Type of Research	Description
Overall prognosis research	Studies that summarise the average risk of an outcome (e.g. death) or expected value of an outcome (e.g. pain score) among people with the health condition of interest in a particular healthcare setting.
Prognostic factor research	Studies that identify factors whose values (levels) are associated with changes in the outcome's risk or expected value.
Prognostic model research	Studies that develop, validate or assess the impact of a prognostic model to predict an individual's outcome risk or expected outcome value using combinations of prognostic factors.
Predictors of treatment effect research	Studies that identify how to tailor treatment decisions for individual patients according to whether they are likely to benefit from particular treatments.

Table 2.2: The PROGRESS framework for prognosis research

2.3.1 Prognosis research topics in spontaneous SAH

Prognosis research in spontaneous SAH predominantly focuses on aneurysmal SAH due to its higher risk of mortality and poor clinical outcomes, making it a significant area of interest. However, some studies also examine non-aneurysmal SAH, including perimesencephalic and non-perimesencephalic types. While non-aneurysmal SAH

generally has better clinical outcomes compared to aneurysmal SAH, understanding its prognosis remains crucial for monitoring potential complications and informing treatment decisions.

Previous prognosis studies in spontaneous SAH have addressed all four types of prognosis research under the PROGRESS framework. In overall prognosis research, studies summarise the average risk of mortality, complications, and poor neurological outcomes over a specified period among patients with spontaneous SAH, or more specifically, aneurysmal SAH. Prognostic factor research aims to identify and select influential predictors associated with mortality, complications, or poor neurological outcomes. These predictors can include demographic characteristics, underlying medical conditions, physical and radiographic examinations, and physiological monitoring indices from vital signs. The selected predictors from prognostic factor research can be combined to develop prognostic models that predict survival probabilities or the risks of complications or poor neurological outcomes.

Research on predictors of treatment effect, particularly in identifying which factors indicate whether an individual will respond to a specific treatment, is relatively scarce. These treatments can include medical management, such as the use of nimodipine, or surgical interventions like aneurysm clipping and coiling. Relevant predictors might include neurological scores, length of hospital stay, or other indicators that help determine the efficacy of a treatment for a specific individual. Generally, prognosis research in this area assumes that treatment effects can vary among individuals based on their unique characteristics and health conditions. The goal is to identify these predictors or factors to assist clinicians in tailoring treatments, thereby optimising benefits and minimising harms for each patient.

Apart from the types of prognosis research under the PROGRESS framework, studies on the prognosis of spontaneous SAH can be categorised according to different types of outcomes, most commonly binary/categorical and time-to-event outcomes. Binary outcomes of interest may include whether individuals develop specific complications, such as re-bleeding or hydrocephalus, or if they die during the study period. Corresponding time-to-event outcomes consider not only whether an event has occurred but also the time to the event. Neurological scores are often used to indicate good or poor neurological outcomes and can be included as categorical outcomes in a prognostic model, such as the Modified Rankin Score (mRS).

2.3.2 Mortality

Research on survival prognosis is of significant importance as it aims to provide accurate predictions of patients' survival outcomes, guide clinical decisions, and improve quality of life. Mortality can be analysed as a binary outcome or a time-to-event outcome, depending on whether the analysis considers the time until death. Studies on spontaneous SAH have identified several key covariates that

influence survival. These include demographic factors such as age, treatment information including choice and timing of treatment, pre-existing medical conditions, clinical scores at the time of admission, radiological and haematological findings like Fisher grade and troponin level, and physiological monitoring indices such as ECG and ABP readings.

Demographic factors play a crucial role in predicting mortality. In a cross-centre prognosis study to develop a prognostic model and predict 60-day case fatality in aneurysmal SAH patients, age was found as one of the most significant predictors of survival in both univariate analysis (*OR=1.43, 95%CI: 1.23-1.66*) for predictor selection and the developed multivariable prognostic model (*p=0.00004, OR=1.32, 95%CI: 1.13-1.55*). [34]

Another study, involving 3,567 patients, transformed age into a categorical covariate by decade (e.g., age 30-39, 40-49) and combined mortality, vegetative states, and severe disability as unfavourable outcomes. These unfavourable outcomes can be treated either as binary outcomes or as time-to-event outcomes, considering the time from admission to death, surgery, and recording of the Glasgow Outcome Scale (GOS). Age was found to be a significant prognostic factor for unfavourable outcomes in both univariate and multivariate analyses, considering only preoperative factors (*p<0.0001, OR=1.53, 95%CI:1.37-1.64*) and all factors (*p<0.0001, OR=1.50. 95%CI: 1.37-1.64*). Multivariate Cox modelling also indicated age as a significant factor when considering preoperative factors (*p<0.0001, HR=1.02, 95%CI: 1.02-1.04*) and all factors. (*p<0.0001, HR=1.03, 95%CI: 1.02-1.04*) [8].

A prognosis study exclusively focusing on elderly patients ($\geqslant$ 60 years) with aneurysmal SAH considered death as the only time-to-event outcome. In this study, age was identified as a significant prognostic factor influencing mortality in the final Cox model (*p=0.0257, HR=1.399*) [35]. Another commonly analysed demographic factor, gender, was included in all these studies but was found to be insignificant [8][35].

Treatment information is considered a key prognostic factor in relevant studies, including aspects such as the timing of treatment (e.g., time to surgery after the onset of SAH) and the type of medical or surgical intervention adopted (e.g., coiling or clipping). A study investigating the ideal timing for surgical treatment, either clipping or coiling, after the onset of aneurysmal SAH found that patients receiving coiling between 5 to 10 days post-SAH have a higher risk of developing DCI. Furthermore, aneurysm treatment administered after day 10, regardless of the treatment modality, is associated with worse outcomes. However, the timing of treatment between day 5 and day 10, whether clipping or coiling, is not a significant prognostic factor for poor outcomes, including high modified Rankin Scale (mRS) scores ($\geqslant$3) and mortality [36].

Compared to the timing of treatment, the effects of different treatment choices on survival are of greater research interest, as they can directly guide treatment decisions for better clinical outcomes. For aneurysmal SAH, the two primary techniques for treating aneurysms, the sources of bleeding, are coiling and clipping. These treatment options have been compared using the complete occlusion rate as a comparative parameter in Chapter 1, where clipping showed a higher complete occlusion rate than coiling. However, coiling is associated with a lower risk of mortality compared to clipping. Specifically, the relative risk reduction in mortality for coiling compared to clipping is 13% (*RR=0.77, 95%CI: 0.61-0.98*) at five-year follow-up and 22% (*RR=0.78, 95%CI: 0.64-0.96*) at ten years [37].

Pre-existing conditions at admission are often included as potential factors in prognostic modelling, including both chronic diseases and complications. Hypertension, a chronic disease, has been identified as a significant prognostic factor for poor outcomes, including mortality, vegetative states, and severe disability. In univariate analysis, hypertension is significant (*p<0.0001, OR=2.10, 95%CI: 1.75-2.51*). However, in multivariate analysis, hypertension remains significant only when considering preoperative factors (*p=0.003, OR=1.32, 95%CI: 1.10-1.58*) [34]. Regarding body mass index (BMI), multivariate analysis has shown that being overweight (*25-29.9* kg/m^2) is a significant predictor of mortality (*p=0.038, OR=0.309, 95%CI: 0.102-0.937*) when adjusting for age, Hunt and Hess scale, modified Fisher grade, and DCI [38].

Although complications are typically included as binary or time-to-event outcomes in prognostic modelling, the occurrence of specific complications can also indicate a higher risk of mortality and should be considered influential factors in prognosis. Re-bleeding and hydrocephalus are both associated with high mortality rates, particularly if re-bleeding occurs within 12 hours after the initial SAH, which can increase the mortality rate by up to 50%-70% [39]. Re-bleeding within 24 hours after the initial SAH is a strong predictor of mortality in both univariate (*p=0.0001, OR=7.12, 95%CI: 2.61-19.42*) and multivariate analyses (*p=0.01, OR=5.38, 95%CI: 1.48-19.52*). Another major complication following SAH, DCI, is associated with higher mortality at discharge (*OR=2.00, 95%CI: 1.08-3.72*) and at 3, 6, and 12 months post-SAH [38][40].

Vasospasm, particularly acute vasospasm, is significantly associated with mortality, vegetative states, and severe disability in both univariate analysis (*p<0.0001, OR=2.19, 95%CI: 1.57-3.07*) and survival modeling (*p=0.009, OR=1.55, 95%CI: 1.12-2.15*), considering only preoperative factors. In addition to these four major complications following SAH, other complications such as cerebral infarction, cerebral edema, cardiac complications, pulmonary complications, and electrolyte imbalances are also linked to an increased risk of mortality [8][39][41].

Unlike other covariates, complications are typically analysed as outcomes rather than

prognostic factors. Studies examining their associations with mortality often focus on overall prognosis, providing statistics on the proportion of mortality in patients with different types of complications. For instance, data from an international cooperative study on the timing of aneurysm surgery indicated that 40% of SAH patients developed at least one severe, life-threatening medical complication, with nearly one-quarter of deaths attributable to complications. Specifically, 19% of deaths were due to the direct effects of the initial haemorrhage, while re-bleeding and vasospasm were responsible for 22% and 23% of deaths, respectively. Pulmonary complications were identified as the most common non-neurological cause of death [41].

Clinical scores measured on admission to evaluate neurological conditions are popular prognostic factors in prognosis research for spontaneous SAH, with the Hunt and Hess grade and World Federation of Neurological Surgeons (WFNS) grade being the two commonly used scales. Using WFNS grade 1 as a reference, higher WFNS grades are associated with increased mortality rates: grade 2 (*OR=1.87, 95%CI: 1.13-1.55*), grade 3 (*OR=1.70, 95%CI: 0.87-3.32*), grade 4 (*OR=4.87, 95% CI: 2.60-9.14*), grade 5 (*OR=7.00, 95% CI: 2.54-19.28*), and grade 6 (*OR=5.75, 95% CI: 1.13-1.55*) [65]. Additionally, the mortality rate for high Hunt and Hess grades (grades 4 and 5) is extremely high, ranging from 71% to 100%, with these patients facing a significantly higher risk of in-hospital mortality (*OR=10.94, 95% CI: 5.55-21.57*) [38][42].

Radiographic investigations, e.g., CT findings, can provide important and valuable prognostic information for mortality and complications. The Fisher grade or modified Fisher grade is the best-known grading system to classify SAH in CT scans and is commonly included in prognosis research of SAH. Adjusting WFNS grade, age and lumen size, with Fisher grade 1 as reference, Fisher grade 2 (*OR=1.43, 95%CI: 0.27-7.65*), 3 (*OR=2.67, 95%CI: 0.53-13.51*), 4 (*OR=2,76, 95%CI: 0.54-14.14*) are increasing associated with higher odds ratio for mortality. ($p < 0.0001$) [65] Additionally, the modified Fisher grade ≥ 3 is a strong and independent risk factor for in-hospital mortality (*OR=20.90, 95%CI: 2.80-55.92*).[38]

For aneurysmal SAH, characteristics of aneurysms found in radiographic investigations provide valuable information of aneurysms and can be included as prognostic factors in prognosis research. Size of aneurysm is the most commonly used prognostic factor in that larger aneurysms are associated with higher risk of mortality after adjusting for other factors (*p=0.0004, OR=1.08, 95%CI: 1.03-1.13*).[64] Location of aneurysm is another important predictor for mortality and severe disability considering only preoperative factors (*p<0.0001, OR=1.21, 95%CI: 1.10-1.34*) where aneurysms located in anterior cerebral (*OR=1.34, 95%CI: 1.07-1.66*) and posterior circulations (*OR=1.53, 95%CI: 1.15-2.03*) are associated with higher risk of poor outcomes compared with other locations, e.g., internal carotid and middle cerebral. [8]

Some biomarkers in blood tests can be included as influential predictors of mortality,

such as troponin and brain natriuretic peptide (BNP) levels, which are associated with cardiac dysfunctions. It has been found that elevated troponin (*RR=2.0, 95% CI: 1.2-3.4*) and BNP levels (*RR=11.1, 95% CI: 4.7-26.0*) are significantly associated with increased mortality. In addition to haematology biomarkers, indices from various physiological monitoring modalities, such as arterial blood pressure (ABP), electrocardiogram (ECG), electroencephalogram (EEG), and others, can serve as prognostic factors for mortality. ECG abnormalities, in particular, have been reported as predictors of mortality. For example, tachycardia (*RR=3.9, 95% CI: 1.7-9.3*), P mitrale (*RR=4.1, 95% CI: 1.6-10.5*), Q wave abnormalities (*RR=2.9, 95% CI: 1.5-5.5*), ST depression (*RR=2.1, 95% CI: 1.5-3.1*), and T wave abnormalities (*RR=1.8, 95% CI: 1.4-2.4*) have all been identified as significant predictors of mortality in a meta-analysis on the impact of cardiac abnormalities, manifested as ECG abnormalities, on outcomes after aneurysmal SAH [43].

In a multivariate analysis on associations between clinical characteristics of the study population and ECG findings, a high ECG score (ECG score$\geqslant$6), which is an overall ECG index defined as the total number of leads that have abnormal Q wave, ST depression, or T wave inversion, has been shown to be the most powerful predictor for in-hospital mortality (*p=0.0026, OR=14.39, 95%CI: 2.54-81.71*). [44]

ABP is another important modality in SAH management, whose indices can contain valuable prognostic information for survival. For example, variability of blood pressure (BPV), which can be further detailed into variability of specific types of blood pressure for analysis, e.g., systolic blood pressure variability (SBPV) and pulse pressure variability (PPV), incorporates dynamic changes of blood pressure over time and has gained recognition as a prognostic factor of mortality (*PPV: p=0.015, OR=1.110. 95%CI: 1.023-1.212; SBPV: p=0.019, OR=1.072, 95%CI: 1.012-1.139*). [45][46]

Indices from other modalities, beyond ECG and ABP, also hold significant prognostic value. For instance, EEG patterns such as non-convulsive status epilepticus (NCSE) are linked to high mortality, though it remains under investigation whether sub-clinical seizures have a deleterious effect on the brain or merely indicate underlying disease [47]. High intracranial pressure (ICP) is critical in the mechanisms of various brain injuries, with elevated mean ICP ($\geqslant$20 mmHg) associated with increased mortality risks (*OR=1.08, 95% CI: 1.04-1.23*) [48]. Additionally, mortality following spontaneous SAH, particularly aneurysmal SAH, is linked to lower mean brain oxygen tension (PbtO2) and prolonged periods of compromised cerebral oxygenation. In one study, mortality was associated with more episodes of compromised PbtO2 (*OR=1.1, 95% CI: 1.003-1.2*) and cerebral hypoxia (*OR=1.3, 95% CI: 1.0-1.7*) [49].

Research on survival prognosis for spontaneous SAH is vital for predicting patient outcomes, and improving quality of life. Mortality can be analysed as either a binary

or time-to-event outcome. Key prognostic factors include demographic variables such as age, which consistently emerges as a significant predictor, and treatment details like timing and type of intervention (e.g., coiling vs. clipping). Pre-existing conditions, particularly hypertension and BMI, and specific complications such as re-bleeding and DCI, significantly impact mortality risk. Clinical scores at admission, including Hunt and Hess and WFNS grades, and radiographic findings like Fisher grade provide valuable prognostic information. Biomarkers (e.g., troponin and BNP levels) and physiological monitoring indices (e.g., ECG and ABP readings) are also crucial, with elevated biomarkers and ECG abnormalities associated with higher mortality. Figure 2.4 reviews and visualises the strength of these prognostic factors for mortality using forest plots.

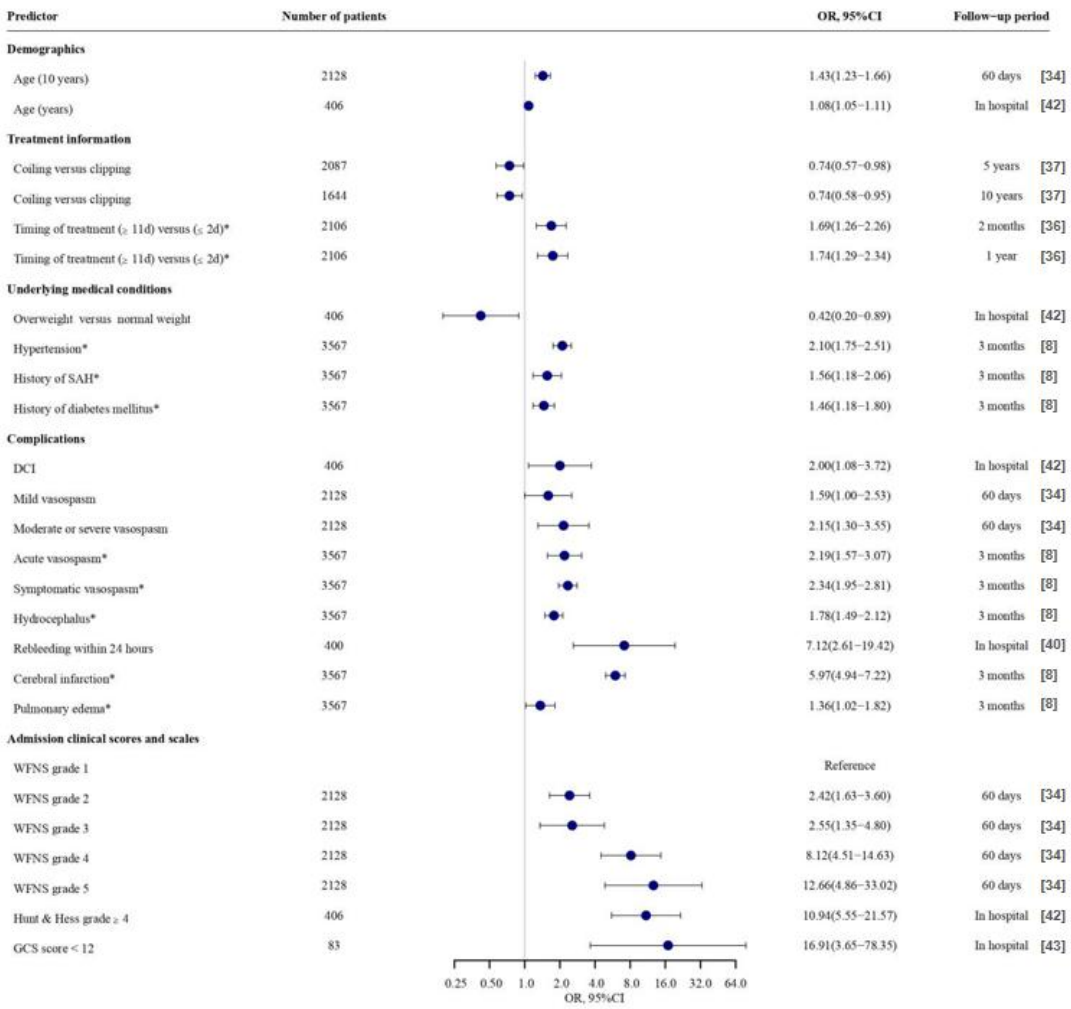


Figure 2.4: Forest plots of prognostic risk factors for mortality in univariate analysis after spontaneous SAH[2]

[2] ***: a composite outcome combined of mortality and other poor outcomes, ^: adjusted for baseline predictors**

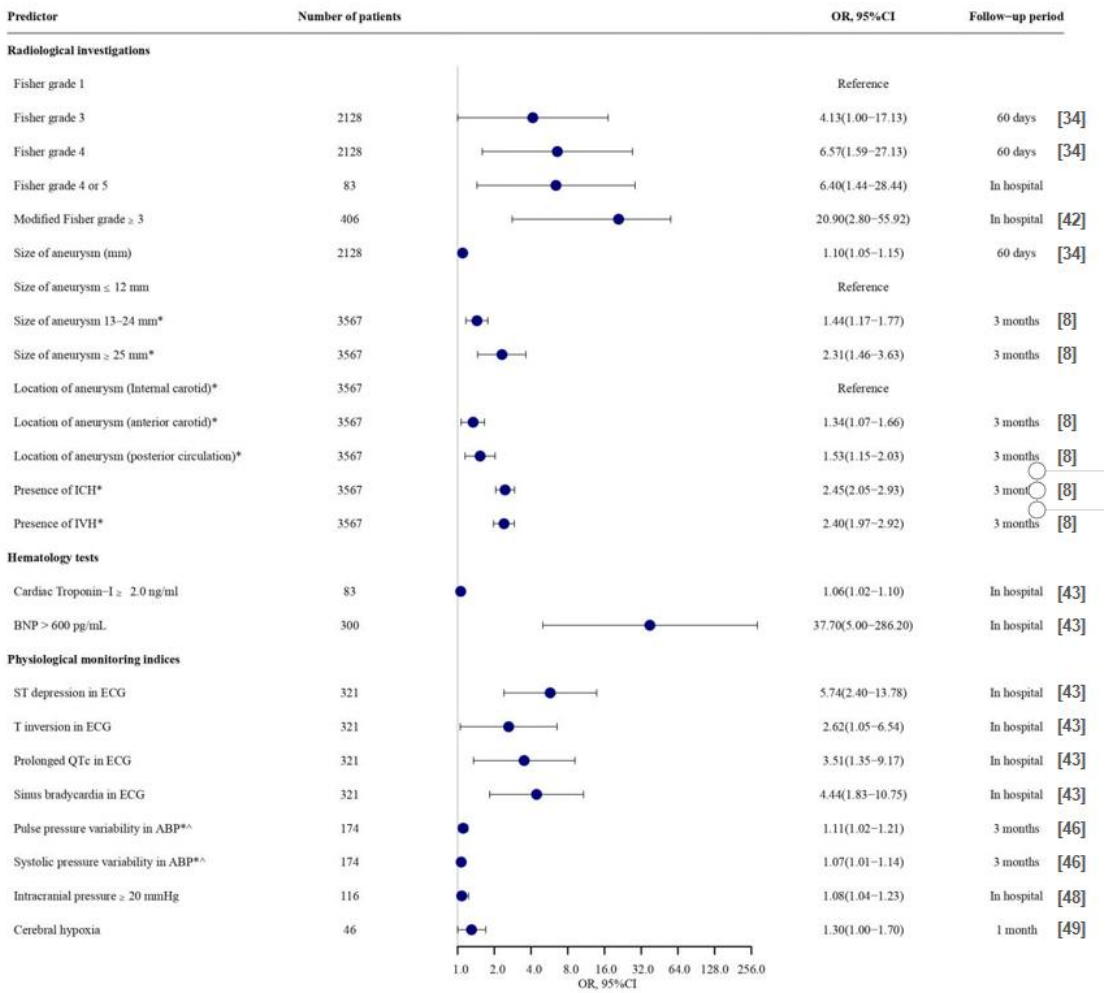


Figure 2.4 Cont.

Research on survival prognosis for spontaneous SAH is vital for predicting patient outcomes, and improving quality of life. Mortality can be analysed as either a binary or time-to-event outcome. Key prognostic factors include demographic variables such as age, which consistently emerges as a significant predictor, and treatment details like timing and type of intervention (e.g., coiling vs. clipping). Pre-existing conditions, particularly hypertension and BMI, and specific complications such as re-bleeding and DCI, significantly impact mortality risk. Clinical scores at admission, including Hunt and Hess and WFNS grades, and radiographic findings like Fisher grade provide valuable prognostic information. Biomarkers (e.g., troponin and BNP levels) and physiological monitoring indices (e.g., ECG and ABP readings) are also crucial, with elevated biomarkers and ECG abnormalities associated with higher mortality. Figure 2.4 reviews and visualises the strength of these prognostic factors for mortality using forest plots.

2.3.3 Neurological outcomes measured by neurological grades

Compared to mortality, neurological outcomes are more frequently used in prognosis research because they include a range of outcomes and are often more sensitive to

neurological changes. This sensitivity allows for a better capture of the effects of covariates on patients' overall quality of life and functional status by focusing on poor neurological outcomes in prognostic modelling. Poor neurological outcomes can be represented by grades such as the modified Rankin Scale (mRS) and Glasgow Outcome Scale (GOS), as well as vegetative states, mild to severe disabilities, or combinations of these measures, sometimes including mortality. Neurological grades like mRS and GOS are more popular than other measures, such as disabilities and vegetative states, because they provide a standardised approach to assessing the overall neurological function of patients.

In this section, the effects of each category of covariates will be reviewed and discussed, ranging from demographics to physiological indices. It is found that overall neurological outcomes ($p<0.001$), assessed using the GOS at 3 months after SAH, worsen with increasing age, remaining significant in multivariate analysis after adjusting for different prognostic factors. Specifically, there is a significantly increased risk of poor outcomes after the age of 60 [50]. Similarly, age is shown to be a significant prognostic factor for poor outcomes (mRS score $\geqslant$ 4) when considered as a continuous covariate [51]. Although gender is not significantly associated with mortality, exploratory analysis reveals that female sex is significantly associated with unfavourable outcomes, defined as mRS score > 2, in both univariate ($p=0.033$, $OR=2.04$, 95% CI: 1.05-3.96) and multivariate analysis ($p=0.011$, $OR=2.63$, 95% CI: 1.22-5.66) [52].

As previously discussed, the timing of treatment, particularly aneurysm treatment after day 10, is a significant prognostic factor for all aneurysmal SAH patients, regardless of treatment modality. This delayed treatment is associated with poorer outcomes at 2 months ($OR=1.84$, 95% CI: 1.36-2.51) and 1 year ($OR=1.89$, 95% CI: 1.38-2.57), when adjusted for other factors, using treatment within 2 days after SAH as a reference [37]. Additionally, the treatment modality can serve as a prognostic factor for neurological outcomes. Specifically, coiling is associated with excellent outcomes, defined as an mRS score of 0 or 1, in univariate analysis ($p=0.01$, $OR=1.80$, 95% CI: 1.15-2.82) [53].

Pre-existing chronic diseases can impact neurological outcomes, as measured by neurological scales. In an exploratory analysis of predictors for unfavourable outcomes after good-grade aneurysmal SAH, where an unfavourable outcome is defined as an mRS score > 2, a history of hypertension was found to be a significant predictor in univariate analysis ($OR=2.19$, 95% CI: 1.26-3.80). However, this significance diminished in multivariate analysis after adjusting for other predictors ($OR=1.45$, 95% CI: 0.75-2.79) [52].

Body mass becomes a more important predictor for poor neurological grades than mortality, since only overweight (25-29.9 kg/m^2) is a significant predictor for mortality. In the same study, for poor neurological outcomes ($\mathrm{mRS} \geq 4$), body mass

index, either as a continuous covariate, or categorised into overweight ($(25-29.9kg/m^2$) and obese ($\geq 30\ kg/m^2$), are significant at 90 days (*BMI continuous: p=0.031, OR=1.050, 95%CI: 1.004-1.098; overweight: p=0.014, OR=0.432, 95%CI: 0.221-0.842; obese: p=0.041, OR=2.067, 95%CI: 1.032-4.139*) and at 180 days (*BMI continuous: p=0.037, OR=1.048, 95%CI: 1.003-1.096; overweight: p=0.001, OR=0.311, 95%CI: 0.156-0.622; obese: p=0.049, OR=1.947, 95%CI: 1.105-3.888*) in univariate analysis. [38]

Multivariate analysis with BMI as a categorical variable along with other significant variables for poor neurological grades also shows that BMI category is a significant predictor at both 90 days (O*verweight: p=0.008, OR=0.243, 95%CI: 0.085-0.692; obese: p=0.003, OR=5.064, 95%CI: 1.753-14.627*) and 180 days (O*verweight: p=0.001, OR=0.122, 95%CI: 0.039-0.383; obese: p=0.043, OR=2.918, 95%CI: 1.036-8.220*). [38]

In the study on predictors of unfavourable outcomes (mRS $\geq$ 3) after good-grade aneurysmal SAH (WFNS grade I or II), various complications, including DCI, respiratory complications, and intracranial haemorrhage, were associated with unfavourable outcomes at 12 weeks. This association was evident in both univariate (DCI: *OR=4.10, 95% CI: 2.07-8.12*; respiratory complications: *OR=3.27, 95% CI: 1.86-5.73*; intracranial haemorrhage complications: *OR=3.71, 95% CI: 1.60-8.58*) and multivariate analyses (DCI: *OR=2.60, 95% CI: 1.05-6.43*; respiratory complications: *OR=2.62, 95% CI: 1.35-5.09*; intracranial haemorrhage complications: *OR=3.19, 95% CI: 1.19-8.56*) [52].

In another study investigating predictors of excellent functional outcomes (mRS < 2) in aneurysmal SAH identified several complications that were significantly associated with lower likelihood of favorable recovery. Specifically, hydrocephalus ($p < 0.01$, *OR = 0.41, 95% CI: 0.27 – 0.66*), vasospasm ($p < 0.01$, *OR = 0.49, 95% CI: 0.30 – 0.80*), seizures ($p < 0.01$, *OR = 0.33, 95% CI: 0.18 – 0.58*), cerebral infarction ($p < 0.01$, *OR = 0.23, 95% CI: 0.14 – 0.37*), and acute lung injury/acute respiratory distress syndrome ($p = 0.05$, *OR = 0.59, 95% CI: 0.35 – 0.99*) were all associated with poorer neurological recovery. [53] Furthermore, additional complications, including cerebral oedema, electrolyte disturbances, and cardiac and pulmonary dysfunction, are also linked to worse neurological grades [39][41]. These findings showed the significant impact of secondary complications on patient outcomes following aneurysmal SAH.

The type of spontaneous SAH significantly affects prognosis, with aneurysmal SAH widely accepted as being associated with poorer outcomes. A prospective study on the effects of categories of spontaneous SAH, either aneurysmal SAH or non-aneurysmal SAH, also known as angiogram-negative SAH and which can be further divided into non-perimesencephalic SAH and perimesencephalic SAH, on neurological outcomes has shown that aneurysmal SAH patients are less likely (*p=0.0264*) to have excellent

neurological outcomes (mRS < 2) (*64/102, 62.7%*), than non-perimesencephalic SAH (*15/18, 83.3%*) and perimesencephalic SAH patients (*13/14, 92.9%*). [54]

A meta-analysis of six studies considering the differences in prognosis of patients with non-perimesencephalic SAH and perimesencephalic SAH has shown that the overall odds ratio of good neurological outcome (mRS score < 3 or GOS score > 3) for the perimesencephalic SAH subgroup is 6.23 (*p<0.0001, 95%CI: 2.65-14.65*) compared with non-perimesencephalic SAH subgroup. No statistically significant heterogeneity is found among the studies, which indicates that these studies included in the meta-analysis have reached similar conclusions. [55]

Alcohol consumption, particularly heavy drinking (*>300g/week*), significantly increases the risk of poor outcomes one year after aneurysmal SAH, including mortality, vegetative states, or severe disability, as measured by the GOS (*p=0.0023*) [56]. Similarly, patients with poor neurological grades upon admission, such as those assessed by the Hunt and Hess grade and WFNS grade, are more likely to have poor neurological outcomes. For instance, a study on the preoperative prediction of long-term outcomes in poor-grade aneurysmal SAH (Hunt and Hess grade 4 or 5) found that the worst preoperative Hunt and Hess grade 5 strongly predicts one-year outcomes (*p<0.0001*). Additionally, a high WFNS score (WFNS score $\geqslant$ 3) is significantly associated with poor outcomes, defined as mortality and mRS score $\geqslant$ 4, in both univariate analysis (*OR=8.1, 95% CI: 3.4-19.0*) and multivariate analysis (*OR=4.3, 95% CI: 1.4-13.7*) after adjusting for ventricular score and ECG abnormalities [51].

Radiological information plays a crucial role in the prognosis of spontaneous SAH when measured by neurological grades. In a study on predictors of excellent functional outcomes (mRS < 2) in aneurysmal SAH, certain radiological findings were associated with lower rates of excellent outcomes. These included a higher modified Fisher grade (*p<0.01, OR=0.49, 95% CI: 0.38-0.65*), presence of ICH (*p<0.01, OR=0.24, 95% CI: 0.14-0.40*), and intraventricular haemorrhage (IVH) (*p<0.01, OR=0.42, 95% CI: 0.27-0.65*) [53]. Additionally, large aneurysms ($\geqslant$ 13 mm) were indicative of poor outcomes (mRS score $\geqslant$ 4) at 12 months (*p=0.005, HR=5.202, 95% CI: 1.629-16.614*) [57].

In addition to findings from radiological examinations, certain biomarkers in blood tests can also predict neurological outcomes. Elevated troponin levels are not only a marker for increased mortality risk but also remain a significant prognostic factor (p<0.05, RR=2.3) for poor neurological outcomes, defined as mortality, GOS score < 4, or mRS score $\geqslant$ 3. Similarly, elevated creatine kinase MB (CK-MB) levels are associated with poor neurological outcomes (*p<0.05, RR=2.3*) [43]. High blood sugar (hyperglycemia) is another predictor of poor outcomes at 12 months, being significant in univariate analysis (*p=0.03, HR=3.039, 95% CI: 1.096-8.430*) and included in the final multivariate model (*p<0.03*) [57].

Finally, indices from various modalities of physiological monitoring in vital signs can serve as prognostic predictors for neurological outcomes. In ABP monitoring, systolic blood pressure metrics such as variability measured by standard deviation (*p=0.014*), minimum (*p<0.001*), peak (*p=0.021*), trough (*p=0.007*), and the coefficient of variation (p=0.004) can predict good neurological outcomes at the last clinical follow-up, where an mRS score ≥ 4 indicates poor outcome. However, only the minimum systolic blood pressure (1-mmHg increment) remains statistically significant in multivariate analysis (*p=0.03, OR=1.03, 95% CI: 1.002-1.067*) [45]. Similarly, changes in mean ABP during the follow-up period, such as within the first 4 or 8 days, are significantly associated with clinical outcomes measured by GOS score [58].

ECG indices remain important prognostic factors for neurological outcomes. ST depression, T wave inversion, and U waves have shown significant relationships with poor outcomes, defined as mortality or an mRS score ≥ 4, in univariate analysis (ST depression: *OR=10.6, 95% CI: 2.3-48.8*; T wave inversion: *OR=2.5, 95% CI: 1.5-5.5*; U wave: *OR=0.4, 95% CI: 0.2-0.9*). In multivariate analysis, after adjusting for WFNS and ventricular scores, ST depression (*OR=6.2, 95% CI: 1.2-33.7*) and U waves (*OR=0.4, 95% CI: 0.2-0.98*) remain significant prognostic factors [51]. Additionally, intracranial pressure (ICP) is another vital sign monitoring modality that provides prognostic information for neurological outcomes. High mean ICP (≥20 mmHg) is associated with unfavourable outcomes at 6 months (*p=0.003*), defined as a GOS score < 4, although it becomes insignificant (*p=0.146, OR=1.05, 95% CI: 0.99-1.12*) after adjusting for other predictors [48].

Neurological outcomes, often assessed by scales such as the modified Rankin Scale (mRS) and Glasgow Outcome Scale (GOS), are critical in prognosis research for spontaneous SAH. Age and treatment timing are significant predictors, with poorer outcomes associated with advanced age and delayed treatment beyond 10 days. Gender differences indicate that female patients are more likely to experience unfavourable outcomes. Pre-existing chronic conditions like hypertension and higher body mass index (BMI) also impact neurological outcomes, although their significance may vary in multivariate analyses.

Radiological findings, such as higher modified Fisher grades and the presence of intracerebral or intraventricular haemorrhage, and large aneurysm size are associated with poorer outcomes. Biomarkers like elevated troponin and CK-MB levels, and hyperglycemia, alongside physiological monitoring indices from ABP and ECG, contribute valuable prognostic information. Figure 2.5 reviews these associations, visualising the prognostic powers of these prognostic factors for neurological grades in univariate analysis with forest plots.

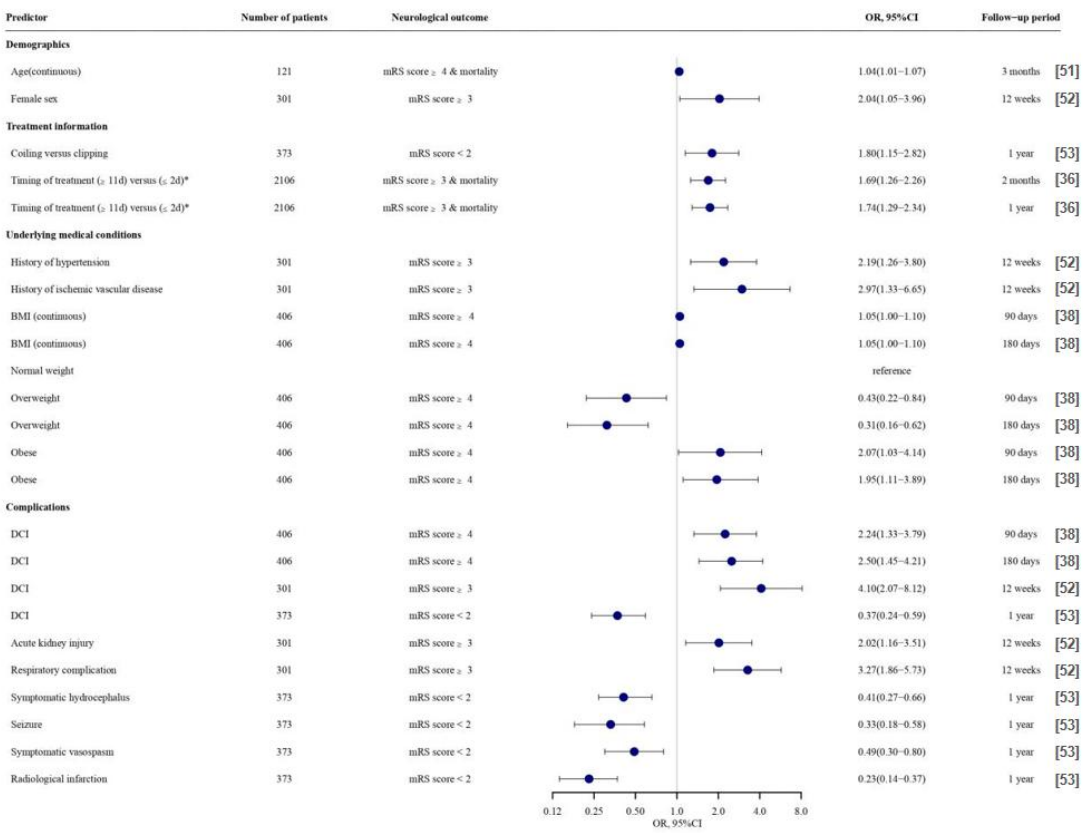


Figure 2.5: Forest plots of prognostic risk factors for neurological grades in univariate analysis after spontaneous SAH

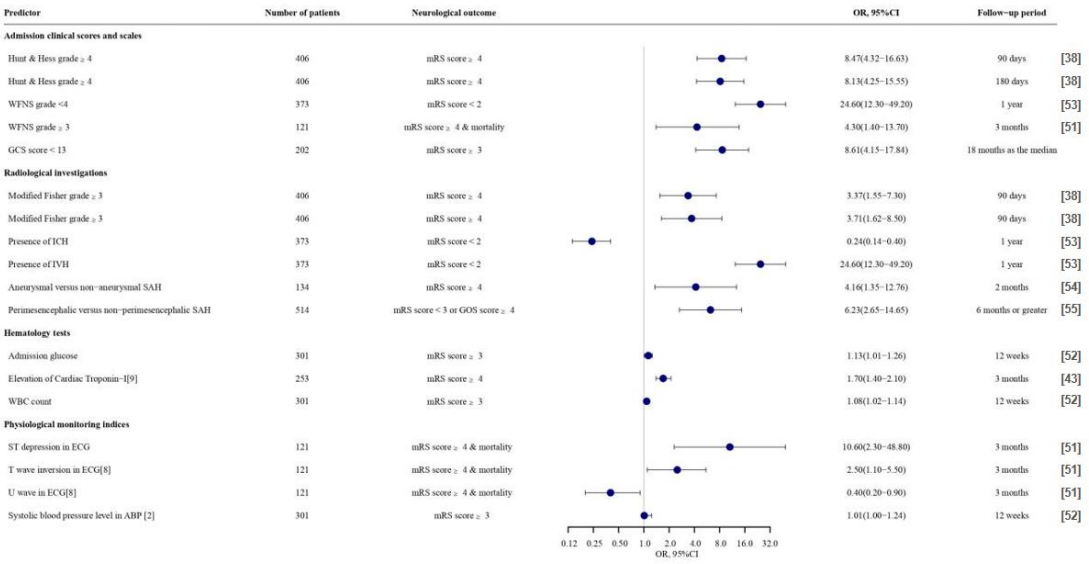


Figure 2.5 Cont.

2.3.4 Re-bleeding

As discussed in the previous chapter, re-bleeding is a serious early complication in spontaneous SAH, particularly aneurysmal SAH, occurring when the sources of haemorrhage, such as aneurysms, burst again after initially being sealed. Re-bleeding

is associated with high mortality and morbidity rates and is often considered a critical indicator of high mortality risk in prognosis research. However, re-bleeding can also be included as an outcome in prognostic modelling to guide early decision-making and prevent the recurrence of haemorrhage sources.

Compared to prognosis studies of spontaneous SAH that include mortality or neurological outcomes, there are significantly fewer studies focusing on re-bleeding as an outcome. Nevertheless, several covariates have been identified as predictive of re-bleeding occurrence, aiding clinicians in acute-phase management to mitigate the risk. These covariates include age, causes of spontaneous SAH, neurological scores on admission, radiographic findings, and physiological monitoring indices in vital signs. Monitoring these prognostic factors can help healthcare providers identify patients at higher risk of re-bleeding and implement timely interventions to prevent re-bleeding after the initial haemorrhage.

Increased age is not only an influential predictor for mortality and poor neurological outcomes but also provides significant prognostic information for re-bleeding, making it one of the most critical risk factors. A study on the relationship between age and outcome after aneurysmal SAH found that the re-bleeding rate increases from 4.5% in the youngest age group ($\leq$ 40 $years$) to 16.4% in patients over 70 years old [50].

Neurological status on admission, as measured by the Hunt and Hess scale, and radiological factors such as the modified Fisher grade and aneurysmal characteristics are among the most important risk factors for re-bleeding. A modified Fisher grade of 3 or 4 is a strong predictor of re-bleeding within the first 24 hours, independent of the patient's WFNS score on admission [39]. In a study on risk factors for aneurysmal re-bleeding, increased age (*$p<0.001$, OR=1.167, 95% CI: 1.116-1.220*), Hunt and Hess grade 4 or 5 (*$p<0.001$, OR=2.512, 95% CI: 1.734-3.639*), aneurysm size greater than 10 mm (*$p=0.002$, OR=1.624, 95% CI: 1.188-2.221*), and systolic blood pressure higher than 160 mmHg (*$p<0.001$, OR=3.338, 95% CI: 1.734-3.639*) were identified as independent risk factors for re-bleeding [59]. Additionally, aneurysms located in the posterior cerebral circulation are at a higher risk of re-bleeding compared to those in the anterior cerebral circulation, and the number of aneurysms also serves as an influential predictor of re-bleeding [39][60].

Besides high SBP, variability in SBP has also been identified as a novel risk factor for re-bleeding, which measures the degree of haemodynamic instability. Re-bleeding is associated with both the standard deviation of SBP (*$p<0.001$, OR=1.254, 95% CI: 1.131-1.391*) and the successive variation of SBP (*$p<0.001$, OR=1.131, 95% CI: 1.039-1.231*) [61]. Apart from ABP indices, ICP also provides important prognostic information. A high mean ICP ($\geqslant$ 20 mmHg) is significantly associated with an increased risk of aneurysmal re-bleeding (*$p=0.008$, OR=3.47, 95% CI: 1.38-8.69*) [48].

Re-bleeding is a serious early complication in spontaneous SAH, especially aneurysmal SAH, associated with high mortality and morbidity rates. Although less studied than mortality or neurological outcomes, several covariates can predict re-bleeding risk. These include age, admission neurological scores (Hunt and Hess scale), radiographic findings (modified Fisher grade, aneurysm size, and location), and physiological monitoring indices (SBP, SBP variability, and ICP). Increased age, particularly in patients over 70, significantly raises re-bleeding risk. High SBP and its variability, along with elevated ICP, are critical risk factors. Figure 2.6 reviews these prognostic risk factors for re-bleeding in univariate analysis after spontaneous SAH, visualised with forest plots.

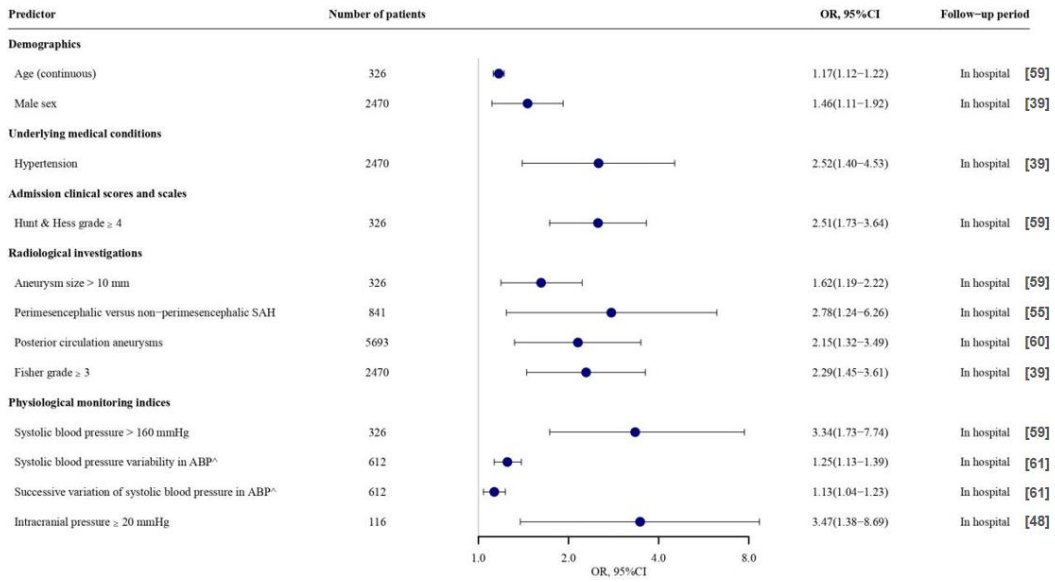


Figure 2.6: Forest plots of prognostic risk factors for re-bleeding in univariate analysis after spontaneous SAH

2.3.5 Vasospasm and delayed cerebral ischaemia (DCI)

Vasospasm and DCI are closely related in the context of SAH, with vasospasm being a contributing factor to the development of DCI. Their associations have been detailedly discussed in Chapter 1, and they will be jointly discussed in this section. Vasospasm and DCI are commonly used as outcomes in prognostic models of SAH because they are common complications and are associated with worse outcomes. DCI, in particular, is the most preventable cause of mortality and poor neurological outcomes, making early detection of risk factors and timely interventions crucial. Prognosis studies and adequate monitoring can facilitate early detection and intervention. [62] Consequently, research into the prognosis of DCI and vasospasm after spontaneous SAH draws considerable interest and has the potential to significantly improve patient outcomes.

Age, as a baseline demographic factor, is commonly included as a predictor in the

prognosis of vasospasm and DCI after SAH. However, the results of different studies can be contradictory. An investigation on age-associated vasospasm found a greater risk of vasospasm in younger patients compared to older patients (Any vasospasm: *OR=5.83, 95% CI: 2.41-14.12*; symptomatic vasospasm: *OR=2.66, 95% CI: 1.008-7.052*) in multivariate analysis, while another study reported that symptomatic vasospasm is more frequently observed in older patients [50][63].

The conflicting results of these two studies likely arise from differences in study settings, methodology, and population characteristics. Therefore, further investigation is necessary to better understand the relationship between age and the incidence of vasospasm. Regarding gender differences, women tend to have a higher risk of developing vasospasm, but this finding is only significant in univariate analysis (*OR=1.33, 95% CI: 1.10-1.63*) and becomes insignificant after adjusting for other predictors (*OR=1.2, 95% CI: 0.95-1.52*), such as age, history of hypertension, and neurological grades on admission [64].

Treatment modalities for aneurysms can also affect the rate of developing DCI or vasospasm. A study including 203 patients treated with clipping and 52 with coiling showed that a higher proportion of patients treated with clipping developed moderate or severe vasospasm compared to those treated with coiling in multivariate analysis (*p=0.01, OR=2.32, 95% CI: 1.21-4.47*). Additionally, clipping was associated with a greater number of affected territories than coiling (*p=0.03*) [65]. Regarding the timing of treatment, the adjusted odds ratio of DCI for treatment on days 5 to 10 was 1.18 (*95% CI: 0.91-1.53*) for the entire cohort, 1.68 (*95% CI: 1.17-2.43*) for patients receiving coiling, and 0.79 (*95% CI: 0.54-1.16*) for patients receiving clipping [36].

Pre-existing chronic diseases and lifestyle factors can significantly impact the incidence of DCI. A systematic review of 52 studies on DCI after SAH found that a higher risk of DCI is associated with a history of hypertension (*OR=1.5, 95% CI: 1.3-1.7*), diabetes mellitus (*OR=6.7, 95% CI: 1.7-26*), and smoking (*OR=1.2, 95% CI: 1.1-1.4*). The review also identified that certain complications, such as hydrocephalus (*OR=1.5, 95% CI: 1.3-1.7*), hyperglycemia (*OR=3.2, 95% CI: 1.8-5.8*), and early systemic inflammatory response syndrome (*OR=2.1, 95% CI: 1.4-3.3*), are associated with a higher risk of DCI [66].

Another systematic review on vasospasm following aneurysmal SAH identified several influential predictors of angiographic vasospasm. These include re-bleeding (*OR=1.25, 95% CI: 1.00-1.56*), hypertension (*OR=1.47, 95% CI: 1.29-1.68*), smoking (*OR=1.34, 95% CI: 1.07-1.68*), acute hydrocephalus (*OR=1.54, 95% CI: 1.31-1.79*), Hunt and Hess grade ≥ 3 (*OR=2.26, 95% CI: 1.82-2.82*), WFNS grade ≥ 4 (*OR=2.08, 95% CI: 1.81-2.39*), Fisher grade ≥ 3 (*OR=2.61, 95% CI: 1.85-3.67*), and the presence of IVH (*OR=1.55, 95% CI: 1.35-1.78*) and ICH (*OR=1.35, 95% CI: 1.31-1.79*) [67]. Additionally, the incidence of symptomatic vasospasm is significantly higher in patients with pulmonary complications after aneurysmal SAH

(*p=0.001*) [41]. Considering the incidence rate of DCI in different types of SAH, the complication rate of DCI and DCI related infarction is higher in non-perimesencephalic SAH than in aneurysmal SAH, while this complication is almost absent in non-aneurysmal perimesencephalic SAH [54].

Additionally, abnormalities biomarkers from haematology tests and indices from physiological monitoring in vital signs are also associated with an increased risk of DCI. A meta-analysis of SAH has concluded that the occurrence of DCI is associated with haematological biomarkers of cardiac damage and dysfunction, such as elevated levels of troponin (*RR=3.2, 95% CI: 2.3-4.4*), CK-MB (*RR=2.9, 95% CI: 1.9-4.5*), and BNP (*RR=4.5, 95% CI: 1.8-11.4*). Additionally, ST depression, an ECG monitoring index, is a significant predictor of DCI in this meta-analysis (*RR=2.4, 95% CI: 1.2-4.9*) [43]. Other ECG indices are also reported to be associated with DCI or vasospasm after SAH. An exploratory analysis of 413 patients showed that QT interval prolongation (*RR=1.86, 95% CI: 1.00-3.45*) and tachycardia (*RR=10.83, 95% CI: 1.17-100.50*) on the baseline ECG are linked to angiographic vasospasm [68].

For other modalities of physiological monitoring in vital signs, continuous EEG after SAH can detect an increased number of subclinical seizures and predict DCI many hours in advance. Various EEG patterns, such as the alpha/delta ratio, relative alpha variability, and total power, are suggestive of DCI [48]. Additionally, impaired cerebral autoregulation, assessed with transcranial Doppler (TCD) and evaluated using the moving correlation coefficient Mx, calculated from spontaneous fluctuations of cerebral blood flow velocities (CBFV) and ABP, is predictive of DCI in patients with large artery vasospasm after SAH. This finding suggests that including CBFV and cerebral autoregulation in prognosis research of DCI after SAH may improve the prediction of DCI [69].

Vasospasm and DCI, are critical outcomes in post-SAH management due to their frequent occurrence and significant associations with poor outcomes. DCI is a significant, preventable cause of mortality and poor neurological outcomes, making early detection vital. Age, gender, treatment modalities, and timing of treatments influence the risk of vasospasm and DCI, though studies show conflicting results on age-related risk. Pre-existing conditions like hypertension, diabetes, and smoking increase DCI risk. Elevated biomarkers, such as troponin, CK-MB, BNP, and ECG abnormalities, such as ST depression, QT prolongation, are significant predictors. Continuous EEG and TCD can also predict DCI by detecting subclinical seizures and impaired cerebral autoregulation. Figure 2.7 reviews prognostic risk factors for DCI and vasospasm in univariate analysis after spontaneous SAH, visualised with forest plots.

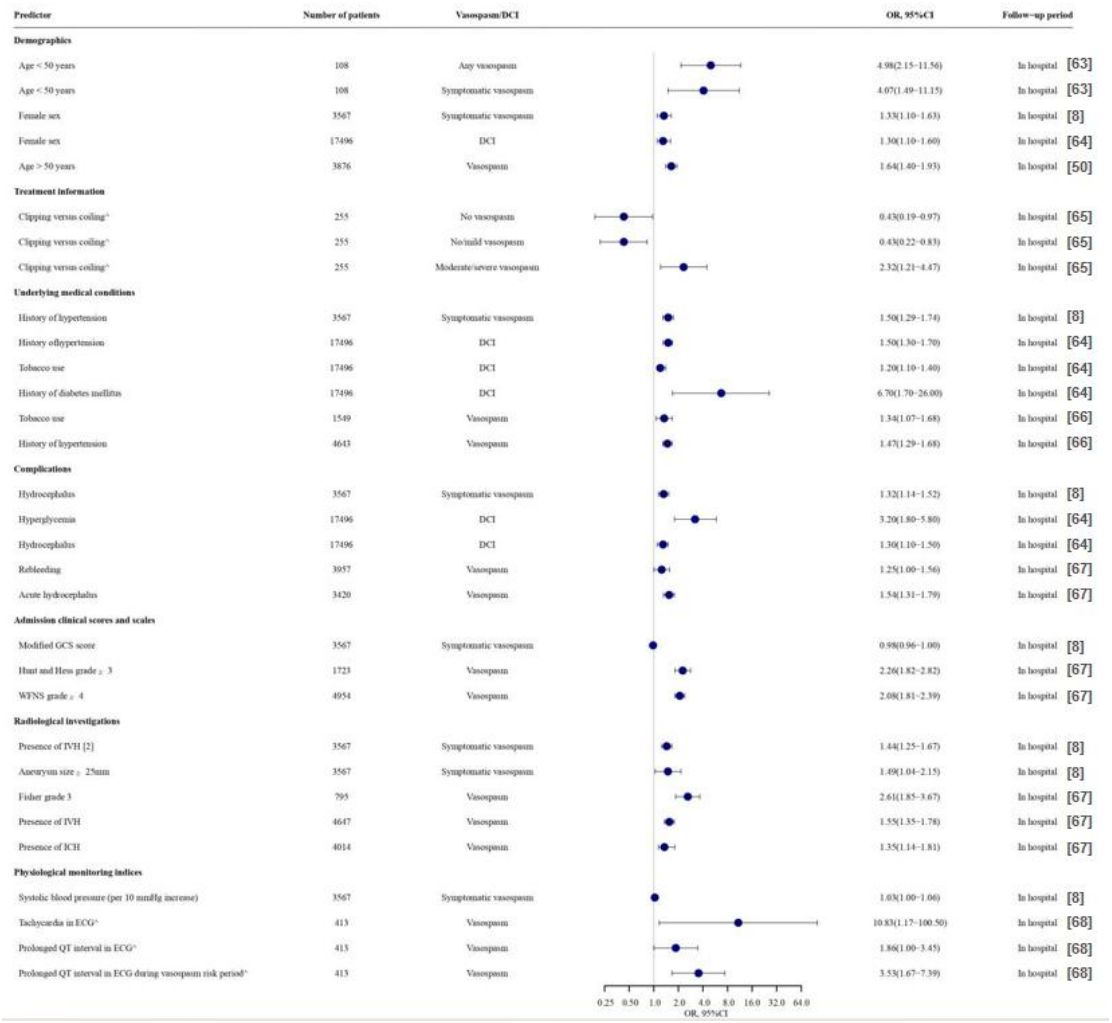


Figure 2.7: Forest plots of prognostic risk factors for DCI and vasospasm in univariate analysis after spontaneous SAH

2.3.6 Hydrocephalus

Hydrocephalus, one of the four major complications following SAH, can lead to severe neurological deterioration and increased mortality risk, which may occur at various stages post SAH. Compared to vasospasm and DCI, there is a lack of sufficient studies on the prognostic factors of hydrocephalus. However, early detection of hydrocephalus risk is crucial for monitoring symptom development and initiating prompt treatment. Reported prognostic factors for hydrocephalus can be broadly categorised into demographics, medical conditions on admission, and radiological findings.

Age significantly influences the prognosis of hydrocephalus after spontaneous SAH. A previously discussed study reported a strong association between age and hydrocephalus on admission (*p=0.0001*) [50]. Additionally, patients older than 60 years are at higher risk for developing shunt-dependent hydrocephalus, allowing for early CSF diversion to reduce parenchymal damage. Other independent risk factors

for shunt-dependent hydrocephalus include poor Hunt and Hess scores, presence of IVH, aneurysms located on the posterior circulation, and complications such as re-bleeding (*p<0.05*) [40][70].

The causes of SAH significantly affect the incidence of post-SAH acute hydrocephalus. A prospective cohort study comparing aneurysmal and non-aneurysmal SAH found that acute hydrocephalus is more common in non-aneurysmal non-perimesencephalic SAH than in aneurysmal SAH, and it is rare in non-aneurysmal perimesencephalic SAH (*p<0.0001*) [54].

Finally, prognostic factors for secondary normal-pressure hydrocephalus (NPH) have been reported. These factors include age (≥60 years) (*Age-adjusted: p<0.001, OR=2.44, 95%CI: 1.94-3.10; multivariate: p<0.001, OR=1.96, 95%CI: 1.47-2.62*), acute hydrocephalus (*Age-adjusted: p<0.001, OR=3.62, 95%CI: 2.87-4.57; multivariate: p<0.001, OR=3.60, 95%CI: 2.77-4.69*), aneurysm located on anterior cerebral artery compared with middle cerebral artery (*Age-adjusted: p<0.001, OR=1.93, 95%CI: 1.42-2.61; multivariate: p<0.001, OR=2.02, 95%CI: 1.39-2.62*), clipping versus coiling (*Age-adjusted: p=0.002, OR=1.59, 95%CI: 1.18-2.14; multivariate: p<0.001, OR=1.97, 95%CI: 1.36-2.85*), Hunt and Hess scale 3 (*Age-adjusted: p<0.001, OR=2.92, 95%CI: 2.17-3.91; multivariate: p<0.001, OR=2.32, 95%CI: 1.63-3.29*), 4 or 5 (*Age-adjusted: p<0.001, OR=3.78, 95%CI: 2.88-4.96; multivariate: p<0.001, OR=2.62, 95%CI: 1.85-3.73*), and the Fisher grade 3 (*Age-adjusted: p<0.001, OR=2.15, 95%CI: 1.53-3.01; multivariate: p=0.001, OR=1.95, 95%CI: 1.30-2.91*), and 4 (*Age-adjusted: p<0.001, OR=3.34, 95%CI: 2.21-5.05; multivariate: p<0.001, OR=2.99, 95%CI: 1.750-5.10*) in CT findings. [71]

Hydrocephalus, a major complication of SAH, causes severe neurological deterioration and increased mortality risk. Although fewer prognosis studies focus on hydrocephalus compared to vasospasm and DCI, early detection of hydrocephalus is important for prompt treatment and improving clinical outcomes. As discussed in section 2.3.6, key prognostic factors include demographics, medical conditions on admission, and radiological findings. Patients over 60 are at higher risk for shunt-dependent hydrocephalus. Other risk factors are poor Hunt and Hess scores, IVH, posterior circulation aneurysms, and re-bleeding.

Acute hydrocephalus is more common in non-aneurysmal non-perimesencephalic SAH and rare in non-aneurysmal perimesencephalic SAH. Secondary NPH risk factors include age, acute hydrocephalus, anterior cerebral artery aneurysms, clipping versus coiling, higher Hunt and Hess scales, and higher Fisher grades on CT. Identifying at-risk patients improves outcomes. Figure 2.8 reviews prognostic risk factors for hydrocephalus in univariate analysis after spontaneous SAH, visualised with forest plots.

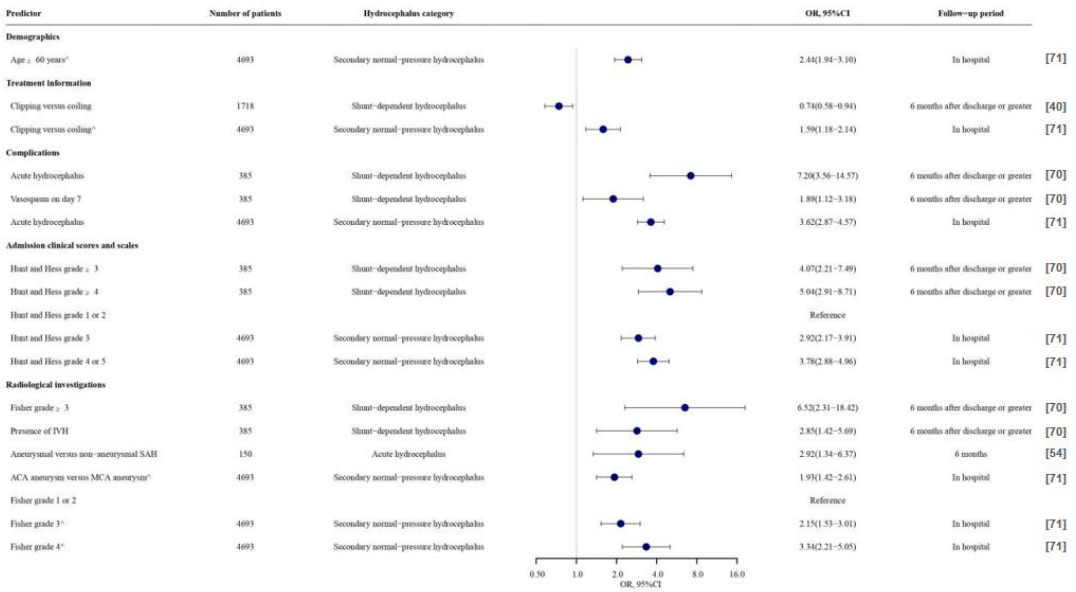


Figure 2.8: Forest plots of prognostic risk factors for hydrocephalus in univariate analysis after spontaneous SAH

2.3.7 Other complications

In addition to mortality and major complications commonly examined in prognosis studies of spontaneous SAH, other complications and their associated risk factors have also drawn research interest. These complications, often associated with better clinical outcomes and lower incidence compared with major complications, can be either neurological, e.g., seizures and cerebral infarction, or non-neurological, e.g., cardiac and pulmonary complications. This section will briefly discuss these complications and their associated risk factors.

Seizures occur in only 1% to 7% of patients with SAH. Their development is associated with older age, aneurysms located in the middle cerebral artery, a history of seizure disorders, and other post-SAH complications such as intracerebral hematoma, cerebral infarction, re-bleeding, and poor neurological grades [39]. Additionally, EEG monitoring and derived indices are crucial for detecting and predicting seizures [47].

Cerebral infarction, the death of brain tissue due to a lack of blood supply, can be predicted by various factors. These include the neurological grade on admission (e.g., Hunt and Hess grade, $p<0.0001$), radiological findings (e.g., Fisher grade, $p<0.0001$), and the presence of IVH and/or ICH on CT scan ($p=0.0005$). Chronic diseases such as hypertension ($p=0.0010$) and complications like re-bleeding ($p=0.0014$) are also significant predictors. Biomarkers in haematological tests and indices from vital signs, such as serum glucose level ($p=0.0133$), QTc time ($p=0.0376$), LVH ($p=0.0001$), and ST depression ($p=0.0207$) on ECG, are important indicators. In multivariate analysis, Fisher grade $\geqslant$ 3 ($p=0.0001$, $OR=7.64$, 95% $CI: 2.94$-24.05), hypertension

(*p=0.0284, OR=2.18, 95% CI: 1.09-3.36*), and LVH (*p=0.0224, OR=2.19, 95% CI: 1.11-4.32*) on ECG remain significant predictors [72].

Cardiac complications, such as arrhythmia and myocardial infarction, and pulmonary complications, such as acute respiratory distress syndrome (ARDS), are common non-neurological complications following spontaneous SAH. These categories include various specific diseases and will be briefly discussed here. For example, age (per 10-year increment) (*p=0.0018, OR=0.59, 95% CI: 0.38-0.91*) and aneurysm position (anterior versus posterior) (*p=0.028, OR=4.00, 95% CI: 1.12-13.8*) have been reported to predict patterns of left ventricular dysfunction after SAH [73]. Age is also significantly associated with the incidence of pulmonary complications after SAH (*p=0.0084*) [53].

Other predictors of left ventricular dysfunction include elevated CK-MB levels, female gender, and poor neurological grade [39]. Troponin, a key biomarker for cardiac failure, serves as a strong predictor for both cardiac complications, e.g., left ventricular dysfunction and pulmonary complications, e.g., pulmonary oedema. Arrhythmias, often manifesting as ECG changes such as ST segment and T wave alterations, are common in SAH patients, with repolarisation abnormalities being the most frequent. Notably, ST depression is associated with higher Hunt and Hess grades and WFNS scores [39].

2.4 Datasets of this thesis

This study utilises multiple datasets across different chapters to support the development of the proposed modeling framework. Each dataset contains specific prognostic factors and outcome events. In this section, data contained in each chapter's study, sampling frequency, and limitations of dataset will be discussed in details.

The dataset used in Chapter 3 is derived from MIMIC-3, a publicly available, large-scale critical care database containing clinical data, physiological waveforms, and clinical outcomes of ICU patients. Specifically, this study utilises a matched waveform subset from MIMIC-3, which provides high-frequency physiological monitoring waveforms alongside structured clinical data.

This dataset includes two key components: baseline covariates and continuous physiological monitoring data. Baseline covariates, obtained from the MIMIC-3 clinical database, include demographic factors such as age and sex, as well as underlying conditions such as hypertension, diabetes, and cardiovascular disease.

The physiological monitoring data, extracted from the matched waveform subset, consists of high-resolution ABP and ECG waveforms (125 Hz sampling frequency), allowing for the calculation of haemodynamic indices used in the study, including ECG indices and blood pressure variabilities. Population characteristics of patients

included in Chapter 3 are presented by Table 2.3.

Covariate		All (n=108)	Death (n=27)	Survival (n=81)
Demographics	Age⩾ 65 years	40 (37.04%)	14 (51.85%)	26 (32.10%)
	Female	66 (61.11%)	16 (59.26%)	50 (61.73%)
Chronic diseases	Hypertension	53 (49.07%)	17 (62.96%)	36 (44.44%)
Complications and comorbidities	Cerebral oedema	25 (23.15%)	11 (40.74%)	14 (17.28%)
	Hydrocephalus	39 (36.11%)	10 (37.04%)	29 (35.80%)
	Seizures	10 (9.26%)	1 (3.70%)	9 (11.11%)
	Atrial fibrillation	10 (9.26%)	3 (11.11%)	7 (8.64%)

Table 2.3: Clinical characteristics of patients included in Chapter 3

A major limitation of this dataset is the presence of artefacts and missing data in the physiological waveforms. While artefact rejection techniques help improve signal quality, this process may lead to data exclusion and potential selection bias. Additionally, not all SAH patients in MIMIC-3 have matched waveform data, limiting the sample size for dynamic haemodynamic analysis.

In Chapter 4, ABP waveforms from the UCI dataset are included for assessing curve-fitting performance and evaluating artefact rejection methods. The UCI dataset is a filtered version of the MIMIC-II waveform database, containing 12,000 instances of ABP waveforms from 942 patients. Since short waveform recordings are more susceptible to artefacts and noises, only instances with waveform lengths longer than 5 minutes were selected.

Upon manual inspection, among 4124 instances of waveforms longer than 5 minutes, 3,600 instances were identified as abnormal waveforms, with the most common abnormality being the absence of a dicrotic notch (1,058 instances). Other waveform

irregularities included bisferiens pulse (307 instances), dicrotic pulse (407 instances), arrhythmias (626 instances), bigeminal pulse (60 instances), and pulsus paradoxus (43 instances). Additionally, 560 waveform instances were excluded due to severe artifacts, ensuring that only high-quality waveforms were used for further analysis. Abnormal waveform instances and clinical associations are presented in Table 2.4.

Waveform Abnormality	Instances (3600 in total)	Percentage (%)
Absence of Dicrotic Notch	1058	29.39%
Bisferiens Pulse	307	8.53%
Arrhythmias	626	17.39%
Bigeminal Pulse	60	1.67%
Pulsus Paradoxus	43	1.19%
Dicrotic Pulse	407	11.31%
Severe Artifacts	560	15.56%
Multiple Abnormalities	539	14.97%

Table 2.4: Summary of ABP instances and identified abnormalities included in Chapter 3

A major limitation is that this study primarily includes normal-morphology ABP waveforms, excluding many pathological waveforms due to concerns about curve-fitting accuracy. This exclusion may limit the applicability of the proposed methods to real-world clinical settings, where waveform abnormalities are common due to underlying cardiovascular conditions and haemodynamic instability.

The dataset in Chapter 5 was sourced from MIMIC-IV, a publicly available critical care database containing electronic health records from Beth Israel Deaconess Medical Center (2008–2019). A total of 766 spontaneous SAH patients were initially identified using ICD-9-CM code 430 and ICD-10-CM code I60, with 65 patients excluded due to short hospital stays (<24 hours) or missing vital signs and neurological assessments, resulting in a final cohort of 701 patients.

As shown in Table 2.5, the median age was 59 years (IQR: 50-70), and 58.35% (409/701) were female, aligning with SAH epidemiology. Hypertension (48.50%) was the most common comorbidity, followed by hydrocephalus (31.53%), respiratory failure (21.56%), and cerebral edema (18.69%), indicating frequent neurological complications. Outcomes were classified based on discharge destinations, with 48.93% (343/701) achieving good recovery (discharge to home/rehabilitation) and 51.07% (358/701) having poor outcomes (mortality, long-term care, hospice).

Summary of neurosurgeries received by these patients is also shown in Table 2.5. This table reflects modern neurosurgical trends, with coiling (235 patients) being the preferred treatment over clipping (37 patients) due to its minimally invasive nature. The small number of patients receiving coiling and clipping is likely due to factors

such as non-aneurysmal SAH cases, early mortality, and poor clinical status, making intervention unfeasible. Craniotomies (35 patients) were performed for tumor resection, haemorrhage evacuation, or trauma, while spinal decompression (92 patients) suggests a notable presence of spinal pathology.

Covariate		All (n = 701)	Good outcome (n = 343)	Poor outcome (n = 358)
Demographics	Age	Median: 59 (IQR: 50 - 70)	Median: 49.25 (IQR: 56 - 68)	Median: 61 (IQR: 51 - 73)
	Female	409 (58.35%)	192 (55.98%)	217 (60.61%)
Underlying conditions	Alcohol	23 (3.28%)	9 (2.62%)	14 (3.91%)
	Tobacco	132 (18.83%)	68 (19.83%)	64 (17.88%)
	Diabetes	76 (10.84%)	32 (9.33%)	44 (12.29%)
	Essential hypertension	340 (48.50%)	154 (44.90%)	186 (51.96%)
Complications	Cerebral oedema	131 (18.69%)	24 (7.00%)	107 (29.89%)
	Cerebral infarction	69 (9.84%)	15 (4.37%)	54 (15.08%)
	Respiratory failure	149 (21.56%)	11 (3.21%)	138 (38.55%)
	Hydrocephalus	221 (31.53%)	34 (3.21%)	187 (52.23%)
	Vasospasm	55 (7.85%)	15 (4.37%)	40 (11.17%)
Neurosurgeries	Clipping	37 (5.28%)	25 (7.29%)	12 (3.35%)
	Coiling	239 (34.09%)	168 (48.98%)	71 (19.83%)
	Craniotomies	39 (5.56%)	20 (5.83%)	19 (5.31%)
	Spinal decompression	96 (13.69%)	44 (12.83%)	52 (14.53%)

Table 2.5: Clinical characteristics and neurosurgeries of included dataset in Chapter 5

Despite its strengths in longitudinal neurological and intervention data, this dataset has limitations. The exclusion of short-stay patients may introduce selection bias, and changes in clinical practices over time could impact outcome trends.

The dataset used in Chapter 6 was also sourced from MIMIC-IV. A total of 612 spontaneous SAH patients were included to investigate the pharmacological effects on SAH recovery, selected based on hospital stays longer than one day, documented neurological assessments, and identified pharmacological records, including detailed medication administration data. All patients were aged 18 or over, and each had identifiable records of medication usage, enabling the analysis of drug exposure in relation to neurological recovery and outcomes.

The cohort had a median age of 58 years (IQR: 49-69), with 58.33% (357/612) being

female. Essential hypertension was the most common comorbidity, followed by hydrocephalus, respiratory failure, and cerebral oedema. Outcomes were assessed over a 14-day study period, covering both acute and sub-acute SAH phases. Table 2.6 presents the clinical characteristics of dataset included in Chapter 6, while Table 2.7 presents of details of pharmacological information.

Covariate		All (612)	Good outcome(283)	Poor outcome(329)
Demographics	Age	Median: 58	Median: 49.25	Median: 61
	Female	409	156	201
Underlying conditions	Alcohol	21	9	12
	Tobacco	117	57	60
	Diabetes	61	24	37
	Essential hypertension	294	125	169
Complications	Cerebral oedema	128	24	106
	Cerebral infarction	65	13	52
	Respiratory failure	148	10	138
	Hydrocephalus	213	31	182
	Vasospasm	55	15	40

Table 2.6: Clinical characteristics of included dataset in Chapter 6

Medication	Patients (All=612)	Percentage (%)
Nimodipine	474	77.45%
Hydralazine	185	30.23%
Acetaminophen	413	67.48%
Levetiracetam	220	35.95%
Morphine	189	30.88%
Mannitol	63	10.29%
Labetalol	161	26.31%
Nicardipine	144	23.53%
Heparin	222	36.27%

Table 2.7: Pharmacological details of included dataset in Chapter 6

The dataset used in Chapter 6, while rich in pharmacological and clinical detail, has several limitations. Medication administration records from MIMIC-IV may be incomplete or imprecise, particularly in terms of dosage timing and discontinuation. Moreover, treatments were not randomised, introducing potential confounding by indication, as more severely ill patients were more likely to receive certain drugs. Additionally, the temporal resolution of dynamic covariates such as GCS scores and biomarkers varies, making it difficult to align drug exposure precisely with clinical responses.

The dataset used in Chapter 7 combines both real-world clinical data and simulated data to support the development of a multi-state prognostic model for SAH progression. The real-world component is derived from the dataset introduced in Chapter 6, sourced from the MIMIC-IV database. To supplement this, simulated data representing time-to-complication events, such as vasospasm and hydrocephalus, were generated based on transition patterns and time distributions observed in the real cohort.

However, this dataset has limitations. The real-world data are constrained to short-term follow-up, limiting the ability to capture late-onset complications or recovery trajectories. Furthermore, simulated time-to-event data, while informed by empirical distributions, rely on assumptions that may not fully reflect the complexity or variability of actual patient pathways.

2.5 Summary and discussion

This chapter reviews and discusses relevant concepts, methodologies, and prognosis studies for spontaneous SAH. It examines the evolution of prognosis from experience-based to evidence-based, generalised to personalised, and static to dynamic approaches. Evidence-based prognosis utilises scientific research and clinical trials for more reliable predictions. Generalised models like the Hunt and Hess scale have evolved into personalised models such as the WFNS grading system and FRESH score. Dynamic prognosis allows continuous updates of prognostic factors, capturing changes during disease progression. These advancements significantly enhance prognosis research and improve the clinical utility of prognostic models.

We then reviewed statistical tools for analysing continuous, binary, and time-to-event outcomes, as well as common metrics for quantifying predictor effects. For continuous outcomes, linear regression models are used to estimate relationships between predictors and the outcome variable, with the R^2 measuring the proportion of variance explained and RMSE quantifying prediction accuracy. For binary outcomes, logistic regression models often employ the OR to measure the odds of an event occurring in one group relative to another, preferred over RR in multivariate analysis. For time-to-event outcomes, survival analysis uses the HR to assess the effect of a prognostic factor on the risk of an event, with AUC and the Brier score evaluating the predictive performance, which can be time-dependent for dynamic prognosis. Other model performance measures, such as calibration, interpretability, and reproducibility, are also discussed to ensure the robustness and clinical applicability of prognostic models.

Finally, we reviewed previous studies on spontaneous SAH, focusing on common clinical outcomes like mortality and post-SAH complications, and their associated prognostic factors. These factors include demographics, treatment information, pre-existing medical conditions, clinical scores on admission, radiological findings,

haematological test results, and physiological monitoring of vital signs. Forest plots based on odds ratios from univariate analyses were used to visualise the effects of these prognostic factors on outcomes. In addition to reviewing prognostic methodologies and studies, this chapter also outlines the datasets employed across Chapters 3 to 7, which collectively support the development and evaluation of the proposed prognostic models.

Age, Hunt and Hess/WFNS grades, and Fisher grade consistently provided valuable insights across different outcomes, while specific predictors strongly indicated particular outcomes, such as high BNP levels indicating an increased mortality risk. Other outcome measures, including ICU/hospital discharges, length of ICU/hospital stay, pathophysiological outcomes, and biomarkers like inflammatory markers, have also been employed in SAH research to provide a comprehensive understanding of patient prognosis. [74] Beyond these prognostic factors, genetic determinants of vasospasm, DCI, and clinical outcomes have also drawn substantial research interest. The increasing availability of genetic datasets, such as those from Biobank, has facilitated the exploration of genetic risk factors associated with SAH outcomes, further enriching comprehensive and personalised prognosis. [75]

In reviewing prognostic studies for SAH, it becomes evident that while most focus on identifying prognostic factors, there is a lack of comprehensive prognostic model research aimed at clinical utility. Existing prognostic tools, such as the FRESH and WFNS scales, while useful, do not fully provide comprehensive and personalised prognostic profiles. Comprehensive and personalised models can improve prediction accuracy by integrating various types and modalities of prognostic information, including different aspects of measuring patients' clinical conditions.

Another potential improvement for SAH prognostication is the implementation of dynamic prognostic models. Current studies often rely on static prognostications at specific time points, limiting their effectiveness in monitoring disease progression. Dynamic models, which adjust predictions with new prognostic information available, offer improved clinical utility, particularly given the rapid evolving nature of SAH. Furthermore, the potential of multi-state modelling to account for the various prognostic stages and complications in SAH progression remains underexplored. Such models can capture changes of medical conditions in disease progression, improving personalised and comprehensive prognosis as well as enabling the simultaneous predictions of complications and clinical outcomes. These research gaps will be covered in the studies of this thesis.

Reference for chapter 2

[1] Sackett, D.L., Rosenberg, W.M. and Gray, J.A., 1996. AM, Haynes, RB, & Richardson, WS (1996). Evidence based medicine: what it is and what it isn't. British Medical Journal, 312(7023), pp.71-72.

[2] Symonds, C.P., 1924. Spontaneous sub-arachnoid haemorrhage.

[3] Hunt, W.E. and Hess, R.M., 1968. Surgical risk as related to time of intervention in the repair of intracranial aneurysms. Journal of neurosurgery, 28(1), pp.14-20.

[4] Teasdale, G.M., Drake, C.G., Hunt, W., Kassell, N., Sano, K., Pertuiset, B. and De Villiers, J.C., 1988. A universal subarachnoid hemorrhage scale: report of a committee of the World Federation of Neurosurgical Societies. Journal of neurology, neurosurgery, and psychiatry, 51(11), p.1457.

[5] Witsch, J., Frey, H.P., Patel, S., Park, S., Lahiri, S., Schmidt, J.M., Agarwal, S., Falo, M.C., Velazquez, A., Jaja, B. and Macdonald, R.L., 2016. Prognostication of long-term outcomes after subarachnoid hemorrhage: The FRESH score. Annals of neurology, 80(1), pp.46-58.

[6] Zolfaghari, B., Mirsadeghi, L., Bibak, K. and Kavousi, K., 2023. Cancer prognosis and diagnosis methods based on ensemble learning. ACM Computing Surveys, 55(12), pp.1-34.

[7] Kumarakulasinghe, N.B., Blomberg, T., Liu, J., Leao, A.S. and Papapetrou, P., 2020, July. Evaluating local interpretable model-agnostic explanations on clinical machine learning classification models. In 2020 IEEE 33rd international symposium on computer-based medical systems (CBMS) (pp. 7-12). IEEE.

[8] Rosengart, A.J., Schultheiss, K.E., Tolentino, J. and Macdonald, R.L., 2007. Prognostic factors for outcome in patients with aneurysmal subarachnoid hemorrhage. Stroke, 38(8), pp.2315-2321.

[9] Cox, D.R., 1972. Regression models and life-tables. Journal of the Royal Statistical Society: Series B (Methodological), 34(2), pp.187-202.

[10] Kuitunen, I., Ponkilainen, V.T., Uimonen, M.M., Eskelinen, A. and Reito, A., 2021. Testing the proportional hazards assumption in cox regression and dealing with possible non-proportionality in total joint arthroplasty research: methodological perspectives and review. BMC musculoskeletal disorders, 22(1), p.489.

[11] Wulfsohn, M.S. and Tsiatis, A.A., 1997. A joint model for survival and longitudinal data measured with error. Biometrics, pp.330-339.

[12] Thorsen-Meyer, H.C., Nielsen, A.B., Nielsen, A.P., Kaas-Hansen, B.S., Toft, P., Schierbeck, J., Strøm, T., Chmura, P.J., Heimann, M., Dybdahl, L. and Spangsege, L., 2020. Dynamic and explainable machine learning prediction of mortality in patients in the intensive care unit: a retrospective study of high-frequency data in electronic patient records. The Lancet Digital Health, 2(4), pp.e179-e191.

[13] Ding, H., Yuan, M., Yang, Y., Gupta, M. and Xu, X.S., 2024. Evaluating prognostic value of dynamics of circulating lactate dehydrogenase in colorectal cancer using modeling and machine learning. Clinical Pharmacology & Therapeutics, 115(4), pp.805-814.

[14] Rajkomar, A., Dean, J. and Kohane, I., 2019. Machine learning in medicine. New England Journal of Medicine, 380(14), pp.1347-1358.

[15] Erango, M.A., Goshu, A.T., Buta, G.B. and Dessisoa, A.H., 2017. Bayesian joint modelling of survival of HIV/AIDS patients using accelerated failure time data and longitudinal CD4 cell counts. Br J Med Med Res, 20(6), pp.1-12.

[16] Ingall, T., Asplund, K., Mähönen, M. and Bonita, R., 2000. A multinational comparison of subarachnoid hemorrhage epidemiology in the WHO MONICA stroke study. Stroke, 31(5), pp.1054-1061.

[17] Mine, T., Sato, I., Kishima, H., Kodani, T. and Masuyama, T., 2013. Brain Natriuretic Peptide as a Predictor of Outcome for Non-traumatic Subarachnoid Hemorrhage.

[18] Chen, H., Cohen, P. and Chen, S., 2010. How big is a big odds ratio? Interpreting the magnitudes of odds ratios in epidemiological studies. Communications in Statistics — simulation and Computation®, 39(4), pp.860-864.

[19] Hammer, A., Steiner, A., Ranaie, G., Yakubov, E., Erbguth, F., Hammer, C.M., Killer-Oberpfalzer, M., Steiner, H. and Janssen, H., 2018. Impact of comorbidities and smoking on the outcome in aneurysmal subarachnoid hemorrhage. Scientific Reports, 8(1), pp.1-7.

[20] Zou, G., 2004. A modified poisson regression approach to prospective studies with binary data. American journal of epidemiology, 159(7), pp.702-706.

[21] Barros, A.J. and Hirakata, V.N., 2003. Alternatives for logistic regression in cross-sectional studies: an empirical comparison of models that directly estimate the prevalence ratio. BMC medical research methodology, 3(1), pp.1-13.

[22] Collett, D., 2015. Modelling survival data in medical research. CRC press.

[23] Lin, F., He, Q., Zhuo, L., Zhao, M., Ye, G., Gao, Z., Huang, W., Cai, L., Wang, F., Shangguan, H. and Fang, W., 2023. A nomogram predictive model for long-term survival in spontaneous intracerebral hemorrhage patients without cerebral herniation at admission. Scientific Reports, 13(1), p.3126.

[24] Faruk, A., 2018, March. The comparison of proportional hazards and accelerated failure time models in analyzing the first birth interval survival data. In Journal of Physics: Conference Series (Vol. 974, No. 1, p. 012008). IOP Publishing.

[25] Alsefri, M., Sudell, M., García-Fiñana, M. and Kolamunnage-Dona, R., 2020. Bayesian joint modelling of longitudinal and time to event data: a methodological review. BMC medical research methodology, 20, pp.1-17.

[26] Lázaro, E., Armero, C. and Alvares, D., 2021. Bayesian regularization for flexible baseline hazard functions in Cox survival models. Biometrical Journal, 63(1), pp.7-26.

[27] DeLong, D.M., Guirguis, G.H. and So, Y.C., 1994. Efficient computation of subset selection probabilities with application to Cox regression. Biometrika, 81(3), pp.607-611.

[28] Bender, R., Augustin, T. and Blettner, M., 2005. Generating survival times to simulate Cox proportional hazards models. Statistics in medicine, 24(11), pp.1713-1723.

[29] Chapman, J.W., O'callaghan, C.J., Hu, N., Ding, K., Yothers, G.A., Catalano, P.J., Shi, Q., Gray, R.G., O'connell, M.J. and Sargent, D.J., 2013. Innovative estimation of survival using log-normal survival modelling on ACCENT database. British journal of cancer, 108(4), pp.784-790.

[30] Fisher, L.D. and Lin, D.Y., 1999. Time-dependent covariates in the Cox proportional-hazards regression model. Annual review of public health, 20(1), pp.145-157.

[31] Asar, Ö., Ritchie, J., Kalra, P.A. and Diggle, P.J., 2015. Joint modelling of repeated measurement and time-to-event data: an introductory tutorial. International journal of epidemiology, 44(1), pp.334-344.

[32] Rizopoulos, D., 2012. Joint models for longitudinal and time-to-event data: With applications in R. CRC press.

[33] Lubbock, A.L. and Lopez, C.F., 2021. Programmatic modeling for biological systems. Current opinion in systems biology, 27, p.100343.

[34] Risselada, R., Lingsma, H.F., Bauer-Mehren, A., Friedrich, C.M., Molyneux, A.J., Kerr, R.S.C., Yarnold, J., Sneade, M., Steyerberg, E.W. and Sturkenboom, M.C.J.M., 2010. Prediction of 60 day case-fatality after aneurysmal subarachnoid haemorrhage: results from the International Subarachnoid Aneurysm Trial (ISAT). European journal of epidemiology, 25, pp.261-266.

[35] Schöller, K., Massmann, M., Markl, G., Kunz, M., Fesl, G., Brückmann, H., Pfefferkorn, T., Tonn, J.C. and Schichor, C., 2013. Aneurysmal subarachnoid hemorrhage in elderly patients: long-term outcome and prognostic factors in an interdisciplinary treatment approach. Journal of neurology, 260, pp.1052-1060.

[36] Dorhout Mees, S.M., Molyneux, A.J., Kerr, R.S., Algra, A. and Rinkel, G.J., 2012. Timing of aneurysm treatment after subarachnoid hemorrhage: relationship with delayed cerebral ischemia and poor outcome. Stroke, 43(8), pp.2126-2129.

[37] van der Schaaf, I., Algra, A., Wermer, M., Molyneux, A., Clarke, M.J., van Gijn, J. and Rinkel, G.J., 2005. Endovascular coiling versus neurosurgical clipping for patients with aneurysmal subarachnoid haemorrhage. Cochrane Database of Systematic Reviews, (4).

[38] Damodara, N., Amuluru, K., Nuoman, R., Bowers, C.A., Khandelwal, P., Moseley, S., Al-Shammari, H., El-Ghanem, M., Gandhi, C.D. and Al-Mufti, F., 2020. Body mass index and overall outcome following subarachnoid hemorrhage: an obesity paradox?. World Neurosurgery, 144, pp.e679-e684.

[39] Ganaw, A.E.A., Ahmed, S.M.G., Ehfeda, M. and Belkhair, S., 2022. Complications and Critical Care Management of Aneurysmal Subarachnoid Hemorrhage. Management of Subarachnoid Hemorrhage, pp.139-165.

[40] Duan, W., Pan, Y., Wang, C., Wang, Y., Zhao, X., Wang, Y., Liu, L. and CNSR Investigators, 2018. Risk factors and clinical impact of delayed cerebral ischemia after aneurysmal subarachnoid hemorrhage: analysis from the China National Stroke Registry. Neuroepidemiology, 50(2-3), pp.128-136.

[41] Friedman, J.A., Pichelmann, M.A., Piepgras, D.G., McIver, J.I., Toussaint III, L.G., McClelland, R.L., Nichols, D.A., Meyer, F.B., Atkinson, J.L. and Wijdicks, E.F., 2003. Pulmonary complications of aneurysmal subarachnoid hemorrhage. Neurosurgery, 52(5), pp.1025-1032.

[42] Weir, R.U., Marcellus, M.L., Do, H.M., Steinberg, G.K. and Marks, M.P., 2003. Aneurysmal subarachnoid hemorrhage in patients with Hunt and Hess grade 4 or 5: treatment using the Guglielmi detachable coil system. American journal of neuroradiology, 24(4), pp.585-590.

[43] Van der Bilt, I.A.C., Hasan, D., Vandertop, W.P., Wilde, A.A.M., Algra, A., Visser, F.C. and Rinkel, G.J.E., 2009. Impact of cardiac complications on outcome after aneurysmal subarachnoid hemorrhage: a meta-analysis. Neurology, 72(7), pp.635-642.

[44] Kawasaki, T., Azuma, A., Sawada, T., Sugihara, H., Kuribayashi, T., Satoh, M., Shimizu, Y. and Nakagawa, M., 2002. Electrocardiographic score as a predictor of mortality after subarachnoid hemorrhage. Circulation journal, 66(6), pp.567-570.

[45] Ascanio, L.C., Enriquez-Marulanda, A., Maragkos, G.A., Salem, M.M., Alturki, A.Y., Ravindran, K., Fehnel, C.R., Hanafy, K., Ogilvy, C.S., Thomas, A.J. and Moore, J.M., 2020. Effect of blood pressure variability during the acute period of subarachnoid hemorrhage on functional outcomes. Neurosurgery, 87(4), pp.779-787.

[46] Dowlati, E., Triano, M.J., Felbaum, D.R., Mai, J.C., Aulisi, E.F., Armonda, R.A. and Chang, J.J., 2021. Increased pulse pressure variability within the first 24 hours leads to poor disposition in subarachnoid hemorrhage patients. American Journal of Hypertension, 34(6), pp.645-650.

[47] Kondziella, D., Friberg, C.K., Wellwood, I., Reiffurth, C., Fabricius, M. and Dreier, J.P., 2015. Continuous EEG monitoring in aneurysmal subarachnoid hemorrhage: a systematic review. Neurocritical care, 22, pp.450-461.

[48] Zoerle, T., Lombardo, A., Colombo, A., Longhi, L., Zanier, E.R., Rampini, P. and Stocchetti, N., 2015. Intracranial pressure after subarachnoid hemorrhage. Critical care medicine, 43(1), pp.168-176.

[49] Ramakrishna, R., Stiefel, M., Udoteuk, J., Spiotta, A., Levine, J.M., Kofke, W.A., Zager, E., Yang, W. and LeRoux, P., 2008. Brain oxygen tension and outcome in patients with aneurysmal subarachnoid hemorrhage. Journal of neurosurgery, 109(6), pp.1075-1082.

[50] Lanzino, G., Kassell, N.F., Germanson, T.P., Kongable, G.L., Truskowski, L.L., Torner, J.C. and Jane, J.A., 1996. Age and outcome after aneurysmal subarachnoid hemorrhage: why do older patients fare worse?. Journal of neurosurgery, 85(3), pp.410-418.

[51] Schuiling, W.J., Algra, A., de Weerd, A.W., Leemans, P. and Rinkel, G.J., 2006. ECG abnormalities in predicting secondary cerebral ischemia after subarachnoid haemorrhage. Acta neurochirurgica, 148, pp.853-858.

[52] Eagles, M.E., Tso, M.K., Ayling, O.G., Wong, J.H. and MacDonald, R.L., 2020. Unfavorable outcome after good grade aneurysmal subarachnoid hemorrhage: exploratory analysis. World Neurosurgery, 144, pp.e842-e848.

[53] Pegoli, M., Mandrekar, J., Rabinstein, A.A. and Lanzino, G., 2015. Predictors of excellent functional outcome in aneurysmal subarachnoid hemorrhage. Journal of neurosurgery, 122(2), pp.414-418.

[54] Conzen, C., Weiss, M., Albanna, W., Seyfried, K., Schmidt, T.P., Nikoubashman, O., Stoppe, C., Clusmann, H. and Schubert, G.A., 2022. Baseline characteristics and outcome for aneurysmal versus non-aneurysmal subarachnoid hemorrhage: a prospective cohort study. Neurosurgical Review, pp.1-8.

[55] Boswell, S., Thorell, W., Gogela, S., Lyden, E. and Surdell, D., 2013. Angiogram-negative subarachnoid hemorrhage: outcomes data and review of the literature. Journal of Stroke and Cerebrovascular Diseases, 22(6), pp.750-757.

[56] Juvela, S., 1992. Alcohol consumption as a risk factor for poor outcome after aneurysmal subarachnoid haemorrhage. British Medical Journal, 304(6843), pp.1663-1667.

[57] Mocco, J., Ransom, E.R., Komotar, R.J., Schmidt, J.M., Sciacca, R.R., Mayer, S.A. and Connolly Jr, E.S., 2006. Preoperative prediction of long-term outcome in poor-grade aneurysmal subarachnoid hemorrhage. Neurosurgery, 59(3), pp.529-538.

[58] Faust, K., Horn, P., Schneider, U.C. and Vajkoczy, P., 2014. Blood pressure changes after aneurysmal subarachnoid hemorrhage and their relationship to cerebral vasospasm and clinical outcome. Clinical neurology and neurosurgery, 125, pp.36-40.

[59] Guo, L.M., Zhou, H.Y., Xu, J.W., Wang, Y., Qiu, Y.M. and Jiang, J.Y., 2011. Risk factors related to aneurysmal rebleeding. World neurosurgery, 76(3-4), pp.292-298.

[60] Beck, J., Raabe, A., Szelenyi, A., Berkefeld, J., Gerlach, R., Setzer, M. and Seifert, V., 2006. Sentinel headache and the risk of rebleeding after aneurysmal subarachnoid hemorrhage. Stroke, 37(11), pp.2733-2737.

[61] Lin, Q.S., Lin, Y.X., Lin, Z.Y., Yu, L.H., Dai, L.S. and Kang, D.Z., 2016. Systolic blood pressure variability is a novel risk factor for rebleeding in acute subarachnoid hemorrhage: a case‐control study. Medicine, 95(11).

[62] Francoeur, C.L. and Mayer, S.A., 2016. Management of delayed cerebral ischemia after subarachnoid hemorrhage. Critical care, 20, pp.1-12.

[63] Kale, S.P., Edgell, R.C., Alshekhlee, A., Haghighi, A.B., Sweeny, J., Felton, J., Kitchener, J., Vora, N., Bieneman, B.K., Cruz-Flores, S. and Abdulrauf, S., 2013. Age-associated vasospasm in aneurysmal subarachnoid hemorrhage. Journal of Stroke and Cerebrovascular Diseases, 22(1), pp.22-27.

[64] Macdonald, R.L., Rosengart, A., Huo, D. and Karrison, T., 2003. Factors associated with the development of vasospasm after planned surgical treatment of aneurysmal subarachnoid hemorrhage. Journal of neurosurgery, 99(4), pp.644-652.

[65] Gross, B.A., Lai, P.M.R., Frerichs, K.U. and Du, R., 2014. Treatment modality and vasospasm after aneurysmal subarachnoid hemorrhage. World neurosurgery, 82(6), pp.e725-e730.

[66] de Rooij, N.K., Rinkel, G.J., Dankbaar, J.W. and Frijns, C.J., 2013. Delayed cerebral ischemia after subarachnoid hemorrhage: a systematic review of clinical, laboratory, and radiological predictors. Stroke, 44(1), pp.43-54.

[67] Inagawa, T., 2016. Risk factors for cerebral vasospasm following aneurysmal subarachnoid hemorrhage: a review of the literature. World neurosurgery, 85, pp.56-76.

[68] Ibrahim, G.M. and Macdonald, R.L., 2012. Electrocardiographic changes predict angiographic vasospasm after aneurysmal subarachnoid hemorrhage. Stroke, 43(8), pp.2102-2107.

[69] Calviere, L., Nasr, N., Arnaud, C., Czosnyka, M., Viguier, A., Tissot, B., Sol, J.C. and Larrue, V., 2015. Prediction of delayed cerebral ischemia after subarachnoid hemorrhage using cerebral blood flow velocities and cerebral autoregulation assessment. Neurocritical care, 23, pp.253-258.

[70] de Oliveira, J.G., Beck, J., Setzer, M., Gerlach, R., Vatter, H., Seifert, V. and Raabe, A., 2007. Risk of shunt-dependent hydrocephalus after occlusion of ruptured intracranial aneurysms by surgical clipping or endovascular coiling: a single-institution series and meta-analysis. Neurosurgery, 61(5), pp.924-934.

[71] Yamada, S., Ishikawa, M., Yamamoto, K., Ino, T., Kimura, T. and Kobayashi, S., 2015. Aneurysm location and clipping versus coiling for development of secondary normal-pressure hydrocephalus after aneurysmal subarachnoid hemorrhage: Japanese Stroke DataBank. Journal of neurosurgery, 123(6), pp.1555-1561.

[72] Inagawa, T., Yahara, K. and Ohbayashi, N., 2014. Risk factors associated with cerebral vasospasm following aneurysmal subarachnoid hemorrhage. Neurologia medico-chirurgica, 54(6), pp.465-473.

[73] Khush, K., Kopelnik, A., Tung, P., Banki, N., Dae, M., Lawton, M., Smith, W., Drew, B., Foster, E. and Zaroff, J., 2005. Age and aneurysm position predict patterns of left ventricular dysfunction after subarachnoid hemorrhage. Journal of the American Society of Echocardiography, 18(2), pp.168-174.

[74] Andersen, C.R., Fitzgerald, E., Delaney, A. and Finfer, S., 2019. A systematic review of outcome measures employed in aneurysmal subarachnoid hemorrhage (aSAH) clinical research. Neurocritical care, 30, pp.534-541.

[75] Biobank, U.K., 2014. About uk biobank.

Chapter 3 Personalised dynamic survival prediction with vital sign indices in SAH patients

In Chapter 2, prognostic factors for clinical outcomes following spontaneous SAH were investigated. Among these factors, indices extracted from the physiological monitoring of vital signs emerged as critical sources of dynamic prognostic information. These indices not only aid in the development of dynamic prognostic models for SAH patients but also play a pivotal role in predicting the risks of mortality, re-bleeding, vasospasm, DCI, and poor neurological outcomes, as discussed in the previous chapter.

Among the various modalities of physiological monitoring, indices extracted from arterial blood pressure (ABP) and electrocardiogram (ECG) are the most prevalent in prognostic studies and serve as common risk predictors for various complications and mortality. These two modalities are also the most frequently used in the critical care of spontaneous SAH patients. Consequently, dynamic prognostic models incorporating ABP and ECG indices are more practical and clinically applicable.

This chapter will explore the prognostic value of vital sign indices, particularly those derived from ABP and ECG measurements, and examine how these indices can be utilised to develop prognostic models for spontaneous SAH. We will start by outlining the methods for extracting prognostic information from ABP and ECG waveforms. Using these extracted indices, we will develop a personalised dynamic prediction model. Finally, we will discuss the main findings, clinical significance, and limitations of this study.

3.1 Feature extraction from ABP and ECG measurements

This section will focus on extracting prognostic factors from ABP and ECG measurements for use in dynamic prognostic models. First, we will define and discuss common prognostic features that can be utilised as predictors for various clinical outcomes following spontaneous SAH, based on the preliminary discussion in Chapter 2. Next, we will outline the methods for waveform annotation and the subsequent feature extraction and calculation based on these annotations.

3.1.1 Prognostic features in ABP and ECG measurements

According to the review on indices of ABP monitoring in spontaneous SAH prognosis research in chapter 2, ABP indices can be loosely categorised into characteristic pressure values and the variability of these pressures. As illustrated in Figure 3.1, waveforms are segmented into cardiac cycles based on the location of the diastolic trough. The characteristic pressure values include systolic pressure P_s, dicrotic notch

P_n, dicrotic peak P_v, and diastolic pressure P_d. These values can be directly recorded from the waveforms, with systolic pressure being the most significant in prognosis research for spontaneous SAH. Its level can be used as a risk factor for mortality, re-bleeding, and neurological outcomes, as discussed in the previous chapter.

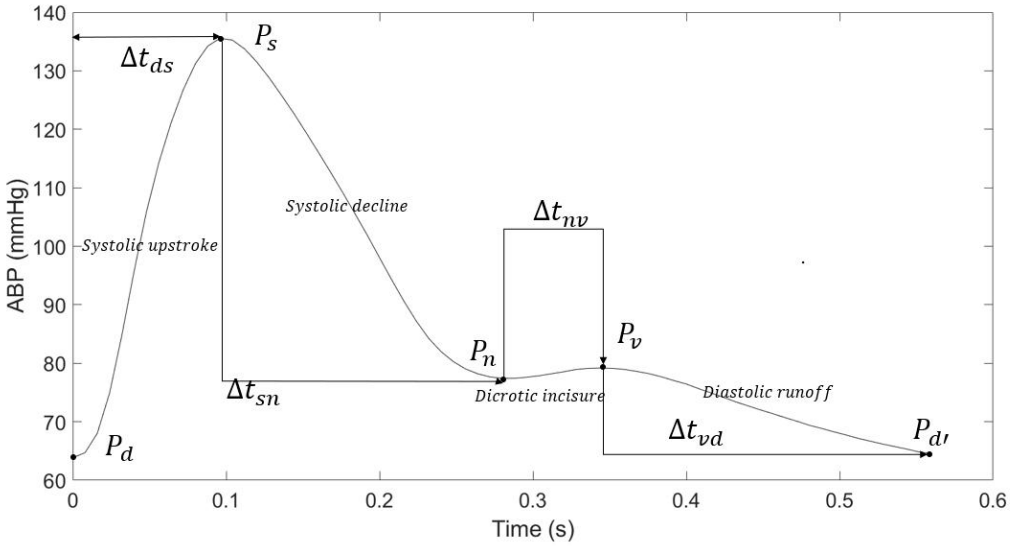


Figure 3.1: ABP waveform of a single typical cardiac cycle

Other prognostic metrics can be derived from these characteristic pressure values. For instance, pulse pressure, which is the difference between systolic and diastolic pressure levels, represents the force generated by the heart with each contraction and can indicate arterial stiffness and cardiovascular health. The variability of these metrics, such as pulse pressure variability (PPV) and systolic pressure variability (SBPV), reflects the dynamic nature of blood pressure and provides insights into cerebrovascular health.

As previously mentioned, PPV and SBPV have been recognised as significant prognostic factors for mortality. (*PPV: p=0.015*, *OR=1.110， 95%CI: 1.023-1.212; SBPV: p=0.019, OR=1.072, 95%CI:1.012-1.139*) [1] The variability of these pressures is assessed using the standard deviation or coefficient of variation, which respectively indicate the absolute variability of the pressure values and their relative variability compared to the mean systolic pressure or pulse pressure. [2]

Compared to ABP waveforms, ECG waveforms are more complex and require specialized knowledge and experience to fully understand and interpret the underlying diagnostic and prognostic information. This complexity arises from the cardiac electrical activity, which involves an intricate sequence of depolarisation and repolarisation events. An illustration of the ECG waveform for a single cardiac cycle is provided in Figure 3.2.

As illustrated in Figure 3.2, the ECG waveform consists of several basic components that represent cardiac electrical activities, including the P wave, QRS complex, T wave, U wave, ST segment, PQ interval, and QT interval. The duration and amplitude of these components provide crucial prognostic information about cardiac conditions, aiding in the assessment of an individual's cardiac health.

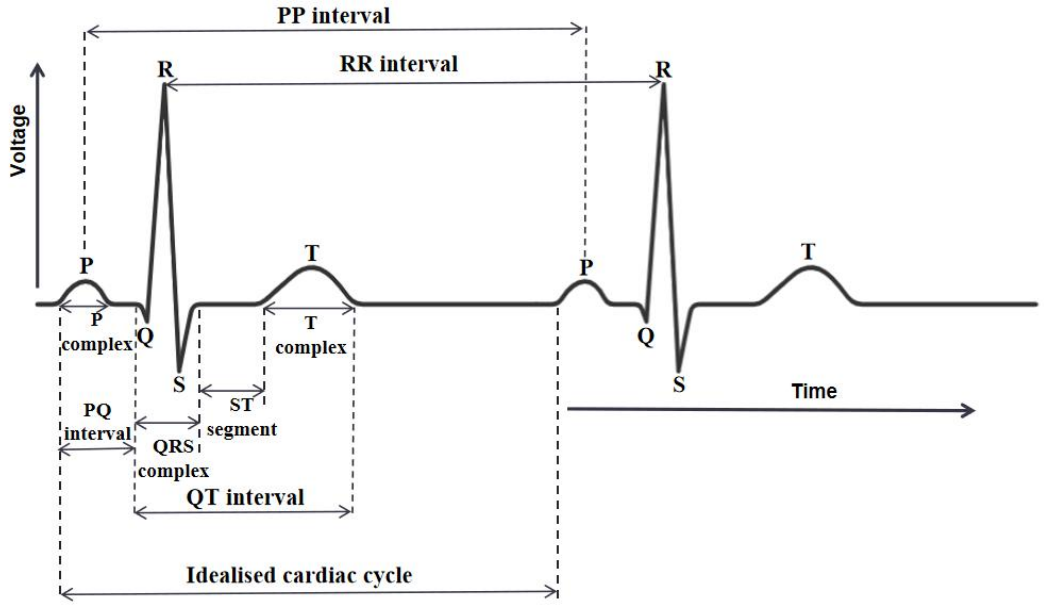


Figure 3.2: ECG waveform of a cardiac cycle and its constituent patterns

ECG indices with prognostic value in spontaneous SAH can be computed from these components and categorised into rhythm indices, amplitude indices, interval indices, and morphology indices. For example, tachycardia (a fast heart rate >100 bpm) is a typical rhythm index associated with a higher risk of mortality (*RR=3.9, 95%CI: 1.7-9.3*) and angiographic vasospasm (*RR=10.83, 95%CI: 1.17-100.50*). [3][4] The ST segment is depressed, denoted as ST depression, if it lies more than 0.1mV below the baseline. [5] ST depression is often a sign of myocardial ischaemia and has been shown to be prognostically valuable in predicting mortality (*RR=2.1, 95%CI: 1.5-3.1*), poor neurological grades and DCI. (*RR=2.4, 95%CI: 1.2-4.9*) [3][6]

A prolonged QT (corrected for heart rate > 410 ms) is associated with higher risk of ventricular arrhythmias, and is a typical interval index associated with angiographic vasospasm (*OR=2.4, 95%CI: 1.00-3.45*). [4] A more commonly adopted criteria for QT prolongation is > 440 ms, corrected for heart rate. [7] Morphological changes such as P mitrale, T wave inversion, and U wave are also used in SAH prognosis research. In P mitrale, the P wave is notched and biphasic, typically seen in patients with left atrial enlargement, and has been reported to predict mortality (*RR=4.1, 95%CI: 1.6-10.5*). [3][8] T wave inversion, occurring when the T wave is inverted below the baseline, has a significant relationship with poor outcomes, including mortality or an mRS score $\geqslant$4 (*OR=2.5, 95%CI: 1.5-5.5*). The U wave, typically a rounded low-amplitude component during the repolarisation phase of the ventricles,

has been found to significantly predict a favorable outcome. (*OR=0.4, 95%CI: 0.2-0.9*). However, the protective effect of the U wave is difficult to explain and has not been consistently reported in other studies. [6]

Some studies may not report the prognostic effects of specific indices but rather general types of indices. As discussed in chapter 2, pathological Q wave (*RR=2.9, 95%CI: 1.5-5.5*) and T wave abnormalities (*RR=1.8, 95%CI: 1.4-2.4*) have been reported as predictive of mortality. Pathological Q wave can be characterised by abnormalities in its duration, depth and in which specific leads this pathological Q wave are shown, while T wave abnormalities can include T wave inversion, peaking or flattening, T wave alternans, notched or biphasic T waves. [3] These general ECG indices combine various abnormalities for each component and serve as optimal prognostic factors, particularly when instances of explicit waveform abnormalities, such as T wave inversion, are insufficient.

3.1.2 Annotation of waveforms for feature extraction

In Section 3.1.1, indices from previous SAH prognosis studies were revisited and discussed in greater detail, focusing on their definitions and associated abnormalities in cardiovascular conditions. It is evident that these indices are localised and extracted based on characteristic points. For the ABP waveform, these characteristic points include systolic pressure $\boldsymbol{P_s}$, dicrotic notch $\boldsymbol{P_n}$, dicrotic peak $\boldsymbol{P_v}$, and diastolic pressure $\boldsymbol{P_d}$. For ECG indices, the characteristic points are those used to detect the PQRST complex, the PQ junction for computing the QTc interval, and the J point to determine whether the ST segment is normal, depressed, or elevated.

To facilitate the extraction of indices for dynamic prognosis research, methods based on the Pan-Tompkins algorithm have been proposed for detecting characteristic points in both ABP and ECG waveforms. [9] The algorithms for detecting these waveform feature points are illustrated in Figure 3.3.

First, the ABP and ECG signals are pre-processed to remove noise and enhance the QRS complexes, diastole, and systole. For ABP signals, low-pass filtering is used for noise reduction and smoothing. Since ECG signals represent electrical activity and have lower amplitude compared to ABP signals, they are more susceptible to interference from external sources, such as EMG interference, and are more prone to noise. Therefore, the pre-processing of ECG signals involves Gaussian moving average filtering and high-pass digital filtering to handle high-frequency noise and baseline drift. Additionally, a band-stop filter and a low-pass filter are used to remove 60-Hz hum and EMG interference, respectively.
Second, a derivative filter followed by a squaring operation is applied to both pre-processed ABP and ECG signals to enhance the morphological characteristics of the waveforms, such as the slopes of QRS complexes, systole, and diastole, aiding in the detection of characteristic points. Subsequently, a moving window integration is

performed to smooth the squared signals within short moving windows, further increasing the signal-to-noise ratio (SNR).

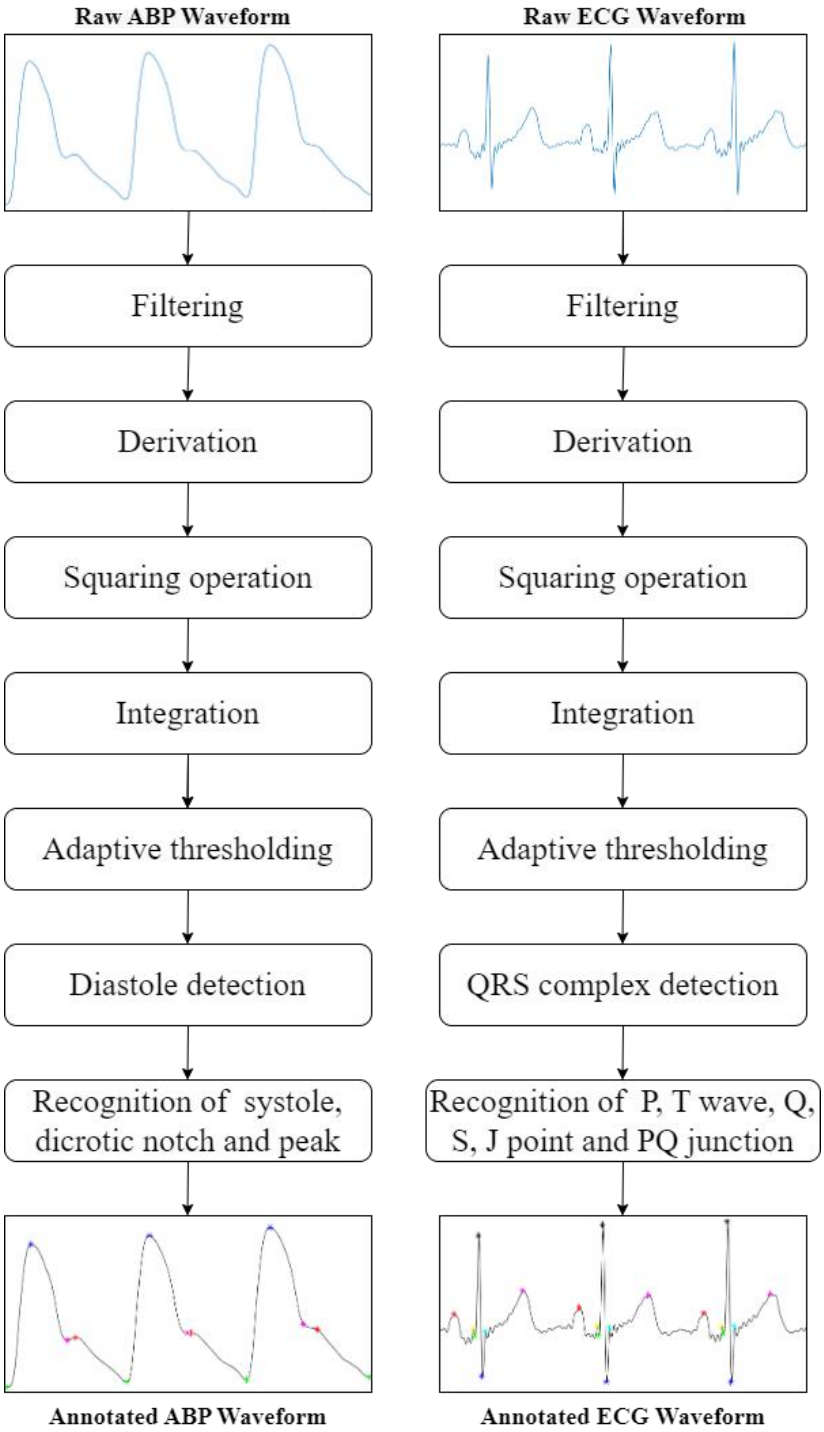


Figure 3.3: Block diagram of ABP and ECG annotation algorithms

Finally, a moving average threshold is determined based on the signal characteristics for the detection of R peaks in ECG waveforms. For ABP waveforms, the diastolic pressure point is identified as the maximum of the second derivative within each interval. Other characteristic points are then identified with reference to the R peaks and diastolic pressure points.

For ECG waveforms, after detecting the R peaks, the Q point is identified as the first significant negative deflection within a specific time window before the R peak, while the S point is the first significant negative deflection after the R peak. Similarly, the T point is found as the first significant positive deflection after the QRS complex, and the P point is identified as the nearest significant positive deflection before the QRS complex.

Based on the detected PQRST complex, the PQ junction and J point correspond to the transition between the P wave and the QRS complex, and the transition between the S wave and the ST segment, respectively. The J point can be detected as the inflection point where the QRS complex meets the ST segment and the slope change is most rapid, marking the end of depolarization and the beginning of repolarisation. [10] Similarly, the PQ junction marks the point where the P wave ends and the QRS complex starts, identified by a rapid change in slope.

For ABP waveforms, after detecting the diastolic pressure point as the maximum of the second derivative where the second derivative exceeds an adaptive threshold, the systolic peak is defined as the maximum of the waveform following the diastolic pressure point. For dicrotic indices, the dicrotic notch is identified as the minimum value resulting from subtracting the signal from the straight line connecting the systole and diastole. The dicrotic peak is defined as the minimum of the second derivative of the time series following the dicrotic notch. If local waveform minima and maxima exist, they are refined to these points. This criterion is adopted due to its robustness compared to other approaches. [11]

After detecting the characteristic points, refining these points is crucial to ensure the accuracy and reliability of the identified points for ECG waveforms. ECG waveforms are significantly affected by noise, artifacts, and individual variations, which can cause spikes and fluctuations that interfere with detection. To refine ECG annotations, the waveforms are smoothed using Gaussian moving average filtering with different orders.

Low-order filters enhance the detection of less conspicuous characteristic points, such as the Q and S points, while high-order filters improve the detection of the T and P points by reducing interference effects. The characteristic points annotated on waveforms smoothed with Gaussian moving average filters of different orders are then compared and analyzed to determine the final annotations. This refinement and validation step significantly improves annotation accuracy.

Figure 3.4 illustrates the annotation of ECG and ABP waveforms, demonstrating that characteristic points in simultaneous ABP and ECG waveforms are accurately detected even in the presence of noise and waveform abnormalities. These detected characteristic points can then be used to compute dynamic prognostic factors.

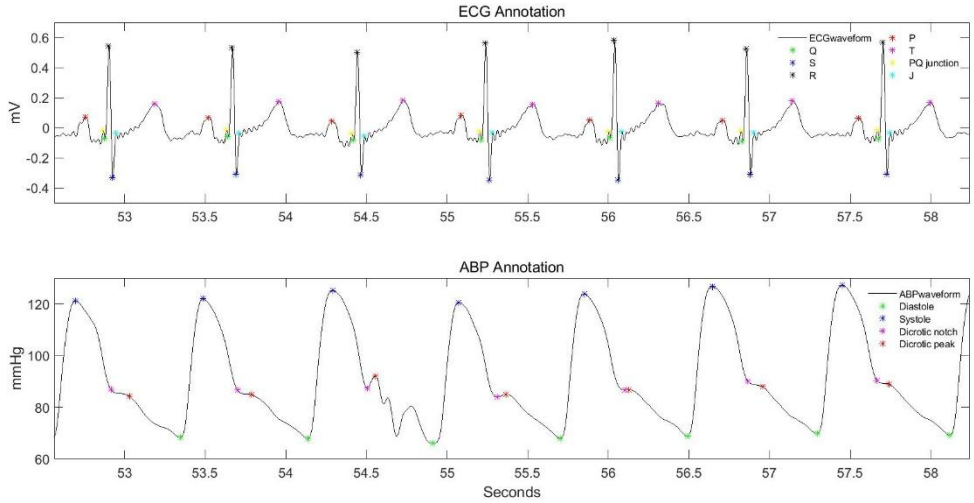


Figure 3.4: Annotation of a short segment of simultaneous ABP and ECG waveform

3.2 Dynamic prognostic modelling with vital sign indices

3.2.1 Introduction

Spontaneous SAH, particularly aneurysmal SAH, is associated with higher mortality rate and worse functional outcome compared with traumatic SAH. The critical care of spontaneous SAH patients is often accompanied by both neurological and non-neurological complications, wherein aneurysmal re-bleeding, DCI, together with initial bleed, account for the majority of mortalities following spontaneous SAH. [12]

Given the high mortality rate, poor neurological outcomes, and complications following the initial haemorrhage, prognosis is particularly important for spontaneous SAH patients. Early prognosis, such as on admission, guides timely intervention and effective treatment. Additionally, prognosis during critical care management helps identify risks, prevent potential complications, and improve survival outcomes.

Previous prognosis research on spontaneous SAH has primarily focused on identifying risk factors for clinical outcomes. Commonly adopted clinical outcomes include mortality, neurological grades (e.g., Glasgow Outcome Scale (GOS) and the modified Rankin Scale (mRS)), length of ICU/hospital stay, and discharge status (good/poor). Survival prognosis draws the most research interest as it aims to provide accurate predictions of patient survival, guide clinical decisions, and improve quality of life. This study, therefore, aims to develop a personalised dynamic prediction model for survival probabilities in spontaneous SAH patients.

Prognostic risk factors for mortality can be broadly categorised into demographics, family history and genetic factors, treatment information, underlying medical conditions, complications, clinical scores and scales, radiological investigations,

hematology biomarkers, and indices from vital signs. Commonly used prognostic tools in clinical practice include the Hunt and Hess scale, the World Federation of Neurological Surgeons (WFNS) grading system, the Glasgow Coma Scale (GCS), and the Fisher and modified Fisher scales. Figure 3.5 reviews these prognostic risk factors for mortality, compiled from previous research examining their effects on mortality after spontaneous SAH, primarily in cases of aneurysmal SAH.

In Figure 3.5, we have reviewed prognostic risk factors identified as independent predictors of mortality in previous studies (Note that these references are from chapter 2). Mortality is typically included as a binary outcome in these studies but can also be analysed as a time-to-event outcome in survival analysis. Some studies on spontaneous SAH have included mortality as a time-to-event outcome. For example, WFNS score ($p < 0.0001$, $HR = 1.843$), age ($p = 0.0257$, $HR = 1.399$), clipping ($p < 0.0001$, $HR = 0.164$) and coiling ($p < 0.0001$, $HR = 0.177$) were included as prognostic factors for mortality in a Cox model in studying the long-term outcome in elderly patients with aneurysmal SAH. [13]

Most previous prognosis studies on spontaneous SAH have focused on identifying risk factors associated with clinical outcomes. However, to utilise these influential risk factors for survival prediction, prognostic model research is needed. This research aims to develop a prognostic model that predicts an individual's mortality risk using combinations of these prognostic factors.

For prognosis and clinical utility, a key issue must be addressed. To support clinical decision-making and individualised treatments, the rapid evolution of clinical conditions should be monitored to update prognostic information and track disease progression. Previous studies have mostly focused on the prognostic value of fixed-time predictors, primarily baseline covariates at admission.

However, dynamic covariates, which can be repeatedly measured during the hospital stay, provide up-to-date prognostic information on disease progression. Incorporating dynamic covariates into prognostication can potentially improve the predictive accuracy of survival probabilities. Therefore, simultaneous analysis of repeated measurements of dynamic covariates and survival data should be implemented for dynamic prognosis.

Joint modelling methods were initially implemented in AIDS studies to investigate the effects of repeatedly measured CD4 counts on survival. These methods were later adopted in other fields of clinical research, such as cancer and cardiovascular diseases. [14] However, joint modelling methods have not been applied in SAH prognosis research. This is not only due to the lack of awareness of available tools for simultaneous analysis of repeated measurements and survival outcomes but also because of a lack of awareness of the values in dynamic prognostic information provided by routine monitoring of vital signs.

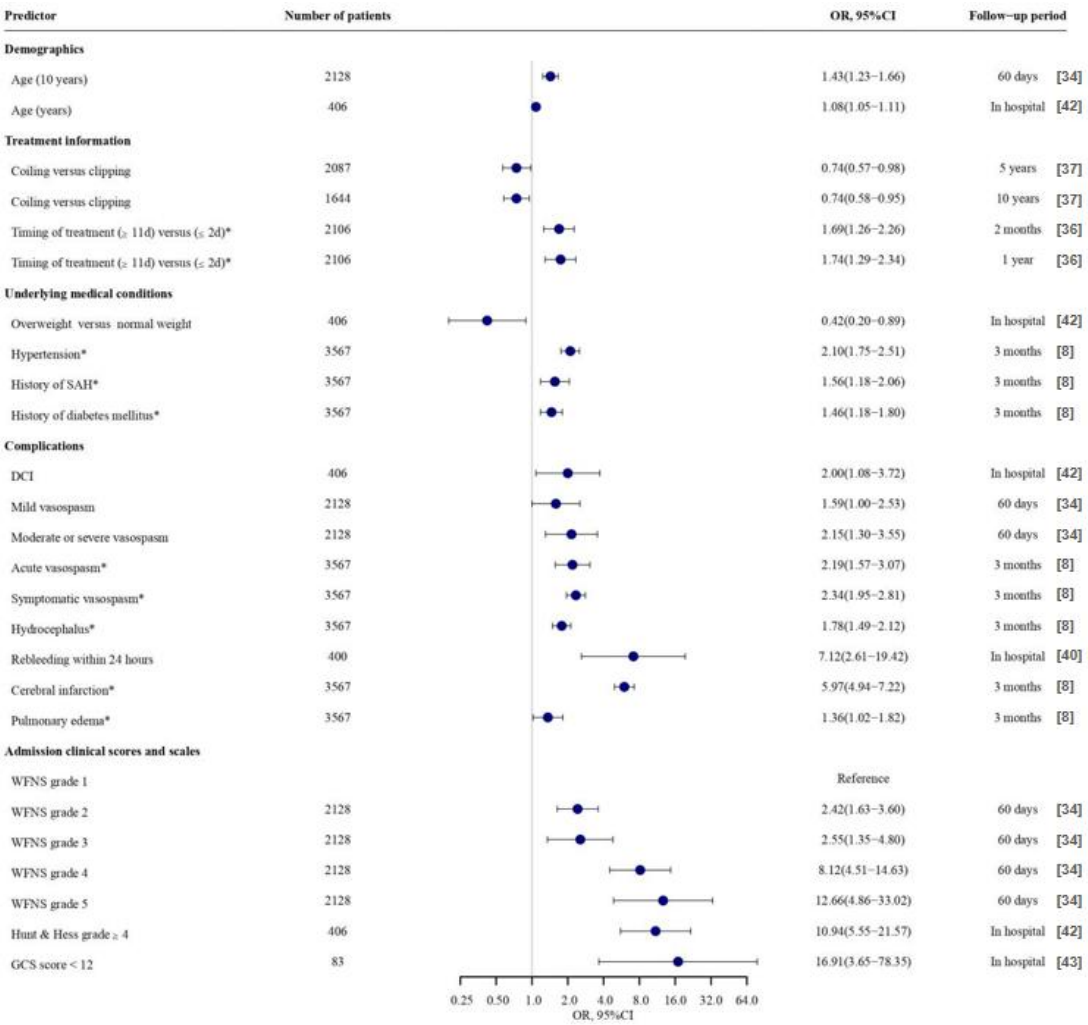


Figure 3.5: Review of prognostic risk factors for mortality in univariate analysis after spontaneous SAH[3]

This section is structured as follows: First, we will discuss the inclusion criteria for patient selection and baseline clinical characteristics. Second, we will extract longitudinal predictors from ECG and ABP waveforms to serve as time-varying covariates in our joint model, based on the feature extraction approaches discussed in Section 3.1. Finally, we will implement simultaneous analysis of the longitudinal and event processes using joint modelling methods. The performance of the dynamic prognosis and personalised survival prediction will be assessed, discussed, and compared with a traditional prognostic model based on survival analysis.

[3] ***: a composite outcome combined of mortality and other poor outcomes, ^: adjusted for baseline predictors**

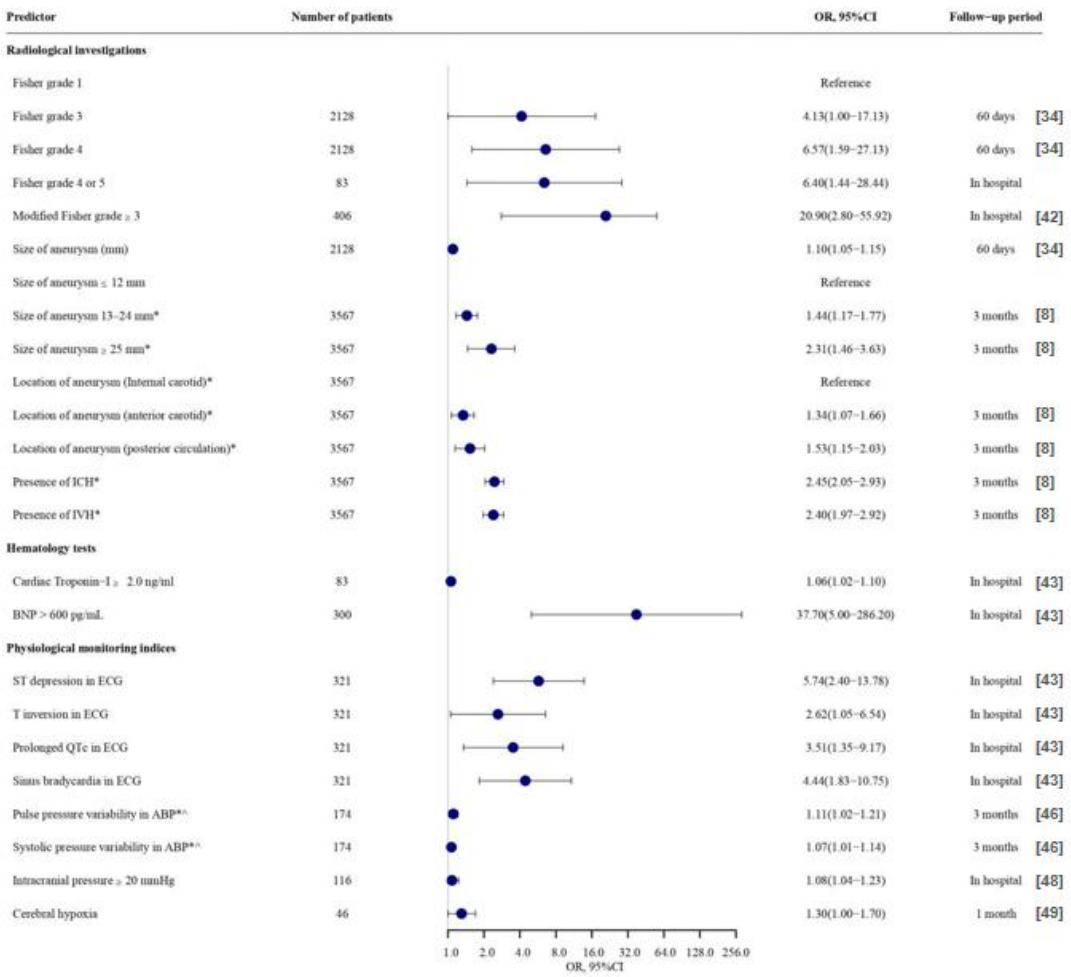


Figure 3.5: Cont.

3.2.2 Patient population and clinical characteristics

Patients for this study were selected from the publicly available MIMIC-III database, a retrospective dataset of patients who stayed in critical care units (CCUs) at Beth Israel Deaconess Medical Center between 2001 and 2012. [15] We specifically selected spontaneous SAH patients with recorded ECG and ABP waveforms and conducted a retrospective cohort study with up to 14 days of follow-up in the CCUs from the time of admission.

178 patients with a primary diagnosis of spontaneous SAH were initially included in this study. Patients without simultaneous ECG and ABP monitoring records were excluded from the analysis. After pre-processing and feature extraction, additional patients were excluded due to artefacts, lack of valid ECG and ABP features within the follow-up periods, or mismatched clinical and waveform information. Furthermore, patients with a length of stay longer than 30 days or who died within 12 hours of admission were excluded, as dynamic trajectories representing the evolution of medical conditions could not be observed. The flowchart for patient inclusion is shown in Figure 3.6.

A total of 108 patients were included in the study, with 27 mortalities and 81 survival cases, resulting in a 14-day mortality rate of 25%. The characteristics of demographics, pre-existing chronic diseases, and complications are detailed in Table 3.1. Survival analysis was conducted using the Cox proportional hazards model to identify baseline covariates from the admission data. Significant results ($p < 0.05$) are highlighted in bold. Based on this analysis, cerebral oedema on admission was identified as the only influential baseline covariate to be analysed jointly with dynamic prognostic information.

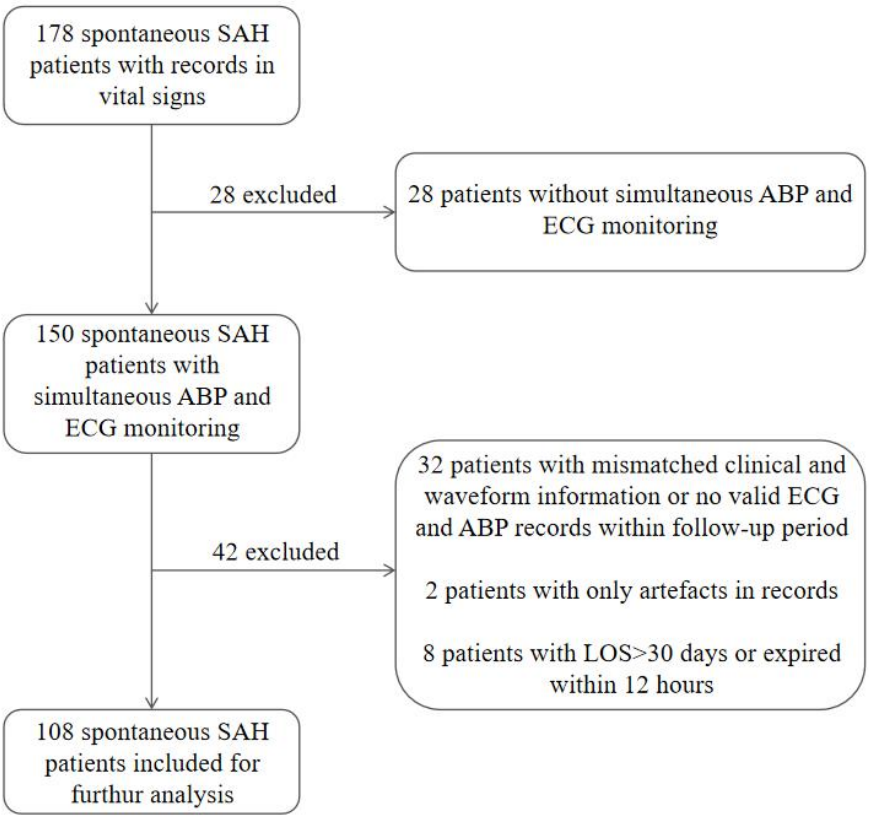


Figure 3.6: Flowchart for patient inclusion for this study

3.2.3 Dynamic predictor extraction

Dynamic predictors were extracted from raw ABP and ECG waveforms as dynamic covariates to be jointly analysed with the baseline covariates. Four commonly used influential predictors of mortality from vital signs (ST depression, T wave inversion from ECG waveforms as well as variability of systolic blood pressure (SBPV) and pulse pressure (PPV) from ABP waveforms) were extracted from waveforms and included for analysis. [16][17]

Extraction of predictors mainly consists of two steps: waveform annotation and

computation of dynamic covariates. Firstly, annotation of ECG and ABP waveforms implies detection of feature points based on the waveform morphology for subsequent predictor computation. For ABP waveforms, the feature points of interest are in the order of diastole, systole, dicrotic notch, and dicrotic peak, and for ECG waveforms, we detected features of P-QRS-T waves to determine segments, intervals, and amplitudes. The feature detection procedures for both the ECG and ABP waveforms are based on the Pan-Tompkins algorithm and are illustrated in Figures 3.3 and 3.4. [9] In each cardiac cycle, if no complete set of feature points in the correct order was identified, this cycle was labelled as an anomaly and excluded from further analysis.

Covariate		**All (n=108)**	**Death (n=27)**	**Survival (n=81)**	**Hazard ratio (95% CI)**	**p-value**
Demographics	**Age⩾ 65 years**	40 (37.04%)	14 (51.85%)	26 (32.10%)	1.988 (0.958 - 3.500)	0.075
	Female	66 (61.11%)	16 (59.26%)	50 (61.73%)	0.903 (0.419 - 1.946)	0.794
Chronic diseases	**Hyper tension**	53 (49.07%)	17 (62.96%)	36 (44.44%)	1.815 (0.830 - 3.967)	0.135
Complications and comorbidities	**Cerebral oedema**	25 (23.15%)	11 (40.74%)	14 (17.28%)	2.736 (1.269 - 5.894)	**0.010**
	Hydrocephalus	39 (36.11%)	10 (37.04%)	29 (35.80%)	0.935 (0.427 - 2.048)	0.867
	Seizures	10 (9.26%)	1 (3.70%)	9 (11.11%)	0.306 (0.041 - 2.662)	0.245
	Atrial fibrillation	10 (9.26%)	3 (11.11%)	7 (8.64%)	1.172 (0.705 - 1.948)	0.796

Table 3.1: Clinical characteristics on admission, including demographics, chronic diseases, complications and comorbidities, and results of univariate survival analysis

ECG and ABP waveforms from the 108 patients, were divided into 5-min non-overlapping segments. For each segment, ST depression and T wave inversion were represented by the ratio of ST depression (ST segment < $-0.1mV$) and T wave inversion (T wave amplitude < $0.1mV$) across all cardiac cycles with PR segment as the isoelectric baseline; and SBPV and PPV were measured by the standard deviations of systolic and pulse pressure within each 5-min waveform segment. Then we computed mean levels across segments on each day of CCU stay for patients. The generated within-day mean values of selected covariates from ECG and ABP waveforms were taken as dynamic covariates in modelling spontaneous SAH prognosis in this study.

3.2.4 Statistical explanations

As discussed, the primary objective of this study is to model the dynamic changes in disease progression of spontaneous SAH and predict survival outcomes using both baseline covariates at admission and dynamic covariates extracted from vital signs. To achieve this, we begin by investigating the effect of baseline covariates on survival outcomes, which is commonly modeled using a Cox proportional hazards model:

$$h_i(t) = h_0(t)\exp(\sum_j \gamma_j \omega_{j_i}) \quad (3.1)$$

where $h_i(t)$ denotes the instantaneous hazard of mortality for the i^{th} patient at time *t.* $h_0(t)$ is the baseline hazard function, while ω_{j_i} is the value of the j^{th} baseline covariate for patient the i^{th} patient with the corresponding coefficient γ_j. A positive coefficient indicates an increase in the hazard of mortality, whereas a negative coefficient implies a protective effect from the event of mortality.

In our study, cerebral oedema was identified as the only significant baseline covariate in the univariate survival analysis, as shown in Table 3.1. The results of the Cox regression indicate that the estimated coefficient for cerebral oedema was 1.0064 ($p=0.010$, $HR=2.736$, 95% $CI: 1.269\text{-}5.894$). This suggests that, when considering only the effects of baseline covariates on survival, a diagnosis of cerebral oedema ($\omega_{co} = 1$) on admission increases the hazard of mortality by 2.736 times compared to patients without this complication ($\omega_{co} = 0$).

The coefficients and standard errors were estimated based on survival data and a baseline covariate vector representing whether the i^{th} patient was diagnosed with cerebral oedema on admission. The available survival data of i^{th} patient consists of observed time of event of mortality T_i and indicator of mortality δ_i. For the i^{th} patient, observed event time $T_i = min\,(T_i^*, C_i)$, where T_i^* is the true event time and C_i is the censoring time.

The true event time T_i^* is known if event of mortality is observed by the end of the study, corresponding to the maximal follow-up period of 14 days. Otherwise, event time is censored, meaning that the exact value of T_i^* is unknown, but it is known that the censoring time C_i occurred since the event had not happened up until the patient was lost to follow-up. Observations are termed censored if the patient was lost to follow-up due to reasons such as discharge home, transfer to other hospital units, or if the patient was still alive at the end of the study.

With survival data, the coefficient of cerebral oedema and its standard error can be estimated based on the log partial likelihood function:

$$L(\gamma) = \sum_i \delta_i (\gamma^T \omega_i - \log(\sum_{j \in \chi(t_i)} \exp(\gamma^T \omega_j))) \quad (3.2)$$

where coefficients are estimated by maximising the log partial likelihood, and the set $\chi(t_i)$ denotes the set of individuals still at risk just before time t_i.

Dynamic covariates of vital sign indices were then incorporated into the model to be analysed simultaneously with the effects of baseline covariates on survival outcomes. To handle multiple dynamic covariates and baseline covariates, a straightforward approach is to use the counting-process form of Cox model, given by:

$$h_i(t) = h_0(t) R_i(t) \exp(\gamma^T \omega_i + \sum_j \alpha_j y_{j_i}(t)) \quad (3.3)$$

$R_i(t)$ indicates whether the i^{th} patient still at risk at time t, which takes 1 if $t < T_i$. In this context, $y_{j_i}(t)$ represents the value of j^{th} dynamic covariate for patient i at time t. Similarly, the coefficients of both baseline and dynamic covariates can also be estimated based on the use of the log partial likelihood function.

However, the counting-process form of the Cox model, also known as the time-varying Cox model, assumes no measurement error and exogenous time-varying covariates. This means that the existence and value of these covariates are not influenced by events that have already occurred. [18] These assumptions do not hold for the dynamic covariates included in this study, where waveform-derived covariates are measured with error and become unavailable after an event of mortality. Misusing the counting-process form of the Cox model to analyze dynamic covariates can lead to an underestimation of the effects of these covariates on survival, reducing their estimated effects towards zero. [19]

These limitations of the time-varying Cox model can be addressed by the use of a joint model. For this study, a joint model for longitudinal process and survival data can be formulated in the following two equations:

$$y_{j_i}(t) = m_{j_i}(t) + \varepsilon_{j_i}(t) = \beta_j x_{j_i}^T(t) + b_{j_i} z_{j_i}^T(t) + \varepsilon_{j_i}(t) \quad (3.4)$$

$$h_i(t) = h_0(t)\exp(\gamma^T \omega_i + \sum_j \alpha_j m_{j_i}(t)) \quad (3.5)$$

In Equation 3.4, $y_{j_i}(t)$ denotes the j^{th} longitudinal outcome or the observed value of j^{th} dynamic covariate, measured with error, for i^{th} patient at time t. The term $m_{j_i}(t)$ is the corresponding unobserved true value of the j^{th} longitudinal outcome, composed of fixed-effect term $\beta_j x_{j_i}^T(t)$ and random-effect term $b_{j_i} z_{j_i}^T(t)$. Fixed and random effects are respectively used to describe population-level trajectories and individual-specific deviations, where these deviations are assumed to be normally distributed, i.e., $b_{j_i} \sim N(0, D_j)$.

To model the trajectories of different dynamic covariates during disease progression, both at the population level and individual-specific level, measurement time is included in both the fixed and random-effect terms. Additionally, since blood pressure variability has been observed to be age-dependent, patient age at admission is incorporated as an explanatory factor into the fixed effects for modeling SBPV and PPV. [20] The measurement error, denoted by $\varepsilon_{j_i}(t)$, is assumed to be normally distributed, i.e., $\varepsilon_{j_i} \sim N(0, \sigma^2)$.

After modelling the longitudinal process with linear mixed-effects models (LMMs), the unobserved true values of dynamic covariates are incorporated into the survival analysis to be jointly analysed with baseline covariates. As mentioned, four dynamic covariates were included as potentially influential dynamic prognostic factors of survival outcome: ST depression, T wave inversion, SBPV and PPV. Each dynamic covariate is jointly analysed with the baseline covariate, cerebral oedema, as formulated by Equations 3.4 and 3.6:

$$h_i(t) = h_0(t) exp\,(\gamma_{co}\omega_{co_i} + \alpha_j m_{j_i}(t)) \quad (3.6)$$

where α_j quantifies the association of the j^{th} dynamic covariate with mortality risk, adjusting for baseline covariates. A significant α_j ($p<0.05$) indicates that the j^{th} dynamic covariate is an influential prognostic factor for survival outcome and is thus included in Equation 3.5.

The parameters of all joint models were estimated using the Bayesian approach with the R package JMbayes2[4]. Inference was based on a joint posterior distribution, which is the product of the joint likelihood of the observed data and the prior distribution.

[4] **JMbayes2: Extended Joint Models for Longitudinal and Time-to-Event Data (cran.r-project.org/web/packages/JMbayes2)**

Markov chain Monte Carlo (MCMC) techniques, specifically a combination of Gibbs and Metropolis-Hastings algorithms, were used to implement the Bayesian approach.

3.3 Results

3.3.1 Joint analysis of vital sign indices and baseline covariates

Table 3.2 presents the results of joint analysis of survival data and each potential dynamic covariate. The joint shared parameter α_j measures the effect of the j^{th} dynamic covariate on survival, while adjusting for the effect of cerebral oedema on admission. Positive estimates of α_j indicate a risk factor of mortality, whereas negative estimates represent protective effects.

Covariate	Estimate (95% CI)	Hazard ratio (95% CI)	Std	p-value
ST depression	-1.1229 (-3.8778 – 1.1027)	0.3253 (0.0207– 3.0122)	1.2787	0.394
T wave inversion	0.5991 (-0.9757 - 2.1725)	1.8205 (0.3769– 8.7802)	0.7997	0.452
Systolic pressure variability	0.3129 (0.0985 - 0.5553)	1.3674 (1.1035- 1.7390)	0.1180	**0.006**
Pulse pressure variability	0.0759 (-0.0809 - 0.2114)	1.0789 (0.9223- 1.2354)	0.0747	0.305

Table 3.2: Results of joint shared parameters in survival sub-model for simultaneous analysis of each dynamic covariate and survival data

From the results shown in Table 3.3, it can be seen that systolic blood pressure variability is the only significant dynamic prognostic factor for mortality. Therefore, the survival sub-model of our final joint model can be described by:

$$h_i(t) = h_0(t)exp\ (\gamma_{co}\omega_{co_i} + \alpha_{SBPV}m_{SBPV_i}(t))\ (3.7)$$

where the longitudinal behavior of systolic blood pressure variability measurements is modelled using a linear mixed-effects model (LMM). The results of the joint modeling of influential baseline and dynamic covariates are presented in Table 3.3.

In the longitudinal sub-model, systolic blood pressure variability was found to increase with both measurement time after admission and patient age. A one-day longer stay in the CCU was associated with an increase in systolic pressure variability of 0.1732 mmHg (*p = 0.0371, 95% CI: 0.0087 - 0.3527*). Also, an increase of one year in age was associated with an increase of 0.0661 mmHg (*p < 0.001, 95% CI:*

0.0256 - 0.1080) in the true unobserved systolic pressure variability.

Cerebral oedema was associated with an increased hazard of mortality, with the estimated hazard ratio (HR) rising from 2.736 in the separate survival analysis to 3.300 when accounting for confounding effects with dynamic covariates. When jointly modelled with longitudinal information, patients diagnosed with cerebral edema had a 3.300 times higher mortality hazard compared to those without this condition. Most importantly, systolic blood pressure variability was significantly associated with the hazard of mortality. An increase of 1 mmHg in systolic blood pressure variability corresponded to a 37.97% higher hazard of mortality (*p = 0.0060, HR = 1.3797, 95% CI: 1.1035 - 1.7390*).

	Variable	**Coefficient (95% CI)**	**Hazard ratio (95% CI)**	**p-value**
Survival process	**Cerebral oedema**	1.1938 (0.0361- 2.2237)	3.2996 (1.0368 - 9.2415)	**0.0416**
	SBPV	0.3219 (0.0985 - 0.5533)	1.3797 (1.1035 - 1.7390)	**0.0060**
Longitudinal process	**Variable**	**Coefficient (95% CI)**	**Std**	**p-value**
	Intercept	9.1067 (6.4671 - 11.6127)	1.3152	**<0.001**
	Age	0.0661 (0.0256 - 0.1080)	0.0208	**<0.001**
	Time	0.1732 (0.0087 - 0.3527)	0.0869	**0.0371**

Table 3.3: Results for the proposed joint model of longitudinal and survival data for spontaneous SAH prognosis

3.3.2 Dynamic survival prediction and assessment

The proposed joint model can be used as a prognostic tool to monitor disease progression from the aspect of haemodynamic stability, evaluate real-time mortality risks, and guide personalised medical care for patients. Based on the fitted joint model, we can estimate the conditional survival probability of the i^{th} patient at time t, denoted by $\pi_i(t|T_s)$, given the information whether this patient was diagnosed with cerebral oedema on admission and measures of systolic blood pressure variability up until the starting time of prediction T_s. Here, dt represents the prediction interval, indicating how many days into the future the survival probability is being estimated. Thus, the targeted time of prediction is T_p, such that $T_p = T_s + dt$.

The survival probability of the i^{th} patient at time *t* can then be computed based on

known baseline and dynamic covariates as well as the fact that the patient is still alive at T_s. The predictions of survival probabilities were calculated using a Monte Carlo method. The accuracy of survival prediction, or the discriminative power of the proposed joint model, was evaluated using the area under the ROC curve (AUC). In this study, we compared the predictive accuracy of the proposed prognostic model, which incorporates dynamic prognostic information from continuously measured SBPV, with that of a traditional prognostic model that does not, across different starting points of prediction and targeted prediction time points, as shown in Table 3.4.

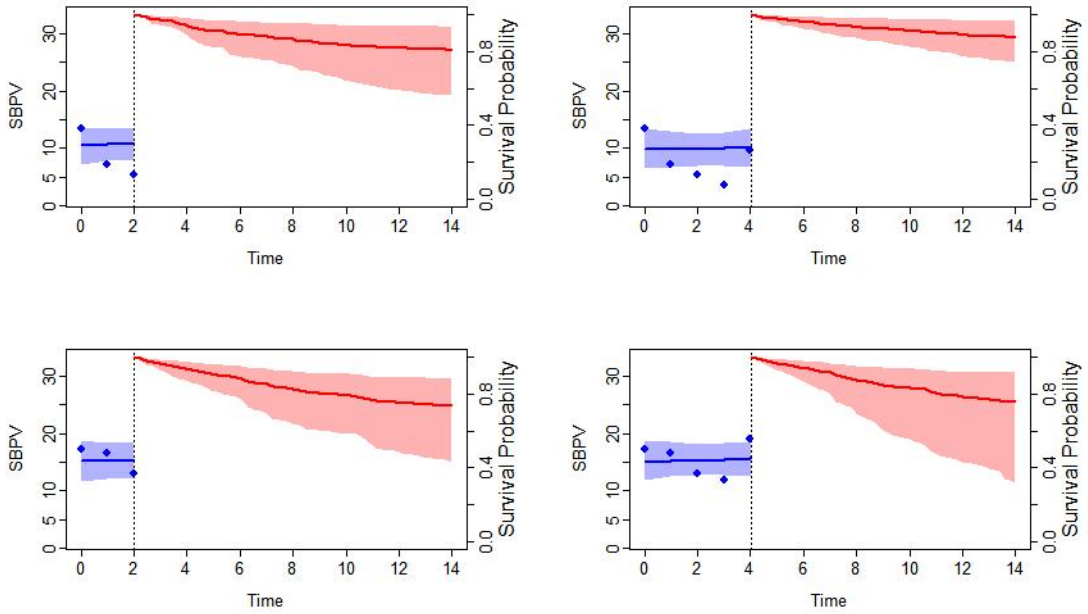


Figure 3.7: Dynamic survival prediction plots for two patients, two plots on the top for one patient while two plots on the bottom for another patient. (The blue dots represent observed values of systolic blood pressure. The blue lines and surrounding light blue regions respectively represent estimated true values and corresponding 95% confidence intervals. The red lines and surrounding light red regions respectively denote the estimated dynamic survival probability and 95% confidence interval)

Figure 3.7 compares the estimated survival probabilities between two randomly selected patients, starting from $T_s = 3$ and $T_s = 5$. It can be observed that the patient with low levels of systolic pressure variability has a higher estimated survival probability at the end of the follow-up period compared to the patient with high levels of systolic pressure variability. With updated measurements showing extremely high systolic pressure variability above the upper bound of the confidence interval (as shown in the bottom right plot), the confidence interval becomes wider, indicating greater uncertainty in the survival prediction.

According to Table 3.4, we can find that systolic pressure variability, as a dynamic covariate, provides valuable up-to-date prognostic information. Incorporating systolic pressure variability into prognostication significantly improves the predictive accuracy of model, especially in the first week post-SAH, compared to the traditional prognostic model which only considers baseline covariates at admission. In the second week after the onset of SAH, prognostic modeling approaches provide only satisfactory predictive accuracy. While the proposed joint model still improves prediction accuracy in the second week compared to the traditional prognostic model, the improvement is not as significant as it is in the first week.

	AUC	**Tp = 3**	**Tp = 5**	**Tp = 7**	**Tp = 10**	**Tp = 12**
Proposed joint model	**Ts = 2**	0.6569	0.7385	0.7713	0.7206	0.7111
	Ts = 3	-	0.7606	0.7588	0.7215	0.7028
	Ts = 5	-	-	0.6391	0.5857	0.5644
	Ts = 7	-	-	-	0.6421	0.5862
	Marginal	0.6569	0.7496	0.7231	0.6675	0.6411
	AUC	**Tp = 3**	**Tp = 5**	**Tp = 7**	**Tp = 10**	**Tp = 12**
Traditional prognostic model	**Ts = 2**	0.5619	0.6140	0.5866	0.6097	0.5957
	Ts = 3	-	0.6479	0.5903	0.6151	0.5984
	Ts = 5	-	-	0.5559	0.5995	0.5798
	Ts = 7	-	-	-	0.6551	0.6008
	Marginal	0.5619	0.6310	0.5776	0.6199	0.5937

Table 3.4: Predictive accuracy of proposed joint model and traditional prognostic model across different starting points of prediction and targeted prediction time points

3.4 Discussion

The primary objective of this study is to explore dynamic prognostic values of vital sign indices and investigate how they can be used to improve prognostic models for SAH. This study is the first to implement the simultaneous analysis of repeated measurements and survival outcomes to model SAH prognosis. Key findings, clinical significance, and future directions are discussed below.

In this study, all baseline and dynamic covariates in the proposed joint model, including cerebral oedema and SBPV in the survival sub-model, as well as intercept, age, and measurement time to model SBPV in the longitudinal process, were statistically significant. SBPV increases with time, is higher in older patients, and

correlates with a higher mortality risk and cerebral oedema diagnosis. Additionally, SBPV is associated with re-bleeding and poor neurological outcomes, suggesting its potential use in predicting these probabilities in future studies. [21]

Given that the normal assumption for random effects is robust to misspecification and has a negligible effect on parameter estimation, we did not further examine this assumption. [22] To check the normality of residuals, we used a Q-Q plot, as shown in Figure 3.5. The plot shows that while residuals align well with a normal distribution in the central region, they have slightly heavier tails, indicating outliers or extreme values not fully captured by the model. These slight deviations, particularly in the tails, do not substantively impact the robustness or the interpretability of the model results, and the robustness can be improved with larger dataset.

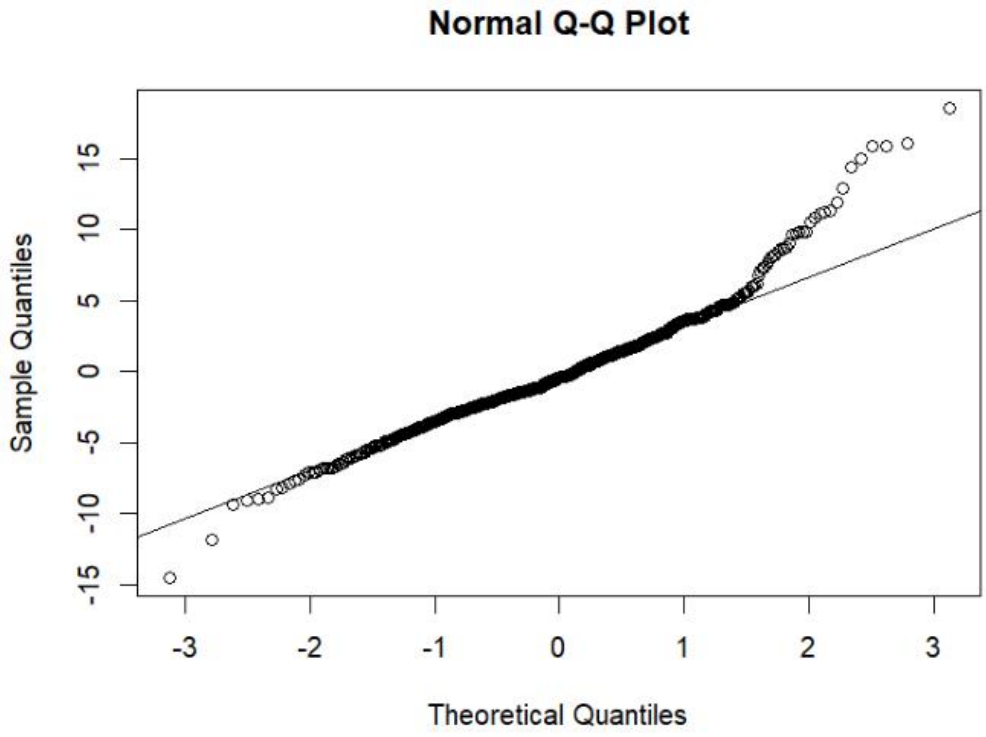


Fig. 3.5: Normal Q-Q plot of residuals for checking normality assumption

The predictive accuracy of the fitted model was evaluated using AUC values across various starting points and targeted prediction times. The model showed good predictive accuracy in the first week following spontaneous SAH, significantly outperforming the traditional prognostic model. However, it fails to provide reliable survival predictions beyond this period. In the first week after SAH onset, SBPV likely reflects the physiological response to acute injury and impairment in cerebrovascular autoregulation, making it a strong predictor of mortality. [23]

However, as the disease progresses, events such as treatment interventions and complications like DCI become more influential in determining clinical outcomes.

Consequently, the predictive power of SBPV may diminish over time. While SBPV is a useful early predictor of mortality, it cannot be solely relied upon for SAH prognosis in critical care. A comprehensive prognosis requires incorporating other clinical and radiological predictors, such as neurological assessments, radiological findings, and haematological biomarkers, to ensure accurate dynamic prognosis as the disease evolves.

There are several limitations to this study. Firstly, the limited dataset restricted the number of baseline and dynamic covariates included in the analysis, which is insufficient to fully capture the multi-factorial nature of SAH prognosis. As more clinical data becomes available, additional prognostic factors and intermediate events, particularly complications critical to SAH patient care, should be included to provide a more comprehensive understanding of SAH prognosis and improve prediction accuracy. Additionally, the study's retrospective nature and reliance on a single-center dataset may limit the generalisability of the findings. The potential for unmeasured confounding variables and selection bias also poses challenges. Future research should aim to validate these findings in larger, multi-center prospective studies to enhance the robustness and applicability of the prognostic models.

Secondly, for the interpretability of our results, we only selected covariates and corresponding functional forms that have been shown to be statistically significant in previous SAH prognosis studies. This constraint limits the selection and inclusion of potentially relevant prognostic factors. With more clinical evidence supporting the prognostic significance of additional covariates, more interpretable dynamic predictors will become available, further enhancing SAH prognostic models.

Finally, many SAH patients require inotropic support to maintain CPP, but these drugs can significantly affect blood pressure variability. Thus, raw recordings of blood pressure variability may not fully reflect haemodynamic instability of SAH patients, potentially confounding predictions in prognostic models. Adjusting for inotropic drug use or incorporating dose-adjusted BP indices in prognostic models may improve the accuracy of outcome predictions. [24]

The joint modeling framework in this study offers a novel approach to incorporating various prognostic information into prognostication, with the potential to include intermediate events such as complications and neurological interventions, thereby improving predictive accuracy. The Bayesian approach used for parameter estimation allows for the integration of expert knowledge and existing clinical findings as prior information, facilitating clinical application. This framework has significant clinical implications, enabling healthcare providers to more accurately predict survival outcomes for SAH patients.

By integrating dynamic health data as covariates and baseline patient characteristics into prognostic modeling, healthcare providers can better understand patients'

baseline medical conditions and individual disease progression and recovery trajectories, allowing for personalised care plans. Additionally, dynamic prognostic modeling transforms health data and patient characteristics into comprehensible survival probabilities and actionable insights, enabling real-time adjustments to treatment strategies.

Future work of this study should aim to model the complete mechanism of SAH prognosis, where major complications are suggested by corresponding risk factors, and mortality as a clinical outcome is predicted by combinations of these risk factors and the occurrence of complications. This mechanism can be viewed as a multi-state process, with transitions between different states defined by complications. These transitions still need to be investigated and will be covered in Chapter 7. Multi-state joint modeling approaches can provide a comprehensive, accurate, and dynamic understanding of SAH prognosis, potentially facilitating personalised prognosis and improving patient outcomes.

Reference for chapter 3

[1] Dowlati, E., Triano, M.J., Felbaum, D.R., Mai, J.C., Aulisi, E.F., Armonda, R.A. and Chang, J.J., 2021. Increased pulse pressure variability within the first 24 hours leads to poor disposition in subarachnoid hemorrhage patients. American Journal of Hypertension, 34(6), pp.645-650.

[2] Ascanio, L.C., Enriquez-Marulanda, A., Maragkos, G.A., Salem, M.M., Alturki, A.Y., Ravindran, K., Fehnel, C.R., Hanafy, K., Ogilvy, C.S., Thomas, A.J. and Moore, J.M., 2020. Effect of blood pressure variability during the acute period of subarachnoid hemorrhage on functional outcomes. Neurosurgery, 87(4), pp.779-787.

[3] Van der Bilt, I.A.C., Hasan, D., Vandertop, W.P., Wilde, A.A.M., Algra, A., Visser, F.C. and Rinkel, G.J.E., 2009. Impact of cardiac complications on outcome after aneurysmal subarachnoid hemorrhage: a meta-analysis. Neurology, 72(7), pp.635-642.

[4] Ibrahim, G.M. and Macdonald, R.L., 2012. Electrocardiographic changes predict angiographic vasospasm after aneurysmal subarachnoid hemorrhage. Stroke, 43(8), pp.2102-2107.

[5] Ford, R.B. and Mazzaferro, E., 2011. Kirk & Bistner's handbook of veterinary procedures and emergency treatment. Elsevier Health Sciences.

[6] Schuiling, W.J., Algra, A., de Weerd, A.W., Leemans, P. and Rinkel, G.J., 2006. ECG abnormalities in predicting secondary cerebral ischemia after subarachnoid haemorrhage. Acta neurochirurgica, 148, pp.853-858.

[7] Johnson, J.N. and Ackerman, M.J., 2009. QTc: how long is too long?. British journal of sports medicine, 43(9), pp.657-662.

[8] Haugaa, K.H., Johnson, J.N., Bos, J.M., Phillips, B.L., Eidem, B.W. and Ackerman, M.J., 2013. Subclinical cardiomyopathy and long QT syndrome: an echocardiographic observation. Congenital Heart Disease, 8(4), pp.352-359.

[9] Pan J, Tompkins WJ. A real-time QRS detection algorithm. IEEE transactions on biomedical engineering. 1985 Mar(3):230-6.

[10] Prineas, R.J., Crow, R.S. and Zhang, Z.M., 2009. The Minnesota code manual of electrocardiographic findings. Springer Science & Business Media.

[11] Sun, J.X., Reisner, A.T. and Mark, R.G., 2006, September. A signal abnormality index for arterial blood pressure waveforms. In 2006 Computers in Cardiology (pp. 13-16). IEEE.

[12] JA HUTCHINSON P, Seeley HM, Kirkpatrick PJ. Factors implicated in deaths from subarachnoid haemorrhage: are they avoidable?. British journal of neurosurgery. 1998 Jan 1;12(1):37-40.

[13] Schöller, K., Massmann, M., Markl, G., Kunz, M., Fesl, G., Brückmann, H., Pfefferkorn, T., Tonn, J.C. and Schichor, C., 2013. Aneurysmal subarachnoid

hemorrhage in elderly patients: long-term outcome and prognostic factors in an interdisciplinary treatment approach. Journal of neurology, 260, pp.1052-1060.

[14] Tsiatis AA, Degruttola V, Wulfsohn MS. Modeling the relationship of survival to longitudinal data measured with error. Applications to survival and CD4 counts in patients with AIDS. Journal of the American statistical association. 1995 Mar 1;90(429):27-37.

[15] Pollard TJ, Johnson AE. The mimic-iii clinical database. The MIMIC-III Clinical Database. 2016.

[16] Kumar, S.M., Choudhary, D., Arulkumar, A., Anees, T., Nair, S. and Tharakan, J.A., 2013. Prevalence of electrocardiographic changes in patients with acute aneurysmal subarachnoid hemorrhage and their relationship with outcome. Indian Journal of Neurosurgery, 2(01), pp.052-056.

[17] Dowlati, E., Triano, M.J., Felbaum, D.R., Mai, J.C., Aulisi, E.F., Armonda, R.A. and Chang, J.J., 2021. Increased pulse pressure variability within the first 24 hours leads to poor disposition in subarachnoid hemorrhage patients. American Journal of Hypertension, 34(6), pp.645-650.

[18] Kalbfleisch JD, Prentice RL. The statistical analysis of failure time data. John Wiley & Sons; 2011 Jan 25.

[19] Rizopoulos D. Joint models for longitudinal and time-to-event data: With applications in R. CRC press; 2012 Jun 22.

[20] Imai Y, Aihara A, Ohkubo T, Nagai K, Tsuji I, Minami N, Satoh H, Hisamichi S. Factors that affect blood pressure variability. American journal of hypertension. 1997 Nov 1;10(11):1281-9.

[21] Lin, Q.S., Lin, Y.X., Lin, Z.Y., Yu, L.H., Dai, L.S. and Kang, D.Z., 2016. Systolic blood pressure variability is a novel risk factor for rebleeding in acute subarachnoid hemorrhage: a case‐control study. Medicine, 95(11).

[22] Rizopoulos D, Verbeke G, Molenberghs G. Shared parameter models under random effects misspecification. Biometrika. 2008 Mar 1;95(1):63-74.

[23] Ascanio, L.C., Enriquez-Marulanda, A., Maragkos, G.A., Salem, M.M., Alturki, A.Y., Ravindran, K., Fehnel, C.R., Hanafy, K., Ogilvy, C.S., Thomas, A.J. and Moore, J.M., 2020. Effect of blood pressure variability during the acute period of subarachnoid hemorrhage on functional outcomes. Neurosurgery, 87(4), pp.779-787.

[24] Salvagno, M., Geraldini, F., Coppalini, G., Robba, C., Gouvea Bogossian, E., Annoni, F., Vitali, E., Sterchele, E.D., Balestra, C. and Taccone, F.S., 2024. The impact of inotropes and vasopressors on cerebral oxygenation in patients with traumatic brain injury and subarachnoid hemorrhage: A narrative review. Brain sciences, 14(2), p.117.

Chapter 4 Synthetic ABP modeling and artefact rejection within digital twin for SAH management

Control of arterial blood pressure (ABP) plays a crucial role in the management of spontaneous subarachnoid haemorrhage (SAH). Appropriate ABP management is essential for preventing re-bleeding and cerebral vasospasm, as well as reducing secondary brain injury. [1] Additionally, maintaining a stable ABP level ensures a steady supply of oxygenated blood to brain tissues, which is vital for the recovery of neurological functions after SAH. It was shown in Chapter 3 that variability of systolic blood pressure (SBPV) is a useful risk factor for post-SAH mortality, especially in acute phases. These findings suggest that both maintaining proper ABP levels and ensuring their stability are critical in post-SAH management.

The measurement of ABP in the management of SAH patients, especially in the acute phase, is often through an arterial catheter invasively. This involves inserting a catheter directly into an artery, which is connected to a pressure transducer to provide real-time, continuous, and accurate blood pressure readings. However, invasive ABP is associated with bleeding, infection risk, and nerve damage, and should not be performed for extend periods. Non-invasive ABP measurement techniques such as the auscultatory method, and the oscillometric method lack the capability for accurate and continuous long-term monitoring, while advanced measurement techniques such as machine learning-based are still in their preliminary stage. [2]

Digital twins of personalised ABP can serve as a substitute for invasive ABP measurements for short-term monitoring or relatively long-term monitoring with the aid of finger cuff technique, due to its non-invasiveness and ease of use. A digital twin is a digital representation of a physical entity, such as an object, system, or process. In the context of physiological monitoring, digital twin technology allows for the construction of personalised and dynamic representations of a patient's physiological status. These digital twins can be continuously updated and refined with real-time data, such as continuously monitored ABP waveforms.

By utilising synthetic ABP models, digital twins enable clinicians to simulate comprehensive ABP datasets that accurately reflect the physiological processes of individual patients. These models can reconstruct invasive ABP waveforms with personalised characteristics based on finger cuff measurements. This approach also offers valuable insights into how patients might respond to various treatment options without the need for physical interventions, thereby enhancing patient care and improving treatment outcomes.

This chapter will begin by discussing common artefacts in ABP measurements and approaches for artefact rejection. Ensuring artefact-free ABP waveforms is crucial for developing personalised synthetic ABP models and pre-processing raw ABP

waveforms for dynamic prognostic modelling. Following this, a synthetic ABP model will be proposed, focusing on its mathematical expressions and physiological interpretations. The model's performance will be compared with other piecewise ABP models by evaluating their fitting accuracy on ABP waveforms from the MIMIC-II database. Additionally, this model's capability to learn personalised ABP characteristics and reconstruct waveforms that reflect a patient's unique blood pressure profile will be illustrated. Finally, potential applications of the proposed synthetic ABP models in the context of digital twins will be explored.

4.1 Common artefacts and their rejection in ABP waveforms

Real-time measurements of ABP waveforms are often contaminated with artefacts, complicating the extraction of useful physiological features and the development of personalised synthetic ABP models that require artefact-free waveforms. Therefore, artefact detection and rejection are essential pre-processing steps for raw ABP waveforms before further analysis. This section will begin by introducing common artefacts in ABP measurements, discussing their morphology, causes, and mathematical models. Subsequently, synthetic artefacts will be simulated on the basis of these models to develop and refine artefact rejection algorithms.

4.1.1 Common artefacts in ABP measurements

Various types of common artefacts that have been identified clinically are included in our study. Each artefact can be classified as either physiological, such as arrhythmia, or non-physiological, such as measurement problems or operational errors [3]. For ease of comparison and analysis, we have collected and briefly introduced the possible causes of artefacts from relevant literature, along with their mathematical models and morphological properties in simulations. Different types of artefacts with varying intensities are illustrated in Figures 4.1 to 4.8, with high-intensity artefacts represented by solid lines and low-intensity artefacts by dashed lines.

(1) **Saturation to ABP Maximum Artefact** ($\boldsymbol{A_{max}}$) (Figure 4.1): Saturation to ABP maximum artefact A_{max} results in a rapid increase in ABP waveform from its normal value to saturate at the maximal ABP value $\boldsymbol{P_{max}}$, dependent on the equipment used for ABP measurements. The morphological behaviour of this type of artefact can be simulated with a hyperbolic tangent function $tanh$. This type of artefact is likely caused by arterial line flushing, and its severity is defined by the length of the duration $\boldsymbol{L_{max}}$. [3]

Also $\boldsymbol{P_d^{n'}}$ is the closest diastolic pressure prior to the occurrence of the artefact. The duration of the rapid increase is denoted as $\boldsymbol{L_{max_tanh}}$, and is relatively stable in $\boldsymbol{A_{max}}$ artefacts. Thus, for convenience of analysis, we also fix this parameter at a

typical value. The duration of the saturation part prior to resuming normal ABP levels $\boldsymbol{L_{max_saturation}}$ is used to evaluate the severity of this type of artefacts. Thus, the piece-wise function of $\boldsymbol{A_{max}}$ artefact can be expressed as:

$$\boldsymbol{F_{max}} = \begin{cases} \boldsymbol{tanh}\left(\frac{\boldsymbol{\eta_{smax}\pi}}{\boldsymbol{f_s}}\boldsymbol{x}\right)\left(\boldsymbol{P_{max}} - \boldsymbol{P_d^{n'}}\right) + \boldsymbol{P_d^{n'}},\ \boldsymbol{A_{max-1}}\ (\boldsymbol{L = L_{max_tanh}}) \\ \boldsymbol{P_{max}},\ \boldsymbol{A_{max-2}}\ \left(\boldsymbol{L = L_{max_saturation}}\right) \end{cases} \quad (4.1)$$

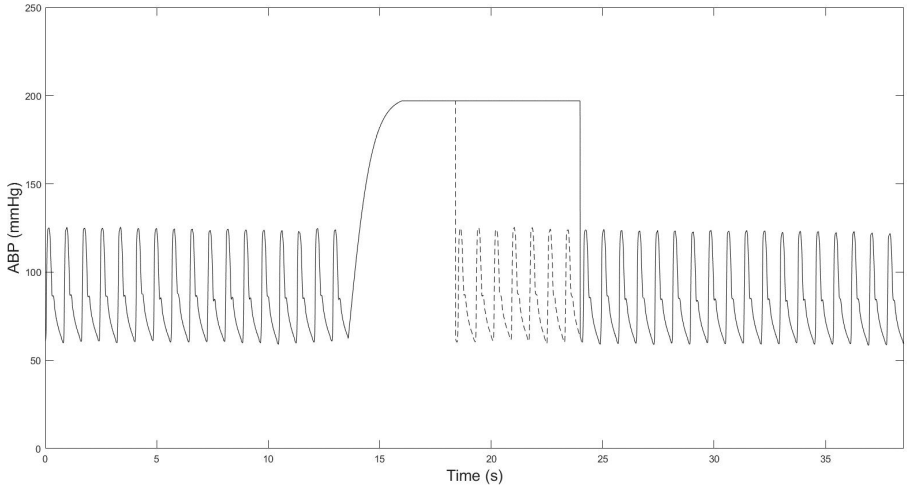


Figure 4.1: Saturation to ABP maximum artefact with different intensity

In this formula, we denote two parts of $\boldsymbol{A_{max}}$ artefacts as $\boldsymbol{A_{max-1}}$ and $\boldsymbol{A_{max-2}}$, followed by the corresponding durations of each part. Similar expressions are also adopted in other types of artefacts.

(2) **Saturation to ABP Minimum Artefact** ($\boldsymbol{A_{min}}$) (Figure 4.2): The morphological changes caused by saturation to ABP minimum artefact $\boldsymbol{A_{min}}$ can be decomposed into a series of characteristic waveforms. These series of changes can be modeled with a piece-wise function with four consecutive parts: 1) rapid diastolic pressure exponentially increase to some value $\boldsymbol{P_m}$; 2) exponential decay from a certain ABP value to some minimum value $\boldsymbol{P_{min}}$; 3) transition back to normal systolic blood pressure; 4) diastolic pressure gradually resumes its unaffected pressure levels. Saturation to ABP Minimum Artefact can be caused by a transient arterial line constriction. Adjusting the severity of $\boldsymbol{A_{min}}$ artefact is mainly implemented by controlling the duration of the decaying section $\boldsymbol{L_{smin-decay}}$.

The morphological changes caused by saturation to ABP minimum artefact ($\boldsymbol{A_{min}}$) can be decomposed into a series of characteristic waveforms. These series of changes can be modeled with a piecewise function with four consecutive parts:

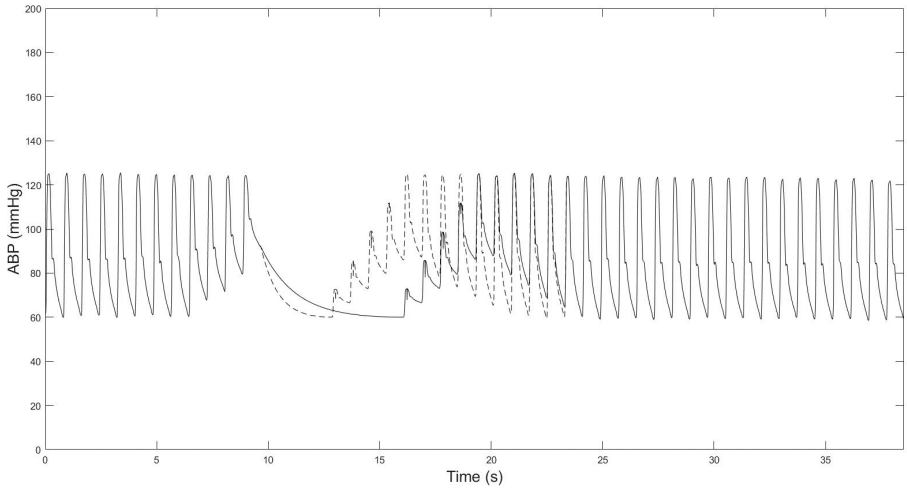


Figure 4.2: Saturation to ABP minimum artefact with different intensity

1. Rapid diastolic pressure increases from $\boldsymbol{P_d^n}$ to some value $\boldsymbol{P_m}$ with rate $\boldsymbol{\eta_{min-1}}$, where this diastolic increase can be modelled with either linear or exponential approach since it lasts only a few cardiac cycles. The waveforms of the cardiac cycles within this part are scaled with reference to the values of systolic and modified diastolic pressure. The duration of this part is denoted as $\boldsymbol{L_{min-1}}$; and $\boldsymbol{D_{min-1}}$ represents the distance between current time points and the point with pressure $\boldsymbol{P_m}$.

2. Exponential-decay from certain ABP value to some minimum value $\boldsymbol{P_{min}}$, which varies with measurement conditions and is usually around $50mmHg$. The decaying waveform is modeled using hyperbolic function $\cosh$, and the steepness of the decay can be fitted with parameter $\boldsymbol{\eta_{min-2}}$. Severity of this artefact type is directly correlated with duration of this decaying section since other parts of the artefact is rather machine intrinsic. Thus, we denote the duration of this section as $\boldsymbol{L_{min-2}}$ and adjust it for the severity effect assessment.

3. Both diastolic and systolic pressure increase linearly or exponentially, waveforms are then generated by a simplified waveform generator using increasing pressure sequences. Since waveforms of this section are restrained within mild fluctuations, the waveform generator is simplified to a piecewise function with only two sub-functions where the effects of $\boldsymbol{P_n^n}$ and $\boldsymbol{P_v^n}$ are ignored. An increase in diastolic and systolic pressure terminates at $\boldsymbol{P_{min-d}}$ and normal value $\boldsymbol{P_s^n}$ respectively, which are defined clinical practically. The duration of this part is denoted as $\boldsymbol{L_{min-3}}$. Noting that $\boldsymbol{N_{min-3}}$ represents the total number of cardiac cycles contained in this part, while $\boldsymbol{D_{min-3}}$ represents the distance between current points and the start of this part in cycles.

4. In this part, systolic pressure has resumed to normal systolic pressure values. Meanwhile, diastolic pressure decreases from $\boldsymbol{P_{min-d}}$ to normal levels. Similarly, changes of pressure points can be approximated with linear, exponential, or

hyperbolic functions. Similarly, the duration of this part is denoted as L_{min-4}. Similar to part 3, N_{min-4} represents the total number of cardiac cycles contained in this part, while D_{min-4} represents the distance between current points and start of this part in cycles.

Also, for the convenience of expression, we use P_i^n $(i \in \{d, s, n, v\})$ to denote the pressure points of current cardiac cycles, while F is used to represent the original value of waveform used to simulate artefacts. Thus, the Saturation to ABP Minimum Artefact (A_{min}) can be modelled using:

$$F_{min} = \begin{cases} \frac{P_s^n - F(x)}{P_s^n - P_d^n}(P_d^n - P_s^n + P_m e^{\eta_{min-1} D_{min-1}}) + P_s^n, \ A_{min-1}(L = L_{min-1}) \\ \frac{cosh(x)acosh(\eta_{min-2}) + (L_{min-2} - x)}{L_{min-2}} + P_{min} + \eta_{min-2}, A_{min-2}(L = L_{min-2}) \\ \frac{P_s^n - F(x)}{P_s^n - P_d^n}\left(\frac{D_{min-3}(P_{min-d} - P_s^n)}{N_{min-3}}\right) + P_{min}, \ A_{min-3}(L = L_{min-3}) \\ \frac{P_s^n - F(x)}{P_s^n - P_d^n}\left(P_{min-d} + \frac{D_{min-4}(P_d^n - P_{min-d})}{N_{min-4}} - P_s^n\right) + P_s^n, A_{min-4}(L = L_{min-4}) \end{cases} \quad (4.2)$$

(3) Reduced Pulse Pressure Artefact (A_{pp}) (Figure 3.13): In reduced pulse pressure artefacts (A_{pp}), pulse pressure gradually declines as the artefact continues due to thrombosis-induced damping in the arterial line. This type of artefact is simulated with gradually decreasing systolic pressure over the artefact window, while the severity of this artefact is described by the duration L_{pp}.

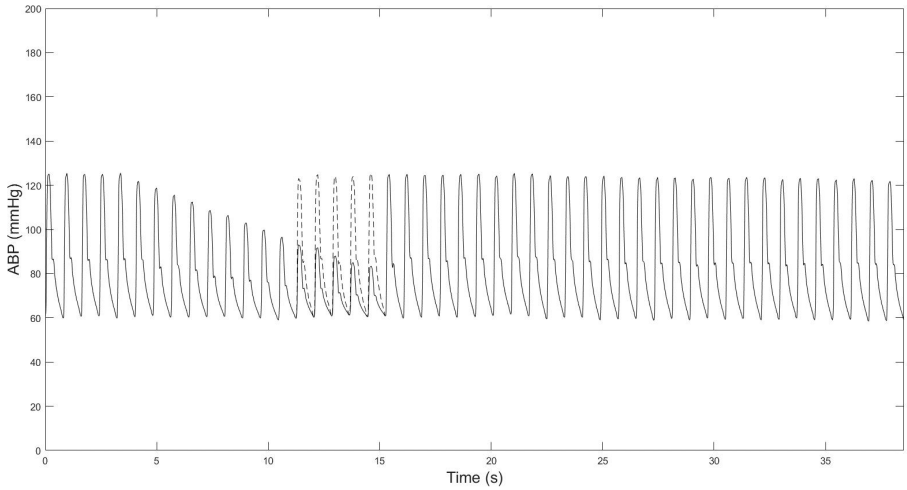


Figure 4.3: Reduced pulse pressure artefact with different intensity

In reduced pulse pressure artefacts (A_{pp}), pulse pressure gradually declines as the artefact continues due to thrombosis-induced damping in the arterial line. We simulate this decline with a linear pattern that the systolic pressure decreases by a fixed rate η_{pp} each cycle, while the severity of this artefact is described by the duration L_{pp}.

Similarly, $\boldsymbol{D_{pp}}$ denotes the number of cardiac cycles of the start of this artefact to current time points. Thus, this type of artefact can be formulated as:

$$\boldsymbol{F_{pp} = \frac{F(x) - P_s^n}{P_s^n - P_d^n}\left(P_s^n - \eta_{pp} D_{pp}\right) + P_d^n,\ A_{pp}\left(L = L_{pp}\right)} \quad (4.3)$$

(4) **Square Wave Artefact** $(\boldsymbol{A_{sw}})$ (Figure 4.4): Square wave artefact ($\boldsymbol{A_{sw}}$) consists of a series of random square waveforms, varying between maximum $\boldsymbol{P_{sw-max}}$ and minimum $\boldsymbol{P_{sw-min}}$, simulating a fast flush test of the sensor. The severity of $\boldsymbol{A_{sw}}$ artefact is strongly correlated with its duration $\boldsymbol{L_{sw}}$.

$\boldsymbol{A_{sw}}$ artefact usually occurs on and off, thus each continuous random square waveform is considered as a single artefact for convenience of further analysis; a simulated $\boldsymbol{A_{sw}}$ artefact can be modeled with:

$$\boldsymbol{F_{sw} = SW_{random}(P_{sw-max}, P_{sw-min}, N_{sw}),\ A_{sw}(L = L_{sw})} \quad (4.4)$$

where $\boldsymbol{SW_{random}}$ is a random square wave generator, simulating square waveforms varying between maximum $\boldsymbol{P_{sw-max}}$ and minimum $\boldsymbol{P_{sw-min}}$, while $\boldsymbol{N_{sw}}$ denotes the number of square waves within the duration $\boldsymbol{L_{sw}}$. The intensity of $\boldsymbol{A_{sw}}$ artefact is adjusted by $\boldsymbol{L_{sw}}$, while $\boldsymbol{N_{sw}}$ are set at a reasonable value.

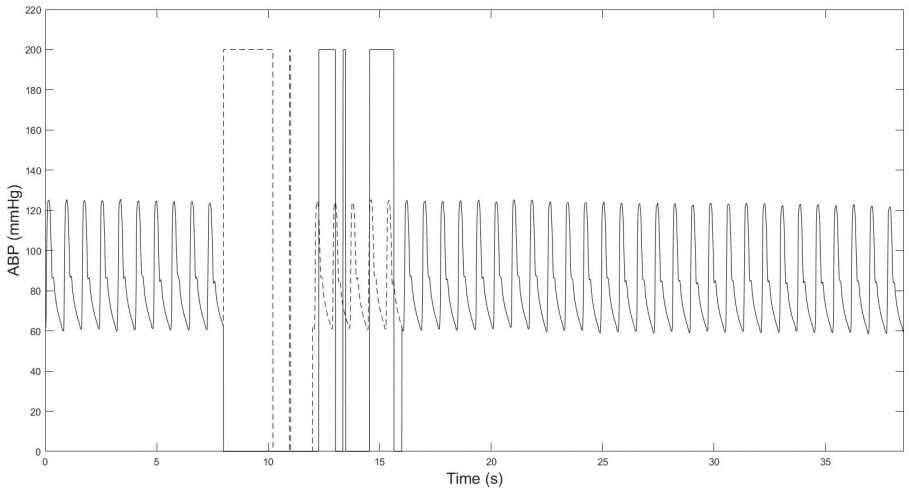


Figure 4.4: Square wave artefact with different intensity

(5) **High Frequency Artefact** $\left(\boldsymbol{A_{hf}}\right)$ (Figure 4.5): The effect of a high frequency artefact ($\boldsymbol{A_{hf}}$) is simulated with additive noise produced by brown noise generator and band-pass filtered over a pass band $[1.5Hz\ 18Hz]$. Occurrence of this type of artefact is correlated with movement and disturbance of the transducer, while the duration of the artefact $\boldsymbol{L_{hf}}$ as well as the noise level $\boldsymbol{NL_{hf}}$ define the severity of the type of artefact. [2]

This type of artefact is simulated brown noise which is then band-pass filtered with passband $[1.5\text{Hz}\ 18\text{Hz}]$. The resultant filtered noise signal is then added to real ABP waveforms. The intensity of $\boldsymbol{A_{hf}}$ artefact is controlled by both the noise level $\boldsymbol{A_{hf}}$ and artefact length $\boldsymbol{L_{hf}}$. Thus, this type of artefact can be formulated by:

$$\boldsymbol{F_{hf} = F(x) + BPF\left(Brownian\left(L_{hf}, NL_{hf}\right)[1.5Hz, 18Hz]\right),\ A_{hf}\left(L = L_{hf}\right)} \quad (4.5)$$

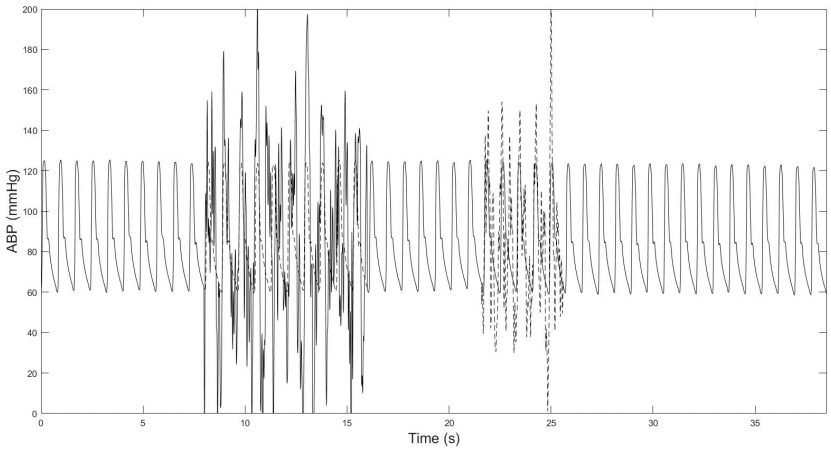


Figure 4.5: High frequency artefact with different intensity

(6) **Impulse Artefact** $\left(\boldsymbol{A_{imp}}\right)$ (Figure 4.6): Impulse artefact ($\boldsymbol{A_{imp}}$) is simulated with an additive main lobe section of the sinc function. Impulse artefacts normally result from motion or mechanical artefact. The severity of $\boldsymbol{A_{imp}}$ artefact is studied by controlling its amplitude $\boldsymbol{M_{imp}}$ and parameter $\boldsymbol{\eta_{imp}}$, related to the main lobe width of the sinc function.

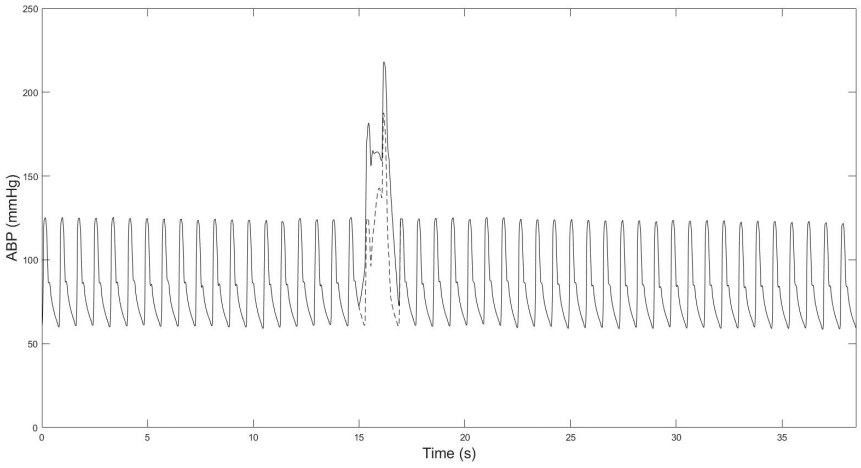


Figure 4.6: Impulse artefact with different intensity

Impulse Artefact is simulated by an additive central lobe of sinc function. The severity of A_{imp} artefact is studied by controlling its amplitude M_{imp} and parameter L_{imp}, which is related to the main lobe width of sinc function. We use $\lfloor ... \rfloor$ to denote that we select the central lobe of sinc function to be added to real ABP waveform for artefact simulation. This type of artefact can be expressed by:

$$F_{imp} = F(x) + M_{imp} \left\lfloor sinc\left(\frac{x}{L_{imp} f_s}\right)\right\rfloor,\ A_{imp}(L = L_{imp}) \quad (4.6)$$

(7) **Ectopic Beat Artefact** (A_{ect}) (Figure 4.7): Ectopic beat artefacts (A_{ect}) are naturally occurring episodes, characterised by extended diastolic runoff, where the corresponding diastolic pressure of that cycle is lower than normal. The length of extended diastolic runoff L_{ect} and the corresponding ectopic diastolic pressure P_{d-ect} jointly determine the severity of a single ectopic beat.

This type of artefact is simulated by modifying the waveform of a single cardiac cycle, where we extend the diastolic runoff of that cycle from original length L_{ect0} to length L_{ect} as well as reduce the diastolic pressure of that cycle from P_d to P_{d-ect} by ΔP_{d-ect}. These two parameters together determine the severity of this artefact. We use P_s to denote the corresponding systolic pressure of that cycle, and then real diastolic runoff can be replaced by A_{ect} artefact which is expressed as:

$$F_{ect} = \frac{F\left(\frac{xL_{ect}}{L_{ect0}}\right) - P_s}{P_s - P_d}\Delta P_{d-ect} + P_s,\ A_{ect}(L = L_{ect}) \quad (4.7)$$

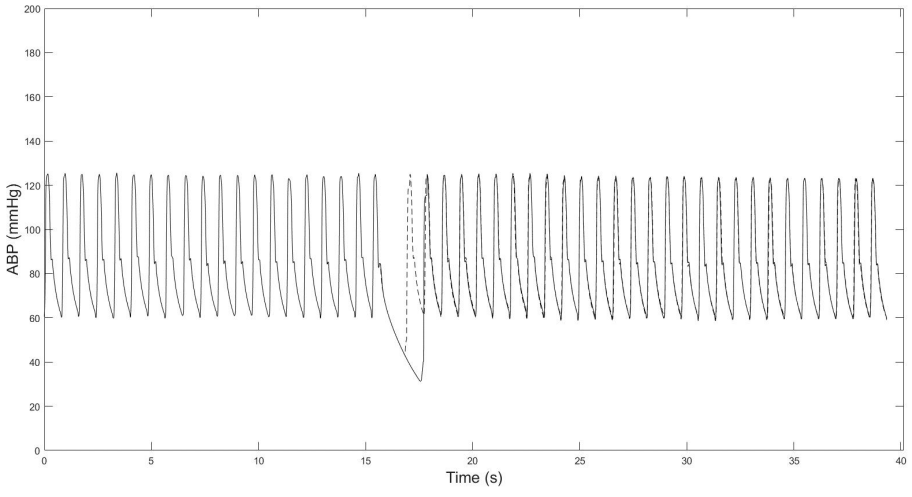


Figure 4.7: Ectopic beat artefact with different intensity

(8) Dicrotic Peak Artefact (A_{dp}) (Figure 4.8): Dicrotic Peak Artefact (A_{dp}) is correlated with arrhythmia, where the secondary peak of that cycle P_v is obviously higher than normal as is shown on BP morphology. The severity of P_v artefact is

defined by the effected pressure level of dicrotic peak $\boldsymbol{P_{v-dp}}$.

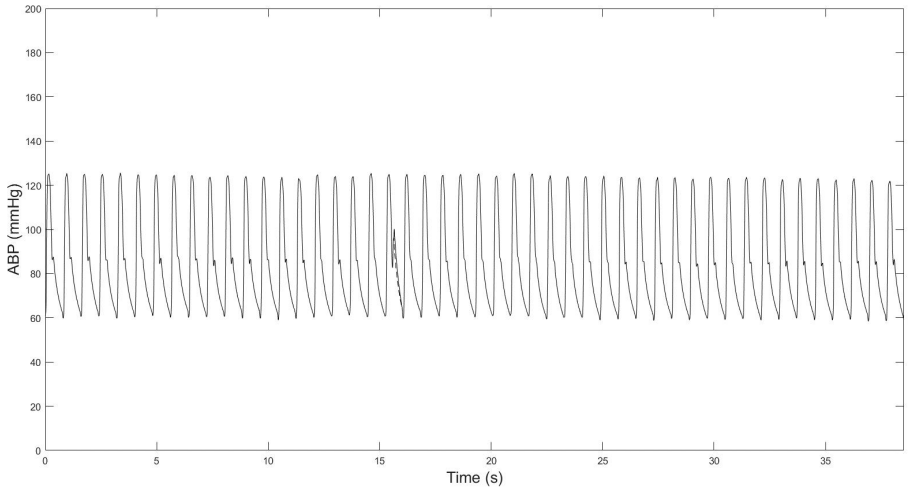


Figure 4.8: Dicrotic peak artefact with different intensity

Dicrotic peak artefact can be also simply simulated by modifying the waveform of dicrotic incisure and diastolic runoff in a single cycle, where we increase the pressure value of secondary peak from $\boldsymbol{P_v}$ to $\boldsymbol{P_{v-dp}}$ by $\boldsymbol{\Delta P_{v-dp}}$, the amplitude of this increase defines the severity of this artefact. Thus, dicrotic peak artefact can be formulated as:

$$\boldsymbol{F_{dp}} = \begin{cases} \dfrac{\boldsymbol{F(x) - P_n}}{\boldsymbol{P_v - P_n}}\left(\boldsymbol{P_{v-dp} - P_n}\right) + \boldsymbol{P_n},\ \boldsymbol{A_{dp-dicrotic\ incisure}} \\ \dfrac{\boldsymbol{F(x) - P_d}}{\boldsymbol{P_v - P_d}}\left(\boldsymbol{P_{v-dp} - P_d}\right) + \boldsymbol{P_d},\ \boldsymbol{A_{dp-diastolic\ runoff}} \end{cases} \quad (4.8)$$

Artefact Type	Notation	Parameters
Saturation to ABP Maximum Artefact	A_{max}	$\eta_{smax},\ P_{max},\ L_{max}$
Saturation to ABP Minimum Artefact	A_{min}	$\eta_{min-1},\ \eta_{min-2},\ L_{min-1},\ L_{min-2},$ $L_{min-3},\ L_{min-4},\ P_{min},\ P_{min-d}$
Reduced Pulse Pressure Artefact	A_{pp}	L_{pp}
Square Wave Artefact	A_{sw}	$P_{sw-max},\ P_{sw-min},\ L_{sw}$
High Frequency Artefact	A_{hf}	$L_{hf},\ NL_{hf}$
Impulse Artefact	A_{imp}	$M_{imp},\ \eta_{imp}$
Ectopic Beat Artefact	A_{ect}	$L_{ect},\ P_{d-ect}$
Dicrotic Peak Artefact	A_{dp}	P_{v-dp}

Table 4.1: Common artefacts and associated parameters

Common artefacts discussed in this section, as well as their associated parameters are summarised in Table 4.1.

4.1.2 Artefact detection and rejection in ABP measurements

Since various types of artefacts severely degrade the quality of ABP recordings, we aim to mitigate these effects by identifying and rejecting contaminated regions in the recordings. Artefact detection focuses on accurately locating the occurrences of artefacts. To accurately identify anomalies in time series, removing the seasonal components, such as the pulsatile waveforms, can help reveal unexpected waveform changes caused by artefacts or noise that are otherwise obscured by these regular fluctuations.

Various signal decomposition approaches have been applied in seasonal-trend decomposition, among which STL (Seasonal-Trend decomposition using Loess) is the most widely used method. STL decomposes time-series signals into a trend component $\boldsymbol{T_t}$, a seasonality component $\boldsymbol{S_t}$ and a remainder component $\boldsymbol{R_t}$ in an iterative way, [4] where:

$$\boldsymbol{Y_t = T_t + S_t + R_t} \quad (4.9)$$

To handle the seasonality shift of ABP signals with which the classical STL algorithm is unable to cope, Robust STL is adopted where the seasonality component $\boldsymbol{S_t}$ is extracted by iterated non-local seasonal filtering. [5] Decomposition of each type of artefact into trend, seasonality, and remainder terms are illustrated in Figure 4.9 to Figure 4.16. In these figures, the original artefact sequences are shown in the upper left; the trend term, characterised by the shape the artefact, is shown in the upper right; the seasonal terms, which denotes the pulsatile waveforms after the artefact component is removed, is shown in the lower left; and the remaining components are shown in the lower right.

After seasonal-trend decomposition, the trend component can be considered as a combination of flat trend with mild fluctuations and outliers caused by artefacts. To detect and to locate these outliers, we propose a dynamic envelope threshold strategy tailored for ABP measurements, inspired by a dynamic thresholding approach to detect spacecraft anomalies by NASA. [6]

In our dynamic thresholding strategy, the statistical properties of input trend components are learnt from the past $\boldsymbol{h}$ observations to determine the threshold level of the current state. We propose an iterated unsupervised threshold strategy to complete artefact regions without the need for labelling anomalies, as shown in Table 4.2.

Given an input trend sequence for artefact detection, all samples of this time series are initialised as non-anomalous. We then use dual sliding windows to capture long-term and short-term statistics of historical observations, termed as $\boldsymbol{y^t}$ and $\boldsymbol{y_s^t}$, respectively

with length $\boldsymbol{h}$ and $\boldsymbol{l}$. The values of $\boldsymbol{h}$ and $\boldsymbol{l}$ are prescribed by following these principles: 1) $\boldsymbol{h}$ should be at least larger than the maximal length across all artefacts to mitigate the impacts of artefacts on baseline statistics; 2) a short sliding window with length $\boldsymbol{l}$ is used for capturing regional statistics, thus $\boldsymbol{l}$ should be larger than the length of any flat local waveforms contained in artefacts, e.g., the saturation part of $\boldsymbol{A_{max}}$ artefacts.

$i = 0$;

$\boldsymbol{is_anomaly_{(0)} = initialise(is_anomaly) = 0}$;

$\boldsymbol{y^t} = [y^{t-h}, \ldots, y^{t-n}, \ldots, y^{t-1}]$;

$\boldsymbol{y_s^t} = [y^{t-l}, \ldots, y^{t-n}, \ldots, y^{t-1}]$;

$z^t = \frac{z_0}{\sqrt{1+\beta_0\sigma^2(\boldsymbol{y_s^t})}}$;

while not converge

$\boldsymbol{y_is_normal_{(i)}^t} = \{y^{t'} \in \boldsymbol{y^t} | is_anomaly_{(i-1)}^t = 0\}$;

$\boldsymbol{normal_range_{(i)}^t} = [\mu(\boldsymbol{y_is_normal_{(i)}^t}) - z^t\sigma(\boldsymbol{y_is_normal_{(i)}^t}), \mu(\boldsymbol{y_is_normal_{(i)}^t})$

Table 4.2: Dynamic thresholding strategy for artefact detection

Then the threshold of the current time is computed from a long sliding window of length $\boldsymbol{h}$ to learn the baseline statistics of the input trend components. A short sliding window of length $\boldsymbol{l}$ is adopted to capture transient anomalies. If the differences of observations and current baseline level are more than $\boldsymbol{z^t}$ times of the standard deviation of the non-anomalous observations within the longer sliding window, observation of current time point is then identified as anomaly. These detected outliers are then marked as anomalous in the next iteration. Observations classified as anomalies by dynamic thresholding are excluded from the threshold calculation in the next iteration.

$\boldsymbol{z^t}$ measures how we can tolerate the degree of deviation from baseline statistics calculated from long sliding windows, where $\boldsymbol{z_0}$ and $\boldsymbol{\beta_0}$ are adjustable parameters and the chosen values. When these parameters are determined, the value of $\boldsymbol{z^t}$ is determined by the variance of the observations within short sliding windows. Intuitively, if recent historical values exhibit severe fluctuations, when the variance is high, $\boldsymbol{z^t}$ would be reduced, implying possible occurrences of artefacts and fewer deviations are tolerated in order to fully locate the region of artefacts.

On the other hand, when the variance is low, the threshold $\boldsymbol{z^t}$ for detecting artefacts would be high, as it is likely that no significant artefacts are present within the short window, aside from some small sharp spikes. In this case, higher deviations from the baseline are tolerated to avoid false positives where normal fluctuations might be misclassified as anomalies. Iteratively, each data point in the trend term is reclassified, and the algorithm is considered converged when the labels of all data points remain unchanged in the final iteration.

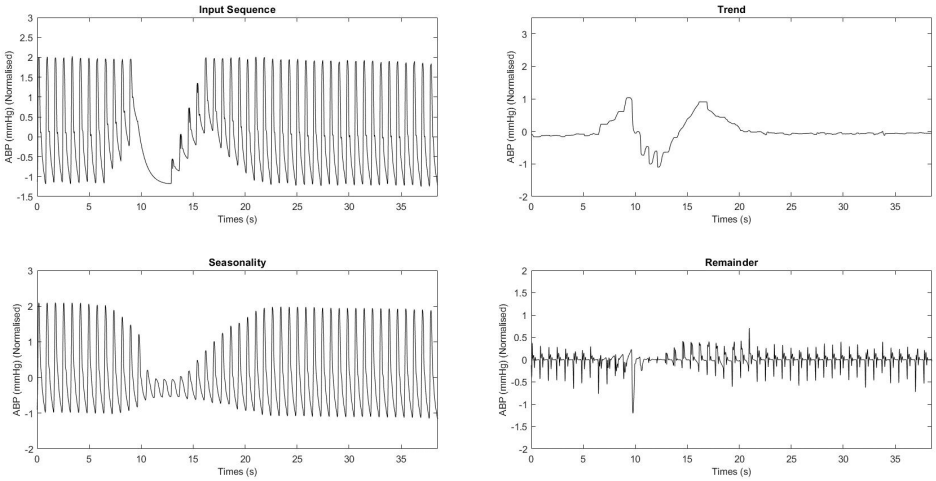


Figure 4.9: Decomposition results of saturation to ABP minimum artefact

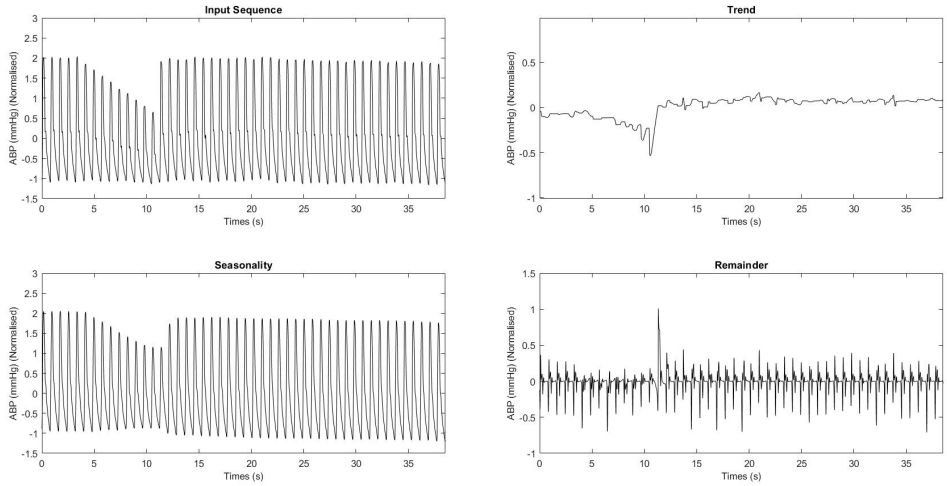


Figure 4.10: Decomposition results of reduced pulse pressure artefact

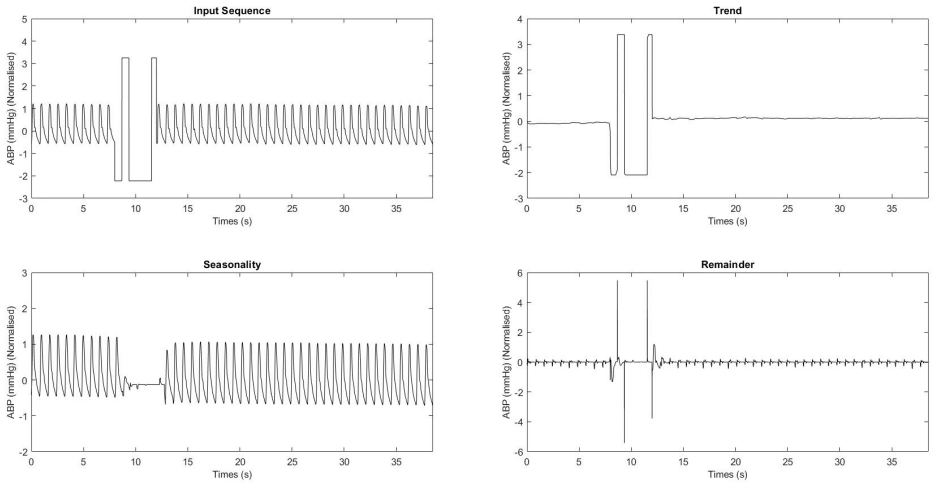


Figure 4.11: Decomposition results of square wave artefact

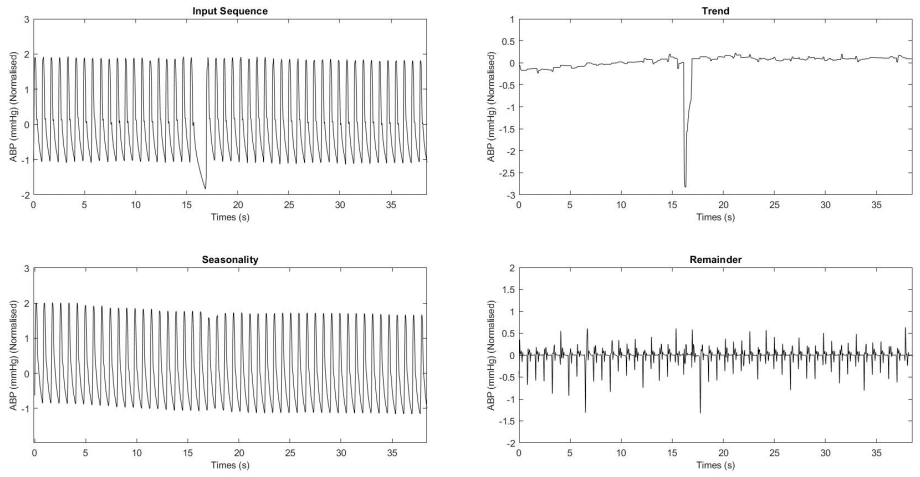


Figure 4.12: Decomposition results of ectopic beat artefact

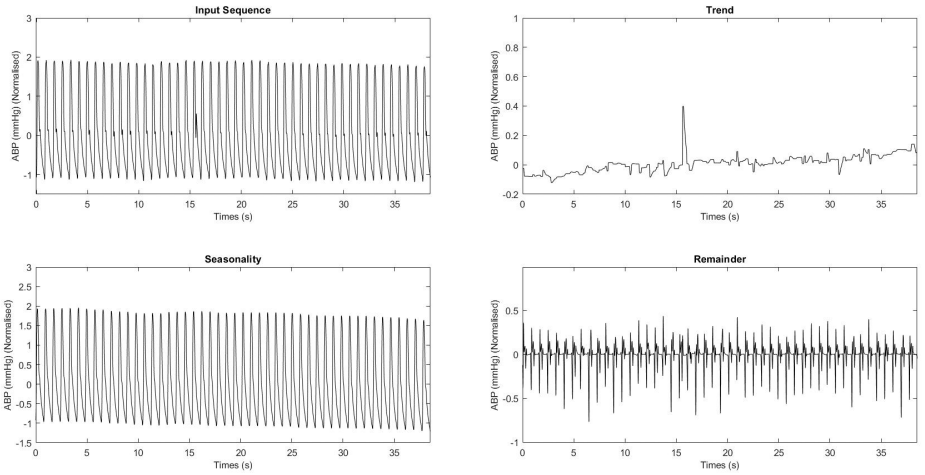


Figure 4.13: Decomposition results of dicrotic peak artefact

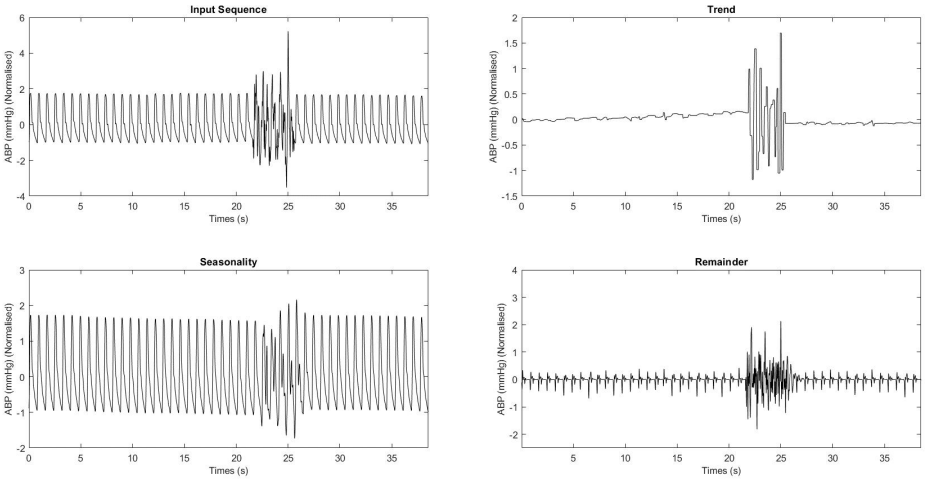


Figure 4.14: Decomposition results of high frequency artefact

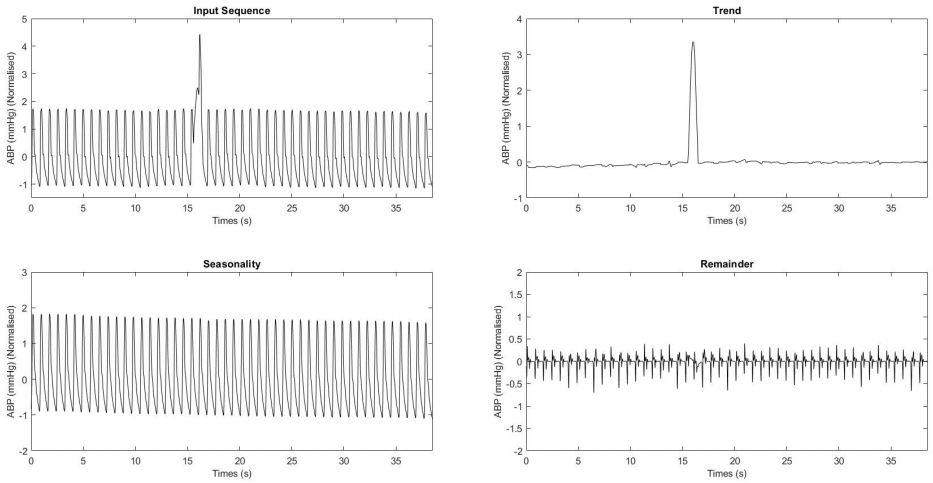


Figure 4.15: Decomposition results of impulse artefact

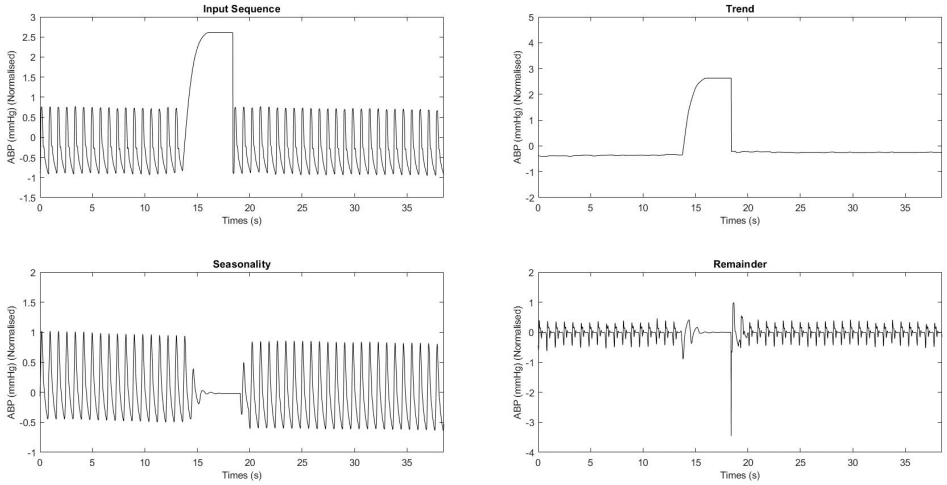


Figure 4.16: Decomposition results of saturation to ABP maximum artefact

Regions of artefacts can be accurately detected and located using our dynamic thresholding strategy, as illustrated in Figure 4.17, where the detected contaminated regions are plotted in red. We have implemented this dynamic thresholding detection strategy on the trend component of Robust STL decomposition and labeled the detected anomaly regions in the original artefact sequences.

The trend term can then be fed into the reconstruction procedure for artefact correction. To maintain the reliability of ABP recordings contaminated by artefacts, we exclude the affected cardiac cycles from further analysis or replace all cardiac cycles containing anomalies with those generated by the proposed synthetic ABP generator. The features required for ABP generation are learned from adjacent cycles.

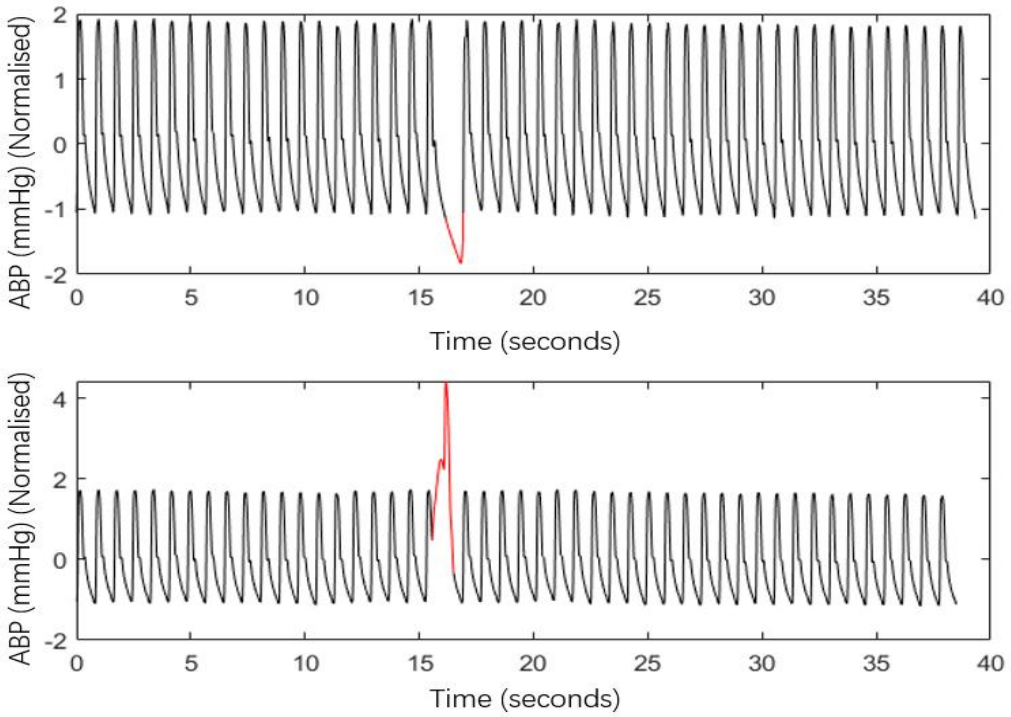


Figure 4.17: Artefact detection (labelled red) of ectopic beat and impulse artefact

4.1.3 Discussion on proposed methods for ABP artefact rejection

In Section 4.1, an artefact rejection algorithm is proposed, specifically designed for the detection and rejection of common artefacts that occur clinically in ABP measurement and monitoring. To facilitate understanding, Figure 4.18 provides a flowchart illustrating the workings of this algorithm.

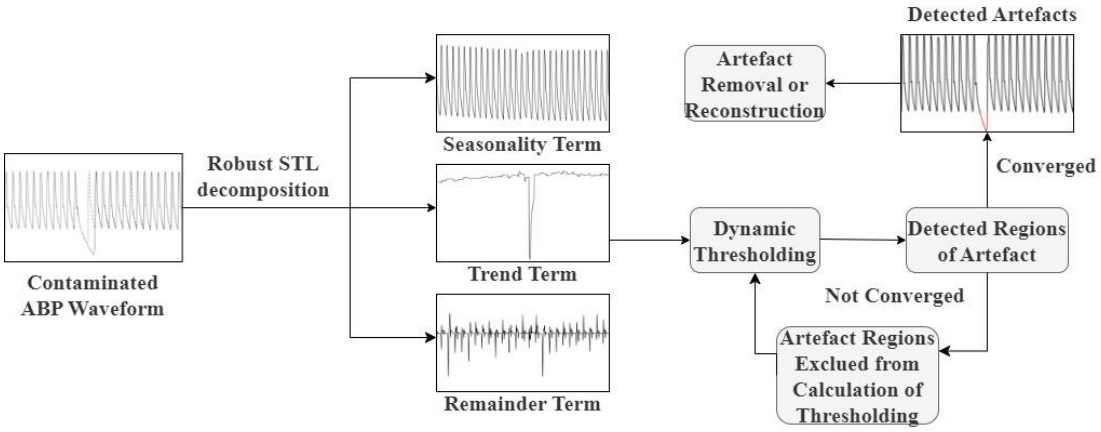


Figure 4.18: Flowchart of proposed artefact detection method for ABP measurement

Artefact rejection is a common task in signal processing, and various methods have

been proposed to handle artefacts, such as template matching, independent component analysis (ICA), statistical thresholding, and machine learning techniques. The optimal choice of artefact rejection approach depends on the type of signal, characteristics of the artefacts, and specific applications. For example, statistical thresholding is suitable for artefact rejection in physiological signals, such as fully automated statistical thresholding for EEG artefact rejection. [7] Physiological signals often exhibit certain statistical characteristics, temporal dependencies, and normal signal variations that statistical thresholding methods can capture, allowing them to differentiate between normal signal variations and artefacts effectively.

Another advantage of this thresholding-based artefact detection approach is that it is fully automated, eliminating the need for manual inspection, labelling of data, and subjective judgments. Statistical thresholding allows for customisation by combining multiple statistical measures, enabling the adjustment of thresholds based on specific requirements and applications.

The artefact rejection approach based on dynamic thresholding, proposed in this section, is suitable for ABP waveforms for several reasons. Firstly, ABP waveforms exhibit long-term trend patterns and short-term variations, such as cyclic patterns. The STL decomposition technique can separate ABP waveforms into seasonal, trend, and residual components, allowing for the identification of artefacts that deviate from these underlying patterns. This separation preserves meaningful physiological information while effectively removing artefacts. The dynamic thresholding strategy adjusts the threshold for artefact detection based on the statistical properties of the trend component. Additionally, the dynamic thresholding can be fine-tuned via parameters to balance sensitivity and specificity.

4.2 Arterial blood pressure modelling

After raw ABP waveforms are processed with artefact rejection procedures, artefacts and noises that could potentially contaminate physiological characteristics are eliminated. Based on segments of these artefact-free ABP waveforms, a personalised synthetic ABP model can be developed, representing a personalised and dynamic digital version of a patient's haemodynamics and enabling the setup of digital twins. This section will begin by examining the morphology and characteristics of ABP waveforms. Building on this foundation, a piecewise, physiologically interpretable ABP model will be developed, with its fitting performance assessed using ABP waveforms from the MIMIC-II database and compared to other ABP models. Finally, methods to generate personalised synthetic ABP waveforms based on the developed models will be discussed.

4.2.1 The morphology of arterial blood pressure waveform

The morphology of ABP, in a single cardiac cycle, exhibits regular fluctuations along

with left ventricular constriction and dilation. The anacrotic limb correlates with aortic valve opening and left ventricular ejection, followed by the anacrotic shoulder, which primarily reflects volume displacement. Systolic pressure $\boldsymbol{P_s}$ is defined by the peak of the ABP waveform, also implying the onset of the dicrotic limb. Then the dicrotic notch $\boldsymbol{P_n}$, representing aortic valve closure, demarcates the dicrotic limb. Shortly after the dicrotic notch, the dicrotic peak $\boldsymbol{P_v}$, primarily caused by retrograde flow, is measured at the secondary peak located on the dicrotic limb and marks the onset of the diastolic phase. During the diastolic phase of the left ventricle, ABP gradually declines until the bottom of the waveform, denoted as diastolic pressure $\boldsymbol{P_d}$, marking the beginning of the systolic upstroke of the next cardiac cycle.

We refer to systolic pressure $\boldsymbol{P_s}$, dicrotic notch $\boldsymbol{P_n}$, dicrotic peak $\boldsymbol{P_v}$ and diastolic pressure $\boldsymbol{P_d}$ as the feature points in the ABP waveforms. These feature points characterise the beat-to-beat fluctuations of ABP and are important in haemodynamic analysis; they also demarcate the ABP waveform throughout a cardiac cycle into four components as shown in Figure 4.19.

Since arterial blood pressure exhibits obvious morphological characteristics, several models have been proposed to describe cardiac cycles. For example, a model has been proposed to describe the time series of ABP signals using both data-driven approaches and physiological principles. [8] In this model, diastolic pressure, systolic pressure, dicrotic notch and dicrotic peak are respectively denoted as $\boldsymbol{P_d}$, $\boldsymbol{P_s}$, $\boldsymbol{P_n}$ and $\boldsymbol{P_v}$,while $\boldsymbol{\Delta t_{ds}}$, $\boldsymbol{\Delta t_{dn}}$, $\boldsymbol{\Delta t_{dv}}$ denote the intervals between the onset of cardiac cycles and systolic, dicrotic notch, and dicrotic peak pressure points, as illustrated in Figure 4.19.

The blood pressure waveform of the $\boldsymbol{j^{th}}$ cardiac cycle can then be approximated by a simple piecewise-linear approach, which can be formulated as:

$$\boldsymbol{f_{ds}(t) = \frac{P_s - P_d}{t_s - t_d} \bullet (t - t_d) + P_d} \quad (4.10)$$

$$\boldsymbol{f_{sn}(t) = \frac{P_n - P_s}{t_n - t_s} \bullet (t - t_d) + P_s} \quad (4.11)$$

$$\boldsymbol{f_{nv}(t) = \frac{P_v - P_n}{t_v - t_n} \bullet (t - t_n) + P_n} \quad (4.12)$$

$$\boldsymbol{f_{vd}(t) = \frac{P_{d'} - P_v}{t_{d'} - t_v} \bullet (t - t_v) + P_v} \quad (4.13)$$

To model the characteristic exponential decay during diastole, $\boldsymbol{f_{vd}(t)}$ can be alternatively given by:

$$\boldsymbol{f_{vd}(t) = P_{d'} + (P_v - P_{d'}) \bullet \left[\frac{t_{d'} - t}{t_{d'} - t_v}\right] \bullet F(t)} \quad (4.14)$$

$$\boldsymbol{F(t) = c_d \, exp\left[m_1(t_{d'} - t_v)\right] + (1 - c_d) \, exp\left[m_2(t_{d'} - t_v)\right]} \quad (4.15)$$

wherein $\boldsymbol{c_d}$, $\boldsymbol{m_1}$ and $\boldsymbol{m_2}$ are shaping parameters of the exponential decay.

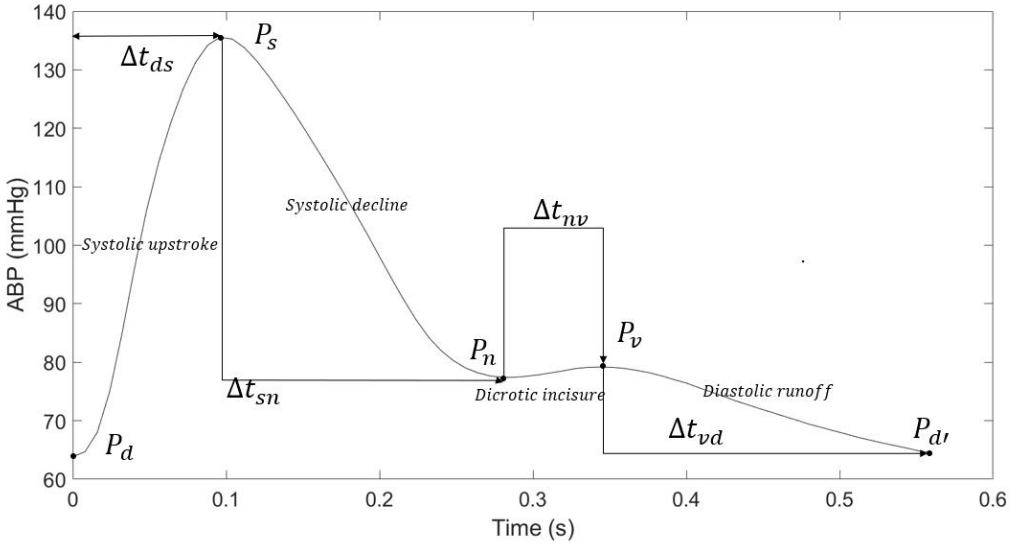


Figure 4.19: ABP waveform of a typical single cardiac cycle

This morphological modelling framework serves as a realistic blood pressure generator to compile a virtual database based on prescribed parameters, e.g., mean systolic pressure $\overline{\boldsymbol{P_S}}$, mean diastolic pressure $\overline{\boldsymbol{P_d}}$, baroreflex sensitivity coefficient $\boldsymbol{\alpha_0}$ and Windkessel time constant $\boldsymbol{\tau}$, which determine the spectral content and other dynamic features of simulated time series.

Besides this parametric framework, many other approaches have been adopted to quantitatively describe ABP signals, such as Gaussian, Rayleigh, Log-normal, and Double-exponential kernel functions. [9] For example, an ABP waveform model has been proposed with three Gaussian functions, respectively corresponding to systolic wave, tidal wave, and dicrotic wave.

In this modelling strategy, the ABP signal is segmented into a series of cardiac cycles, which are then quantitatively described using the pulse decomposition analysis (PDA) approach. The recorded ABP signals commonly consist of systolic wave and several reflection waves due to some vessel bifurcations. Specifically, single-cycle ABP waveform is approximated by three Gaussian functions and an integrated straight-line baseline, which can be formulated as:

$$\widehat{\boldsymbol{y}}_{\boldsymbol{i}}(\boldsymbol{n}) = \sum_{\boldsymbol{l}=\boldsymbol{1}}^{\boldsymbol{3}} \boldsymbol{g}_{\boldsymbol{i}}^{\boldsymbol{l}}\left(\boldsymbol{n}, \boldsymbol{a}_{\boldsymbol{i}}^{\boldsymbol{l}}, \boldsymbol{b}_{\boldsymbol{i}}^{\boldsymbol{l}}, \boldsymbol{c}_{\boldsymbol{i}}^{\boldsymbol{l}}\right) + \boldsymbol{k}_{\boldsymbol{i}}\boldsymbol{n} + \boldsymbol{b}_{\boldsymbol{i}} = \sum_{\boldsymbol{l}=\boldsymbol{1}}^{\boldsymbol{3}} \boldsymbol{a}_{\boldsymbol{i}}^{\boldsymbol{l}} \exp\left[-\frac{\left(\boldsymbol{n}-\boldsymbol{b}_{\boldsymbol{i}}^{\boldsymbol{l}}\right)^{\boldsymbol{2}}}{\left(\boldsymbol{c}_{\boldsymbol{i}}^{\boldsymbol{l}}\right)^{\boldsymbol{2}}}\right] + \boldsymbol{k}_{\boldsymbol{i}}\boldsymbol{n} + \boldsymbol{b}_{\boldsymbol{i}}, \boldsymbol{n} \in [\boldsymbol{1}, \boldsymbol{PPI}(\boldsymbol{i})] \quad (4.16)$$

Similar to the three-Gaussian-function-based PDA model, other models based on kernel functions can also provide parametric expressions of ABP waveforms, providing a compact representation of physiological features.

As has been discussed in this section, many approaches have been proposed for ABP waveform modelling. However, to simulate synthetic artifacts for developing and assessing artifact rejection algorithms, the morphological characteristics of

waveforms should be adjustable via parameters according to artificial ABP artifact models developed from clinical findings. In this context, the three-Gaussian-function-based PDA model is not optimal for this application as morphological characteristics, e.g., systolic pressure, cannot be directly adjusted via parameters. Thus, a parametric synthetic ABP model that can mimic specific patterns, e.g., RSA and Mayer waves, and morphological characteristics needs to be developed.

4.2.2 Piece-wise parametric ABP model

The feature points $\boldsymbol{P_s}$, $\boldsymbol{P_n}$, $\boldsymbol{P_v}$, $\boldsymbol{P_d}$ demarcate a single cardiac cycle into four components. We propose a piecewise parametric curve to fit realistic ABP waveforms according to their morphological features. The systolic upstroke begins along with the onset of rapid ejection and terminates at the intersection of rapid and slow ejection. Since the spine of this component is characterised by a rapid rise while both tails are flat, this component can be modelled using a sigmoidal function. Considering the feasibility of parameterisation among a series of sigmoidal functions, the logistic function is selected due to the physiological interpretability of its parameters. Thus, the systolic upstroke component can be modelled as:

$$\boldsymbol{f_{ds}} = -\frac{\boldsymbol{\alpha_{ds}}}{\boldsymbol{1 + e^{-\beta_{ds}(x-\gamma_{ds})}}} + \boldsymbol{c_{ds}} \quad (4.17)$$

where the parameters are described in Table 4.3.

Parameter	Physical Interpretation	Physiological Interpretation
α_{ds}	Amplitude of upstroke	Pulse pressure
β_{ds}	Steepness of upstroke	Level of myocardial contractility, etc.
γ_{ds}	Time shift	Time shift
c_{ds}	Lower baseline amplitude	Diastolic blood pressure level

Table 4.3: Physical and physiological interpretations of systolic upstroke parameters

The systolic decline component is defined by a slow ejection period that terminates at the opening of the aortic valve. In this period, the blood ejected from the ventricle is not enough to compensate for that flowing out from the aortic root, when ABP declines in an approximately inverse sigmoidal pattern. Similarly, the systolic decline component can be modelled as:

$$\boldsymbol{f_{sn}} = \frac{\boldsymbol{\alpha_{sn}}}{\boldsymbol{1 + e^{\beta_{sn}(x-\gamma_{sn})}}} + \boldsymbol{c_{sn}} \quad (4.18)$$

where the parameters are described in Table 4.4.

The dicrotic incisure component correlates with the dicrotic pulse, which, under widely adopted ABP sampling rates, will only cover a few samples. Thus, knowing $\boldsymbol{P_n}$ and $\boldsymbol{P_v}$ as both ends of this component, we can simplify this component $\boldsymbol{f_{nv}}$ using a linear model passing through feature points at both ends, which reduces the complexity of our model compared to parametrically modelling this component.

Parameter	Physical Interpretation	Physiological Interpretation
α_{sn}	Amplitude of decline	Systolic-dicrotic notch pressure difference
β_{sn}	Steepness of decline	Level of aortic elasticity, etc.
γ_{sn}	Time shift	Time shift
c_{sn}	Upper baseline amplitude	Systolic blood pressure level

Table 4.4: Physical and physiological interpretations of systolic decline parameters

The diastolic runoff component is primarily composed of rapid and slow filling periods, when the negative pressure formed by left ventricular myocardial relaxation pumps the blood from the left atrium to the left ventricle. The waveform of the diastolic runoff exhibits the shape of exponential decay; thus, we adopt two exponential functions to model these two filling periods:

$$\boldsymbol{f_{vd} = \alpha_{vd-rapid} e^{-\beta_{vd-rapid}} + \alpha_{vd-slow} e^{-\beta_{vd-slow}}, \left(\beta_{vd-rapid} > \beta_{vd-slow}\right)} \quad (4.19)$$

where the parameters are described in Table 4.5.

Parameter	Physical Interpretation	Physiological Interpretation
$\alpha_{vd-rapid}$	Weight of rapid decay	Weight of rapid filling period
$\alpha_{vd-slow}$	Weight of Slow Decay	Weight of Slow Filling Period
$\beta_{vd-rapid}$	Rapid Decaying rate	Level of Peripheral Resistance, etc.
$\beta_{vd-slow}$	Slow Decaying rate	Level of Peripheral Resistance, etc.

Table 4.5: Physical and physiological interpretations of diastolic runoff parameters

Based on the morphological features of the ABP waveform, we have proposed a piecewise curve-fitting strategy using the method of non-linear least squares. However, this strategy cannot guarantee that the fitted curves pass through the feature points. To preserve these physiological features as well as to improve the fitting performance of our model, we apply a Gaussian-curve optimiser to our existing model. Having detected values of feature points, this optimiser can improve our model in various aspects: 1) preserve feature points for further analysis; 2) reduce fitting errors; 3) smooth the fitting curves at intersections between components, especially for dicrotic incisure, which feature points at both ends are already preserved.

The Gaussian-curve optimiser is deployed centered at component intersections, which replace the fitted values of intersections with detected realistic feature point values. We term the corresponding optimiser centered at $\boldsymbol{t_d}$, $\boldsymbol{t_s}$, $\boldsymbol{t_n}$ and $\boldsymbol{t_v}$ as $\boldsymbol{G_d}$, $\boldsymbol{G_s}$, $\boldsymbol{G_n}$ and $\boldsymbol{G_v}$ respectively. An optimiser is composed of two half-Gaussian distribution curves extended to left and right with different standard deviations dependent on the duration of the component on either side. For example, the weight of the optimiser centred at $\boldsymbol{t_s}$ can be expressed as:

$$G_s = \begin{cases} e^{\frac{-(t-t_s)^2}{(\sigma \Delta t_{ds})^2}}, & t < t_s \\ e^{\frac{-(t-t_s)^2}{(\sigma \Delta t_{sn})^2}}, & t \geq t_s \end{cases} \quad (4.20)$$

The weight of optimisers centred at other feature points, G_d, G_n and G_v, can be expressed in similar formulae. σ is the parameter denoting the attenuation rate of the effect of the optimiser, which is fine-tuned to minimize the RMSE. Thus, the fitted model of each component can be modified as equations:

$$\widehat{f_{ds}} = P_d G_d + P_s G_s + (1 - G_d - G_s) f_{ds} \quad (4.21)$$

$$\widehat{f_{sn}} = P_s G_s + P_n G_n + (1 - G_s - G_n) f_{sn} \quad (4.22)$$

$$\widehat{f_{nv}} = P_n G_n + P_v G_v + (1 - G_n - G_v) f_{nv} \quad (4.23)$$

$$\widehat{f_{vd}} = P_v G_v + P_d G_d + (1 - G_v - G_d) f_{vd} \quad (4.24)$$

Parametric modelling of the ABP waveform expresses ABP signals in a compact representation, enabling us to capture the temporal variability of physiological features. Generation of synthetic ABP signals provides a platform for control, prediction, identification, detection, and simulation of occurrences of various types of artefacts.

4.2.3 Assessing the fitting performance of ABP models

The fitting accuracy of a synthetic ABP model is important for ensuring that the research findings based on these models are reliable and applicable to real-world clinical situations. Thus, the fitting performance of different ABP models should be compared. Meanwhile, the effects of Gaussian curve optimiser on curve fitting should also be examined.

For assessment of curve fitting performance, real ABP waveforms are included in this study, selected from the UCI dataset. The UCI dataset is a filtered version of MIMIC-II waveform database and contains 12000 instances of ABP data from 942 patients. The data inclusion process is illustrated in Figure 4.20. Only instances with waveform length longer than 5 minutes are selected since short waveform recordings can be significantly affected by artefacts.

In inspection of ABP instances, 3600 ABP instances were found as abnormal waveforms. The absence of dicrotic notch was found to be the most common waveform abnormality (1058 instances), associated with significant peripheral vascular disease, followed by bisferiens pulse (307 instances), dicrotic pulse (407 instances), arrhythmias (626 instances), bigeminal pulse (60 instances), and pulses paradoxus (43 instances). 560 waveform instances contaminated with severe artefacts were also excluded. Examples of these waveform abnormalities are shown in Figure 4.21.

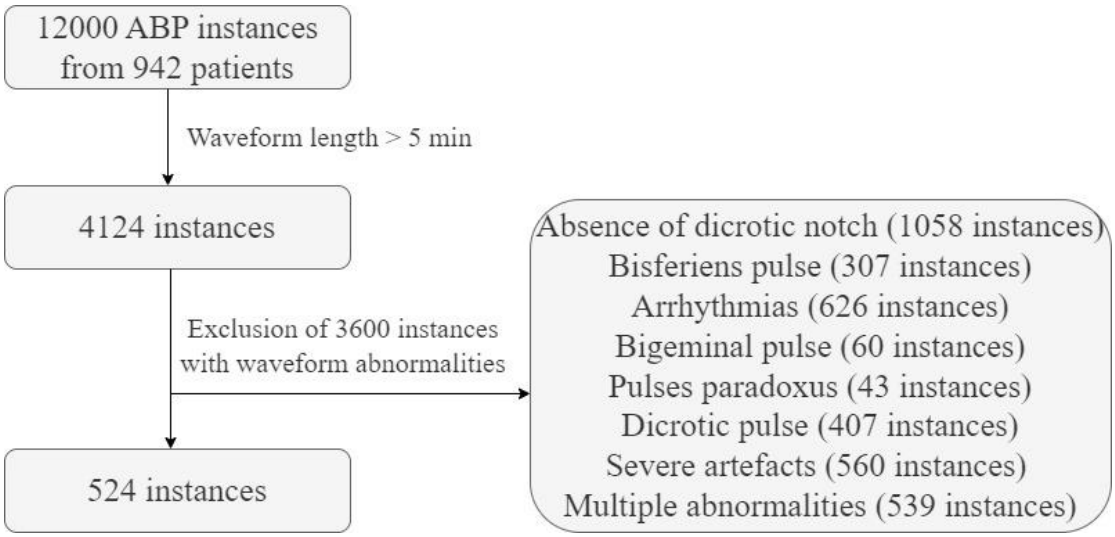


Figure 4.20: Data inclusion process for fitting performance assessment

Cardiac cycle waveforms were extracted from 524 ABP instances, and the distributions of their characteristic pressure values, including systolic pressure $\boldsymbol{P_s}$, dicrotic notch $\boldsymbol{P_n}$, dicrotic peak $\boldsymbol{P_v}$ and diastolic pressure $\boldsymbol{P_d}$ are shown in Figure 4.22.

Then the fitting performance of different ABP models and different attenuation rates of the Gaussian curve optimiser, as shown in Table 4.6, is compared with the mean RMSE and corresponding standard deviation across cardiac cycle waveforms.

Model	***No σ***	**$\sigma = 0.05$**	**$\sigma = 0.10$**	**$\sigma = 0.15$**	**$\sigma = 0.20$**	**$\sigma = 0.25$**	**$\sigma = 0.30$**
Linear	2.4425	2.0581	1.8998	1.7901	1.7692	2.0146	2.5086
Double Exponential Diastole	2.5808	2.1927	2.0123	1.8892	1.8690	2.1216	2.6260
Triple Gaussian	1.7750	1.5470	1.4139	1.4090	1.6619	2.1844	2.8018
Our Model	1,1743	0.9919	0.9047	1.0624	1.5468	2.2405	2.9534

Table 4.6: Mean RMSE across cardiac cycle waveforms of different ABP models

Our proposed parametric ABP model outperforms other models regarding the fitting performance and variance of parameters. The Gaussian-function optimiser with fine-tuned $\boldsymbol{\sigma}$ improves the fitting accuracy in all models. $\boldsymbol{\sigma = 0.10}$ is the optimal setting for our proposed model. The optimiser can improve the performance of curve fitting since the feature points in ABP waveforms can serve as reference landmarks for model calibration. By incorporating these points into a ABP model, the fitting process can be optimised to closely match the observed ABP waveform, which improves the overall accuracy and reliability. The fitting performance of all considered models is illustrated in Figure 4.23 with a single cardiac cycle, where the real waveform to fit to is also shown.

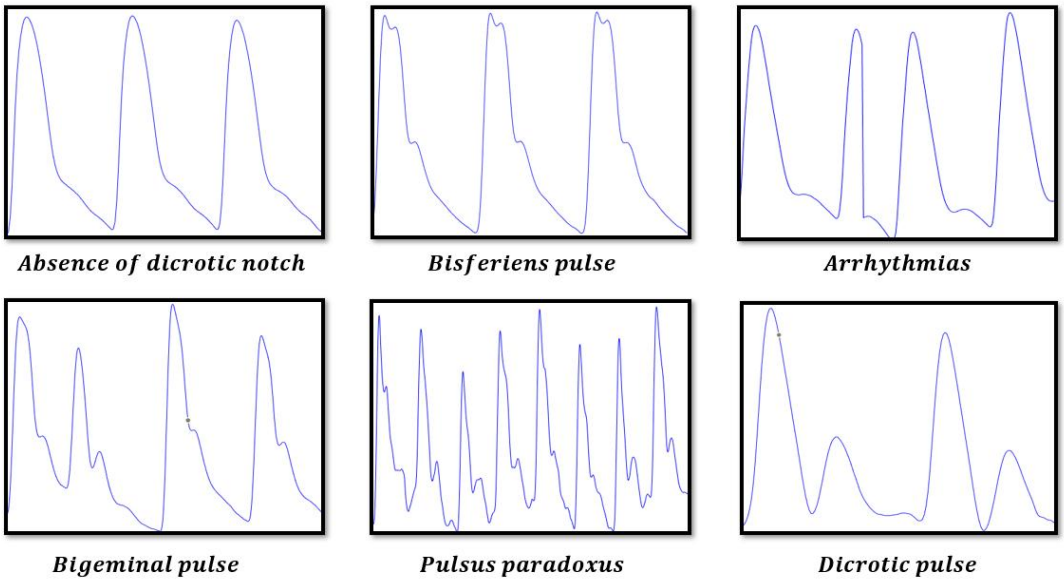


Figure 4.21: Waveform abnormalities in ABP recordings

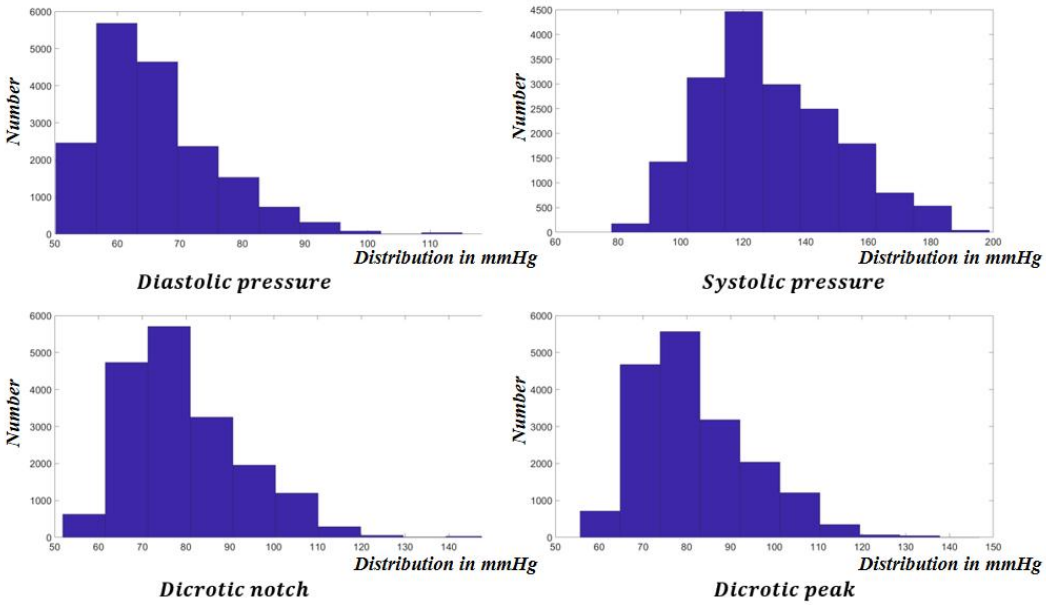


Figure 4.22: Distribution of characteristic pressure values

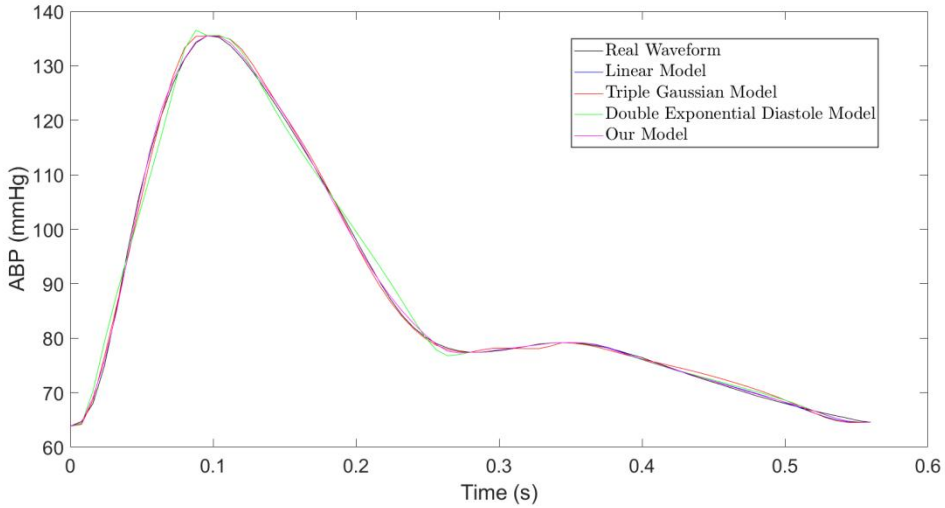


Figure 4.23: Curve fitting performance of different models with the optimiser

Despite good fitting accuracy of the proposed model, there are some limitations. The model accuracy has only been assessed based on ABP recordings with normal morphology, which results in insufficient representation of pathological conditions. This proposed synthetic ABP model is suitable as a platform for artefact simulation and development of artefact rejection methods since artefact models are developed based on ABP waveforms of normal physiological conditions. However, the value of this proposed model in other applications remains to be explored and validated.

4.2.4 Personalised synthetic ABP generation

The parametric ABP model proposed in our study can be used, combined with detected feature points and relevant temporal information, to generate synthetic ABP signals of individuals under normal physiological conditions. The auto-regressive integrated moving average (ARIMA) model can be suitable for modeling sequences of pressure points and time intervals between as well as suitable for generation of feature sequences for constructing synthetic ABP waveforms due to the following reasons.

The ARIMA model captures relationships between current and past values through its auto-regressive (AR) component, modeling dependencies such as systolic pressure values across cardiac cycles. Its integrated (I) component achieves stationarity by differencing the time series, removing trends, seasonality, and other non-stationary elements due to physiological variations. The moving average (MA) component then models dependencies between current pressure values and past residual errors, capturing remaining dependencies or noise to improve accuracy. Together, these components enable ARIMA to forecast future values based on historical data, generating sequences that simulate the continuation of original feature sequences.

To simulate the dependencies among feature sequences, we refer to the antecedent

pressure feature $\boldsymbol{P_d}$, the first feature point in a cardiac cycle, and the duration of a cardiac cycle T, as independent variables. These two features are directly simulated using the ARIMA model from pressure and temporal feature sequences of realistic signals. The remaining features are termed dependent variables, where the pressure variables are dependent on the pressure feature $\boldsymbol{P_d}$ and temporal sequences are dependent on $\boldsymbol{T}$. Generation of feature sequences follows the following procedures and is illustrated in Figures 4.24 and 4.25, where we find that simulated and real features have similar statistical properties.

(1) We denote paired independent and dependent feature sequences detected from realistic signals as $\boldsymbol{x_0}$ and $\boldsymbol{y_0}$, which are used to train corresponding ARIMA models. The pre-trained models are then applied to simulate an example pair of feature sequences $\boldsymbol{x}$ and $\boldsymbol{y}$ as preparation for determining our proposed synthetic feature sequences $\hat{\boldsymbol{x}}$ and $\hat{\boldsymbol{y}}$.

(2) Since the temporal patterns of $\boldsymbol{x_0}$ have been captured in training the ARIMA model, a random sequence of $\boldsymbol{x}$ can be directly adopted as $\hat{\boldsymbol{x}}$. To determine $\hat{\boldsymbol{y}}$ that inherits the statistical properties and the correlation with the paired independent sequence, we propose a mixed strategy to determine $\hat{\boldsymbol{y}}$, where:

$$\hat{\boldsymbol{x}} = \boldsymbol{x} \quad (4.25)$$

$$\hat{\boldsymbol{y}} = \boldsymbol{k_x x} + \boldsymbol{k_y y} + \boldsymbol{c} \quad (4.26)$$

such that:

$$\boldsymbol{k_x} = \frac{\boldsymbol{\sigma(x_0)\sigma(y_0)cov(x,y) - \sigma(x)\sigma(y)cov(x_0,y_0)}}{\boldsymbol{\sigma(x_0)\big(\sigma(x)cov(x,y) - \sigma(y)var(x)\big)}} \quad (4.27)$$

$$\boldsymbol{k_y} = \frac{\boldsymbol{var(x)\big(cov(x_0,y_0) - \sigma(x_0)\sigma(y_0)\big)}}{\boldsymbol{\sigma(x_0)\big(\sigma(x)cov(x,y) - \sigma(y)var(x)\big)}} \quad (4.28)$$

$$\boldsymbol{c} = \boldsymbol{\mu(y_0) - k_x\mu(x) - k_y\mu(y)} \quad (4.29)$$

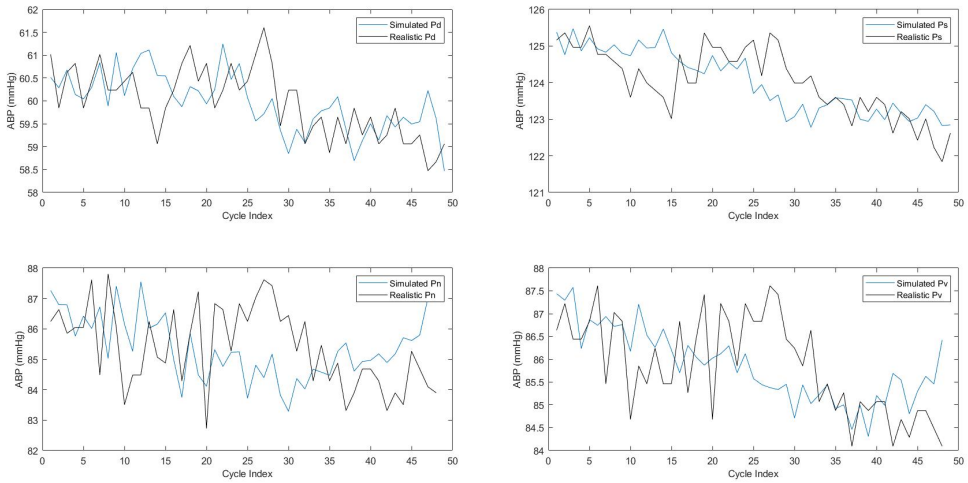


Figure 4.24: Comparison of simulated (blue solid) and realistic (black solid) pressure features

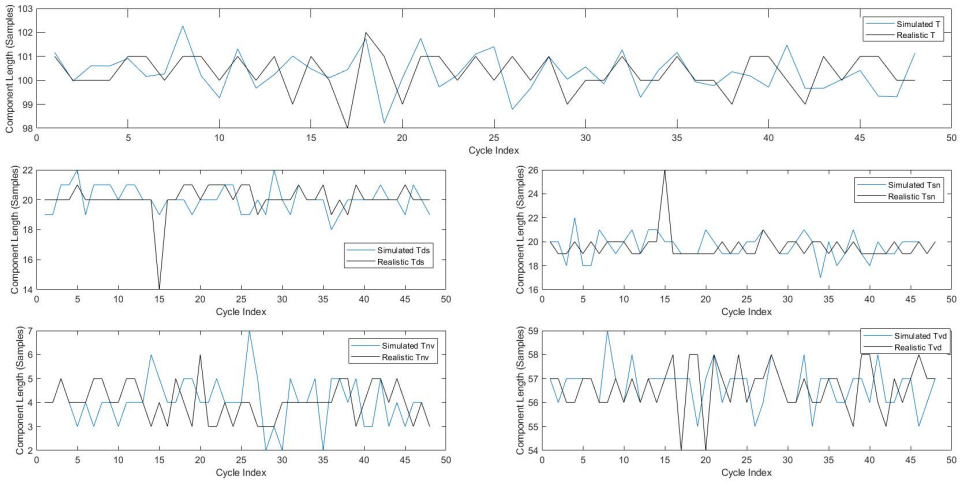


Figure 4.25: Comparison of simulated (blue solid) and realistic (black solid) temporal features

This guarantees that the mean, variance of $\hat{\boldsymbol{y}}$ and its degree of correlation with matched $\hat{\boldsymbol{x}}$ are consistent with the realistic feature sequence $\boldsymbol{y_0}$ statistically.

(3) Having simulated a series of synthetic feature sequences from realistic physiological properties of candidates, the waveforms of components can then be constructed by taking simulated feature sequences into our synthetic parametric model as a waveform generator, while the input-output relationship is shown in Table 4.7. The parameters of the components required to build the waveform are computed by regression techniques corresponding to the relevant feature variables, where $\boldsymbol{P_{d'}}$ denotes the diastolic pressure of next cardiac cycle.

Parameters to Predict	***Input Variables***
$\alpha_{ds}, \beta_{ds}, \gamma_{ds}, c_{ds}$	$P_d, P_s, \Delta t_{ds}$
$\alpha_{sn}, \beta_{sn}, \gamma_{sn}, c_{sn}$	$P_s, P_n, \Delta t_{sn}$
$\alpha_{vd-rapid}, \alpha_{vd-slow}, \beta_{vd-rapid}, \beta_{vd-slow}$	$P_v, P_{d'}, \Delta t_{vd'}$

Table 4.7: Input variables and parameters to predict in waveform generation

Our proposed parametric ABP generator thus is capable of simulating synthetic ABP signals and artefacts with controlled settings, which inherits important physiological information from realistic signals as well as providing sufficient and reliable datasets for developing and assessing artefact rejection approaches.

In section 4.2, a piece-wise parametric ABP model has been proposed to fit different components of ABP waveforms and can be utilised to generate simulated ABP waveforms as well. To make all these procedures easier to understand, Figure 4.26 provides a schematic of how they work.

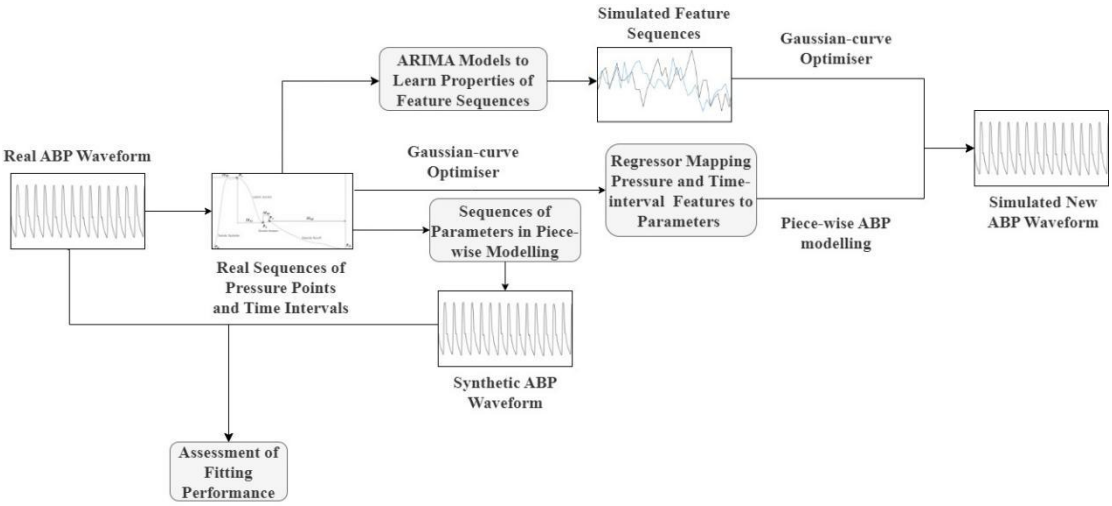


Figure 4.26: Flowchart of construction of proposed ABP model and generation of simulated ABP waveform

Firstly, sequences of pressure points, e.g., $\boldsymbol{P_d}$, and time intervals, e.g., $\Delta \boldsymbol{t_{ds}}$, are extracted from real ABP waveforms, dividing a single cycle of waveform into four components: systolic upstroke, systolic decline, dicrotic incisure, and diastolic runoff. Each component is fitted with a specific piece-wise parametric model. Sequences of fitted parameters of these four components of a series of cardiac cycles are then used to simulate original ABP waveforms with a Gaussian-curve optimiser, which are compared with original real ABP waveforms to assess the fitting performance.

Next, extracted features and corresponding parameters are used to train multivariate regression models, mapping features to related piece-wise parameters. ARIMA models are adopted to learn the temporal patterns of feature sequences and can be used to generate new feature sequences. With the multivariate regression models, simulated feature sequences with ARIMA models are used to estimate corresponding piece-wise parameters. These parameters are then used to simulate new ABP waveforms, with simulated sequences pressure points ensuring the waveforms passing through pressure points with Gaussian-curve optimisers.

4.3 Applications with digital twins in SAH management

After developing personalised synthetic ABP models, it is important to explore their applications as digital twins, within the management of SAH. There are three main applications of proposed synthetic ABP models as digital twins representing patients' haemodynamics.

Firstly, our proposed synthetic ABP models can represent ABP monitoring with continuous sequences of haemodynamic factors, e.g., levels of myocardial contractility, aortic elasticity, and peripheral resistance, and vital signs, e.g., SBP and DBP. Real-time sequences of these haemodynamic factors and vital signs reflect on

cardiovascular status of patients, which can be potentially incorporated as dynamic covariates in SAH prognosis. Personalised synthetic ABP models can also predict and generate future sequences of these haemodynamic factors and vital signs, which can be ultilised in predicting clinical outcomes and occurrences of cardiovascular complications.

Secondly, personalised synthetic ABP models, as digital twins, can be used to simulate how various haemodynamic factors and vital signs potentially respond to different treatment options, especially pharmacological agents for blood pressure control, e.g., hydralazine and nicardipine, without physically subjecting these patients to use of these medications. The application of digital twins in SAH management could help treatment options more tailored and optimised for patients with risk-free simulation. Besides, digital twins can serve as an advanced educational tool for training medical staff and students without the pressure of real-life consequences.

Most importantly, personalised synthetic ABP models can be valuable when invasive ABP measurement is not appropriate or feasible. In situations where invasive procedures pose significant risks or are contraindicated, digital twins can provide a non-invasive alternative by simulating the patient's haemodynamics. This allows caregivers to monitor and assess the patient's cardiovascular status continuously and accurately for short periods without the need for invasive measurements, as illustrated in Figure 4.27.

Additionally, these models can potentially reconstruct ABP using finger cuff measurements, providing a practical and non-invasive method to gather critical haemodynamic data. In the context of SAH prognostic modelling, this non-invasive approach can provide continuous monitoring of haemodynamics and cardiovascular status, contributing to a more comprehensive understanding of disease progression.

4.4 Summary and discussion

This chapter has primarily focused on methods for artefact rejection and the development of synthetic models for ABP monitoring within the context of SAH management. The contents of this chapter can be summarised into three main sections: the identification and simulation of common artefacts in ABP measurements, the development of personalised synthetic ABP models, and the exploration of their potential applications in SAH management and prognosis.

Firstly, this chapter began by introducing common artefacts in ABP monitoring, including their morphology, causes, e.g., unintended movement, and mathematical models to simulate these artefacts. Dynamic thresholding algorithms were then proposed to reject these artefacts effectively.

Secondly, Section 4.2 introduced a piece-wise parametric ABP model and techniques for simulating ABP waveforms that accurately replicate real ABP waveforms and

capture individual cardiovascular conditions. These simulated ABP waveforms provide a platform for generating synthetic artefacts, which are crucial for developing and testing artefact rejection algorithms.

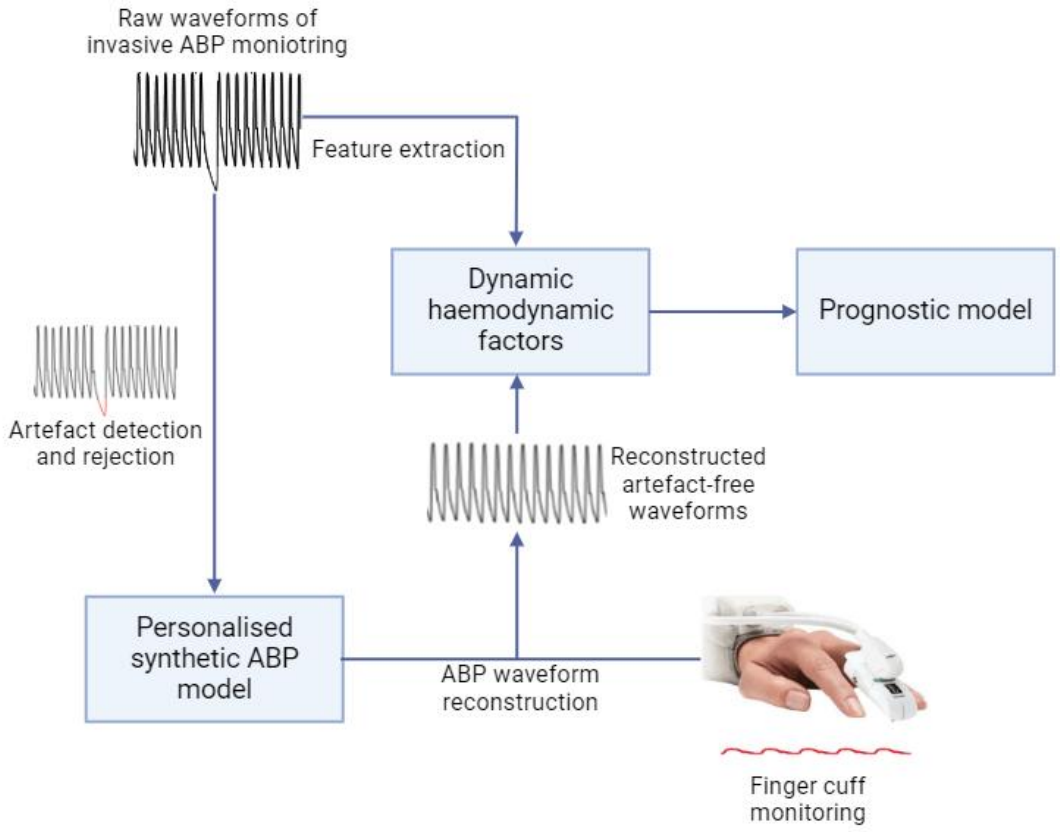


Figure 4.27: Applications of personalised synthetic ABP models in SAH management and prognosis

Moreover, the proposed method for generating synthetic ABP waveforms, when integrated into a digital twin, offers a dynamic representation and virtual model of a patient's physiological processes and health status. This integration provides a robust platform for understanding, simulating, predicting, and intervening in patients' cardiovascular health scenarios, as discussed in Section 4.3.

There are three main applications of the proposed synthetic ABP models as digital twins representing patients' haemodynamics:

- **Haemodynamic prediction**: Personalised synthetic ABP models can predict future sequences of haemodynamic factors and vital signs as predicted future dynamic covariates in prognostic modelling. This capability enhances the ability to forecast clinical outcomes and potential cardiovascular complications in SAH management.

- **Simulation of treatment responses:** Personalised synthetic ABP models as digital twins can simulate patients' responses to different treatment options, especially pharmacological agents for blood pressure control, without the risks associated with actual medication use. This allows for tailored and optimised treatment plans through risk-free simulation. For example, by integrating pharmacokinetic (PK) and pharmacodynamic (PD) models, digital twins can predict how drugs such as vasopressors, and calcium channel blockers, e.g., nimodipine, affect blood pressure variability, and systemic circulation. These simulations allow clinicians to explore dose-response relationships, drug interactions, and individualised treatment strategies without the risks associated with real-world medication use. Additionally, digital twins can serve as advanced educational tools for training medical staff and students without the pressure of real-life consequences.
- **Non-invasive monitoring enhancement:** Long-term use of invasive ABP measurement is not feasible due to risks such as bleeding, and infection. Alternatively, the synthetic ABP model can provide continuous cerebrovascular status (CUS) monitoring without requiring an arterial line by ultilising non-invasive physiological signals and computational modelling techniques such as signal fusion. Instead of direct intra-arterial measurements, machine learning algorithms, e.g., regression-based models and deep learning approaches, and physiological modelling techniques can potentially estimate blood pressure dynamics using non-invasive inputs such as non-invasive cuff-based BP readings, PPG, and HRV. While these advanced modeling approaches enable non-invasive estimation of ABP and CUS monitoring, the most accurate and reliable measurement of ABP remains direct intra-arterial monitoring via an arterial line, which provides real-time, high-fidelity pressure waveforms essential for critical care settings.

However, while artefact rejection methods and synthetic ABP models show promising clinical applications, there are limitations to the studies presented in this chapter. The primary limitation is that model accuracy has only been assessed based on ABP waveforms with normal morphology. The high rejection rate (87%) due to pathological waveforms highlights a key challenge, as many SAH patients exhibit abnormal haemodynamic patterns that our method could not effectively capture. This limitation risks excluding valuable physiological information and reducing the model' s applicability to patients with severe conditions. Future work should focus on developing methods to incorporate abnormal waveforms and extract meaningful features from them. One possible solution is to use unsupervised learning techniques, such as auto-encoders, to learn the intrinsic patterns of both normal and abnormal waveforms.

Consequently, while the synthetic ABP models are adequate for simulating artefacts, testing artefact rejection methods, and evaluating treatment responses, their effectiveness and applicability in other clinical situations or with different patient conditions remain to be investigated. Another significant limitation is that

non-invasive monitoring without a finger cuff is not suitable for long-term use, as cardiovascular status can change over time. For relatively long-term monitoring, the use of a finger cuff is necessary to supplement and ensure accurate and reliable measurements.

This chapter detailed methods for artefact rejection and synthetic ABP model development for SAH management. It covered the identification and simulation of ABP artefacts, development of personalised synthetic ABP models, and their applications in haemodynamic prediction, treatment response simulation, and non-invasive monitoring enhancement. Despite potential applications, limitations include the need for validation with pathological conditions and challenges in ensuring accurate long-term non-invasive monitoring without supplementary devices such as finger cuffs.

Reference for chapter 4

[1] Psychogios, K., Tsivgoulis, G. and FESO, F., 2019. Subarachnoid hemorrhage, vasospasm, and delayed cerebral ischemia. Pract Neurol, 9, pp.37-41.

[2] Rastegar, S., GholamHosseini, H. and Lowe, A., 2020. Non-invasive continuous blood pressure monitoring systems: current and proposed technology issues and challenges. Physical and Engineering Sciences in Medicine, 43, pp.11-28.

[3] Li, Q., Mark, R.G. and Clifford, G.D., 2009. Artificial arterial blood pressure artifact models and an evaluation of a robust blood pressure and heart rate estimator. Biomedical engineering online, 8(1), pp.1-15.

[4] Cleveland, R.B., Cleveland, W.S., McRae, J.E. and Terpenning, I., 1990. STL: A seasonal-trend decomposition. J. Off. Stat, 6(1), pp.3-73.

[5] Wen, Q., Gao, J., Song, X., Sun, L., Xu, H. and Zhu, S., 2019, July. RobustSTL: A robust seasonal-trend decomposition algorithm for long time series. In Proceedings of the AAAI Conference on Artificial Intelligence (Vol. 33, No. 01, pp. 5409-5416).

[6] Hundman, K., Constantinou, V., Laporte, C., Colwell, I. and Soderstrom, T., 2018, July. Detecting spacecraft anomalies using lstms and nonparametric dynamic thresholding. In Proceedings of the 24th ACM SIGKDD international conference on knowledge discovery & data mining (pp. 387-395).

[7] Lim, P.K., Ng, S.C., Lovell, N.H., Yu, Y.P., Tan, M.P., McCombie, D., Lim, E. and Redmond, S.J., 2018. Adaptive template matching of photoplethysmogram pulses to detect motion artefact. Physiological measurement, 39(10), p.105005.

[8] Mahdi, A., Clifford, G.D. and Payne, S.J., 2017. A model for generating synthetic arterial blood pressure. Physiological measurement, 38(3), p.477.

[9] Chou, Y., Wang, P. and Feng, Y., 2019. The Optimal Morphological Model for Arterial Blood Pressure Wave Related Classification: Comparison of Two Types of Kernel Function Mixtures. IEEE Access, 8, pp.4133-4148.

Chapter 5 Neurological intervention transition model for dynamic prediction of good outcome in spontaneous SAH[5]

Deterioration of neurovascular conditions can be rapid in patients with spontaneous subarachnoid haemorrhage (SAH), often leading to poor outcomes. Therefore, it is crucial to promptly assess and continually track the progression of the disease. This study incorporates baseline clinical conditions, repeatedly measured neurological grades, and biomarkers for the dynamic outcome prediction of patients with spontaneous SAH. Neurological interventions, primarily aneurysm clipping and endovascular embolisation, were also incorporated as intermediate events in developing the neurological intervention transition (NIT) joint model.

A retrospective cohort study was performed on 701 patients with spontaneous SAH, using data from the MIMIC-IV dataset over a study period of 14 days, encompassing both the acute and sub-acute phases of SAH. A dynamic prognostic model was developed to predict patient outcomes by combining a Cox proportional hazards model with piece-wise linear mixed-effects models, thereby incorporating various types of prognostic information.

Baseline clinical conditions, including cerebral oedema, cerebral infarction, respiratory failure, hydrocephalus, and vasospasm, as well as repeatedly measured GCS scores, glucose levels, and white blood cell (WBC) counts, were included as covariates in the optimal model. Incorporating neurological interventions, such as aneurysm clipping and endovascular embolisation, as intermediate events enhanced the prediction performance compared to the baseline joint modelling approach.

The average AUC of the optimal model proposed in this study is 0.7783 across different starting points and prediction intervals. This model offers dynamic prognosis for spontaneous SAH patients and has significant potential benefits for critical care management in clinical practice.

5.1 Introduction

Spontaneous SAH is characterised by sudden bleeding into the subarachnoid space due to non-traumatic causes, mostly arising from a ruptured cerebral aneurysm. It is considered as a medical emergency due to various associated complications and its life-threatening nature, such that the 28-day mortality rate is reported as high as 41.7%. [1] Close monitoring of disease progression and prediction of adverse clinical outcomes in the critical care are thus required to identify risks of deterioration and track changes in neurological status, which can change rapidly. This allows for timely

[5] **Available at: https://www.nature.com/articles/s41598-024-51684-6**

neurological intervention, adjustments in treatment strategies, and proactive preventive measures to optimise critical care management and improve patient outcomes.

The prognostication of spontaneous SAH is intricate and multi-factorial. In clinical practice, the prognosis is commonly made through patients' medical conditions and various assessments. These medical conditions include underlying conditions, e.g., hypertension, and diabetes, as well as complications, e.g., re-bleeding, vasospasm, hydrocephalus, and cerebral oedema. Clinical assessments used for prognostication of spontaneous SAH include clinical examinations, e.g., Glasgow Coma Scale (GCS) to assess the level of consciousness, radiological investigations on brain imaging, haematological biomarkers, e.g., white blood cell (WBC) count, and vital signs, e.g., blood pressure and oxygen saturation, that provide information about a patient's physiological status.

Clinical tools for prognosis of spontaneous SAH have been mostly developed based on baseline medical conditions and clinical assessments. The Hunt and Hess scale and the World Federation of Neurological Surgeons (WFNS) scale are the two most widely used prognostic scoring systems for SAH, focusing on the patient's level of consciousness and neurological deficits. [2][3] Another scoring system, the Fisher grade or modified Fisher grade uses findings of the amount of blood and intraventricular haemorrhage (IVH) on brain computed tomography (CT) scans to assess the severity of SAH. [4][5] A multidimensional tool, the FRESH score was also proposed for prognostication of outcomes after spontaneous SAH, incorporating Hunt and Hess and APACHE-II physiologic scores on admission, age and re-bleeding within 48 hours. [6]

The prognostication of spontaneous SAH can be potentially improved in several aspects. Firstly, these prognostic scoring systems focus on a specific aspect of medical conditions, particularly patient's consciousness level and neurological deficits. Although this could be the most critical aspect of prognosis and is valuable in clinical practice for risk identification, other prognostic factors can provide additional prognostic information and should be included in multi-factorial prognostic models for more comprehensive and customised prognostication.

Secondly, vital signs and neurological status, usually measured by GCS score, are repeatedly measured and recorded routinely to monitor disease progression and assess treatment response. They provide up-to-date dynamic prognostic information on patients' evolving conditions. Incorporation of up-to-date dynamic prognostic information in prognostic modelling enables clinicians to determine and adjust treatment plans effectively and provide realistic expectations on patients' clinical outcomes.

Finally, intermediate events, e.g., neurological interventions and occurrences of

complications, can significantly impact the progression and clinical outcomes. Incorporating these intermediate events in prognostication of spontaneous SAH can help improve the prediction accuracy of prognostic models, allowing for a more comprehensive and dynamic approach to prognostication to enhance the management and prognosis of patients suffering spontaneous SAH.

This study aims to develop a dynamic prognostic model for spontaneous SAH to improve prognostication as well as explore the prognostic values of neurological interventions when jointly analysed with baseline and dynamic covariates. For the multi-factorial nature of SAH prognostication, various clinical conditions on admission, e.g., demographics and underlying medical conditions, will be incorporated as baseline covariates, which are unaltered during the study period, for prognostic modelling.

Dynamic prognostic information, provided by repeated measured vital signs, haematological biomarkers, and neurological grades, as well as a neurological intervention, is then simultaneously analysed and modelled with baseline covariates for monitoring the disease progression of each patient. The proposed prognostic model takes various medical conditions on admission, multiple dynamic factors providing up-to-date prognostic information, and the effect of neurological interventions into account for prognostication. These advantages make it an novel clinical tool for risk assessment, customised treatment optimisation, and disease progression monitoring.

5.2 Methods

5.2.1 Data Collection and Visualisation

Patient recruited in this study were selected from MIMIC-IV, a publicly available database sourced from the electronic health record of the Beth Israel Deaconess Medical Center between 2008 to 2019. [7] 766 patients with spontaneous SAH as the primary diagnosis were initially included in the study, identified by ICD-9-CM code 430 or ICD-10-CM code I60 and their specifiers. 65 patients were excluded due to too short hospital stay (< 24 hours) or having no identified records in vital signs and neurological assessments.

A final total of 701 patients were included in this study, all patients aged 18 and over. Among them, 409 (58.35%) patients were females, and the median age was 59 (IQR: 50-70). Essential hypertension is the most common medical condition on admission (340, 48.50%), followed by hydrocephalus (221, 31.53%), respiratory failure (149, 21.56%), and cerebral oedema (131, 18.69%). Clinical outcomes were measured by discharge destinations at the end of study period. Good outcome (343, 48.93%) was defined by returning home or rehabilitation, while poor outcome (358, 51.07%) includes mortality, long-term acute care, and hospice care. The clinical characteristics

of the dataset are shown in Table 5.1.

Covariate		All (n = 701)	Good outcome (n = 343)	Poor outcome (n = 358)
Demographics	Age	Median: 59 (IQR: 50 - 70)	Median: 49.25 (IQR: 56 - 68)	Median: 61 (IQR: 51 - 73)
	Female	409 (58.35%)	192 (55.98%)	217 (60.61%)
Underlying conditions	Alcohol	23 (3.28%)	9 (2.62%)	14 (3.91%)
	Tobacco	132 (18.83%)	68 (19.83%)	64 (17.88%)
	Diabetes	76 (10.84%)	32 (9.33%)	44 (12.29%)
	Essential hypertension	340 (48.50%)	154 (44.90%)	186 (51.96%)
Complications	Cerebral oedema	131 (18.69%)	24 (7.00%)	107 (29.89%)
	Cerebral infarction	69 (9.84%)	15 (4.37%)	54 (15.08%)
	Respiratory failure	149 (21.56%)	11 (3.21%)	138 (38.55%)
	Hydrocephalus	221 (31.53%)	34 (3.21%)	187 (52.23%)
	Vasospasm	55 (7.85%)	15 (4.37%)	40 (11.17%)
Neurosurgeries	Clipping	37 (5.28%)	25 (7.29%)	12 (3.35%)
	Coiling	239 (34.09%)	168 (48.98%)	71 (19.83%)
	Craniotomies	39 (5.56%)	20 (5.83%)	19 (5.31%)
	Spinal decompression	96 (13.69%)	44 (12.83%)	52 (14.53%)

Table 5.1: Clinical characteristics and neurosurgical information of included dataset

Summary of neurosurgeries received by these patients is also shown in this table, which reflects modern neurosurgical trends, with coiling being the preferred treatment over clipping due to its minimally invasive nature. The small number of patients receiving coiling and clipping is likely due to factors such as non-aneurysmal SAH cases, early mortality, and poor clinical status, making intervention unfeasible. Craniotomies (35 patients) were performed for tumor resection, haemorrhage evacuation, or trauma, while spinal decompression (92 patients) suggests a notable presence of spinal pathology.

Six indices were included as dynamic covariates for prognostic modelling: one neurological grade (GCS score), three haematological biomarkers (creatinine, WBC, and glucose), and two vital signs (systolic blood pressure (SBP) and oxygen saturation (SpO2)). These indices have been shown to be valuable in SAH prognosis research [8-13]. Table 5.2 presents the statistics of these dynamic covariates for the two outcome groups, expressed as means and standard deviations.

Covariate		All	Good outcome	Poor outcome
Neurological Score	GCS Score	11.89 ± 3.72	14.57 ± 3.72	10.58 ± 3.84
Haematological Biomarkers	Creatinine (mg/dL)	0.75 ± 0.72	0.84 ± 1.06	0.70 ± 0.37
	WBC (10^9/L)	11.57 ± 5.19	9.68 ± 4.04	12.68 ± 5.46
	Glucose (mg/dL)	129.29 ± 37.74	117.69 ± 32.49	136.30 ± 38.95
Vital Signs	SBP (mmHg)	141.99 ± 20.76	134.66 ± 17.03	144.03 ± 21.24
	SpO2 (%)	97.08 ± 3.54	96.72 ± 4.67	97.26 ± 2.82

Table 5.2: Statistics of all observations of six dynamic covariates

Figure 5.1 visualises the trajectories and corresponding 95% confidence intervals of these dynamic covariates during the study period, using the locally estimated scatter-plot smoothing (LOESS) method. The LOESS method was separately applied to each group, estimating a smoothed curve that best represents the trend of each dynamic covariate for each group.

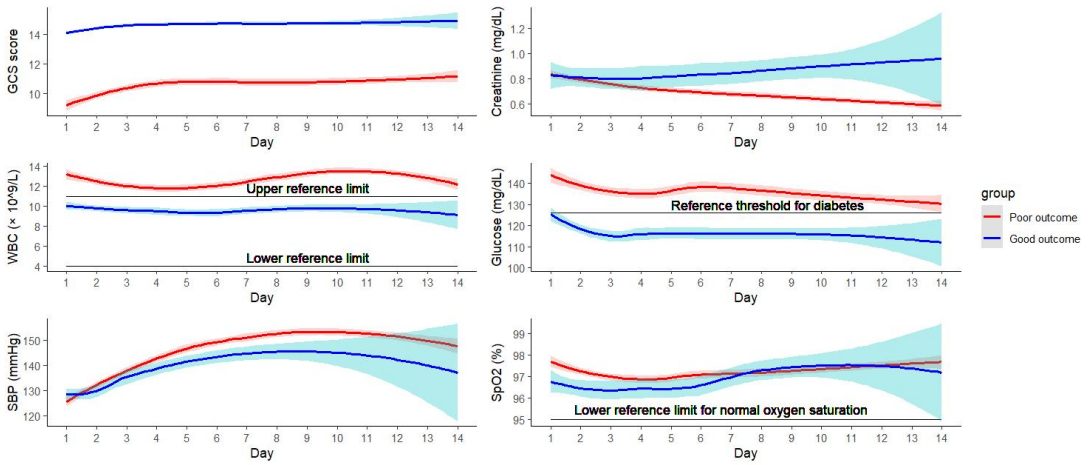


Figure 5.1: Trajectories of six dynamic prognostic covariates with LOESS method

According to the trajectory visualisation in Figure 5.1 and statistics shown in Table 5.2, GCS score is a highly discriminative dynamic covariate between the two groups, while the trajectories of WBC and glucose also demonstrate good discrimination between good and poor outcomes. These three dynamic covariates were subsequently included as potential predictors in prognostic modelling.

The GCS score effectively differentiates between good and poor outcomes by reflecting better neurological recovery in the good outcome group. WBC count indicates that a controlled inflammatory response is associated with good outcomes, whereas elevated levels correlate with poorer outcomes. Similarly, glucose levels show that stable and lower levels are linked to better recovery, while persistent hyperglycemia is indicative of poor prognosis.

In contrast, the other three covariates do not exhibit significant discriminative power. Visualisation of the trajectories of dynamic prognostic covariates allows for the observation of patterns and trends within each group, providing initial insights into the dynamic nature of these covariates. The prognostic significance of these dynamic covariates needs to be jointly analysed with baseline covariates and intermediate events, which will be presented later.

5.2.2 Prognostic modelling

The prognostic modelling process starts with examining the effects of baseline covariates on outcomes, which can be modelled using a Cox proportional hazard model. The Cox model is the most widely used method in survival analysis and can be used to investigate the effects of baseline covariates on clinical outcomes, given by :

$$h_i(t) = h_0(t)\exp(\sum_j \gamma_j \omega_{j_i}) \quad (5.1)$$

where $h_i(t)$ denotes the instantaneous rate of experiencing a good clinical outcome for patient *i* at time *t,* while ω_{j_i} is the value of the j^{th} baseline covariate for the i^{th} patient with corresponding coefficient γ_j. A positive coefficient indicates increasing chance of a good outcome, whereas a negative coefficient implies higher risk of poor outcomes. The effect of j^{th} baseline covariate on outcome is measured by hazard ratio (HR), computed as $exp(\gamma_j)$.

Covariate	Univariate analysis			Multivariate analysis		
	HR	95%CI	P value	HR	95%CI	P value
Age	0.9944	0.9870 – 1.0019	0.144	–	–	–
Female	0.8856	0.7155 – 1.0961	0.264	–	–	–
Alcohol	0.6952	0.3586 – 1.3480	0.282	–	–	–
Tobacco	0.9890	0.7584 – 1.2898	0.935	–	–	–
Diabetes	0.7400	0.5142 – 1.0649	0.105	–	–	–
Essential hypertension	0.8566	0.6924 – 1.0598	0.154	–	–	–
Cerebral oedema	0.2661	0.1757 – 0.4031	**< 0.001**	0.5626	0.3680 – 0.8600	**0.008**
Cerebral infarction	0.2913	0.1736 – 0.4889	**< 0.001**	0.3644	0.2169 – 0.6124	**< 0.001**
Respiratory failure	0.0767	0.0420 – 0.1400	**< 0.001**	0.1345	0.0727 – 0.2488	**< 0.001**
Hydrocephalus	0.1280	0.0897 – 0.1828	**< 0.001**	0.1821	0.1271 – 0.2609	**< 0.001**
Vasospasm	0.3316	0.1975 – 0.5566	**< 0.001**	0.4092	0.2430 – 0.6891	**< 0.001**

Table 5.3: Results of univariate and multivariate survival analysis of baseline covariates

The estimated HRs of all analysed baseline covariates are less than 1, indicating a lower likelihood of good outcomes, as shown in Table 5.3. The univariate analysis revealed the effects of individual variables on clinical outcomes, while the multivariate analysis considered the simultaneous effects of multiple covariates, estimating the effect of each covariate while accounting for others. Among these baseline covariates, cerebral oedema, cerebral infarction, respiratory failure, hydrocephalus, and vasospasm are significant in univariate survival analysis and remain significant in multivariate survival analysis.

Dynamic prognostic covariates can be measured with errors and influenced by caregivers, such as human biases in neurological assessments. To address this, linear mixed-effects models (LMM) are adopted to model the longitudinal properties of these covariates and handle unobserved heterogeneity. Since each patient corresponds to repeated measurements of dynamic covariates, these measurements within the same patient are likely to be correlated. An LMM accounts for this within-subject correlation by including random effects. The fixed-effect and random-effect terms in an LMM for a dynamic covariate respectively describe its population-level mean trajectory and individual-specific deviations.

The longitudinal property of the j^{th} dynamic covariate for the i^{th} patient at time *t* is thus given by:

$$y_{j_i}(t) = m_{j_i}(t) + \varepsilon_{j_i}(t) = \beta_j x_{j_i}^T(t) + b_{j_i} z_{j_i}^T(t) + \varepsilon_{j_i}(t) \quad (5.2)$$

where $y_{j_i}(t)$ denotes the observed value of j^{th} dynamic covariate for the i^{th} dynamic covariate, measured with error, while $m_{j_i}(t)$ is the corresponding unobserved true value, composed fixed-effect term $\beta_j x_{j_i}^T(t)$ representing the overall trend for all patients, and random-effect term $b_{j_i} z_{j_i}^T(t)$ for explaining patient-specific deviations from the overall trend.

These dynamic covariates are then simultaneously modelled with baseline covariates to incorporate up-to-date dynamic prognostic information in prognostication with joint modelling approach. A joint model for multiple dynamic dynamic covariates and baseline survival analysis is given by:

$$h_i(t) = h_0(t) \exp(\gamma^T \omega_i + \sum_j \alpha_j m_{j_i}(t)) \quad (5.3)$$

In comparison with Equation 5.1, Equation 5.3 simultaneously analyses the effects of baseline and dynamic covariates on clinical outcomes by incorporating longitudinal sub-models for these dynamic covariates as described in Equation 5.2.

Next, another valuable source of prognostic information that can be incorporated into prognostic modelling is intermediate events, specifically neurological interventions in this study. For the prognostication of spontaneous SAH, neurological interventions can directly impact disease progression and clinical outcomes. These interventions can stabilise patients, prevent complications like re-bleeding, and improve neurological recovery. Incorporating these events into the modelling framework allows for more comprehensive prognostication.

To incorporate the effects of neurological interventions on disease progression, the longitudinal sub-model of the prognostic model, as denoted by Equation 5.2, can be reformulated as follows:

$$y_{j_i}(t) = m_{j_i}(t) + \varepsilon_{j_i}(t) = \begin{cases} \beta_j x_{j_i}^T(t) + b_{j_i} z_{j_i}^T(t) + \varepsilon_{j_i}(t), & 0 < t < \tilde{t}_i \\ \beta_j x_{j_i}^T(t) + b_{j_i} z_{j_i}^T(t) + \tilde{\beta}_j \tilde{x}_{j_i}^T(t_+) + \tilde{b}_{j_i} \tilde{z}_{j_i}^T(t_+) + \varepsilon_{j_i}(t), & t \geq \tilde{t}_i \end{cases} \quad (5.4)$$

where $\tilde{t}_i$ is the time of the neurological intervention of the i^{th} patient, while t_+ denotes the time relative to neurological intervention. For the i^{th} patient, $t_+ = max(0, t - \tilde{t}_i)$. The effects of neurological interventions are modelled as additive terms on both overall population-level trend and individual-specific terms of dynamic covariates after the intervention time point.

Correspondingly, Equation 5.3 can be extended as:

$$h_i(t) = \begin{cases} h_0(t) \exp(\gamma^T \omega_i + \sum_j \alpha_j (\beta_j x_{j_i}^T(t) + b_{j_i} z_{j_i}^T(t))), & 0 < t < \tilde{t}_i \\ h_0(t) \exp(\gamma^T \omega_i + \sum_j \alpha_j (\beta_j x_{j_i}^T(t) + b_{j_i} z_{j_i}^T(t) + \tilde{\beta}_j \tilde{x}_{j_i}^T(t_+) + \tilde{b}_{j_i} \tilde{z}_{j_i}^T(t_+))), & t \geq \tilde{t}_i \end{cases} \quad (5.5)$$

Equation 5.5 describes the prognosis of spontaneous SAH in two states, obtained from the combination of Equation 5.3 and Equation 5.4. Patients who have not received neurological interventions are considered to be in the first state of prognosis, while those who have been treated with neurological interventions are in the second state of prognosis. The time point $\tilde{t}_i$ marks the state transition. Thus, this model is termed the neurological intervention transition (NIT) joint model. Its performance as a prognostic model will be compared with baseline joint models that do not include neurological interventions in the prognostic modelling.

Parameters in this model are estimated using the Bayesian approach, which infers parameter values from a joint posterior distribution derived from the product of the joint likelihood of the observed data and the prior distribution. In this study, prior beliefs on the parameters within the joint modelling framework are based on values separately estimated in the survival and longitudinal sub-models. The Bayesian approach is implemented via Markov Chain Monte Carlo (MCMC) methods, utilising Gibbs and Metropolis-Hastings algorithms for sampling from the distributions.

5.3 Results

5.3.1 Simultaneous analysis on longitudinal and survival data

The prognostic value of each dynamic covariate was measured by its HR, calculated as the exponential of the coefficient, α_j, when jointly analysed and adjusted for the five significant baseline covariates listed in Table 5.3. Table 5.4 presents the HRs of the included dynamic covariates using both the baseline and the proposed NIT joint modelling approaches.

According to the results in Table 5.4, the GCS score is a strong independent dynamic prognostic factor for clinical outcomes. A one-unit increase in GCS score is associated with a 173.79% higher likelihood of a good outcome when jointly modelled with baseline covariates. Conversely, the presence of WBC abnormalities and hyperglycaemia are negatively associated with good outcomes at 14 days.

Covariate		**Baseline joint model**			**NIT joint model**		
		HR	**95%CI**	**P value**	**HR**	**95%CI**	**P value**
Univariate	**GCS score**	2.7379	2.0044 − 3.7398	**< 0.001**	3.2802	2.2559 − 4.7696	**< 0.001**
	Creatinine abnormality	1.1085	0.7548 − 1.6280	0.584	1.1087	0.7780 − 1.5799	0.580
	WBC abnormality	0.7847	0.5515 − 1.1167	0.170	0.7954	0.5695 − 1.1110	0.197
	Hyperglycemia (Glucose ≥ 126mg/dL)	0.7474	0.4967 − 1.1247	0.151	0.7703	0.5031 − 1.1793	0.213
	SBP	0.9971	0.9862 − 1.0081	0.594	0.9971	0.9868 − 1.0075	0.584
	Low oxygen saturation (SpO2 < 95%)	1.4249	0.7476 − 2.7159	0.288	1.1910	0.6214 − 2.2826	0.600
GCS score + WBC	**GCS score**	2.5713	1.8692 − 3.5370	**< 0.001**	3.2651	2.2583 − 4.7208	**< 0.001**
	WBC abnormality	0.3681	0.2077 − 0.6524	**< 0.001**	0.3882	0.2180 − 0.6912	**0.003**
GCS score + Glucose	**GCS score**	2.5767	1.9580 − 3.3909	**< 0.001**	3.0162	2.0178 − 4.5086	**< 0.001**
	Hyperglycemia (Glucose ≥ 126mg/dL)	0.2790	0.1237 − 0.6294	**0.001**	0.2097	0.0853 − 0.5155	**< 0.001**
	GCS score	2.4322	1.7716 − 3.3392	**< 0.001**	2.8445	2.1522 − 3.7596	**< 0.001**

GCS score + WBC + Glucose	**WBC abnormality**	0.4544	0.2489 − 0.8296	**0.003**	0.5261	0.2899 − 0.9549	**0.038**
	Hyperglycemia (Glucose ≥ 126mg/dL)	0.3722	0.1478 − 0.9370	**0.018**	0.2681	0.0961 − 0.7480	**0.010**

Table 5.4: Results of dynamic covariates in baseline and NIT joint modelling approach

The associations between WBC abnormalities and hyperglycaemia with clinical outcomes are not significant when these haematological biomarkers are solely modelled as dynamic covariates. However, they become significant when jointly analysed with the GCS score. Additionally, the prognostic power of the GCS score decreases when modelled alongside these haematological biomarkers. This suggests that these biomarkers act as confounding variables affecting the relationship between GCS score and outcomes. Including these haematological biomarkers helps control for this confounding effect, providing a more accurate estimate of the HR for the GCS score.

Covariate	**Baseline joint model**						**NIT joint model**					
GCS score	**dt/Ts**	**1**	**2**	**3**	**5**	**7**	**dt/Ts**	**1**	**2**	**3**	**5**	**7**
	1	0.9143	0.7423	0.7016	0.6715	0.7405	**1**	0.8950	0.7250	0.7039	0.6896	0.7335
	2	0.7441	0.7505	0.6391	0.7561	0.7564	**2**	0.7432	0.7509	0.6513	0.7521	0.7534
	3	0.7736	0.7294	0.6791	0.7245	0.7544	**3**	0.7761	0.7383	0.6835	0.7370	0.7685
	5	0.7886	0.7811	0.7046	0.7031	0.7472	**5**	0.7888	0.7924	0.7255	0.7479	0.7799
	7	0.7865	0.7878	0.7511	0.6968	0.7320	**7**	0.7831	0.7976	0.7700	0.7603	0.7705
	Marginal	0.8014	0.7582	0.6951	0.7104	0.7461	**Marginal**	0.7973	0.7609	0.7069	0.7369	0.7611
	Mean AUC: 0.7422 ± 0.0524						**Mean AUC: 0.7526 ± 0.0466**					
GCS score + Glucose	**dt/Ts**	**1**	**2**	**3**	**5**	**7**	**dt/Ts**	**1**	**2**	**3**	**5**	**7**
	1	0.8966	0.7758	0.7285	0.7152	0.7542	**1**	0.9328	0.7510	0.6984	0.6955	0.7468
	2	0.7795	0.7684	0.6554	0.7588	0.7673	**2**	0.7563	0.7645	0.6522	0.7521	0.7634
	3	0.7908	0.7546	0.6875	0.7331	0.7632	**3**	0.7896	0.7581	0.6941	0.7422	0.7669
	5	0.8018	0.8065	0.7205	0.7181	0.7622	**5**	0.8016	0.8080	0.7294	0.7456	0.7814
	7	0.7975	0.8015	0.7526	0.7168	0.7571	**7**	0.7954	0.7991	0.7667	0.7497	0.7792
	Marginal	0.8132	0.7814	0.7089	0.7284	0.7608	**Marginal**	0.8151	0.7761	0.7082	0.7370	0.7675
	Mean AUC: 0.7585 ± 0.0468						**Mean AUC: 0.7608 ± 0.0518**					
GCS score + WBC	**dt/Ts**	**1**	**2**	**3**	**5**	**7**	**dt/Ts**	**1**	**2**	**3**	**5**	**7**
	1	0.8273	0.7714	0.7381	0.7120	0.7476	**1**	0.8271	0.7597	0.7147	0.7115	0.7436
	2	0.7803	0.7917	0.6647	0.7636	0.7668	**2**	0.7400	0.7644	0.6589	0.7589	0.7592
	3	0.8000	0.7626	0.7003	0.7392	0.7684	**3**	0.7938	0.7573	0.6996	0.7416	0.7749
	5	0.8038	0.8095	0.7228	0.7262	0.7675	**5**	0.8062	0.8137	0.7328	0.7527	0.7903
	7	0.8006	0.8047	0.7589	0.7289	0.7614	**7**	0.7991	0.8035	0.7731	0.7654	0.7912
	Marginal	0.8024	0.7880	0.7170	0.7340	0.7623	**Marginal**	0.7932	0.7797	0.7158	0.7460	0.7718
	Mean AUC: 0.7608 ± 0.0384						**Mean AUC: 0.7613 ± 0.0390**					

	dt/Ts	1	2	3	5	7	dt/Ts	1	2	3	5	7
GCS score + Glucose + WBC	1	0.8309	0.7446	0.7176	0.7061	0.7627	1	0.8155	0.7425	0.7520	0.7110	0.7719
	2	0.7815	0.7850	0.6686	0.7626	0.7728	2	0.7469	0.8032	0.6944	0.7767	0.7874
	3	0.8069	0.7684	0.7011	0.7414	0.7700	3	0.8221	0.7879	0.7258	0.7626	0.7892
	5	0.8144	0.8155	0.7340	0.7245	0.7751	5	0.8192	0.8313	0.7636	0.7654	0.7972
	7	0.8061	0.8025	0.7618	0.7196	0.7749	7	0.8138	0.8177	0.7930	0.7715	0.7957
	Marginal	0.8080	0.7832	0.7166	0.7308	0.7711	Marginal	0.8035	0.7965	0.7458	0.7574	0.7883
	Mean AUC: 0.7619 ± 0.0407						Mean AUC: 0.7783 ± 0.0356					

Table 5.5: Prediction performance (measured by AUCs) of different joint model settings, different starting times of predictions and prediction intervals

Vital signs, however, are not found to be significantly associated with clinical outcomes, with HR values around 1. This may be explained by their dynamic nature, as vital signs can fluctuate and change rapidly in response to various physiological and environmental factors. While abnormal vital signs may indicate physiological instability, they may not necessarily correlate with clinical outcomes. Close monitoring and management of vital signs remain important for patients with SAH, but their prognostic value for clinical outcomes may be limited compared to neurological assessments.

Table 5.5 presents the prediction performance of different models, where T_s denotes the starting point of prediction, and dt is the prediction interval. Prognostic information available up to T_s is used to predict clinical outcomes at the targeted time point $T_s + dt$. The AUC represents the overall discriminative ability of the prognostic model in distinguishing between patients with good and poor outcomes. The mean AUC is calculated by averaging the predictive performance over all T_s and dt. Variability across starting points and prediction intervals for each model was also calculated, with low variability indicating that the model was robust over time and could consistently provide reliable predictions of clinical outcomes.

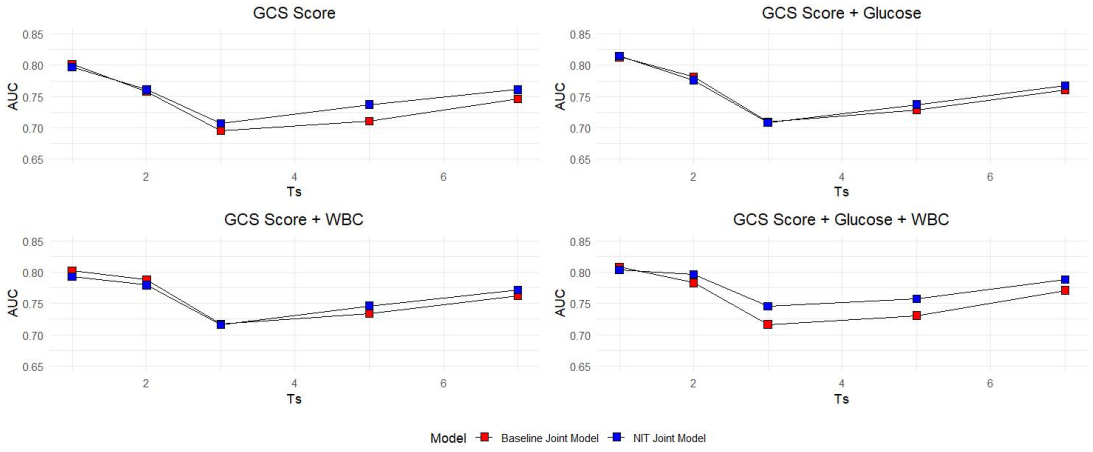


Figure 5.2: Comparisons in prediction accuracy between baseline and NIT joint models

Figure 5.2 compares the prediction accuracy with time between two modelling approaches and combinations of dynamic covariates, measured by marginal AUC by the time of prediction. It can be found that, with all combinations of dynamic covariates, the prediction performance of proposed NIT joint model is better than the corresponding model developed by baseline joint modelling methods. This figure also shows that the prediction performance of proposed NIT joint model with GCS score, glucose and WBC as dynamic covariates is good and consistent with different prediction time, where the AUC is at least around 0.75 for all starting points of prediction. Moreover, prognostic NIT joint model can provide good prediction performance in both acute phase ($T_s + dt \leq 3$, Mean AUC: 0.7683) and sub-acute phase ($3 < T_s + dt \leq 14$, Mean AUC: 0.7796) of spontaneous SAH.

Based on the predictive performance of different dynamic prognostic models, this study presents several main findings. Firstly, the repeatedly measured neurological status, as indicated by the GCS score, is a strong dynamic predictor of clinical outcomes, even after adjusting for baseline medical conditions upon admission. Secondly, incorporating haematological biomarkers, such as WBC and glucose, provides additional prognostic information by reflecting the patient's immune response, infection status, and metabolic changes. This integration can enhance the prediction accuracy of the prognostic models.

Secondly, intermediate events, such as neurological interventions, provide valuable prognostic information on disease progression. Incorporating these intermediate events as transitions between prognostic states adds granularity to the model by segmenting the overall prognostication process into multiple states. This allows for a more detailed analysis of disease progression. Compared to baseline joint models, NIT joint models demonstrate better predictive accuracy when including the same baseline and dynamic covariates.

Moreover, NIT joint models enhance personalised prognosis by modelling the time point of neurological intervention as an individualised transition point between prognostic states. This approach incorporates individual-specific characteristics into the prognostic model, allowing it to account for personalised milestones in disease progression and tailor outcome predictions accordingly.

Finally, compared to baseline joint models, NIT joint models perform better in relative long-term outcome prediction. The average improvement in prediction accuracy from baseline to the NIT joint model across four covariate combinations is 0.0101 (1.34%) for predictions in the sub-acute phase, with an overall improvement of 0.0074 (0.98%). This merit of the NIT joint model likely results from its ability to account for changes in disease progression due to neurological interventions, which become more pronounced during the sub-acute phase of prognostication.

The multivariate NIT joint model, which incorporates GCS score, WBC, and glucose as dynamic prognostic covariates, is identified as the optimal model in this study. This model increases the predictive accuracy of outcomes from 0.7422 in the baseline joint model, which only considers neurological grades, to 0.7783, reflecting an improvement of 4.86%. This optimal model serves as an accurate and comprehensive clinical tool for personalised prognosis in patients with spontaneous SAH, potentially benefiting disease progression monitoring and personalised post-neurosurgery management for improved clinical outcomes.

5.4 Discussion

This study has proposed a multivariate NIT joint model for prognosticating outcomes in patients with spontaneous SAH. Unlike traditional tools such as the Hunt and Hess grade, which rely heavily on neurological status, this model incorporates a broader range of prognostic factors, including medical conditions, haematological biomarkers, and neurological interventions besides neurological assessments. This comprehensive approach better captures the multi-factorial nature of SAH prognosis. By integrating individual-specific prognostic information and modelling disease progression through personalised state transitions, the NIT model can potentially serve as useful clinical tool for personalised prognosis, offering tailored insights and improving patient management.

The optimal NIT joint model comprises five baseline covariates (cerebral oedema, cerebral infarction, respiratory failure, hydrocephalus, and vasospasm), three dynamic covariates (GCS score, WBC count, and glucose levels) and a state transition indicator represented by intermediate neurological interventions. This model can provide accurate outcome predictions across all starting points of prediction and prediction intervals, with the overall AUC 0.7783, respectively 0.7683 and 0.7796 in the acute and sub-acute phases of spontaneous SAH.

In analysing the predictive power of neurological status, haematological biomarkers, and vital signs, the GCS score was found as the most valuable covariate for prognostication. This finding aligns with the widespread clinical use of neurological scales for SAH prognosis, which estimate patient outcomes based on neurological assessments. While WBC count and glucose levels are not independent prognostic factors, they offer additional prognostic information that complements neurological status, thereby enhancing the model's prediction accuracy.

Although the prognostic values of vital signs were found to be limited in this study, their variability, e.g., systolic blood pressure variability, which may indicate impaired blood pressure regulation and cardiovascular instability, is drawing research attention in prognosis studies. [14] Variability in blood pressure and ICP can provide valuable prognostic information, particularly in the acute phases when maintaining haemodynamic stability is critical for controlling acute symptoms. With more

frequent measurements of vital signs, their variability and changes during disease progression can be captured and potentially included as influential dynamic covariates for the prognostication of SAH.

This study provides a novel approach to incorporate different types of covariates and events into prognostication of spontaneous SAH, on the basis joint modelling framework. This approach is also suitable and can be extended to model the prognosis of other cerebrovascular diseases due to its ability to incorporate different types of prognostic information.

The prognostic information that can potentially be incorporated includes demographics, medical conditions, neurological status, haematological biomarkers, vital signs, radiological findings, and intermediate events that directly impact disease progression, such as complications and neurological surgeries. Additionally, the Bayesian approach adopted for parameter estimation allows for the integration of expert knowledge into prior distributions, enhancing its clinical utility and improving the model's interpretability for clinicians.

This study not only utilises dynamic health data and baseline patient characteristics to monitor patients' conditions but also explains changes in dynamic covariates through clinical intermediate events. This approach enhances the accuracy of predicting clinical outcomes and increases healthcare providers' engagement in prognostic modelling. Consequently, it facilitates a more transparent modelling mechanism, potentially leading to better acceptance in clinical practice.

However, the study acknowledges a significant limitation: the omission of time-to-complication data, such as DCI and vasospasm, which carries valuable prognostic information and marks pivotal points in disease progression. The failure to integrate this information into the prognostic modelling diminishes its ability to detect critical changes in disease progression, resulting in sub-optimal prediction performance.

Another notable limitation of our study is the potential impact of sedation on GCS assessments. Sedative agents can artificially lower GCS scores, making it difficult to distinguish between true neurological deterioration and drug-induced unconsciousness. This could lead to inaccurate estimates of neurological status and affect the accuracy of predictive models relying on GCS as a primary prognostic factor. Future studies should consider incorporating alternative neurological monitoring methods, such as pupillary reactivity, EEG, or neuroimaging, to improve the reliability and comprehensiveness of neurological status evaluation in sedated patients. Additionally, prognostic models should account for sedation status to minimise potential bias in outcome predictions.

The findings of this study also contribute to the advancement of personalised prognosis, a growing trend in critical care management. Personalised prognosis

considers individual characteristics and can guide tailored treatment decisions, individualised follow-up, and resource allocation. Implementing personalised prognosis in clinical practice can help improve patient outcomes, enhance collaboration between patients and caregivers, and support more patient-centred healthcare. This study is the first to incorporate all three types of individual-specific covariates and events, i.e., baseline medical conditions, dynamic prognostic factors and intermediate events, into prognostic modelling in studies of neurovascular diseases. Findings and approaches proposed in this study can thus potentially contribute to the development of personalised prognosis for neurovascular diseases.

There are three main future directions of this study. Firstly, neurological intervention is not the only intermediate event that can provide additive prognostic information to baseline and dynamic covariates. Occurrences of major complications during critical care, e.g., re-bleeding, and DCI, are also informative indicators for changes in disease progression, which often indicate worsening neurological conditions. Incorporating multiple intermediate outcomes and development of a multi-state prognostic model can potentially provide more accurate and comprehensive prognostication.

Secondly, the application of deep learning strategies in the prognosis of spontaneous SAH can potentially help capture informative features for prognosis research, thereby improving the model's flexibility and adaptability. These enhancements can be integrated with our proposed modelling framework to achieve higher predictive performance. [15] However, it is important to consider the potential challenges of deep learning approaches, such as the difficulty in interpreting the results and understanding disease progression. This lack of interpretability can pose significant challenges in clinical practice, as it may hinder caregivers from trusting and effectively utilising the model's predictions.

Thirdly, in this study, coiling and clipping were analysed together as neurological intervention due to dataset limitations. However, coiling and clipping differ in their procedural risks, impact on cerebral haemodynamics, and functional outcomes, which could influence prognostic modeling. Distinguishing these interventions as separate treatment events is important and would require a larger dataset to ensure sufficient statistical power for meaningful comparisons.

Reference for chapter 5

[1] Ingall T, Asplund K, Mähönen M, Bonita R. A multinational comparison of subarachnoid hemorrhage epidemiology in the WHO MONICA stroke study. Stroke. 2000 May;31(5):1054-61.
[2] Hunt, W.E. and Hess, R.M., 1968. Surgical risk as related to time of intervention in the repair of intracranial aneurysms. Journal of neurosurgery, 28(1), pp.14-20.
[3] Teasdale, G.M., Drake, C.G., Hunt, W., Kassell, N., Sano, K., Pertuiset, B. and De Villiers, J.C., 1988. A universal subarachnoid hemorrhage scale: report of a committee of the World Federation of Neurosurgical Societies. Journal of neurology, neurosurgery, and psychiatry, 51(11), p.1457.
[4] Fisher, C.M., Kistler, J.P. and Davis, J.M., 1980. Relation of cerebral vasospasm to subarachnoid hemorrhage visualized by computerized tomographic scanning. Neurosurgery, 6(1), pp.1-9.
[5] Frontera, J.A., Claassen, J., Schmidt, J.M., Wartenberg, K.E., Temes, R., Connolly, E.S., Macdonald, R.L. and Mayer, S.A., 2006. Prediction of symptomatic vasospasmafter subarachnoid hemorrhage: the modified fisher scale. Neurosurgery, 59(1), pp.21-27.
[6] Witsch, J., Frey, H.P., Patel, S., Park, S., Lahiri, S., Schmidt, J.M., Agarwal, S., Falo, M.C., Velazquez, A., Jaja, B. and Macdonald, R.L., 2016. Prognostication of long-term outcomes after subarachnoid hemorrhage: The FRESH score. Annals of neurology, 80(1), pp.46-58.
[7] Johnson, A.E., Bulgarelli, L., Shen, L., Gayles, A., Shammout, A., Horng, S., Pollard, T.J., Hao, S., Moody, B., Gow, B. and Lehman, L.W.H., 2023. MIMIC-IV, a freely accessible electronic health record dataset. Scientific data, 10(1), p.1.
[8] Rosen, D.S. and Macdonald, R.L., 2005. Subarachnoid hemorrhage grading scales: a systematic review. Neurocritical care, 2, pp.110-118.
[9] Lampmann, T., Hadjiathanasiou, A., Asoglu, H., Wach, J., Kern, T., Vatter, H. and Güresir, E., 2022. Early serum creatinine levels after aneurysmal subarachnoid hemorrhage predict functional neurological outcome after 6 months. Journal of Clinical Medicine, 11(16), p.4753.
[10] Ma, X., Lan, F. and Zhang, Y., 2021. Associations between C-reactive protein and white blood cell count, occurrence of delayed cerebral ischemia and poor outcome following aneurysmal subarachnoid hemorrhage: A systematic review and meta-analysis. Acta Neurologica Belgica, pp.1-14.
[11] Schmutzhard, E., Rabinstein, A.A. and Participants in the International multi-disciplinary Consensus Conference on the Critical care Management of Subarachnoid Hemorrhage, 2011. Spontaneous subarachnoid hemorrhage and glucose management. Neurocritical care, 15, pp.281-286.
[12] Rosengart, A.J., Schultheiss, K.E., Tolentino, J. and Macdonald, R.L., 2007. Prognostic factors for outcome in patients with aneurysmal subarachnoid hemorrhage. Stroke, 38(8), pp.2315-2321.
[13] Ryttlefors, M., Howells, T., Nilsson, P., Ronne-Engström, E. and Enblad, P., 2007. Secondary insults in subarachnoid hemorrhage: occurrence and impact on

outcome and clinical deterioration. Neurosurgery, 61(4), pp.704-715.
[14] Lin, Q.S., Lin, Y.X., Lin, Z.Y., Yu, L.H., Dai, L.S. and Kang, D.Z., 2016. Systolic blood pressure variability is a novel risk factor for rebleeding in acute subarachnoid hemorrhage: a case–control study. Medicine, 95(11).
[15] Lin, J. and Luo, S., 2022. Deep learning for the dynamic prediction of multivariate longitudinal and survival data. Statistics in medicine, 41(15), pp.2894-2907.

Chapter 6 Incorporating pharmacological effects into prognostic models for SAH disease progress

Previous chapters have studied on how to ultilise multiple sources of prognostic information as well as simultaneously analyse baseline and dynamic covariates to monitor disease progression and predict patients' clinical outcomes. Specifically, we have respectively studied prognostic values of baseline covariates, dynamic covariates, e.g., neurological assessments and vital signs, intermediate events during post-SAH care, e.g., neurovascular interventions, and how to combine them into prognostic modelling to predict prognosis.

To more accurately monitor and describe disease progression, thereby enhancing critical care for SAH patients in clinical practice, one important question must be considered: how can the trajectories of longitudinal prognostic factors in SAH prognosis be better represented and explained? Chapter 3 addresses this by modelling longitudinal prognostic factors, such as repeatedly measured ABP and ECG indices, using fixed-term and random-term effects. These effects respectively represent group-level trends and individual-level deviations from these trends over time. In Chapter 5, neurosurgical interventions, such as aneurysm clipping and endovascular embolisation, are incorporated as clinical intermediate events, marking change points in the trajectories of dynamic covariates.

The studies in Chapter 3 and Chapter 5 focus on the temporal patterns and changes of dynamic covariates, highlighting the natural disease progression and recovery patterns of patients over time. This approach provides a clear picture of how the disease evolves. However, relying solely on time-related effects to explain the trajectories of dynamic covariates, while ignoring other influences, especially pharmacological effects, can result in an incomplete representation of patients' clinical profiles and limited clinical significance. Specifically, by neglecting the impact of pharmacological interventions on longitudinal prognostic factors, the prognostic model loses the ability to assess drug effectiveness and thereby guide pharmacological plans.

To address this challenge, this chapter will explore potential improvements in prognostic models by incorporating pharmacological effects, evaluating improvements through prediction accuracy, and discussing the corresponding clinical implications. First, commonly prescribed medications for SAH patients will be examined, detailing their usage scenarios and mechanisms of action. Next, the impact of each medication on the recovery of neurological status in SAH patients will be analysed through dynamic prognostic modelling. Finally, the findings from this chapter will be discussed in terms of their clinical significance and potential contributions to SAH prognosis studies.

6.1 Medication protocols for SAH recovery

Compared to the natural evolution of SAH, which is the inherent progression of the condition without medical intervention, healthcare providers aim to enhance patients' recovery trajectories and clinical outcomes through various treatment strategies, including neurosurgery, pharmacotherapy, and supportive care. The primary goal of neurosurgery is to secure aneurysms via coiling or clipping to prevent re-bleeding. Other neurosurgical interventions are not directly aimed at treating SAH itself but at managing complications and intracranial pressure (ICP). For example, external ventricular drains (EVDs) are used to manage hydrocephalus, and decompressive craniectomy (DC) is performed to treat elevated ICP.

The effects of neurosurgery, including coiling and clipping, on disease progression and their prognostic values were studied in Chapter 5, with these interventions incorporated as clinical intermediate events in dynamic prognostic models. In addition to neurosurgical interventions, understanding the impact of medications on disease progression and clinical outcomes is also of significant clinical importance. This will allow healthcare providers to optimise treatment strategies by referring to predictions from prognostic models that consider pharmacological effects.

Based on their primary uses in clinical practice, common pharmacological agents can be broadly classified into three main categories: complication prevention and management, pain relief and control, and intracranial and blood pressure control. Pharmacological agents aimed at preventing and managing complications include nimodipine for vasospasm prevention, antiepileptic drugs such as levetiracetam for seizure prophylaxis, and heparin for venous thromboembolism prophylaxis to prevent deep vein thrombosis (DVT).

Pain relief and control are crucial for SAH patients to manage both headache and procedural pain. Commonly used medications include non-opioid analgesics like acetaminophen and opioid analgesics like morphine. Intracranial and blood pressure control are also vital in post-SAH care to prevent secondary brain injury, ensure adequate cerebral perfusion, and reduce the risk of further complications. Mannitol is often used to reduce elevated ICP, while antihypertensive agents such as hydralazine are employed to control blood pressure.

The clinical effectiveness of pharmacological agents such as nimodipine, pain relief medications, and antihypertensive agents on the outcomes of SAH patients has been extensively studied [1][2][3]. However, their dynamic effects on SAH recovery, specifically how the administration of these medications impacts recovery trajectories over time, remain unexplored despite their significance for SAH prognosis. Therefore, in Section 6.2, we aim to study the dynamic pharmacological effects on SAH recovery and how incorporating these effects can enhance the prediction performance and comprehensiveness of prognostic models.

6.2 Analysis on pharmacological effects on SAH recovery

6.2.1 Data description and methods

To investigate the pharmacological effects on SAH recovery, we recruited 612 spontaneous SAH patients from MIMIC-IV dataset, a publicly available database sourced from the electronic health record of the Beth Israel Deaconess Medical Center between 2008 to 2019. [4] Included patients were characterised with hospital stays longer than one day, documented neurological assessments, and all aged 18 or over, with comprehensive medication administration records.

Among these patients, 357 (58.33%) patients were females, and the median age was 58 (IQR: 49-69). Essential hypertension is the most common medical condition on admission, followed by hydrocephalus, respiratory failure, and cerebral oedema. The clinical outcomes were assessed based on discharge destinations at the end of 14-day study period, covering both acute and sub-acute phases of SAH. Good outcome (283, 46.24%) was defined by returning home or rehabilitation within the study period, while poor outcome (329, 53.76%) includes mortality, long-term acute care, hospice care, and long-term hospital stay exceeding the study period. Survival analysis was performed on these clinical baseline covariates to assess their impacts on clinical outcomes and determine their inclusion in prognostic modelling. The clinical characteristics of the dataset and statistical significance of each covariate are shown in Table 6.1.

Covariate		All	Good outcome	Poor outcome	P value
Demographics	Age	Median: 58	Median: 49.25	Median: 61	**0.008**
	Female	409	156	201	0.231
Underlying conditions	Alcohol	21	9	12	0.665
	Tobacco	117	57	60	0.867
	Diabetes	61	24	37	0.092
	Essential hypertension	294	125	169	0.137
Complications	Cerebral oedema	128	24	106	**<0.001**
	Cerebral infarction	65	13	52	**<0.001**
	Respiratory failure	148	10	138	**<0.001**
	Hydrocephalus	213	31	182	**<0.001**
	Vasospasm	55	15	40	**<0.001**

Table 6.1: Clinical characteristics of included dataset and P values of baseline covariates

Significant baseline covariates, highlighted in Table 6.1, were then included in further prognostic modelling and jointly analysed with dynamic prognostic factor, Glasgow

Coma Scale (GCS) score, while Table 6.2 summarises the pharmacological treatments administered to patients included in Chapter 6, providing an overview of the frequency and distribution of commonly used medications within the cohort. In Table 6.1, these baseline covariates can provide baseline prognostic information for predicting clinical outcomes and act as confounders, enabling more accurate estimates on the effects of repeatedly measured GCS score on clinical outcomes.

Medication	Patients (All=612)	Percentage (%)
Nimodipine	474	77.45%
Hydralazine	185	30.23%
Acetaminophen	413	67.48%
Levetiracetam	220	35.95%
Morphine	189	30.88%
Mannitol	63	10.29%
Labetalol	161	26.31%
Nicardipine	144	23.53%
Heparin	222	36.27%

Table 6.2: Pharmacological details of included dataset in Chapter 6

The GCS score was included as the longitudinal prognostic factor to represent disease progression and recovery trajectory due to its two primary merits. Firstly, the GCS score is a strong and widely recognised indicator of clinical outcomes in SAH patients, whereas other longitudinal predictors, such as the vital sign indices discussed in Chapter 3 and Chapter 5, did not demonstrate sufficient prognostic power to serve as independent prognostic predictors [5]. Secondly, unlike other grading scales, such as the Hunt and Hess scale, which assesses the initial severity of SAH, the GCS score offers the advantage of dynamic applicability. It can be routinely measured repeatedly over time, allowing for continuous monitoring and providing ongoing prognostic information on a patient's neurological status.

Therefore, the GCS score was utilised in longitudinal analysis and modelled using linear mixed models (LMMs) to represent the up-to-date neurological status of patients. Administered medications were incorporated as explanatory factors to account for changes in GCS scores. The objective of this chapter's study is to examine whether each administration of medication significantly influences changes in GCS scores and its effects on patients' neurological status. Additionally, this study aims to explore potential medical and pharmacological explanations for these outcomes. Finally, the contributions of this chapter's study to SAH prognosis and the comprehensiveness of prognostic modelling will be discussed.

6.2.2 Effects of medications for complication prevention and management on SAH prognosis

Vasospasm narrows blood vessels, reducing blood flow to the brain and potentially

leading to ischaemic brain injury. This condition can result in a decline in neurological status due to clinical deterioration and worsening neurological function. Nimodipine, a calcium channel blocker, helps relax vascular smooth muscle, thereby improving blood flow and reducing ischaemic damage. This relaxation, along with the neuroprotective and neuroregenerative effects of nimodipine, can help reduce neuronal injury and improve neurological outcomes after SAH [6].

The effectiveness of nimodipine in SAH treatment has been demonstrated by improvements in GCS scores [7]. However, the impact of nimodipine administration on the progression of recovery in SAH patients requires further investigation. To address this, nimodipine is incorporated as a fixed effect in the analysis of repeatedly measured GCS scores. This approach allows us to evaluate how nimodipine administration contributes to neurological improvement, accounting for changes in the neurological status of SAH patients that cannot be explained by natural recovery alone during their hospital stay.

An interaction term between time and nimodipine has also been included, allowing the effect of nimodipine to depend on the timing of its administration. The results of this longitudinal analysis are presented in Table 6.3.

Covariate	Value	Std. Error	P value
Intercept	11.0410	0.2830	**<0.001**
Time	0.1680	0.0398	**<0.001**
Nimodipine	0.9485	0.2952	**0.001**
Interaction term	-0.1096	0.0420	**0.009**

Table 6.3: Longitudinal analysis considering administration of nimodipine

The coefficient for time is 0.1680, indicating that for each additional day, the GCS score is expected to increase by 0.1680, representing the patients' average rate of recovery over time with the administration of nimodipine. The effect of nimodipine on the GCS score is estimated to be $0.9485-0.1096t$, suggesting that while nimodipine can improve the neurological status of SAH patients, its relative benefit decreases over time. For instance, administering nimodipine on day 3, at the end of the acute phase, is associated with a 0.6196 increase in GCS scores. However, by day 7, when maximum vasospasm is typically detected, the increase is only 0.1813. This aligns with previous clinical findings that nimodipine is most effective in the early phases (within 96 hours) for preventing complications such as vasospasm and cerebral ischemia, thereby improving clinical outcomes [8].

Besides examining the dynamic effects of nimodipine on GCS scores, we are also interested in the prognostic value of these pharmacological factors in improving the predictive performance of clinical outcomes. To this end, we first computed the predictive performance of a baseline prognostic model that considers the effects of baseline covariates and GCS scores without incorporating the potential effects of

pharmacological agents. Subsequently, we computed the predictive performance of prognostic models with pharmacological effects included and evaluated the improvement compared to the baseline model.

Ts/dt	1	2	3	5	7	Mean
1	0.8926	0.7952	0.7928	0.7942	0.7964	0.8142
2	0.7489	0.7912	0.7628	0.7969	0.8063	0.7812
3	0.7395	0.6691	0.6998	0.7313	0.7642	0.7208
5	0.7354	0.7789	0.7436	0.7178	0.7098	0.7371
7	0.7477	0.7645	0.7609	0.7435	0.7142	0.7462
Overall: 0.7599 ($\pm$0.0439) Acute: 0.7721 ($\pm$0.0503) Sub-acute: 0.7417 ($\pm$0.0217)						

Table 6.4: Prediction performance of baseline prognostic model

Table 6.4 presents the predictive performance across different starting points T_s and prediction intervals dt. The acute phase (first 3 days) is characterised by acute symptoms such as severe headache and risks of re-bleeding, while the sub-acute phase (after 3 days to 2 weeks) involves delayed complications such as DCI, along with the rehabilitation for neurological recovery.

Ts/dt	1	2	3	5	7	Mean
1	0.8941	0.7952	0.8057	0.8123	0.8121	0.8329
2	0.8128	0.8079	0.7876	0.8255	0.8249	0.8117
3	0.7436	0.6936	0.7255	0.7525	0.7833	0.7397
5	0.7448	0.7899	0.7614	0.7383	0.7339	0.7448
7	0.7625	0.7659	0.7624	0.7547	0.7358	0.7562
Overall: 0.7771 ($\pm$0.0416) Acute: 0.7948 ($\pm$0.0465) Sub-acute: 0.7550 ($\pm$0.0164)						

Table 6.5: Prediction performance of prognostic model considering administration of nimodipine

Table 6.5 presents the prediction performance of the prognostic model when considering the administration of nimodipine. The results show that incorporating nimodipine to explain changes in neurological status enhances the model's performance in predicting clinical outcomes, particularly during the acute phases after SAH when nimodipine is commonly administered. By accounting for nimodipine administration, the model gains insights into the biological pathways affected by nimodipine post-SAH and can explain changes in neurological status that natural recovery alone cannot account for. This enhancement in model thus leads to a more accurate prediction of clinical outcomes.

Compared to vasospasm, which more directly leads to severe conditions due to its potential to cause ischaemia and subsequent brain damage, seizures may not have an immediate and severe adverse impact on post-SAH medical conditions. However, seizure burden in SAH is still associated with worse functional and cognitive outcomes [9]. Levetiracetam, with its multifaceted mechanisms, controls seizures and

improves post-SAH outcomes due to its antiepileptogenic, anti-inflammatory, and neuroprotective properties [10]. To measure the impact of levetiracetam on neurological status and evaluate its prognostic value, we first perform a longitudinal analysis of its effects on GCS scores, as shown in Table 6.6.

Covariate	Value	Std. Error	P value
Intercept	11.6427	0.1610	**<0.001**
Time	0.0939	0.0149	**<0.001**
levetiracetam	0.5797	0.0925	**<0.001**
Interaction term	-0.0744	0.0153	**<0.001**

Table 6.6: Longitudinal analysis considering administration of levetiracetam

In addition to natural recovery patterns over time, levetiracetam positively impacts neurological status, although this positive effect diminishes over time, estimated to be *0.5797-0.0744t*. However, compared to the effect of nimodipine, levetiracetam's positive impact and its reduction over time are both less significant. This is because nimodipine targets vasospasm, which can directly influence the neurological recovery trajectory, making its role more critical in the longitudinal analysis of neurological status. While levetiracetam is important for controlling acute neurological symptoms like seizures, its effects on overall neurological recovery, as measured by GCS scores, are less apparent than those of nimodipine. To assess levetiracetam's effectiveness on neurological recovery, especially in seizure control, EEG monitoring or tools like the Chalfont Seizure Severity Scale might be more suitable.

Table 6.7 presents the predictive performance of a prognostic model incorporating levetiracetam's effects in the longitudinal analysis of neurological status. Compared to nimodipine, the prognostic value of levetiracetam in predicting post-SAH outcomes is less significant. Analysis of the results in Tables 6.4 and 6.7 indicates that incorporating levetiracetam into prognostic modelling does not enhance overall prediction accuracy. However, during the sub-acute phases of SAH recovery, levetiracetam demonstrates prognostic value. In the sub-acute phases, patients' neurological conditions have stabilised, and the focus shifts to managing ongoing neurological issues like seizures. It is during this period that levetiracetam's effectiveness in seizure control becomes increasingly significant.

Ts/dt	1	2	3	5	7	Mean
1	0.9027	0.7882	0.7912	0.7985	0.7976	0.8156
2	0.7420	0.7880	0.7604	0.7960	0.8038	0.7780
3	0.7323	0.6665	0.6993	0.7281	0.7609	0.7174
5	0.7087	0.7708	0.7472	0.7254	0.7150	0.7334
7	0.7445	0.7651	0.7619	0.7499	0.7365	0.7516
Overall: 0.7592 ($\pm$0.0450) Acute: 0.7704 ($\pm$0.0529) Sub-acute: 0.7425 ($\pm$0.0200)						

Table 6.7: Prediction performance of prognostic model considering administration of levetiracetam

Besides neurological symptoms such as vasospasm and seizures, cardiovascular deficits like venous thromboembolism (VTE) also require careful attention. VTE is characterized by blood clots in the deep veins of the body, primarily in the legs, known as DVT. Venous stasis, often resulting from immobility during critical care, is a major factor contributing to the development of VTE, significantly impacting clinical outcomes [11].

Heparin is widely used to prevent VTE by inactivating thrombin and factor Xa, and it can be administered subcutaneously or intravenously. According to the results in Table 6.8, heparin administration for VTE prevention is significantly associated with improved neurological status, although this improvement gradually diminishes over time. The effect on GCS scores is estimated as *0.7379-0.0684t*.

Covariate	Value	Std. Error	P value
Intercept	11.6543	0.1599	**<0.001**
Time	0.0755	0.0176	**<0.001**
Heparin	0.7379	0.0836	**<0.001**
Interaction term	-0.0684	0.0152	**<0.001**

Table 6.8: Longitudinal analysis considering administration of heparin

As shown in Table 6.9, we have assessed the prognostic value of heparin administration. Incorporating heparin into the prognostic model significantly improves the model's performance during the sub-acute phases following SAH. In these phases, the risk of developing VTE increases due to prolonged immobilisation, making heparin's efficacy in preventing blood clot formation crucial.

Ts/dt	1	2	3	5	7	Mean
1	**0.9122**	**0.7983**	**0.7869**	**0.7951**	**0.7907**	**0.8166**
2	**0.7502**	**0.7798**	**0.7569**	**0.7897**	**0.7970**	**0.7753**
3	**0.6976**	**0.6468**	**0.6853**	**0.7293**	**0.7617**	**0.7041**
5	**0.7202**	**0.7721**	**0.7488**	**0.7328**	**0.7279**	**0.7404**
7	**0.7462**	**0.7615**	**0.7636**	**0.7539**	**0.7404**	**0.7531**
Overall: 0.7578 (±0.0480) Acute: 0.7652 (±0.0595) Sub-acute: 0.7467 (±0.0158)						

Table 6.9: Prediction performance of prognostic model considering administration of heparin

To visualise the improvement in the model's prediction accuracy brought by these three pharmacological agents for the prevention of complications, Figure 6.1 compares the prediction accuracy of models incorporating these agents with the baseline prognostic model that does not include pharmacological effects.

According to the comparisons in Figure 6.1, nimodipine, administered to prevent vasospasm, demonstrates the highest prognostic value in overall prediction accuracy

among these three agents. This is likely because vasospasm is a major post-SAH complication, significantly associated with poor clinical outcomes, as well as high incidences of morbidity and mortality [12]. In the longitudinal analysis of these three agents, positive associations between their administration and GCS scores have been observed, although these benefits diminish over time. This suggests that these agents should be administered early for maximal effectiveness in improving patients' neurological conditions.

Another valuable finding is that the prognostic values of these agents vary between the acute and sub-acute phases, reflecting the crucial periods for their use and the temporal characteristics of the corresponding complications. For example, nimodipine is recommended to be started within 96 hours to prevent vasospasm, which typically begins on day 3, peaking 7 to 10 days after SAH. [13] Consequently, the inclusion of nimodipine significantly improves prediction accuracy in the acute phase of SAH. In contrast, incorporating heparin into prognostic modelling primarily enhances predictive performance in the sub-acute phase, when acute symptoms have stabilised and morbidity becomes an important factor in discharge decisions.

Section 6.2.2 has examined three pharmacological agents, i.e., nimodipine, levetiracetam, and heparin, for their roles in preventing common complications associated with SAH: vasospasm, seizures, and VTE, respectively. We have evaluated their effectiveness in improving neurological recovery, analysed the temporal dynamics of these effects, and assessed their prognostic value in enhancing prediction accuracy during both the acute and sub-acute phases. Furthermore, these results have been clinically interpreted in the context of SAH, considering the specific characteristics of these complications and the underlying mechanisms of action of the pharmacological agents studied.

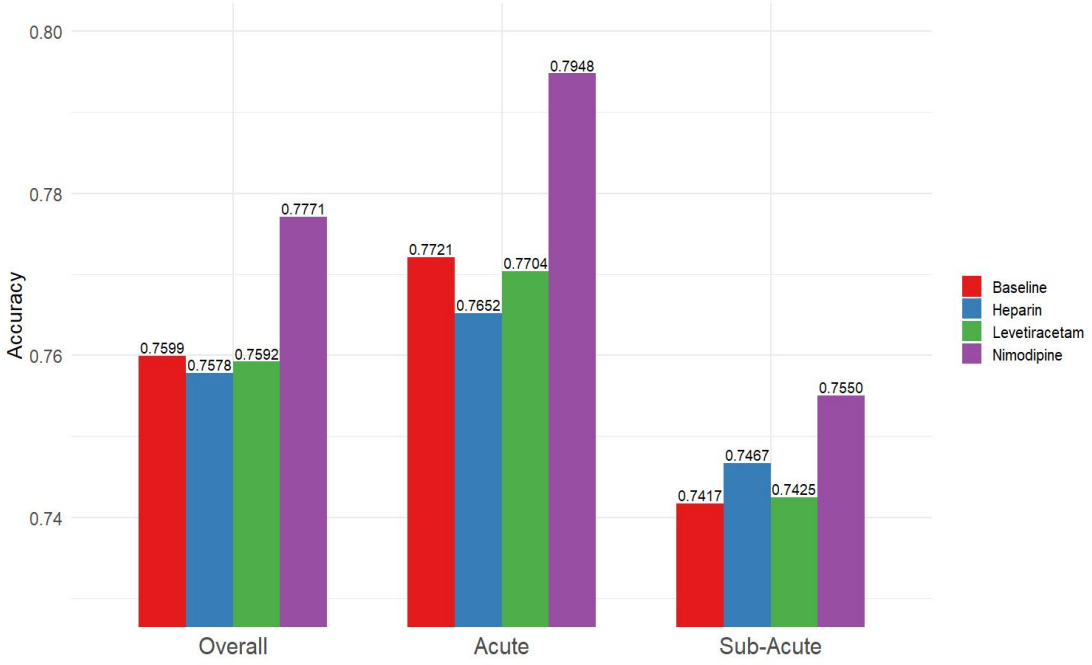


Figure 6.1: Comparison of prediction accuracy for prognostic models with pharmacological agents for complication prevention

6.2.3 Effects of medication for pain relief and control on SAH prognosis

Post-SAH pain relief and control is crucial for SAH patients, as the condition is often accompanied by a sudden, severe headache and neck pain. Pharmacological agents for pain relief are used not only to alleviate pain but also to improve patient comfort and well-being. Analgesics, or pain relievers, can be categorised into two main types: opioid analgesics, such as morphine, and non-opioid analgesics, such as acetaminophen. While the associations between post-SAH pain management and clinical outcomes are not fully understood, Section 6.2.3 aims to explore how these analgesics impact patients' neurological conditions and assess their potential prognostic value for improving predictive accuracy in SAH prognosis.

Opioid analgesics are powerful pain relievers, particularly effective for acute pain, functioning by binding to specific opioid receptors and inhibiting the transmission of pain signals to the brain. Morphine, a common opioid analgesic, is often used to relieve moderate to severe pain by binding to mu-opioid receptors in the central nervous system, thereby inhibiting pain signal transmission. To assess its impact on patients' neurological conditions, a longitudinal analysis was performed, as shown in Table 6.10. The results indicate that morphine has a positive impact on neurological conditions, although this effect gradually diminishes over time.

Covariate	Value	Std. Error	P value
Intercept	11.7261	0.1586	**<0.001**
Time	0.0790	0.0141	**<0.001**
Morphine	0.4846	0.1122	**<0.001**
Interaction term	-0.0420	0.0205	**0.041**

Table 6.10: Longitudinal analysis considering administration of morphine

Ts/dt	1	2	3	5	7	Mean
1	0.9218	0.7954	0.7891	0.7938	0.7942	0.8189
2	0.7891	0.7780	0.7589	0.7970	0.8051	0.7856
3	0.7286	0.6787	0.7062	0.7371	0.7708	0.7243
5	0.7338	0.7815	0.7496	0.7259	0.7195	0.7421
7	0.7560	0.7690	0.7647	0.7517	0.7331	0.7549
Overall: 0.7651(±0.0450) Acute: 0.7763 (±0.0531) Sub-acute: 0.7628(±0.0314)						

Table 6.11: Prediction performance of prognostic model considering administration of morphine

Table 6.11 presents the prognostic values of morphine administration in predicting clinical outcomes. The results illustrate that incorporating morphine improves overall

prediction performance, as well as performance during both acute and sub-acute phases. The improvement is more significant in the sub-acute phases. This suggests that as patients' conditions stabilise, the contributions of morphine to predicting clinical outcomes become more noticeable. Furthermore, as patients recover from acute and severe symptoms in the acute phase, the effects of pain relief medication can be more reliably anticipated and managed, potentially making morphine a more effective tool for controlling ongoing pain.

Unlike opioid analgesics, non-opioid analgesics work through mechanisms other than the opioid receptor pathway and are typically used for controlling mild to moderate pain. Acetaminophen, a widely used non-opioid analgesic in clinical practice, is effective for mild to moderate pain relief and fever reduction. The results in Table 6.12 show that acetaminophen administration is positively associated with improvements in patients' neurological conditions, with this association estimated at *0.4912-0.0419t*.

Covariate	Value	Std. Error	P value
Intercept	11.5202	0.1703	**<0.001**
Time	0.0938	0.0185	**<0.001**
Acetaminophen	0.4912	0.1103	**<0.001**
Interaction term	-0.0419	0.0170	**0.014**

Table 6.12: Longitudinal analysis considering administration of acetaminophen

However, as shown in Table 6.13, incorporating acetaminophen to account for changes in GCS scores does not improve the accuracy of predicting outcomes. This discrepancy between acetaminophen's positive association with improved neurological conditions and its lack of prognostic value for predicting clinical outcomes can primarily be attributed to the complexity of neurological recovery and the limitations of assessment tools.

Ts/dt	1	2	3	5	7	Mean
1	0.9504	0.7705	0.7867	0.7939	0.7903	0.8184
2	0.7463	0.7799	0.7572	0.7944	0.7995	0.7755
3	0.7093	0.6571	0.6898	0.7166	0.7508	0.7047
5	0.7222	0.7721	0.7392	0.7178	0.7128	0.7328
7	0.7352	0.7539	0.7547	0.7496	0.7343	0.7455
Overall: 0.7554(±0.0527) Acute: 0.7662 (±0.0643) Sub-acute: 0.7392(±0.0177)						

Table 6.13: Prediction performance of prognostic model considering administration of acetaminophen

Acetaminophen's effects on alleviating pain and discomfort can be captured as immediate and transient improvements in GCS scores. However, unlike the neuroprotective and neuroregenerative effects of nimodipine, which are critical for neurological recovery, these improvements might not directly correlate with long-term

clinical outcomes. Therefore, while acetaminophen can effectively improve patient comfort and potentially aid neurological conditions, its ability to provide symptomatic relief may not directly translate into better clinical outcomes.

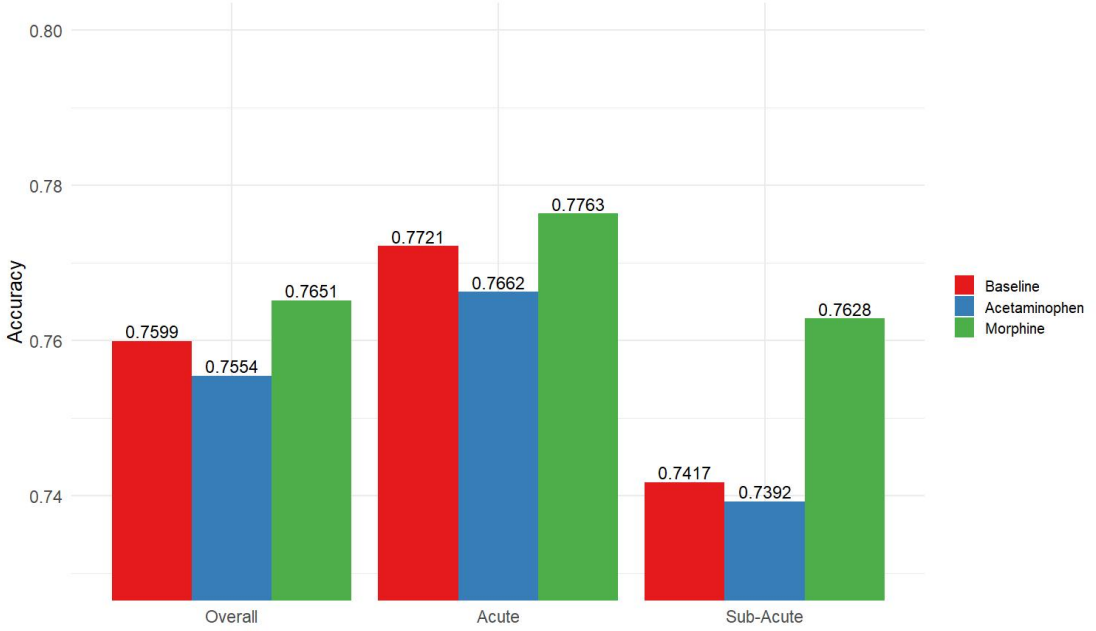


Figure 6.2: Comparison of prediction accuracy for prognostic models with pharmacological agents for pain control and relief

Section 6.2.3 has examined two agents for pain control and relief, focusing on their effectiveness in improving GCS scores, their prognostic value in SAH prognosis, and their underlying mechanisms. The first agent, morphine, is an opioid analgesic primarily used for severe pain, such as post-surgical pain. The second, acetaminophen, is a non-opioid analgesic often used to treat mild to moderate pain, such as headaches and fevers. The analysis in this section shows that both pain relievers are associated with higher GCS scores. Since pain is not only a physical discomfort but also a psychological burden that can reduce responsiveness, these pain relievers may help increase patients' responsiveness during neurological assessments, leading to higher GCS scores.

However, as shown in Figure 6.2, when comparing the prediction accuracy considering these two pain relievers, it is observed that acetaminophen's effectiveness in pain relief and GCS score improvement does not contribute to better predictive performance. Although acetaminophen is commonly used and effectively relieves pain and discomfort, leading to immediate and transient improvements in GCS scores, these short-term improvements may not directly correlate with better clinical outcomes at discharge. In contrast, morphine's ability to manage severe pain from SAH onset or neurosurgeries is crucial for stabilising patients' conditions. This makes morphine's effects more pronounced in improving long-term clinical outcomes, rather than just providing short-term symptomatic relief.

Despite morphine's effectiveness in severe pain relief, enhancing neurological recovery, and potentially improving clinical outcomes, it comes with side effects such as nausea, vomiting, respiratory depression, and a high risk of addiction and tolerance, thus its use should be carefully managed [14]. To maximise the prognostic value of pain relievers and improve their utilisation in SAH prognosis, pain scale tools that can significantly predict clinical outcomes should be employed as longitudinal outcome measures for pain management in SAH prognosis.

6.2.4 Effects of medication for intracranial and blood pressure control on SAH prognosis

In post-SAH management, controlling ICP and maintaining BP are crucial for minimising secondary brain injury. ICP control focuses on managing the pressure within the skull to ensure adequate brain perfusion and prevent mechanical injury. Meanwhile, BP control aims to manage systemic cardiovascular conditions to maintain sufficient overall blood circulation and ensure adequate cerebral circulation.

To manage elevated ICP after SAH, mannitol is administered in response to acute rises in ICP, working by osmotically drawing fluid from brain tissue into the bloodstream. A longitudinal analysis considering mannitol administration was performed to examine its effects on neurological status, as detailed in Table 6.14. However, this analysis found no significant associations between mannitol administration and GCS scores, indicating that mannitol's effectiveness in ICP control may not be reflected in the neurological improvements detected by GCS scores.

Covariate	Value	Std. Error	P value
Intercept	11.8381	0.1564	**<0.001**
Time	0.0742	0.0136	**<0.001**
Mannitol	-0.3798	0.3057	0.214
Interaction term	-0.1024	0.0547	0.061

Table 6.14: Longitudinal analysis considering administration of mannitol

Covariate	Value	Std. Error	P value
Intercept	11.8707	0.1675	**<0.001**
Time	0.0597	0.0158	**<0.001**
Hydralazine	-0.1095	0.1218	0.369
Interaction term	0.0298	0.0185	0.107

Table 6.15: Longitudinal analysis considering administration of hydralazine

Our focus then shifted to hydralazine, which acts directly on vasodilation and reduces blood pressure in the management of post-SAH hypertension. However, similar to mannitol, the analysis in Table 6.15 shows no significant associations between hydralazine administration and changes in patients' neurological status, as measured

by GCS scores. Although hydralazine plays a vital role in controlling blood pressure to manage cerebral perfusion and reduce the risk of re-bleeding, its effects may not directly correlate with improvements in patients' levels of consciousness.

While managing appropriate ICP and BP is essential in post-SAH care, their direct contributions to improvements in neurological conditions, as measured by GCS scores, may not be immediately apparent. Unlike pharmacological agents for complication prevention and acute pain relief, which directly address acute symptoms and complications to facilitate neurological recovery, ICP and BP management focuses on supporting overall brain health and ensuring sufficient circulation. This provides an optimal environment for neurological recovery.

6.3 Summary and discussion

In this chapter, we have studied on three types of pharmacological agents within the context of SAH prognosis: agents for complication prevention and management, pain relief and control, and the management of ICP and blood pressure. To assess the roles and prognostic values of these agents, longitudinal analysis was initially conducted to explore their associations with GCS scores. When significant associations were identified, we have further examined whether incorporating these agents into prognostic models could improve the prediction of clinical outcomes.

After analysing all these three types of pharmacological agents, we have examined and discussed their associations with GCS scores and the resulting effects on prediction accuracy. These discussions covered aspects of specific contexts when these agents are often administrated, their underlying mechanisms of action, and the reasons why these agents may or may not significantly correlate with improved recovery and enhanced predictive performance.

For pharmacological agents for preventing complications in post-SAH management, there are several findings according to the analysis. Firstly, administrations of all three studied agents for preventing complications, i.e., nimodipine for vasospasm, levetiracetam for seizures, and heparin for VTE, were demonstrated associated with improved GCS scores. This suggests that since these complications are directly associated with clinical conditions, administrations for preventing these complications can thus significantly contribute to improved neurological recovery.

Among these three agents, nimodipine administration has shown both the strongest positive associations with GCS scores and the most significant improvement in prediction accuracy. This likely originates from the fact that vasospasm is closely associated with poor clinical outcomes, including high incidences of morbidity and mortality. As a result, effectively preventing vasospasm significantly correlates with improved neurological status and better clinical outcomes.

Secondly, these agents' positive effects on GCS scores all diminish over time,

indicating that these pharmacological agents for preventing complications should be administrated early to maximising their effectiveness in improving GCS scores. Specifically, as we have discussed previously, administrating nimodipine early, ideally within 96 hours, can effectively reduce the risks of vasospasm and associated negative effects. [13] Similarly, it is recommended to initiate early pharmacological thromboprophylaxis with heparin within 24 hours following treatments of aneurysms for preventing VTE in post-SAH management. [15]

After analysing pharmacological agents for complication prevention, we have analysed the effects of two pharmacological agents for pain control and relief: acetaminophen, a non-opioid analgesic for controlling mild to moderate pain, and morphine, an opioid analgesic for severe pain control. Both these two medications have shown positive associations with GCS scores. While the incorporation of morphine into prognostic modelling can lead to improved predictive performance, the effectiveness of acetaminophen in relieving mild to modest pain and its positive association with GCS scores do not necessarily translate into noticeable improvement in clinical outcomes. This is likely because acetaminophen's effectiveness is more about short-term symptomatic relief, whereas morphine not only relieves severe pain but also potentially provides neuroprotective effects, contributing to improvements in long-term clinical outcomes. [16]

For agents for management of ICP and blood pressure, such as mannitol for ICP management and hydralazine for blood pressure control, no significant associations have been identified between administrations of these agents and improvements in patients' neurological status. While managing appropriate ICP and blood pressure is crucial in post-SAH critical care, this management focuses more on supporting overall brain health and sufficient circulation rather than making direct contributions to noticeable improvements in neurological status measured via GCS scores.

Contributions of findings in this chapter are mainly from three aspects. Firstly, studies presented in this chapter introduce a novel approach to incorporate pharmacological agents into prognostic research for SAH and a novel metric to evaluate their effects. Unlike traditional clinical trials or prognostic studies that evaluate the hazard ratio (HR) or odds ratio (OR) of these agents on complications and clinical outcomes, this study incorporates the administration of pharmacological agents in correlation with dynamic prognostic markers, specifically GCS scores.

This approach allows for evaluating real-time effects of administration of an agent on neurological recovery and provides detailed insights into the agent's contributions to SAH prognosis. For instance, nimodipine administration not only effectively prevents vasospasm but also provides neuroprotective and neuroregenerative benefits, leading to better neurological recovery measure by GCS. As a result, incorporating nimodipine administration into SAH prognosis not only contributes to better predictive performance but also improving our understanding and modelling of the

neurological recovery process.

Secondly, this study contributes to the development of a comprehensive framework for prognostic modelling in SAH management. Additionally, the findings from this chapter can be integrated with studies from other chapters for a more comprehensive understanding and modelling of SAH prognosis. For instance, Chapter 3, which incorporates prognostic information from the monitoring of vital signs, and Chapter 5, which examines the roles of neurosurgical interventions in SAH prognosis, can be combined with the studies in this chapter to further enhance our understanding and modelling approaches of SAH prognosis.

Thirdly, prognostic models incorporating pharmacological effects can potentially benefit clinical practice by quantifying medication impacts and supporting personalised medicine. Current strategies often rely on clinical experience and standard protocols for use of medications. Integrating pharmacological data in prognostic models allows for a precise understanding of how specific medications affect prognosis, enabling more accurate adjustments to personalised post-SAH management. For instance, determining the optimal timing and dosage of nimodipine can potentially maximise its benefits in preventing vasospasm and enhancing neurological recovery, leading to better long-term outcomes for SAH patients.

Despite the significant contributions of this chapter's study to SAH prognosis, there are three main limitations that should be addressed for further improvement. Firstly, the study only examined a few representative pharmacological agents. For a more comprehensive understanding of pharmacological effects in SAH prognosis and to optimise the utilisation of prognostic information from medication administration records, a broader range of pharmacological agents should be studied and analysed regarding their effects on neurological recovery and prognostic values.

Secondly, while the GCS score is a widely used marker for neurological recovery and a strong predictor of clinical outcomes, it may not capture the effectiveness of some agents on SAH prognosis, e.g., agents for ICP and blood pressure control. To fully exploit the prognostic information from the administration of these agents, it would be beneficial to include alternative dynamic covariates, such as ICP and cerebral perfusion pressure (CPP) and their variability as longitudinal outcomes that correlate both with the administration of these agents and with clinical outcomes, providing a more comprehensive analysis of the effects of these agents.

A third limitation of this study is the selection bias in the administration of pharmacological interventions, as treatments are given based on clinical severity, prognosis, leading to selection biases. For example, while nimodipine is routinely prescribed to SAH patients, some patients may not receive it, particularly those who are not expected to survive, are on treatment withdrawal, where nimodipine's vasodilatory effects could exacerbate haemodynamic instability. This can create a

selection bias, as patients who do receive nimodipine are typically those expected to recover, making it appear significantly associated with better clinical outcomes.

Similarly, mannitol is administered in cases of elevated ICP, primarily in critically ill patients, making it challenging to separate the drug's effect from the underlying severity of brain injury. Since mannitol is primarily given to patients with high ICP and severe brain injury, those receiving it often have worse baseline clinical conditions, which could create a misleading association between mannitol use and poorer outcomes. Additionally, morphine is only given to patients who are conscious enough to report pain, leading to potential misunderstanding of the association between its use and better neurological outcomes. These treatment-related biases may influence the interpretation of drug effects, and future work should incorporate causal inference methods, to better isolate the true effects of these pharmacological interventions on SAH prognosis.

Chapter 6 investigated the impact of pharmacological agents on SAH recovery by incorporating them into prognostications. Key findings include nimodipine, levetiracetam, and heparin significantly improving GCS scores, especially with early administration, with nimodipine showing the strongest effect. Morphine and acetaminophen also increased GCS scores, but only morphine contributed to relative long-term outcomes. Mannitol and hydralazine, used for intracranial pressure and blood pressure management, did not significantly enhance neurological status. The study presents a novel method for incorporating real-time pharmacological effects into prognostic models for personalised SAH care.

Reference for chapter 6

[1] Hao, G., Chu, G. and Shi, Z., 2022. Clinical effectiveness of nimodipine for the prevention of poor outcome after aneurysmal subarachnoid hemorrhage: A systematic review and meta-analysis. Frontiers in Neurology, 13, p.982498.

[2] Kessler, E.R., Shah, M., K. Gruschkus, S. and Raju, A., 2013. Cost and quality implications of opioid‐based postsurgical pain control using administrative claims data from a large health system: opioid‐related adverse events and their impact on clinical and economic outcomes. Pharmacotherapy: The Journal of Human Pharmacology and Drug Therapy, 33(4), pp.383-391.

[3] Persad-Paisley, E.M., Shamshad, A., Stretz, C., Potter, N.S., Wendell, L.C., Thompson, B.B., Furie, K.L., Reznik, M.E. and Mahta, A., 2022. Association of pre-admission antihypertensive agents and outcomes in aneurysmal subarachnoid hemorrhage. Journal of Clinical Neuroscience, 103, pp.119-123.

[4] Johnson, A.E., Bulgarelli, L., Shen, L., Gayles, A., Shammout, A., Horng, S., Pollard, T.J., Hao, S., Moody, B., Gow, B. and Lehman, L.W.H., 2023. MIMIC-IV, a freely accessible electronic health record dataset. Scientific data, 10(1), p.1.

[5] Gotoh, O., Tamura, A., Yasui, N., Suzuki, A., Hadeishi, H. and Sano, K., 1996. Glasgow Coma Scale in the prediction of outcome after early aneurysm surgery. Neurosurgery, 39(1), pp.19-25.

[6] Li, R., 2014. Hot spots and future directions of research on the neuroprotective effects of nimodipine. Neural regeneration research, 9(21), pp.1933-1938.

[7] Liu, J., Sun, C., Wang, Y., Nie, G., Dong, Q., You, J., Li, Q. and Li, M., 2022. Efficacy of nimodipine in the treatment of subarachnoid hemorrhage: a meta-analysis. Arquivos de Neuro-Psiquiatria, 80, pp.663-670.

[8] Pickard, J.D., Murray, G.D., Illingworth, R., Shaw, M.D., Teasdale, G.M., Foy, P.M., Humphrey, P.R., Lang, D.A., Nelson, R. and Richards, P., 1989. Effect of oral nimodipine on cerebral infarction and outcome after subarachnoid haemorrhage: British aneurysm nimodipine trial. British Medical Journal, 298(6674), pp.636-642.

[9] De Marchis, G.M., Pugin, D., Meyers, E., Velasquez, A., Suwatcharangkoon, S., Park, S., Falo, M.C., Agarwal, S., Mayer, S., Schmidt, J.M. and Connolly, E.S., 2016. Seizure burden in subarachnoid hemorrhage associated with functional and cognitive outcome. Neurology, 86(3), pp.253-260.

[10] Contreras-García, I.J., Cárdenas-Rodríguez, N., Romo-Mancillas, A., Bandala, C., Zamudio, S.R., Gómez-Manzo, S., Hernández-Ochoa, B., Mendoza-Torreblanca, J.G. and Pichardo-Macías, L.A., 2022. Levetiracetam mechanisms of action: from molecules to systems. Pharmaceuticals, 15(4), p.475.

[11] Kshettry, V.R., Rosenbaum, B.P., Seicean, A., Kelly, M.L., Schiltz, N.K. and Weil, R.J., 2014. Incidence and risk factors associated with in-hospital venous thromboembolism after aneurysmal subarachnoid hemorrhage. Journal of clinical neuroscience, 21(2), pp.282-286.

[12] Khanafer, A., Bhogal, P., Hellstern, V., Harmening, C., Bäzner, H., Ganslandt, O. and Henkes, H., 2022. Vasospasm-Related Death after Aneurysmal Subarachnoid Hemorrhage: A Retrospective Case–Control Study. Journal of Clinical

Medicine, 11(16), p.4642.
[13] Ciurea, A.V., Palade, C., Voinescu, D. and Nica, D.A., 2013. Subarachnoid hemorrhage and cerebral vasospasm–literature review. Journal of medicine and life, 6(2), p.120.
[14] Thompson, P.I., Joel, S.P., John, L., Wedzicha, J.A., Maclean, M. and Slevin, M.L., 1995. Respiratory depression following morphine and morphine-6-glucuronide in normal subjects. British journal of clinical pharmacology, 40(2), p.145.
[15] de Oliveira Manoel, A.L., Turkel-Parrella, D., Germans, M., Kouzmina, E., da Silva Almendra, P., Marotta, T., Spears, J. and Abrahamson, S., 2014. Safety of early pharmacological thromboprophylaxis after subarachnoid hemorrhage. Canadian Journal of Neurological Sciences, 41(5), pp.554-561.
[16] Attarian, S., Tran, L.C., Moore, A., Stanton, G., Meyer, E. and Moore, R.P., 2014. The neurodevelopmental impact of neonatal morphine administration. Brain Sciences, 4(2), pp.321-334.

Chapter 7 Multi-state dynamic prognostic modelling for spontaneous SAH

7.1 Introduction

In previous chapters, we have successfully incorporated multiple prognostic factors into modelling SAH prognosis. In these studies, multiple types of prognostic factors have been demonstrated to be valuable in predicting clinical outcomes with clear clinical interpretability. These prognostic factors mainly include base covariates such as age and underlying conditions, and dynamic covariates such as repeated measured neurological assessments.

Baseline covariates capture the baseline clinical conditions of patients upon admission to hospital, while dynamic covariates can be used to depict how patients' clinical conditions evolve during the study period. To enhance the modelling of the longitudinal process, longitudinal explanatory information from treatments such as neurosurgical interventions and administrations of pharmacological agents has included to account for the changes of patients' clinical conditions during hospital stays.

In our previous studies and prognostic research, patients' experiences during hospital stays have been modelled with two possible states: a transient state, such as "alive", and an absorbing state, such as "dead", with only one possible transition between them, from "alive" to "dead". However, in the context of SAH prognosis, the transitioning probability from a transient state to an absorbing state can be significantly influenced by post-SAH complications. For example, cerebral vasospasm is a major contributor to mortality and morbidity following SAH that patients diagnosed with vasospasm are associated with higher risks of poor outcomes. Ignoring the occurrences of complications in prognostic modelling and categorising all patients into a single "alive" state can lead to over-generalisations of patients' clinical conditions that may not effectively capture the true prognostic variability among patients.

In this context, this single transient state for SAH prognosis can be expanded into multiple transient states, each representing a specific clinical scenario characterised by various complications included in the study. With these multiple transient states, multi-state prognostic models can be developed to capture the movement of patients across these potential states. This study is thus particularly focused on addressing modelling issues such as estimating transition probabilities among transient states and from transient states to the absorbing state, evaluating the impact of risk factors, and predicting clinical outcomes.

Besides these modelling issues, this study is also interested in exploring how

transitions between states affect the influence of prognostic factors on other complications and clinical outcomes. Additionally, this study aims to examine how the occurrence of certain complications influences the recovery trajectory and the risks of subsequent complications.

Figure 7.1 illustrates the traditional joint modelling framework for prognostic modelling. In this framework, prognostic information is derived from baseline and dynamic covariates. Baseline covariates provide insights into patients' initial risks at the time of hospital admission, whereas dynamic covariates can provide continually updated information that reflects changes in risk and the disease progresses.

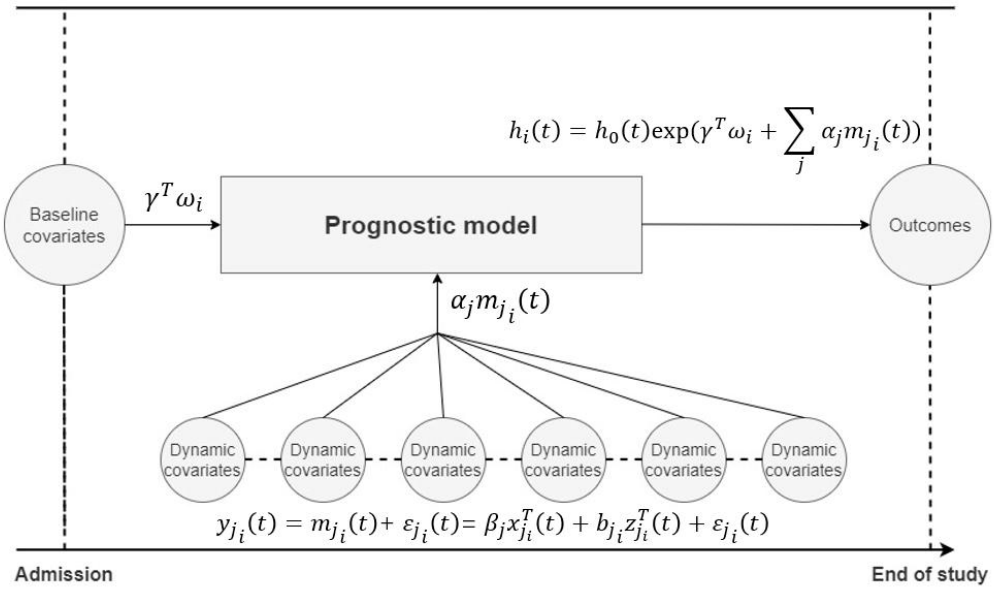


Figure 7.1: Traditional joint modelling framework for prognostic modelling

This framework models disease prognosis with a single transient state, the initial state. This implies that dynamic prognostic factors have the same fixed effects on patients, with random effects allowing for individual variations. For example, when examining the trajectories of dynamic covariates over time, all patients follow a general trend, with random effects allowing for individualised deviations from this average trajectory.

However, as post-SAH management can be accompanied by multiple complications, as shown in Figure 7.2 and discussed previously in Chapter 1, some complications, especially major complications, can significantly impact the prognosis of SAH. Assuming all patients following the same overall trend can result in over-generalisations that fail to accurately capture how specific complications affect disease progression and clinical outcomes.

Besides, in addition to predicting clinical outcomes, it is also of significant interest in predicting the occurrence of complications in the meantime to enable timely

interventions and preventive measures. To fulfill these clinical and research needs, the development of a multi-state prognostic model for spontaneous SAH is important, which will be explored and discussed in this chapter.

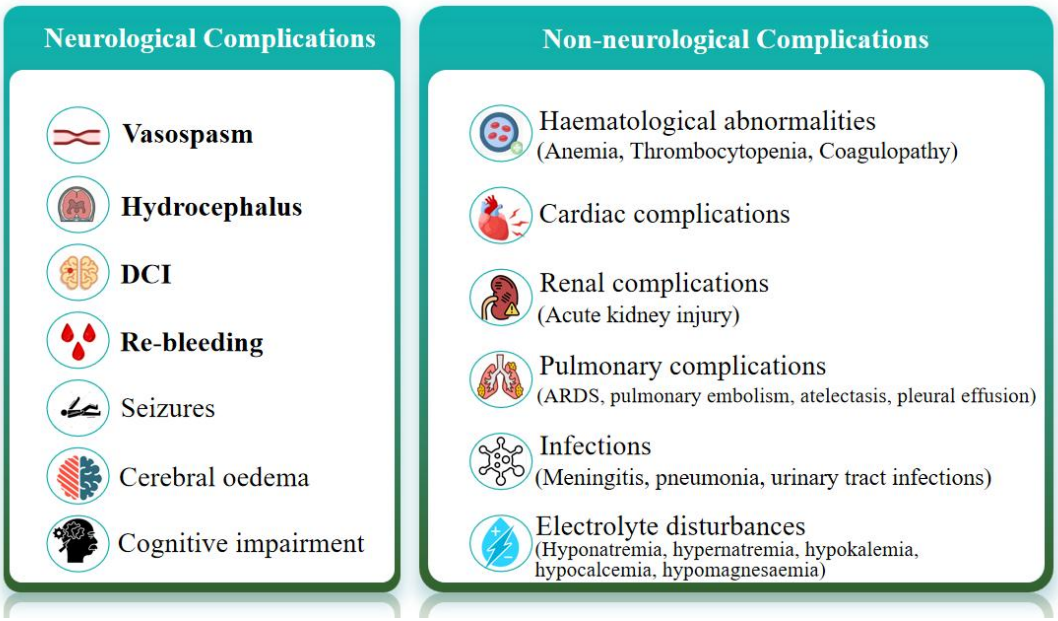


Figure 7.2 Complications after spontaneous SAH with major complications highlighted in bold

7.2 SAH prognostic framework

To develop the framework of multi-state prognostic model for SAH prognosis, we will firstly review key elements for prognostic modelling in the context of post-SAH management. These elements include baseline clinical covariates, dynamic prognostic factors, clinical intermediate events, complications as latent intermediate events, and clinical outcomes. After that, different sub-models that contribute to building this prognostic framework will be discussed, regarding their statistical modelling, and inter-connections. Lastly, methods to estimate parameters included in prognostic modelling will also be discussed.

7.2.1 Key elements in statistical framework

(1) Baseline covariates

Baseline clinical covariates reflect medical conditions of SAH patients at the time of their hospital admission, mainly including demographics, family history and genetic factors, pre-existing medical conditions, neurological status upon admission, and clinical presentations such as severity of headache. These covariates are crucial for characterising each patient's capability of recovering from SAH at the time of their hospital admission. Using age as an example of a baseline covariate, the decrease in physiology reserve and reduced elasticity in vascular structures can affect elder patients' capability of recovery from disease.

Baseline clinical covariates are incorporated into the survival sub-model within the

prognostic framework, which employs a Cox proportional hazard model where baseline covariates have direct impacts on the hazard function. The coefficients of these covariates γ_j have a multiplicative effect on the hazard as shown in Equation 7.1, and $\exp(\gamma_j)$ denotes the corresponding hazard ratio.

$$h_i(t) = h_0(t)\exp(\sum_j \gamma_j \omega_{j_i}) \quad (7.1)$$

In this survival sub-model, baseline covariates are not only directly associated with clinical outcomes but also included to adjust for potential confounding effects. This adjustment allows for more accurate estimates on the associations between other covariates, both baseline and dynamic covariates, and the clinical outcomes.

(2) Dynamic covariates

Dynamic prognostic factors are variables with prognostic information that are updated throughout the study period, typically through repeated measurements. These factors mainly include radiological data, neurological assessments, laboratory haematological biomarkers, physiological monitoring in vital signs, and indices derived from these measurements. These dynamic covariates capture real-time changes and trends in the patient's clinical status, providing continuous prognostic information that is valuable in predicting real-time risks for complications and clinical outcomes.

In a joint modelling framework, dynamic prognostic factors are typically modelled as longitudinal outcomes in longitudinal sub-models, with time included as both fixed and random effects to describe the population-level and individual-specific trajectories of a dynamic prognostic factor over time. The selection and inclusion of additional fixed and random are guided by prior research and characteristics of dataset to capture changes in dynamic covariates, e.g., time to model natural recovery, and pharmacological effects to evaluate the impact of pharmacological administrations on dynamic covariates. Random effects are used to account for inter-individual variability, while the inclusion of a random intercept and random slope allows for individual variations in baseline values and rates of change over time.

As given in Equation 7.2, the longitudinal outcome is represented by $y_{j_i}(t)$, which consists of $m_{j_i}(t)$ and $\varepsilon_{j_i}(t)$. In this equation, $y_{j_i}(t)$ is the observed value of the dynamic prognostic factor, which can be directly measured or derived from measurements, while $m_{j_i}(t)$ is the true underlying value of the dynamic prognostic factor, estimated by the longitudinal sub-model incorporating both fixed and random effects. The error term $\varepsilon_{j_i}(t)$, representing the difference observed value $y_{j_i}(t)$ and

predicted value $m_{j_i}(t)$, accounting for the variability that is not explained by sub-model's fixed or random effects.

$$y_{j_i}(t) = m_{j_i}(t) + \varepsilon_{j_i}(t) = \beta_j x_{j_i}^T(t) + b_{j_i} z_{j_i}^T(t) + \varepsilon_{j_i}(t) \quad (7.2)$$

By incorporating error terms, the proposed longitudinal sub-models are recognised as approximations of actual physiological processes, acknowledging their limitations in capturing all data variabilities. This allows the model to predict future values of dynamic covariates with confidence intervals instead of single point estimates. Furthermore, this enables joint models to estimate patient survival outcomes with confidence intervals rather than precise probabilities. Omitting the error term in longitudinal sub-models would lead to a loss of variability and over-confident predictions characterised by excessively narrow confidence intervals, thereby degrading the reliability and interpretability of the prognostic models.

Dynamic prognostic factors can be categorised as either directly measurable dynamic covariates or derived dynamic covariates. Directly measurable dynamic covariates, such as blood pressure, WBC, and GCS scores, are observed and recorded over time, reflecting changes in a patient's health status and providing insights into the disease trajectory. On the other hand, derived dynamic covariates are calculated from one or more directly measurable covariates; for example, systolic pressure variability derived from systolic blood pressure as discussed in Chapter 4, and WFNS grade, derived from GCS score and the presence of focal neurological deficits. [1]

While derived dynamic covariates offer additional prognostic information for prognostic modeling, they are more vulnerable to measurement errors. Errors in the original measurements can propagate, affecting the accuracy and reliability of derived covariates. Therefore, it is crucial to performance strategies, e.g., data cleaning and validation, to mitigate these measurement errors.

For personalised prognosis, multiple dynamic prognostic factors are modelled simultaneously and incorporated in prognostication to monitor individualised disease progression of patients. Similar to baseline covariates, interaction and confounding effects among dynamic covariates necessitate careful consideration and the application of appropriate methods to effectively manage them.

For example, the study presented in Chapter 5 incorporates three dynamic prognostic factors into its modeling: GCS scores, WBC, and glucose levels. WBC and glucose levels are not independently significant prognostic factors for clinical outcomes without adjusting for confounders. In this case, adjusting for GCS score as a confounder reveals significant associations between these two covariates and clinical outcomes that were previously obscured. By integrating these two dynamic covariates into the prognostic modeling, the predictive performance is improved compared to models that do not include them.

(3) Clinical interventions as clinical intermediate events

In traditional statistical framework of joint modelling with linear mixed models, disease progressions of patients are typically characterised by linear patterns of dynamic covariates. However, while these dynamic covariates can provide some prognostic information in a multivariate manner, they do not fully capture all aspects of disease progression. To achieve a more comprehensive understanding and prognosis, it is essential to incorporate additional prognostic information, such as clinical intermediate events.

Intermediate events are incidents that occur during the study period and can potentially have direct impacts on the outcome. In the prognosis of SAH, these intermediate events typically include, but not limited to, various complications and clinical interventions. These intermediate events can serve as markers for changes in disease progression and provide valuable prognostic information. This subsection will also discuss how to incorporate clinical interventions into prognostic modelling.

Clinical interventions, mainly neurological interventions for SAH patients, either surgical aneurysm clipping or endovascular embolisation, have been shown to effectively prevent re-bleeding and improve patients' outcome. Including these neurological interventions as intermediate events can be an effective method to incorporate their prognostic value into prediction models, potentially enhancing their accuracy. The incorporation of these interventions as intermediate events improved the predictive accuracy of all prognostic models has been discussed in Chapter 5.

The timing and type of clinical intervention for each patient are determined by clinicians and are therefore known in prognostic modeling. Consequently, the current prognostic state—whether non-treated or having received neurological interventions—along with the time point of the intervention, is known. If we are interested in the effect of neurological interventions on disease progression, the longitudinal sub-model of prognostic modeling can be formulated as follows:

$$y_{J_i}(t) = m_{J_i}(t) + \varepsilon_{J_i}(t) = \begin{cases} \beta_J x_{J_i}^T(t) + b_{J_i} z_{J_i}^T(t) + \varepsilon_{J_i}(t), & 0 < t < \tilde{t}_i \\ \beta_J x_{J_i}^T(t) + b_{J_i} z_{J_i}^T(t) + \tilde{\beta}_J \tilde{x}_{J_i}^T(t_+) + \tilde{b}_{J_i} \tilde{z}_{J_i}^T(t_+) + \varepsilon_{J_i}(t), & t \geq \tilde{t}_i \end{cases} \quad (7.3)$$

where $\tilde{t}_i$ is the timing of neurological intervention of the i^{th} patient, while t_+ denotes the time relative to neurological intervention. For the i^{th} patient, $t_+ = max(0, t - \tilde{t}_i)$. When simultaneously modelled with survival data, the hazard function can be formulated as:

$$h_i(t)=\begin{cases} h_0(t)\exp(\gamma^T\omega_i+\sum_j\alpha_j(\beta_j x_{j_i}^T(t)+b_{j_i}z_{j_i}^T(t))), & 0<t<\widetilde{t}_i \\ h_0(t)\exp(\gamma^T\omega_i+\sum_j\alpha_j(\beta_j x_{j_i}^T(t)+b_{j_i}z_{j_i}^T(t)+\widetilde{\beta}_j\widetilde{x}_{j_i}^T(t_+)+\widetilde{b}_{j_i}\widetilde{z}_{j_i}^T(t_+))), & t\geq\widetilde{t}_i \end{cases} \quad (7.4)$$

When multiple intermediate events are incorporated into prognostic modelling. Equation 7.3 can be thus generalised as:

$$y_{j_i}(t)=m_{j_i}(t)+\varepsilon_{j_i}(t)=\beta_j x_{j_i}^T(t)+b_{j_i}z_{j_i}^T(t)+\sum_k\delta_i^k(\widetilde{\beta}_j^k\widetilde{x}_{j_i}^{kT}(t_{k+})+\widetilde{b}_{j_i}^k\widetilde{z}_{j_i}^{kT}(t_{k+}))+\varepsilon_{j_i}(t) \quad (7.5)$$

Assuming $\widetilde{t}_i^k$ is the time of the k^{th} neurological intervention of the i^{th} patient, t_{k+} denotes the time relative to the k^{th} neurological intervention. For the i^{th} patient, $t_{k+}=max(0,t-\widetilde{t}_i^k)$. δ_i^k indicates the already completed k^{th} neurological intervention. $\widetilde{\beta}_j^k\widetilde{x}_{j_i}^{kT}$ and $\widetilde{b}_{j_i}^k\widetilde{z}_{j_i}^{kT}$ respectively represent the fixed-effect and random-effect terms of the k^{th} neurological intervention of the i^{th} patient for the k^{th} longitudinal outcome. The corresponding hazard function can be represented as:

$$h_i(t)=h_0(t)\exp(\gamma^T\omega_i+\sum_j\alpha_j(\beta_j x_{j_i}^T(t)+b_{j_i}z_{j_i}^T(t)+\sum_k\delta_i^k(\widetilde{\beta}_j^k\widetilde{x}_i^{kT}(t_{k+})+\widetilde{b}_{j_i}^k\widetilde{z}_i^{kT}(t_{k+})))) \quad (7.6)$$

By incorporating clinical intermediate events into prognostic modelling, the effects of clinical interventions on clinical outcomes are measured by their additive fixed and random effects on longitudinal outcomes following the intervention points. This modeling approach allows us to precisely measure the impact of interventions, enhance our understanding of SAH disease progression, and improve predictive accuracy.

(4) Complications as latent intermediate events

Complications represent another type of intermediate event in post-SAH management. These complications, which primarily include re-bleeding, vasospasm, delayed cerebral ischemia, and hydrocephalus, have been shown to significantly and typically negatively impact SAH prognosis, as discussed in Chapters 1 and 2. By incorporating complications as latent intermediate events into prognostic modeling, we can assess their effects on disease progression and predict the real-time risks associated with these complications.

The occurrences of complications can serve as clinical indicators of a potentially severer course following SAH. For example, vasospasm, a major cause of DCI, significantly contributes to the morbidity and mortality in SAH patients. The presence of vasospasm can thus signal increased risks of DCI and deteriorating neurological outcomes. These complications can be modeled as intermediate events that directly exacerbate neurological conditions, with additive fixed and random effects on longitudinal outcomes from the time of diagnosis, as demonstrated in Equations 7.3 to

7.6.

For the four major complications following SAH, re-bleeding typically occurs within the first 24 hours post-SAH, with most cases happening within three days of the initial onset. Vasospasm and DCI are both significant complications post-SAH and are closely linked. While vasospasm is considered the primary cause of DCI, the relationship and underlying mechanisms are complex. Vasospasm generally manifests between 3 to 14 days after the initial bleeding, peaking around 7 days, and can lead to DCI. The highest risk period for DCI also spans from 3 to 14 days post-SAH, related to vasospasm and other factors such as impaired cerebral autoregulation. [3][4] Hydrocephalus, on the other hand, can occur at various stages following SAH, classified as acute (0-3 days post-SAH), sub-acute (4-13 days post-SAH), and chronic (beyond 14 days post-SAH). [5]

All these major complications can be integrated as latent intermediate events in the prognostic model, reflecting their interconnected relationships. However, to simplify the explanation of the framework and manage model complexity, we have chosen vasospasm and hydrocephalus as two examples of latent intermediate events for prognostic modeling due to their high incidences and direct impacts on patient morbidity and mortality. These examples provide a comprehensive view of how different types of complications can influence overall prognosis and patient outcomes.

In addition to utilising the prognostic information conveyed by the occurrence of complications in prognostic modeling, there is also interest in predicting the risks of future complications using already obtained prognostic information, including complications that have already occurred. To address this task, multiple transient states based on the occurrence of complications can be included in the prognostic model. This approach allows for a more detailed understanding of SAH patients' prognosis and the progression of their clinical conditions.

(5) Clinical outcomes

In the modeling framework for spontaneous SAH prognosis, clinical outcomes are a key component of the survival sub-model, used to assess patients' prognosis either during or at the end of study period. Common outcome measures in SAH prognosis include mortality, discharge locations at the end of the study, and neurological outcome grades. Many of these outcomes are binary or binarised to provide definitive endpoints that simplify statistical analysis and interpretation. These binary categories, such as survived/died or good/poor clinical outcomes, facilitate the application of statistical models and help clearly categorise patient outcomes for more straightforward interpretations.

These clinical outcomes, modelled as time-to-event outcome O_i, consisting of observed time of event T_i and indicator of event δ_i for the i^{th} patient, where $O_i =$

$\{T_i, \delta_i\}$. For these clinical outcomes, $T_i = min(T_i^*, C_i)$, where T_i^* is the actual time to the clinical outcome for the i^{th} patient, e.g., time to mortality or a poor clinical outcome, and C_i is the censoring time. Typically, the censoring time is at the end of the study period, indicating that the patient did not experience the event by study end, making the time-to-event outcome right-censored. However, it is also possible that an individual may leave or be withdrawn from the study or be lost to follow-up. In these cases, the individual is censored at the last observed follow-up.

In the multi-state prognostic framework, clinical outcomes are conceptualised as absorbing states, in contrast to the transient states previously discussed. This is because once these absorbing states are reached, no further state changes are expected for an individual within the context of the study. For instance, in survival analysis, death is an absorbing state because a patient who dies cannot return to being alive or transition to another clinical state. In various transient states, available prognostic information is utilised to predict real-time probabilities of experiencing these clinical outcomes, which correspond to the transition probabilities from a transient state to an absorbing state.

In Section 7.2.1, various key elements of the SAH prognostic framework are discussed, including their definitions, clinical interpretations, and roles in prognostic modeling. Figure 7.3 illustrates these key elements within the context of post-SAH management. In subsequent sections of this chapter, we will explore how to utilise this prognostic information in modeling through several sub-models.

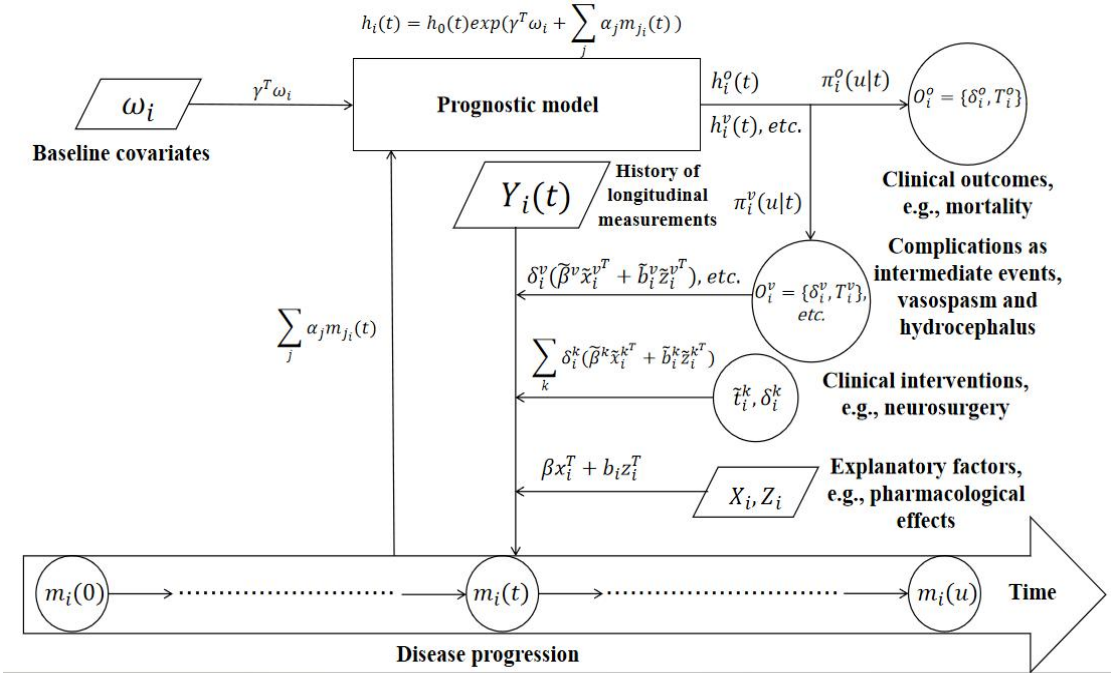


Figure 7.3 Key Elements of the SAH Prognostic Framework

7.2.2 Longitudinal sub-model

Longitudinal sub-models are employed to trace the trajectories of dynamic covariates over time, predicting future values based on existing measurements. These predictions can then be used in survival sub-models to predict the likelihood of complications and clinical outcomes. Additionally, longitudinal sub-models incorporate various explanatory factors, such as pharmacological agents, to explain disease progression. The effects of already occurred complications and clinical interventions are also taken into account.

Generally, the j^{th} dynamic covariate of the i^{th} patient can be represented as:

$$m_{j_i}(t)=\beta_j x_{j_i}^T(t)+b_{j_i} z_{j_i}^T(t)+\sum_{c}^{c=v,h,etc.}\delta_i^c(\tilde{\beta}_j^c\tilde{x}_{j_i}^{c^T}(t_{c+})+\tilde{b}_{j_i}^c\tilde{z}_{j_i}^{c^T}(t_{c+}))+\sum_k\delta_i^k(\tilde{\beta}_j^k\tilde{x}_{j_i}^{k^T}(t_{k+})+\tilde{b}_{j_i}^k\tilde{z}_{j_i}^{k^T}(t_{k+}))+\varepsilon_{j_i}(t) \quad (7.7)$$

where $\sum_{c}^{c=v,h,etc.}\delta_i^c(\tilde{\beta}_j^c\tilde{x}_{j_i}^{c^T}(t_{c+})+\tilde{b}_{j_i}^c\tilde{z}_{j_i}^{c^T}(t_{c+}))$ assesses the effects of documented occurrences of complications while $\sum_k\delta_i^k(\tilde{\beta}_j^k\tilde{x}_{j_i}^{k^T}(t_{k+})+\tilde{b}_{j_i}^k\tilde{z}_{j_i}^{k^T}(t_{k+}))$ quantifies the effects of employed clinical interventions.

Therefore, if we are interested in examining the effects of two major complications, i.e., vasospasm and hydrocephalus, on disease progression. The j^{th} dynamic covariate of the i^{th} patient can be represented as:

$$y_{j_i}(t)=m_{j_i}(t)+\varepsilon_{j_i}(t)=\beta_j x_{j_i}^T(t)+b_{j_i} z_{j_i}^T(t)+\delta_i^v(\tilde{\beta}_j^v\tilde{x}_{j_i}^{v^T}(t_{v+})+\tilde{b}_{j_i}^v\tilde{z}_{j_i}^{v^T}(t_{v+}))+\delta_i^h(\tilde{\beta}_j^h\tilde{x}_{j_i}^{h^T}(t_{h+})+\tilde{b}_{j_i}^h\tilde{z}_{j_i}^{h^T}(t_{h+}))+\varepsilon_{j_i}(t) \quad (7.8)$$

where $\beta_j x_{j_i}^T(t)+b_{j_i} z_{j_i}^T(t)$ denotes the baseline fixed and random terms throughout the entire progress of disease. δ_i^v and δ_i^h respectively indicate documented occurrences of vasospasm and hydrocephalus. Additionally, $\delta_i^v(\tilde{\beta}_j^v\tilde{x}_{j_i}^{v^T}(t_{v+})+\tilde{b}_{j_i}^v\tilde{z}_{j_i}^{v^T}(t_{v+}))$ and $\delta_i^h(\tilde{\beta}_j^h\tilde{x}_{j_i}^{h^T}(t_{h+})+\tilde{b}_{j_i}^h\tilde{z}_{j_i}^{h^T}(t_{h+}))$ respectively correspond to the additive fixed and random terms from already diagnosed vasospasm and hydrocephalus. These additive terms begin to influence longitudinal outcomes following the diagnosis of complications.

7.2.3 Survival sub-model

Survival sub-models can ultilise a wide range of previously gathered prognostic information to predict the likelihood of future complications and clinical outcomes. This prognostic data may include baseline covariates, repeatedly measured longitudinal prognostic factors, as well as documented occurrences of complications, clinical interventions, and pharmacy records.

Taking into account the effects of documented occurrences of complications, specifically vasospasm and hydrocephalus, the predicted value of j^{th} dynamic

covariate of the i^{th} patient is modelled by:

$$m_{j_i}(t)=\beta_j x_{j_i}^T(t)+b_{j_i} z_{j_i}^T(t)+\delta_i^v(\tilde{\beta}_j^v \tilde{x}_{j_i}^{vT}(t_{v+})+\tilde{b}_{j_i}^v \tilde{z}_{j_i}^{vT}(t_{v+}))+\delta_i^h(\tilde{\beta}_j^h \tilde{x}_{j_i}^{hT}(t_{h+})+\tilde{b}_{j_i}^h \tilde{z}_{j_i}^{hT}(t_{h+}))+\varepsilon_{j_i}(t) \quad (7.9)$$

which can then be included in a hazard function (Equation 7.10) to assess its effect on complications and clinical outcomes while being jointly analysed with other prognostic factors.

$$h_i(t)=h_0(t)\exp(\gamma^T \omega_i+\sum_j \alpha_j m_{j_i}(t)) \quad (7.10)$$

As we are interested in predicting not only clinical outcomes but also complications, the hazard function for clinical outcome, vasospasm and hydrocephalus can be respectively denoted as $h_i^o(t)$, $h_i^v(t)$, and $h_i^h(t)$. The hazard function, for example $h_i^v(t)$, describes the instantaneous hazard of developing vasospasm at time *t* given that patient *i* has not yet being diagnosed with vasospasm up to that time.

Correspondingly, the survival $S_i^v(t)$ is the probability that the event of interest, vasospasm, has not occurred by time *t,* and can be derived from $h_i^v(t)$:

$$S_i^v(t) = exp(-\int_0^t h_i^v(s)ds) \quad (7.11)$$

where $\int_0^t h_i^v(s)ds$ is the cumulative hazard function.

In clinical applications, it is essential to condition the hazard function and survival function on the information available up to current time *t*, denoted as $I(t)$. Thus, the hazard and survival function for vasospasm at time *u* given information up to time *t* can be respectively denoted as $h_i^v(u|I(t))$ and $S_i^v(u|I(t))$.

The set of prognostic information available up to current time *t*, $I(t)$ includes the longitudinal history of measurements in dynamic covariates up to time *t*, documented occurrences of complications up to time *t*, and documented administrations of medications and clinical interventions up to time *t*. All this information influences the estimates of longitudinal outcomes and, consequently, the hazard and survival functions. Specifically, $h_i^v(u|I(t))$ and $S_i^v(u|I(t))$ can be represented as:

$$h_i(u \mid I(t))=h_0(u)\exp(\gamma^T \omega_i+\sum_j \alpha_j m_{j_i}(u \mid I(t))) \quad (7.12)$$

and

$$S_i^v(u|I(t)) = exp(-\int_t^u h_i^v(s|I(t))ds) \quad (7.13)$$

given vasospasm has not been diagnosed up to time *t.*

Survival functions utilise all prognostic information gathered during patients' hospital stays, along with baseline covariates collected at admission, to predict clinical outcomes and complications using hazard and survival functions. These functions

could then be employed to generate personalised prognostic profiles, providing a real-time, comprehensive overview of patients' clinical status in state-transition sub-models.

7.2.4 State-transition sub-model

The state-transition sub-model is characterised by a real-time state transition matrix, which is dynamically updated based on current prognostic states and available information. This matrix thus facilitates the derivation of personalised prognostic profiles. By incorporating vasospasm and hydrocephalus into the prognostic modeling, the progression of SAH is structured into four transient states, indicated by documented occurrences of vasospasm δ_i^v and hydrocephalus δ_i^h, as well as one absorbing state:

- Transient states: Diagnosed with SAH without complications (Initial state, State 0,$\delta_i^v = 0, \delta_i^h = 0$), vasospasm (State 1, $\delta_i^v = 1,\ \delta_i^h = 0$), hydrocephalus (State 2, $\delta_i^v = 0,\ \delta_i^h = 1$), and both vasospasm and hydrocephalus (State 3, $\delta_i^v = 1,\ \delta_i^v = 1$).
- Absorbing state: Discharged from hospital with a good clinical outcome (State 4, $\delta_i = 1$).

Using the hazard and survival functions from the survival sub-model, the probabilities of experiencing vasospasm, hydrocephalus, and clinical outcomes during the period from time *t* to time *u*, given the prognostic information available up to time *t*, can be expressed respectively as $P_i^v(u|I(t))$, $P_i^h(u|I(t))$, and $P_i^o(u|I(t))$, give by:

$$P_i(u|I(t)) = [P_i^v(u|I(t)), P_i^h(u|I(t)), P_i^o(u|I(t))] \quad (7.14)$$

which can be computed as:

$$P_i(u|I(t)) = [(1 - S_i^v(u|I(t)))^{1-\delta_i^v},\ (1 - S_i^h(u|I(t)))^{1-\delta_i^h}, 1 - S_i^o(u|I(t))] \quad (7.15)$$

Once a complication is diagnosed, the probability of this complication occurring in the future is considered to be 1. The probabilities of various outcomes of interest can be calculated using survival functions, which integrate the instantaneous risks from time *u* to time *t*, given by:

$$\begin{bmatrix} S_i^v(u|I(t)) \\ S_i^h(u|I(t)) \\ S_i^o(u|I(t)) \end{bmatrix} = \begin{bmatrix} exp(-\int_t^u h_i^v(s|I(t))ds) \\ exp(-\int_t^u h_i^h(s|I(t))ds) \\ exp(-\int_t^u h_i^o(s|I(t))ds) \end{bmatrix} \quad (7.16)$$

At current time point *t*, creating a personalised prognostic profile for a patient involves predicting the probabilities of various outcomes from now until different future time points to provide a comprehensive overview of the patient's prognosis. For

instance, if we aim to forecast the probabilities of these outcomes within specific time frames, such as 1 day, 3 days, and across both the acute and sub-acute phases, the prognostic profile for a patient can be outlined as:

$$\boldsymbol{Prog_i(t)} = \begin{bmatrix} P_i^v(t+1|I(t)) & P_i^v(t+3|I(t)) & P_i^v(14|I(t)) \\ P_i^h(t+1|I(t)) & P_i^h(t+3|I(t)) & \pi_i^h(14|I(t)) \\ P_i^o(t+1|I(t)) & P_i^o(t+3|I(t)) & \pi_i^o(14|I(t)) \end{bmatrix} \quad (7.17)$$

This personalised prognostic profile for a patient at time point *t* predicts probabilities of various outcomes within specific time frames, e.g., 1 day, 3 days, and across the acute and sub-acute phases, which provides crucial information for clinical decision-making. Furthermore, the profile supports continuous monitoring and dynamic adjustment of care plans in response to the patient's changing condition post-SAH, thereby potentially improving the overall efficacy of healthcare delivery. In Section 7.3, we will discuss in detail the role of this prognostic profile in post-SAH management.

7.2.5 Parameter estimation

In joint modelling of longitudinal and time-to-event data, model parameters can be estimated using various statistical techniques. Maximum likelihood estimation (MLE) and Bayesian methods are among the most common approaches in joint modelling. The MLE is used to estimate a set of model parameters $\theta = (\theta_t^T, \theta_y^T, \theta_b^T)^T$ that maximise the log-likelihood function corresponding to the joint distribution of the observed outcomes, including time-to-event outcomes $O_i = \{T_i, \delta_i\}$ and N longitudinal outcomes $Y_i = \{y_{1_i}, \ldots, y_{N_i}\}$. $\theta = (\theta_t^T, \theta_y^T, \theta_b^T)^T$ denotes the parameter vector, with θ_t denoting the parameters in survival sub-model, i.e., coefficients for baseline and dynamic covariates included in survival sub-model and parameters related to baseline hazard function. Likewise, θ_y denotes the parameters included in longitudinal outcomes, i.e., coefficients for fixed and random effects, while θ_b denotes the unique parameters of the random-effects covariance matrix. [6]

To ultilise MLE for parameter estimation, the joint distribution needs to be specified firstly. This involves assuming that a vector of random effects b_{j_i} underlies both the survival and longitudinal processes, indicating that these random effects account for the correlation among repeatedly measured longitudinal outcomes as well as the associations between longitudinal and time-to-event outcomes. [6] Since random effects account for unobserved heterogeneity among individuals, this assumption allows for capturing unobserved individual differences that affect both the longitudinal and survival outcomes.

For correlation among longitudinal outcomes, random effects capture individual variability by representing individual-specific random variation that is not accounted for by fixed effects, while they also incorporate intra-individual correlation by allowing each individual to have their unique baseline level or trajectory as measurements taken from the same individual are likely to be more similar than measurements taken from different individuals.

To link longitudinal and time-to-event outcomes, the same set of random effects is employed to influence both the longitudinal and time-to-event outcomes. The shared random effects structure creates a statistical link between these two processes, reflecting the clinical reality where the same underlying factors such as pharmacological effects, affect both the measurements over time, e.g., neurological assessments, and the risks of clinical outcomes. With *N* longitudinal outcomes, the joint conditional probability for the i^{th} individual is:

$$p(T_i, \delta_i, Y_i \mid \omega_i, X_i, Z_i, b_i; \theta) = p(T_i, \delta_i \mid \omega_i, b_i; \theta) p(Y_i \mid X_i, Z_i, b_i; \theta) \quad (7.18)$$

where:

$$p(Y_i \mid X_i, Z_i, b_i; \theta) = \prod_j p(y_{j_i} \mid X_i, Z_i, b_{j_i}; \theta_j) = \prod_j \prod_l p(y_{j_i}(t_{il}) \mid X_i, Z_i, b_{j_i}; \theta_j) \quad (7.19)$$

In Equation 7.18, the joint probability for observed outcomes of the i^{th} individual is denoted by the multiplication of corresponding survival and longitudinal outcomes, linked by shared random effects. Fixed-effect and random-effect variables are respectively denoted by X_i and Z_i, and will be omitted for simplification in later expressions. In Equation 7.19, the probability of observations in longitudinal outcomes for the i^{th} individual is expressed as the product of each observation in all *N* longitudinal outcomes. $Y_i^T = (y_{1_i}^T, \ldots y_{j_i}^T, \ldots, y_{N_i}^T)$, and $y_{j_i}^T = (y_{j_i}^T(t_{i1}), \ldots, y_{j_i}^T(t_{il}), \ldots, y_{j_i}^T(t_{in_i}))$, where $y_{j_i}^T$ denotes the vector of observations in the j^{th} longitudinal outcome of the i^{th} individual, while $y_{j_i}^T(t_{il})$ is the l^{th} observation of the longitudinal outcome in altogether n_i observations.

The log-likelihood contribution of the i^{th} individual to joint distribution of observed data can thus be formulated as:

$$\log p(T_i, \delta_i, Y_i; \theta) = \log \int p(T_i, \delta_i, Y_i, b_i; \theta) db_i =$$

$$\log \int p(T_i, \delta_i \mid \omega_i, b_i; \theta_t, \beta) [\prod_j \prod_l p\{y_{j_i}(t_{il}) \mid b_{j_i}; \theta_y\}] p(b_i \mid \theta_b) db_i \quad (7.20)$$

with the conditional density for the survival part $p(T_i, \delta_i \mid b_i; \theta_t, \beta)$ given by:

$$p(T_i, \delta_i \mid \omega_i, b_i; \theta_t, \beta) = h_i(\omega_i, M_i(T_i); \theta_t, \beta)^{\delta_i} S_i(T_i \mid \omega_i, M_i(T_i); \theta_t, \beta)$$
$$= [h_0(T_i) \exp(\gamma^T \omega_i + \sum_j \alpha_j m_{j_i}(T_i))]^{\delta_i} \exp(-\int_0^{T_i} h_0(s) \exp(\gamma^T \omega_i + \sum_j \alpha_j m_{j_i}(s)) ds) \quad (7.21)$$

The first part $h_i(\omega_i, M_i(T_i); \theta_t, \beta)^{\delta_i}$ denotes the instantaneous risk of experiencing the event at time T_i given that the individual has survived up to that time and given the history of the longitudinal process up to that time, represented by $M_i(T_i)$, while the second part $S_i(T_i \mid \omega_i, M_i(T_i); \theta_t, \beta)$ represents the probability of the i^{th} individual not experiencing the event up to time T_i.

For patients not experiencing an event of interest in the study period ($\delta_i = 0$), the probability of observed time-to-event outcome is the probability of not experiencing the event up to time T_i, while for patients experiencing event of interest in the study period ($\delta_i = 1$) probability of observed time-to-event outcome is the product of probabilities of not experiencing the event up to time T_i and instantaneous risk of experiencing the event at that time. The product of these two components forms the likelihood for the observed time-to-event data. For each individual, this likelihood is calculated as the hazard at the time of event if the event was observed, multiplied by the survival probability up to the censoring time regardless of whether the event was observed.

The longitudinal part of Equation 7.20 can be formulated as:

$$p(Y_i \mid b_i; \theta) = \prod_j \prod_l p\{y_{j_i}(t_{il}) \mid b_{j_i}; \theta_y\} = \prod_j (2\pi\sigma_j^2)^{-n_i/2} \exp\{-\| y_{j_i} - X_{j_i}\beta_j - Z_{j_i} b_{j_i} \|^2 / 2\sigma_j^2\} \quad (7.22)$$

with $\varepsilon_{j_i} \sim N(0, \sigma_j^2)$, which is derived from the normal distribution's probability density function.

Similarly, the random effect part of Equation 7.20 can be formulated as:

$$p(b_i; \theta) = \prod_j (2\pi)^{-q_j/2} \mid D_j \mid^{-1/2} \exp(-b_{j_i}^T D_j^{-1} b_{j_i} / 2) \quad (7.23)$$

This part is derived from multivariate normal distribution's probability density function, with $b_{j_i} \sim N(0, D_j)$. Unlike the error terms, which are independent of each other, for the j^{th} longitudinal outcome, D_j serves as the covariance matrix for random effects, capturing their variance and correlations between different random effects. The estimation of this covariance matrix in a crucial aspect of parameter estimation of random effects.

The log-likelihood for observed outcomes can then be derived from the joint likelihood of survival, longitudinal and random effects parts over all individuals:

$$L(\theta) = \log \prod_i p(T_i, \delta_i, Y_i \mid \omega_i; \theta) = \sum_i \log\, p(T_i, \delta_i, Y_i \mid \omega_i; \theta) = \sum_i L(T_i, \delta_i, Y_i \mid \omega_i; \theta) \quad (7.24)$$

Set of model parameters θ can be estimated by maximisation of the log-likelihood function denoted in Equation 7.24. This optimisation process can be achieved using algorithms such as the Expectation-Maximisation (EM) algorithm or the Newton-Raphson algorithm, which are well-suited for handling complex models with multiple parameters and latent variables such as random effects. [7][8]

The Bayesian approach can be implemented using Markov Chain Monte Carlo (MCMC) techniques, which is a popular approach for sampling from complex and high-dimensional probability distributions. Several strategies have been developed for sampling from a probability distribution in MCMC. In a methodological review on Bayesian joint modelling of longitudinal and time-to-event data, among 37 studies specifying the sampling algorithm used, Gibbs sampler and Metropolis-Hastings (MH) algorithms was the most widely adopted method (24, 64.86%), followed by Gibbs sampling (9, 24.32%). [9]

Compared to Gibbs sampling alone, a combination of Gibbs sampling and MH algorithms allows for retaining the efficiency of Gibbs while handling intractable or difficult conditional distributions. As has been shown previously, joint distributions of joint models include longitudinal, survival and random-effect parts, resulting in a complex likelihood function with some conditional distributions are not straightforwardly tractable. In such cases, parameters with known and tractable conditional distributions, such as fixed effects in the longitudinal component, can be effectively handled using Gibbs sampling. For other parameters such as random effects where conditional distributions are intractable, MH steps can be employed to facilitate efficient sampling to optimise the overall estimation process.

The tasks of parameter estimation in our proposed modelling framework mainly include three primary sections. Firstly, we aim to predict the occurrence of vasospasm ($O_i^v = \{T_i^v, \delta_i^v\}$), considering hydrocephalus that has already occurred as an intermediate event influencing disease progression. Secondly, we focus on predicting the occurrence of hydrocephalus ($O_i^h = \{T_i^h, \delta_i^h\}$) with previously occurred vasospasm as an intermediate event. Lastly, we are also interested in predicting clinical outcomes ($O_i^o = \{T_i^o, \delta_i^o\}$), taking into account both vasospasm and hydrocephalus as intermediate events that impact the disease's trajectory. To accurately predict these events, it is important to estimate the parameters associated with these three sections using the parameter estimation techniques previously discussed.

Thus, the likelihood for these three sections can be respectively expressed as:

$$L(\theta^v) = \sum_i \log\, p(T_i^v, \delta_i^v, Y_i^v \mid \omega_i^v, \omega_i^h, O_i^h; \theta^v) \quad (7.25)$$

$$L(\theta^h) = \sum_i \log\, p(T_i^h, \delta_i^h, Y_i^h \mid \omega_i^v, \omega_i^h, O_i^v; \theta^h) \quad (7.26)$$

$$L(\theta^o) = \sum_i \log\, p(T_i^o, \delta_i^o, Y_i^o \mid \omega_i^o, \omega_i^v, \omega_i^h, O_i^v, O_i^h; \theta^o) \quad (7.27)$$

and the joint probability of observing the time-to-event data along with the longitudinal outcomes of the i^{th} patient can be re-formulated as Equations 7.28 to 7.30, respectively corresponding to these three components: vasospasm, hydrocephalus, and clinical outcomes:

$$p(T_i^v, \delta_i^v, Y_i^v \mid \omega_i^v, \omega_i^h, b_i^v, O_i^h; \theta^v) = p(T_i^v, \delta_i^v \mid \omega_i^v, \omega_i^h, b_i^v, O_i^h; \theta^v)\, p(Y_i^v \mid b_i^v, O_i^h; \theta^v) \quad (7.28)$$

$$p(T_i^h, \delta_i^h, Y_i^h \mid \omega_i^v, \omega_i^h, b_i^h, O_i^v; \theta^h) = p(T_i^h, \delta_i^h \mid \omega_i^v, \omega_i^h, b_i^h, O_i^v; \theta^h)\, p(Y_i^h \mid b_i^h, O_i^v; \theta^h) \quad (7.29)$$

$$p(T_i^o, \delta_i^o, Y_i^o \mid \omega_i^o, \omega_i^v, \omega_i^h, b_i^o, O_i^v, O_i^h; \theta^o) = p(T_i^o, \delta_i^o \mid \omega_i^o, \omega_i^v, \omega_i^h, b_i^o, O_i^v, O_i^h; \theta^o)\, p(Y_i^o \mid b_i^o, O_i^v, O_i^h; \theta^o) \quad (7.30)$$

Parameters in both the longitudinal sub-models, e.g., coefficients of fixed and random effect variables, and in the survival sub-model, e.g., coefficients of baseline and dynamic covariates, are respectively estimated for three events of interest: vasospasm, hydrocephalus and clinical outcomes. The parameter estimates for different events can vary significantly. For instance, a risk factor associated with vasospasm with a positive coefficient might adversely affect clinical outcomes, as evidenced by a corresponding negative coefficient. Moreover, the risk factors and their effects on vasospasm and hydrocephalus may differ and should be analysed independently to accurately model their impacts on disease progression.

7.3 Simulation and analysis

7.3.1 Dataset and simulation

To implement a multi-state dynamic prognostic model in SAH studies, we have used patient data from MIMIC-IV, a publicly available database sourced from the electronic health record of the Beth Israel Deaconess Medical Center between 2008 to 2019. [10] 612 spontaneous SAH patients with clinical records and records of pharmacy administration were included, with hospital stays of longer than 1 day, identified records in neurological assessments, and patients aged 18 or over.

Among these patients, 357 (58.33%) patients were female, and the median age was 58 (IQR: 49-69). 283 patients (46.24%) were discharged with good outcomes at the end of study period of 14 days, defined by returning home or rehabilitation within the study period, while poor outcome (329, 53.76%) includes mortality, long-term acute care, hospice care, and long-term hospital stay exceeding the study period. Regarding complications considered as intermediate events, 213 patients (34.80%) and 55

patients (8.99%) were diagnosed with hydrocephalus and vasospasm during their hospital stay.

	Number of patients	Good outcomes	Percentage
Hydrocephalus	213	31	14.55%
Vasospasm	55	15	27.27%
Hydrocephalus only	184	29	15.76%
Vasospasm only	26	13	50.00%
Both	29	2	6.90%
Neither	373	239	64.08%
All patients	612	283	46.24%

Table 7.1: Relationship between occurrences of vasospasm/hydrocephalus and good outcomes percentage

The data in Table 7.1, visualised in heatmap Figure 7.4, clearly illustrates that diagnoses of either hydrocephalus or vasospasm negatively impact the likelihood of achieving a good outcome, with the risks increasing when both complications are present. When isolating these conditions, patients diagnosed solely with vasospasm demonstrate a more favourable prognosis compared to those with only hydrocephalus. Analysis of the percentages of good outcomes across these patient groups clearly indicates that the likelihood of a good clinical outcome appears significantly influenced by the presence of either vasospasm, hydrocephalus, or both. For different patient groups, corresponding to different prognostic states, the likelihood of a good clinical outcome is significantly different, necessitating the need for a multi-state prognostic model to enhance our understanding and prediction of patient outcomes.

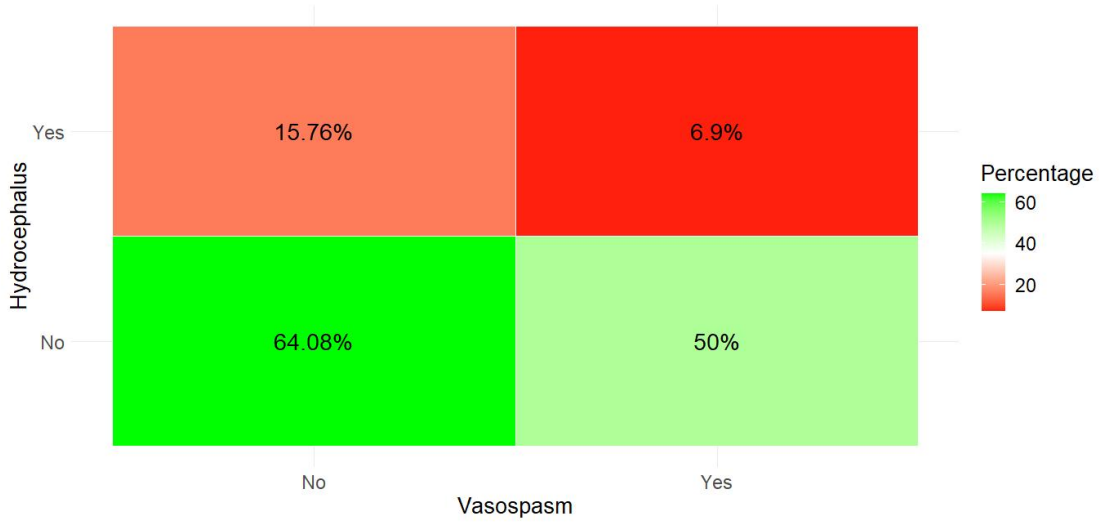


Figure 7.4: Heatmap showing the correlations between occurrences of vasospasm/hydrocephalus and percentage of good outcomes

To develop a multi-state prognostic model for SAH, it is firstly important to identify the baseline covariates for three events, i.e., vasospasm, hydrocephalus, and clinical

outcomes, as the influential covariates for each may differ. Since the time-to-event data for vasospasm and hydrocephalus are not recorded in the dataset, occurrence times for these two complications were simulated to construct the framework for a multi-state prognostic model for SAH.

Occurrences of vasospasm are simulated based on the fact that it usually occurs 4 to 14 days after the initial SAH, peaking at 7 days. [11] Within the study period, hydrocephalus can either develop in the early course of SAH (first 3 days) or later in the sub-acute phase of SAH (4-14 days) as sub-acute hydrocephalus. [12] As log-normal is frequently adopted for modelling time-to-event data in medical research including timing of disease onset, a log-normal distribution is applied to model occurrences time of vasospasm and hydrocephalus, with the statistics derived from these simulations detailed in Table 7.2. [13]

	Mean	Median	Interquartile	Skewness
Vasospasm	7.0	7.0	4.0-9.0	0.1118
Hydrocephalus	6.25	6.0	4.0-8.0	0.3751

Table 7.2: Statistics of simulated occurrence time of vasospasm and hydrocephalus in SAH patients

7.3.2 Survival analysis on baseline covariates

Survival analysis was respectively performed on three targeted events outcomes, i.e., vasospasm, hydrocephalus, and clinical outcomes at discharge, to determine the baseline covariates which can provide a foundation for understanding prognosis of the disease before incorporating dynamic prognostic information. The results of survival analysis on baseline covariates for three targeted event outcomes are detailed in Table 7.3.

Given that the time-to-event data for vasospasm and hydrocephalus are simulated, we opted for a less stringent significance threshold ($p < 0.1$) for covariate selection and inclusion. This approach allows us to include a broader range of baseline covariates, allowing us to explore and illustrate their clinical relevance in the simulated context. Significant results from this survival analysis are highlighted in Table 7.3.

Based on the findings detailed in Table 7.3, we have studied the effects of demographics and three clinical conditions as baseline covariates for targeted event outcomes. These clinical conditions, i.e., cerebral oedema, cerebral infarction and respiratory failure, serve as indicators of both neurological and systemic health in SAH patients. Cerebral oedema is associated with the severity of brain injury and can worsen clinical conditions by increasing intracranial pressure, leading to further neurological damage. As indicated in Table 7.3, it is negatively correlated with positive clinical outcomes.

Event Outcomes	Covariates	Univariate analysis			Multivariate analysis		
		HR	95%CI	P value	HR	95%CI	P value
Vasospasm	Age	0.9743	0.9564 - 0.9925	**0.0059**	0.9746	0.9567 - 0.9928	**0.0064**
	Male	1.6067	0.9463 - 2.7288	**0.0792**	1.6282	0.9515 - 2.7862	**0.0759**
	Cerebral oedema	1.5170	0.8472 - 2.7151	0.1610	-	-	-
	Cerebral infarction	1.7691	0.9140 - 3.4245	**0.0909**	2.0636	1.0534 - 4.0413	**0.0347**
	Respiratory failure	0.9254	0.5097 - 1.6799	0.7990	-	-	-
Hydrocephalus	Age	1.0087	0.9988 - 1.0186	**0.0844**	1.0052	0.9953 - 1.0151	0.3052
	Male	1.0200	0.7763 - 1.33099	0.8870	-	-	-
	Cerebral oedema	1.5759	1.1734 - 2.1168	**0.0025**	1.1802	0.8621 - 1.6151	0.3010
	Cerebral infarction	1.5003	1.0438 - 2.1568	**0.0284**	1.3690	0.9522 - 1.9682	**0.0909**
	Respiratory failure	2.3052	1.7564 - 3.0257	**<0.001**	2.1029	1.5675 - 2.8205	**<0.001**
Clinical outcomes	Age	0.9889	0.9807 - 0.9971	**0.0081**	0.9956	0.9872 - 1.0041	0.3062
	Male	1.1540	0.9130 - 1.4585	0.2310	-	-	-
	Cerebral oedema	0.2987	0.1965 - 0.4539	**<0.001**	0.5355	0.3509 - 0.8178	**0.0039**
	Cerebral infarction	0.2943	0.1688 - 0.5135	**<0.001**	0.3561	0.2040 - 0.6225	**<0.001**
	Respiratory failure	0.0753	0.0401 - 0.1418	**<0.001**	0.0925	0.0486 - 0.1751	**<0.001**

Table 7.3: Results of univariate and multivariate survival analysis of baseline covariates for three targeted outcomes

Respiratory failure occurs when the respiratory system fails to adequately exchange gases, resulting in insufficient oxygenation. This can severely affect clinical outcomes by limiting oxygen delivery to brain tissue, potentially leading to worse overall neurological and systemic outcomes. Additionally, cerebral infarction, which results from a disruption of blood supply to a region of the brain causing tissue death, is found to be a significant risk factor for vasospasm and hydrocephalus, as evidenced by HRs greater than 1. Conversely, it is associated with reduced likelihood of good clinical outcomes, as suggested by HRs less than 1.

Baseline covariates, including demographics and three clinical conditions, can

provide foundational prognostic information that prognosis is based on. For example, after adjusting for all other covariates, patients with cerebral infarction show a 36.9% increased risk of developing hydrocephalus (HR = 1.3690), more than a twofold increase in the risk of vasospasm (HR = 2.0636), and a 64.39% decrease in the likelihood of achieving good clinical outcomes (HR = 0.3561) compared to those without cerebral infarction. Additionally, age, a demographic factor, is positively correlated with the risk of hydrocephalus but inversely related to the risk of vasospasm, aligning with previous findings that younger patients are at higher risk of vasospasm. [14] These baseline covariates establish a solid foundation for dynamic prognostic assessments, facilitating real-time and personalised evaluations of disease progression.

7.3.3 Longitudinal process and dynamic prognosis

The longitudinal process describes the evolving pattern of SAH prognosis by integrating multiple sources of dynamic prognostic information, thereby enhancing the initial prognostic model based on baseline covariates. The dynamic risk profile of a patient mainly is mainly constructed from direct measurements of clinical conditions, e.g., GCS scores to measure neurological status. These dynamic covariates, such as GCS scores, are essential in explaining the changes of patients' clinical conditions over time.

For further clarity and clinical relevance, explanatory factors such as pharmacological effects can be incorporated into the longitudinal sub-models, providing a comprehensive framework for understanding and predicting disease trajectories. Nimodipine is chosen as a representative medication in the longitudinal sub-models for predicting event outcomes due to its strong association with GCS scores and its prognostic power in predicting clinical outcomes, as detailed in Chapter 6.

Covariate	Value	Std. Error	P value
Intercept	11.0674	0.2845	**<0.001**
Time	0.1973	0.0407	**<0.001**
Time since vasosapsm	-0.0704	0.0441	0.1105
Time since hydrocephalus	-0.1301	0.0260	**<0.001**
Nimodipine	0.8069	0.2984	**0.0069**
Interaction term	-0.0930	0.0428	**0.0297**

Table 7.4: Effects of explanatory factors on GCS scores for predicting clinical outcomes at discharge

To predict clinical outcomes at discharge based on GCS scores, a linear mixed model (LMM) was ultilised to assess the effects of time, nimodipine use, and the occurrence of vasospasm and hydrocephalus on GCS scores, as outlined in Table 7.4. "Time" was included as a random effect to model the individualised natural recovery trajectories over time.

According to the analysis in Table 7.4, time is positively correlated with GCS scores, suggesting a general trend of neurological improvement in patients over time. Conversely, occurrences of vasospasm and hydrocephalus were negatively associated GCS scores. Specifically, the presence of vasospasm and hydrocephalus reduces the natural rate of neurological recovery by 35.68% and 65.94%, respectively. For patients with both vasospasm and hydrocephalus, the overall trend of neurological status switches from improvement over time into deterioration, indicating a compounded adverse effect on patient recovery.

In predicting vasospasm or hydrocephalus as event outcomes, the occurrence of the other complication is considered as an intermediate event affecting neurological status. In the longitudinal sub-model for predicting vasospasm, the presence of hydrocephalus is treated as an intermediate event and vice versa, as detailed in Table 7.5 and Table 7.6.

Covariate	Value	Std. Error	P value
Intercept	11.0819	0.2816	**<0.001**
Time	0.1720	0.0396	**<0.001**
Time since vasosapsm	-0.0954	0.0433	**0.0276**
Nimodipine	0.8902	0.2945	**0.0025**
Interaction term	-0.1047	0.0420	**0.0127**

Table 7.5: Effects of explanatory factors on GCS scores for predicting hydrocephalus

Covariate	Value	Std. Error	P value
Intercept	11.0645	0.2845	**<0.001**
Time	0.1980	0.0407	**<0.001**
Time since hydrocephalus	-0.1355	0.0258	**<0.001**
Nimodipine	0.8236	0.2983	**0.0058**
Interaction term	-0.0986	0.0427	**0.0210**

Table 7.6: Effects of explanatory factors on GCS scores for predicting vasospasm

Similarly, we find that in predicting complications, vasospasm and hydrocephalus are correlated with slower recovery rate over time in longitudinal analysis. Use of nimodipine contributes to improvement in neurological status while this positive effect diminishes over time. In longitudinal sub-models, neurological status of patients is modelled with time, effects of complications and administrations of nimodipine, to capture changes in patients' clinical conditions, with random-effect terms allowing for patient-specific deviations from the overall trend.

Neurological conditions, modeled as longitudinal outcomes, are then incorporated into survival sub-models to explain disease progression and changes in prognosis

based on foundational prognostic information. The associations between GCS scores and targeted outcomes, such as vasospasm, hydrocephalus, and clinical outcomes, are presented in Table 7.7.

Outcome event	Value	HR	95% CI	P value
Vasospasm	-0.0515	0.9498	0.8856-1.0226	0.1754
Hydrocephalus	-0.1835	0.8324	0.7966-0.8702	**<0.001**
Good clinical outcome	1.8553	6.3939	3.1950-12.0146	**<0.001**

Table 7.7: Effects of GCS scores on outcome events in joint analysis of longitudinal and time-to-event outcomes

According to the results in Table 7.7, GCS scores are negatively associated with both vasospasm and hydrocephalus. Specifically, increase of one GCS score corresponds to a 5.02% lower risk of developing vasospasm and a 17.76% lower risk of developing hydrocephalus. The association between GCS scores and the occurrence of vasospasm is not statistically significant, likely due to the limited number of observations, as only 8.99% of patients exhibit vasospasm. Importantly, GCS scores exhibit a strong correlation with hydrocephalus and clinical outcomes at discharge. These scores not only provide direct insights into the neurological status of patients in post-SAH management but also guide healthcare providers in deciding discharge destinations.

With these covariates providing real-time prognostic information, we can then predict the real-time probabilities of experiencing outcome events within a specific timeframe. Intermediate events like vasospasm and hydrocephalus can significantly alter the disease progression trajectories of patients. These changes can lead to slower recovery rates than normally expected under critical care, or even deterioration, with multiple complications diagnosed.

7.3.4 Individualised state-transition prediction

With developed prognostic models, we are interested in predicting the probabilities of clinical outcomes and complications for a new individual that has provided a set of dynamic covariates and a vector of baseline covariates, as well as time-to-event data of complications ($O_i^v = \{T_i^v, \delta_i^v\}$, $O_i^h = \{T_i^h, \delta_i^h\}$). A dataset with N patients to fit the prognostic model is given by $D_n = \{\omega_i, O_i^v, O_i^h, O_i^o, y_i; i = 1, \ldots, N\}$. $Y_i(t) = \{y_i(t); 0 \leq s < t\}$ is used denotes the whole set of longitudinal outcomes having observed up to time point t for a new patient that we are interested in predicting his probabilities of experiencing event outcomes.

Based on the observed data of this new patient and parameters estimated for the prognostic model, real-time probabilities event outcomes can be predicted. For this patient, we denote the time to the event of interest T_i^*, which can be either clinical outcomes or complications. Given that the event of interest has not occurred by time t, and considering the observed longitudinal outcomes $Y_i(t)$ up to that time, the

probability that the event of interest will not occur before time u is given by:

$$P(T_i^* \geq u \mid T_i^* > t, \omega_i, Y_i(t); \theta) = \int P(T_i^* \geq u \mid T_i^* > t, \omega_i, Y_i(t), b_i; \theta)\, p(b_i \mid T_i^* > t, \omega_i, Y_i(t); \theta) db_i$$

$$= \int P(T_i^* \geq u \mid T_i^* > t, \omega_i, b_i; \theta)\, p(b_i \mid T_i^* > t, \omega_i, Y_i(t); \theta) db_i$$

$$= \int \frac{S_i(u \mid M_i(u, b_i, \theta), \omega_i; \theta)}{S_i(t \mid M_i(t, b_i, \theta), \omega_i; \theta)}\, p(b_i \mid T_i^* > t, \omega_i, Y_i(t); \theta) db_i \quad (7.31)$$

where the history of true values of longitudinal outcomes M_i is estimated in the longitudinal sub-models. This equation integrates over the distribution of these random effects to provide an overall prediction.

Using an empirical Bayes estimate for b_i, a specific approximation to estimate random effects from data, we can simplify the computation and provide a practical method for obtaining the probabilities of experiencing event outcomes defined by Equation 7.31, which is given by:

$$\widetilde{\pi}_i(u \mid t) = \frac{S_i(u \mid M_i(u, \widetilde{b}_i^{(t)}, \hat{\theta}), \omega_i; \hat{\theta})}{S_i(t \mid M_i(t, \widetilde{b}_i^{(t)}, \hat{\theta}), \omega_i; \hat{\theta})} + O([n_i(t)]^{-1}) \quad (7.32)$$

where $\hat{\theta}$ denotes the maximum likelihood estimates of parameters and $\hat{b}_i^{(t)}$ denotes the mode of posterior distribution of random effects $\log p(b_i \mid T_i^* > t, Y_i(t); \hat{\theta})$.

The mode of this distribution gives the most probable values of b_i based on observed data up to time t and the fact that the event of interest has not occurred by time t. The term $O([n_i(t)]^{-1})$ indicates that the upper bound of the error term of this first-order estimates is $[n_i(t)]^{-1}$, suggesting that the error in this estimation diminishes as $[n_i(t)]^{-1}$ where $n_i(t)$ denotes the number of measurements in longitudinal outcomes by time t. Therefore, the estimator $\widetilde{\pi}_i(u \mid t)$ becomes more accurate with an increasing number of longitudinal measurements, which has been shown to work well in practice. [15]

To determine the standard error and confidence intervals for $\pi_i(u|t)$, we account for the uncertainty in parameter set θ by weighting the probability of survival time beyond u by the posterior distributions of θ, $p(\theta|D_n)$, derived from dataset D_n, which is written as:

$$P(T_i^* \geq u \mid T_i^* > t, \omega_i, Y_i(t), D_n) = \int P(T_i^* \geq u \mid T_i^* > t, \omega_i, Y_i(t); \theta)\, p(\theta \mid D_n) d\theta \quad (7.33)$$

which sums up weighted probabilities of potential values of θ to give a single prediction of event of interest beyond time *u.* The first part of the integrand comes from Equation 7.31, which is the prediction knowing the parameters, while Equation 7.33 computes the prediction over the distribution of parameters given data.

According to central limit theorem and its extension to Bayesian inference with the Bernstein-von Mises theorem, the posterior distribution $p(\theta|D_n)$ can be approximated by a multivariate normal distribution, such that $\{\theta|D_n\}\sim N(\hat{\theta}, Var(\hat{\theta}))$, with the variance $Var(\hat{\theta})$ estimated by the inverse of the Fisher information matrix. Additionally, in Bayesian inference, the Bernstein-von Mises theorem states that as the sample size grows, the posterior distribution of parameters will converge to a multivariate normal distribution. [16]

With Equations 7.31 and 7.33, a Monte Carlo estimate of $\pi_i(u|t)$ can be derived with three steps: (1) draw $\theta^{(l)}\sim N\{\hat{\theta}, Var(\hat{\theta})\}$; (2) draw $b_i^{(l)}\sim\{b_i|T_i^* > t, Y_i(t), \theta^{(l)}\}$ based on MH algorithm; (3) compute $\pi_i^{(l)}(u|t) = \frac{S_i(u|M_i(u,\theta^{(l)},b_i^{(l)}),\, \omega_i;\, \theta^{(l)}))}{S_i(t|M_i(t,\theta^{(l)},b_i^{(l)}),\, \omega_i;\, \theta^{(l)}))}$, which is repeated L times, with L denoting the number of Monte Carlo samples. The L computations of Monte Carlo estimates $\{\pi_i^{(l)}(u|t), l = 1,\ldots,L\}$ can be then used to derive point estimates, and confidence intervals of the probability that this new patient *i* will not experience an event by time *u*, given available prognostic information up to time *t.* [6]

Using these techniques, we can compute the probabilities of vasospasm, hydrocephalus, and clinical outcomes for specific intervals for a new patient. For instance, we can determine the 1-day and 3-day probabilities of these conditions, as well as their probabilities over the entire study period, including the acute and sub-acute phases. Based on these predefined intervals, the prognostic profile of a patient at time point *t* can be described as:

$$\boldsymbol{Prog_i(t)} = \begin{bmatrix} \boldsymbol{\pi_i^v(t+1|t)^T} & \boldsymbol{\pi_i^v(t+3|t)^T} & \boldsymbol{\pi_i^v(14|t)^T} \\ \boldsymbol{\pi_i^h(t+1|t)^T} & \boldsymbol{\pi_i^h(t+3|t)^T} & \boldsymbol{\pi_i^h(14|t)^T} \\ \boldsymbol{\pi_i^o(t+1|t)^T} & \boldsymbol{\pi_i^o(t+3|t)^T} & \boldsymbol{\pi_i^o(14|t)^T} \end{bmatrix} \quad (7.34)$$

where, for example, $\boldsymbol{\pi_i^v(t+1|t)^T} = [\ \hat{\pi}_i^v(t+1|t)\ ,\ \ \pi_i^v(t+1|t)^{Lower}\ ,\ \ \pi_i^v(t+1|t)^{Upper}]$, respectively denote the most probable single prediction, the lower bound of the 95% confidence interval, and the upper bound of the 95% confidence interval.

To understand and visualise the use of this prognostic profile in post-SAH management, we select a patient as an example to demonstrate their prognostic profile at different time points and analyse the effects of complications on disease trajectories. For this purpose, we firstly consider a patient who was diagnosed with both vasospasm and hydrocephalus during their hospital stay.

On day 2, before the diagnosis of hydrocephalus and vasospasm, the prognostic profile for this patient, labeled as Patient A, can be computed using previously developed prognostic models as follows:

$$\boldsymbol{Prog_A(t=2)} = \begin{bmatrix} 0.834\% & 2.755\% & 13.118\% \\ (0.321\% - 1.597\%) & (1.231\% - 5.730\%) & (6.883\% - 24.687\%) \\ 6.487\% & 21.820\% & 64.951\% \\ (3.413\% - 10.418\%) & (12.913\% - 34.266\%) & (39.247\% - 87.962\%) \\ 0.004\% & 0.027\% & 3.433\% \\ (0.000\% - 0.017\%) & (0.001\% - 0.147\%) & (0.001\% - 38.714\%) \end{bmatrix}$$

On day 8, after the patient was diagnosed with vasospasm, continuous monitoring of the patient's neurological conditions revealed an increase in the 1-day and 3-day risks of hydrocephalus. Consequently, the chances of being discharged with good clinical outcomes decreased, primarily due to persistently low Glasgow Coma Scale (GCS) scores and the occurrence of vasospasm.

$$\boldsymbol{Prog_A(t=8)} = \begin{bmatrix} 100\% & 100\% & 100\% \\ 11.937\% & 26.973\% & 45.064\% \\ (6.888\% - 16.046\%) & (16.577\% - 44.354\%) & (28.356\% - 66.915\%) \\ 0.003\% & 0.014\% & 0.096\% \\ (0.000\% - 0.012\%) & (0.000\% - 0.063\%) & (0.002\% - 0.669\%) \end{bmatrix}$$

By day 10, following the occurrences of both vasospasm and hydrocephalus, the short-term probabilities of a good outcome slightly increased, potentially due to some improvement in neurological conditions. However, the overall probabilities of achieving good clinical outcomes remained low, as the GCS score stayed below 8, indicating severe neurological impairment in the late sub-acute phase. Ultimately, the patient was discharged with unsatisfactory clinical outcomes, necessitating chronic or long-term acute care.

$$\boldsymbol{Prog_A(t=10)} = \begin{bmatrix} 100\% & 100\% & 100\% \\ 100\% & 100\% & 100\% \\ 0.005\% & 0.027\% & 0.053\% \\ (0.000\% - 0.019\%) & (0.002\% - 0.113\%) & (0.003\% - 0.247\%) \end{bmatrix}$$

In comparison, Patient B, who maintained good clinical outcomes (GCS scores > 13) without being diagnosed with vasospasm or hydrocephalus during the study period, was selected for analysis. The chances of good clinical outcomes for Patient B are significantly higher, as a high GCS score is a strong predictor of a favorable prognosis. Specifically, the hazard ratio (HR) for GCS scores in predicting good clinical outcomes is 6.3939, indicating that each unit increase in the GCS score is associated with a 6.3939-fold higher likelihood of achieving good clinical outcomes. Despite this, Patient B was at a higher risk of developing vasospasm, which could be attributed to the vasospasm peaks typically occurring around day 7 and the fact that Patient B is younger than Patient A, suggesting a higher inherent risk of vasospasm.

Figures 7.5 and 7.6 respectively illustrate the prognostic profiles of Patient A on day 2 and Patient B on day 6. These two figures reveal that, based on the prognostic information available up to these time points, the cumulative probabilities of

achieving good clinical outcomes, as well as the risks of vasospasm and hydrocephalus, can be predicted with associated confidence intervals.

$$\boldsymbol{Prog_B(t=6)} = \begin{bmatrix} 1.181\% & 3.973\% & 9.121\% \\ (0.429\% - 1.982\%) & (1.303\% - 6.878\%) & (3.658\% - 15.851\%) \\ 3.410\% & 9.893\% & 23.347\% \\ (2.096\% - 5.199\%) & (5.857\% - 15.355\%) & (12.587\% - 38.806\%) \\ 6.638\% & 25.164\% & 69.079\% \\ (0.940\% - 22.993\%) & (2.662\% - 75.698\%) & (7.273\% - 100.000\%) \end{bmatrix}$$

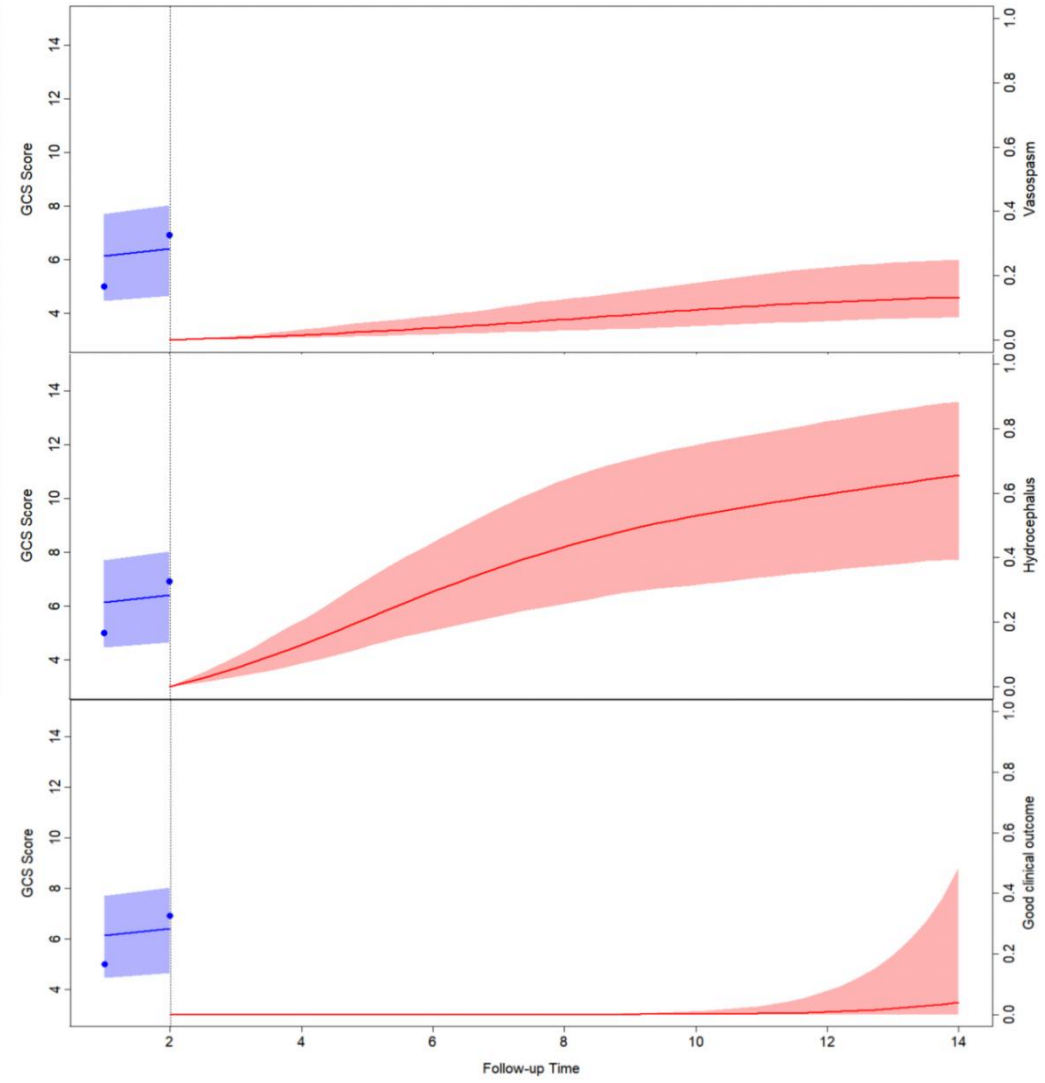


Figure 7.5 Prognostic profile of Patient A on day 2

This figure presents the prognostic profile of Patient A on day 2, showing the predicted probabilities of vasospasm, hydrocephalus, and good clinical outcomes over time. Each plot includes the following elements: the blue shaded area represents the 95% confidence intervals for the predictions based on the data available up to day 2,

the red line indicates the predicted probability trajectory for each outcome, and the red shaded area represents the 95% confidence intervals for the predicted probabilities as time progresses. The top, middle, and bottom plots respectively display the probability of vasospasm, hydrocephalus and achieving good clinical outcomes over time, starting from day 2.

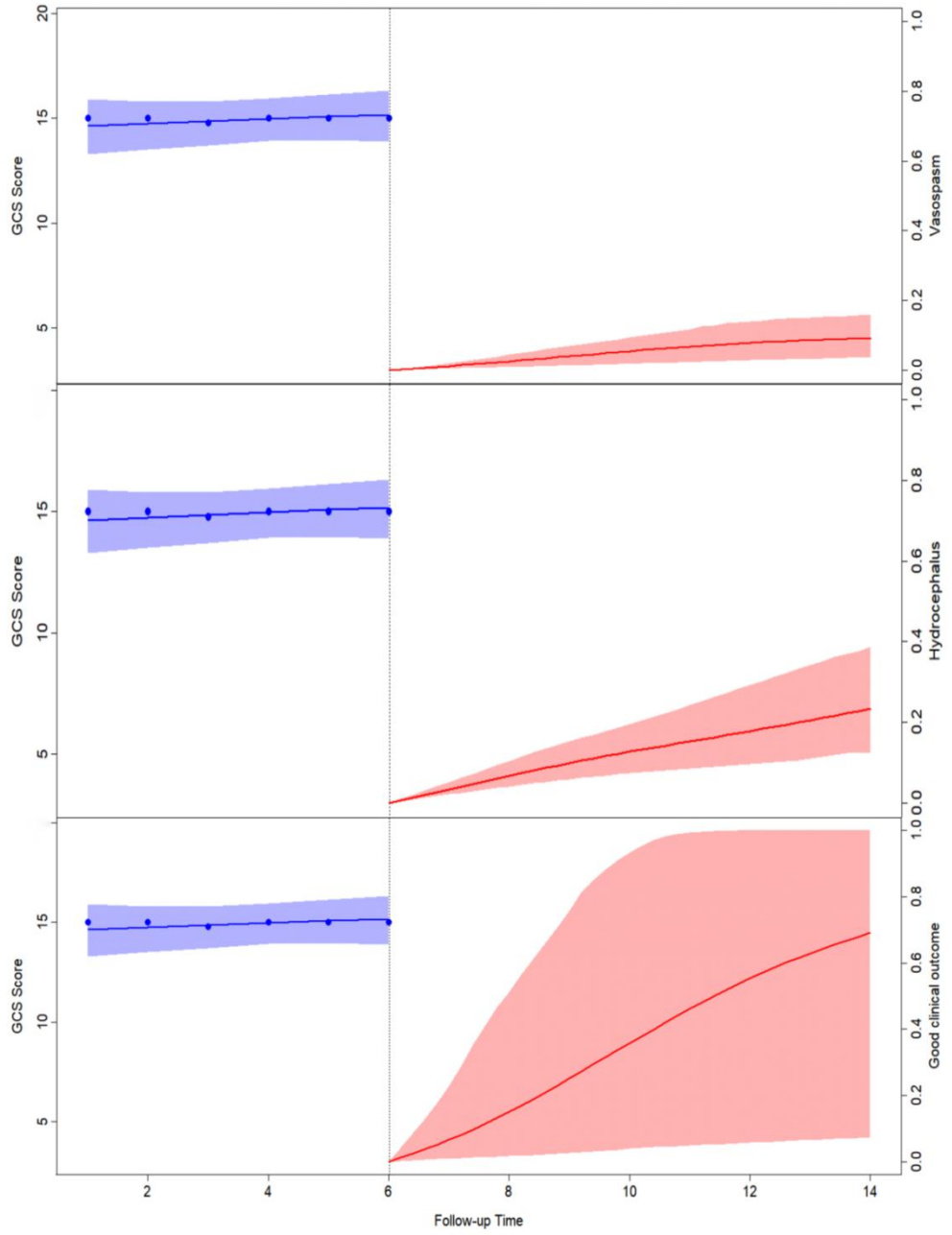


Figure 7.6 Prognostic profile of Patient B on day 6

In Figure 7.5, the predictions of vasospasm, hydrocephalus, and clinical outcomes given prognostic information available within the first two days can be visualised. The predictions indicate that, due to already low GCS score measurements signifying severe neurological deficits, the probability of being discharged with a good clinical outcome is very low. Additionally, it is evident that predictions extending further into

the future are associated with broader confidence intervals, suggesting greater uncertainty about these long-term predictions.

Figure 7.6 presents the prognostic profile of Patient B on day 6, showing the predicted probabilities of vasospasm, hydrocephalus, and good clinical outcomes over time. The elements and figure interpretations are the same as in Figure 7.5. For Patient B, the chances of good clinical outcomes were significantly higher, primarily due to this patient's good and stable neurological conditions, as indicated by consistently high GCS scores. However, our prognostic information may not fully capture a patient's comprehensive medical conditions, leading to uncertainties in our predictions. For example, the broad variance in the final plot suggests that good outcomes are not solely dependent on GCS scores; clinical outcomes depend on multiple factors that our model may not fully capture, including the possibility of complications arising along the way.

7.4 Discussion, limitations and future work

7.4.1 Discussion on multi-state prognostic framework for SAH

This chapter has discussed the comprehensive statistical framework for multi-state prognostic modeling in spontaneous SAH. The key components of the framework include baseline covariates, dynamic covariates with explanatory factors, and intermediate events. Figure 7.7 illustrates the potential usage scenario of this framework in clinical practice.

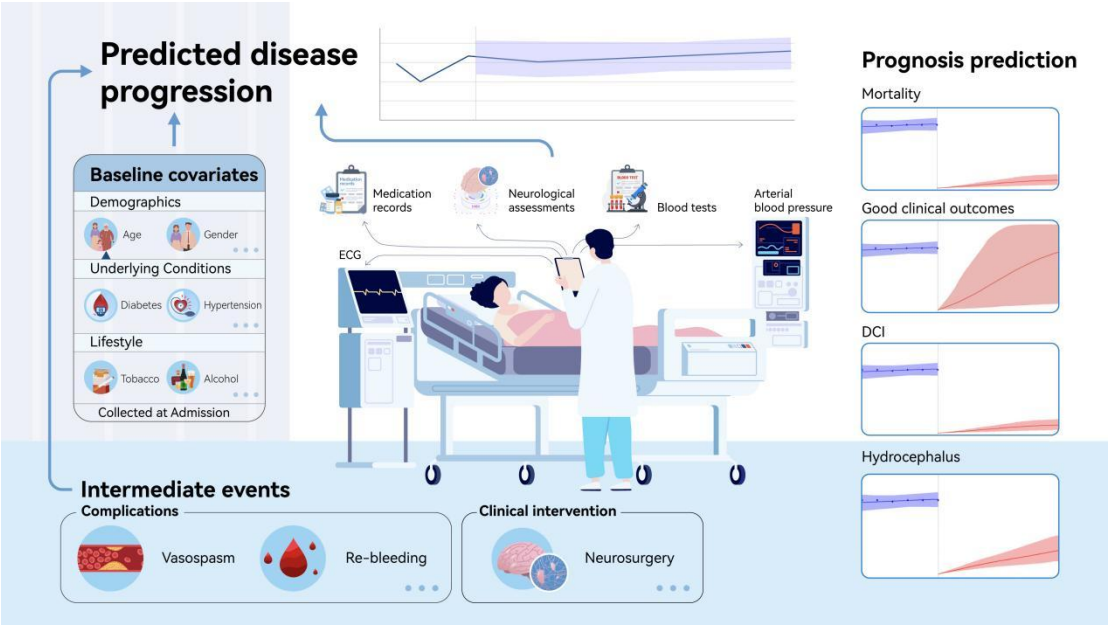


Figure 7.7 Usage scenario of multi-state prognostic framework for SAH

Baseline covariates refer to the initial clinical conditions of patients upon admission, such as age, and pre-existing medical conditions. These are crucial for understanding

each patient's initial risk and capability for recovery. Dynamic covariates are those that change over time and include factors like repeated neurological assessments, radiological data, and laboratory biomarkers. Explanatory factors, such as pharmacological agents, help explain the variations in these dynamic covariates over the course of the disease.

Intermediate events, including clinical interventions, e.g., neurosurgical interventions and pharmacological treatments, and complications, e.g., cerebral vasospasm and hydrocephalus, are incorporated to account for significant shifts in disease progression. These events serve as milestones that can alter the trajectory of a patient's prognosis.

Furthermore, this chapter delves into the structure and function of the three sub-models constituting the prognostic framework: longitudinal sub-models, survival sub-models, and state-transition sub-models. Longitudinal sub-models capture the temporal trajectories of dynamic covariates over time, enabling the prediction of future values based on historical data. These models incorporate both fixed and random effects to account for population-level trends and individual-specific variations.

Survival sub-models use historical and predicted values from longitudinal sub-models, along with prognostic information from baseline covariates, to estimate the probabilities of future complications and clinical outcomes. This integration allows for real-time, personalised risk assessments. Furthermore, the state-transition sub-model characterises a patient's comprehensive real-time prognostic profile, enhancing tailored patient management and personalised treatment plans. This sub-model continuously updates the patient's clinical state based on new prognostic information, providing dynamic prognostic insights. Methods for parameter estimation within these sub-models have also been discussed, employing techniques like MLE and Bayesian methods to handle complex models and latent variables.

The practical application of this framework was demonstrated using a dataset from the MIMIC-IV database, with simulated occurrence times for vasospasm and hydrocephalus. Survival analysis identified significant baseline covariates, which were jointly analysed with dynamic covariates to predict three targeted outcomes: vasospasm, hydrocephalus, and clinical outcomes at discharge. Two patient cases were analysed to illustrate the model's ability in predicting event outcomes. Prognostic profiles showed real-time probabilities of complications and clinical outcomes, demonstrating how the occurrence of complications impacts disease progression and patient prognosis.

7.4.2 Limitations and future work

Despite the promising results, several limitations still need to be acknowledged along

with strategies to address them:

(1) **Simulated data:** The occurrence times of vasospasm and hydrocephalus in this study were based on simulated data due to the lack of documented real-world data in MIMIC-IV database. This simulation, while guided by clinical findings, may not fully capture the variability of actual patient experiences and characteristics of these complications. Future studies should focus on collecting comprehensive real-world data of these complications, while collaborating with multiple hospitals and clinical databases can help gather sufficient real-world data to enhance the model's accuracy and applicability.

(2) **Linear representations of disease progression:** The framework proposed in this chapter's study assumed liner representation, modelled with LMMs, for more straightforward interpretations and reduced modelling complexity. However, disease trajectories in SAH can be highly non-linear, and future work could explore more flexible modeling approaches for better presenting disease progression. For example, non-linear modelling techniques, such as splines or machine learning algorithms could be implemented to better capture the complex and non-linear nature of disease progression. [17] These approaches can potentially accommodate the variability and unexpected changes in patient conditions over time.

(3) **Neurological assessments to represent disease progression:** Disease progression was primarily represented by neurological assessments. While these are critical, they may not fully encompass all aspects of a patient's condition, especially when predicting complications. Incorporating more targeted and a broader range of clinical and biological markers could provide a more comprehensive view of disease progression, e.g., cerebral blood velocities via TCD and blood amount in the subarachnoid space as dynamic covariates for predicting vasospasm, and cerebrospinal fluid biomarkers as predictors of hydrocephalus. [18][19] This will allow for a more comprehensive and accurate representation of the patient's condition and improve predictive performance on various event outcomes.

(4) **More complications as intermediate events:** The current multi-state prognostic model only includes vasospasm and hydrocephalus as intermediate events. Other complications, such as re-bleeding, DCI, and infections, could also significantly impact patient outcomes, as shown in Figure 7.2. Incorporating a wider range of complications into the prognostic models can enhance our understanding on their impact on disease progression as well as provide a more detailed prognostic framework for SAH.

(5) **Lack of external validation:** The prognostic models proposed in this chapter have not undergone external validation with independent datasets. Validation with external dataset is crucial to ensure the generalisability and robustness of the

prognostic framework. In future studies, performing external validation using independent datasets from different populations is essential to validate the model's reliability across various clinical environments. Moreover, conducting multi-center studies can provide broader validation, improving the model's robustness and ensuring its applicability in diverse clinical settings.

(6) **Lack of evidence for predictive accuracy and model stability:** While this chapter establishes a conceptual framework, it lacks direct evidence that the model produces stable and reliable predictions. The highly parametric nature of the approach may lead to optimisation challenges, requiring a dedicated framework for validation. Future work should focus on external validation, stability assessments, and optimisation strategies to improve robustness. The presented results in this chapter serve as illustrative examples, highlighting the need for further improvement before clinical application.

By addressing these limitations through targeted strategies, the prognostic framework can be further refined and enhanced, leading to more accurate and reliable predictions for patients with spontaneous SAH. This will ultimately improve clinical decision-making and patient outcomes. Specifically, the prognostic framework presented in Section 7.4.1 requires multiple intermediate steps before it can be fully implemented in clinical practice.

First, the dynamic prognostic models require rigorous external validation using external datasets and prospective validation in real-time clinical settings to assess their reliability. Next, the framework must improve its modeling of intermediate events, as discussed in this thesis, such as vasospasm, hydrocephalus, and DCI by integrating real time-to-event data of these complications and developing state-transition models to capture disease progression. Additionally, with sufficient dataset, integrating multi-modal data sources, including radiological imaging, continuous physiological monitoring, and laboratory biomarkers, will potentially enhance predictive power.

To facilitate real-time clinical use, computational efficiency must be optimised to handle large-scale patient data with minimal latency. For example, distributed computing is ideal for cloud-based, high-performance parallel processing. Lastly, addressing regulatory challenges and improving usability for healthcare providers will be essential for final implementations.

7.4.3 Summary

In conclusion, this study presents a multi-state dynamic prognostic model for spontaneous SAH, integrating baseline covariates, dynamic covariates, and intermediate events to improve patient prognosis accuracy and monitor disease progression.

Despite the promising results, the study acknowledges several limitations, including the reliance on simulated data for vasospasm and hydrocephalus occurrence times, linear representations of disease progression, solely use of neurological assessments as the primary indicators of disease status, and the absence of external validation. Corresponding strategies have been proposed for each of these limitations to address them, such as collecting comprehensive real-world data, implementing non-linear modeling techniques, incorporating a broader range of dynamic covariates, and conducting external validation with independent datasets.

The inclusion of only vasospasm and hydrocephalus as intermediate events also limits the model's comprehensiveness, highlighting the need to consider additional complications like re-bleeding, DCI, and infections. Addressing these limitations will refine and enhance the prognostic framework, leading to more accurate and reliable predictions for patients with spontaneous SAH. By continuously refining this prognostic framework, we aim to provide a powerful tool for personalised prognosis, facilitating early intervention and tailored treatment strategies for patients suffering from spontaneous SAH and even other cardiovascular diseases.

Reference for chapter 7

[1] CG, D., 1988. Report of World Federation of Neurological Surgeons Committee on a universal subarachnoid hemorrhage grading scale. J neurosurg, 68, pp.985-986.

[2] Naidech, A.M., Janjua, N., Kreiter, K.T., Ostapkovich, N.D., Fitzsimmons, B.F., Parra, A., Commichau, C., Connolly, E.S. and Mayer, S.A., 2005. Predictors and impact of aneurysm rebleeding after subarachnoid hemorrhage. Archives of neurology, 62(3), pp.410-416.

[3] Diringer, M.N., Bleck, T.P., Claude Hemphill, J.I.I.I., Menon, D., Shutter, L., Vespa, P., Bruder, N., Connolly, E.S., Citerio, G., Gress, D. and Hänggi, D., 2011. Critical care management of patients following aneurysmal subarachnoid hemorrhage: recommendations from the Neurocritical Care Society's Multidisciplinary Consensus Conference. Neurocritical care, 15, pp.211-240.

[4] Budohoski, K.P., Czosnyka, M., Smielewski, P., Kasprowicz, M., Helmy, A., Bulters, D., Pickard, J.D. and Kirkpatrick, P.J., 2012. Impairment of cerebral autoregulation predicts delayed cerebral ischemia after subarachnoid hemorrhage: a prospective observational study. Stroke, 43(12), pp.3230-3237.

[5] Dorai, Z., Hynan, L.S., Kopitnik, T.A. and Samson, D., 2003. Factors related to hydrocephalus after aneurysmal subarachnoid hemorrhage. Neurosurgery, 52(4), pp.763-771.

[6] Rizopoulos, D., 2012. Joint models for longitudinal and time-to-event data: With applications in R. CRC press.

[7] Dempster, A.P., Laird, N.M. and Rubin, D.B., 1977. Maximum likelihood from incomplete data via the EM algorithm. Journal of the royal statistical society: series B (methodological), 39(1), pp.1-22.

[8] Lange, K., 2004. Optimization, Springer-Verlag. New York.

[9] Alsefri, M., Sudell, M., García-Fiñana, M. and Kolamunnage-Dona, R., 2020. Bayesian joint modelling of longitudinal and time to event data: a methodological review. BMC medical research methodology, 20, pp.1-17.

[10] Johnson, A.E., Bulgarelli, L., Shen, L., Gayles, A., Shammout, A., Horng, S., Pollard, T.J., Hao, S., Moody, B., Gow, B. and Lehman, L.W.H., 2023. MIMIC-IV, a freely accessible electronic health record dataset. Scientific data, 10(1), p.1.

[11] Bracard, S. and Schmitt, E., 2008. Vasospasm and delayed consequences. Interventional neuroradiology, 14(1_suppl), pp.17-22.

[12] Shaikh, N., Chanda, A., Mohammed, K., Balfaqih, A., Khan, M.M., Nahid, S., Balal, A., Zubair, M., Rahman, M.A., Algallie, H. and Al-Ameri, G., 2023. Aneurysmal Subarachnoid Haemorrhage (aSAH) and Hydrocephalus: Fact and Figures. In Frontiers in Hydrocephalus. IntechOpen.

[13] Chakraborty, H., Hossain, A., Dey, S. and Ghosh, S.K., 2022. Modeling Right-skewed Heavy-tail Right-censored Survival Data with Application to HIV Viral Load. Bulletin of the Malaysian Mathematical Sciences Society, 45(Suppl 1),

pp.365-393.
[14] Kale, S.P., Edgell, R.C., Alshekhlee, A., Haghighi, A.B., Sweeny, J., Felton, J., Kitchener, J., Vora, N., Bieneman, B.K., Cruz-Flores, S. and Abdulrauf, S., 2013. Age-associated vasospasm in aneurysmal subarachnoid hemorrhage. Journal of Stroke and Cerebrovascular Diseases, 22(1), pp.22-27.

[15] Rizopoulos, D. and Ghosh, P., 2011. A Bayesian semiparametric multivariate joint model for multiple longitudinal outcomes and a time‐to‐event. Statistics in medicine, 30(12), pp.1366-1380.

[16] Van der Vaart, A.W., 2000. Asymptotic statistics (Vol. 3). Cambridge university press.

[17] Lin, J. and Luo, S., 2022. Deep learning for the dynamic prediction of multivariate longitudinal and survival data. Statistics in medicine, 41(15), pp.2894-2907.

[18] Gonzalez, N.R., Boscardin, W.J., Glenn, T., Vinuela, F. and Martin, N.A., 2007. Vasospasm probability index: a combination of transcranial doppler velocities, cerebral blood flow, and clinical risk factors to predict cerebral vasospasm after aneurysmal subarachnoid hemorrhage. Journal of neurosurgery, 107(6), pp.1101-1112.

[19] Lenski, M., Biczok, A., Huge, V., Forbrig, R., Briegel, J., Tonn, J.C. and Thon, N., 2019. Role of cerebrospinal fluid markers for predicting shunt-dependent hydrocephalus in patients with subarachnoid hemorrhage and external ventricular drain placement. World Neurosurgery, 121, pp.e535-e542.

Chapter 8 Conclusion and future work

8.1 Conclusion of this thesis

This thesis was devoted to propelling the development of advanced techniques for prognostication of spontaneous SAH. These findings were presented focused on three main aspects related to incorporation a variety of prognostic information into SAH prognostication. Contributions of this thesis, especially proposed prognostic framework, can be extended to the development of prognosis studies for other diseases. Main contributions of studies in this thesis include:

- **Prognostic analysis of a variety of prognostic factors:** This aspect of the thesis assesses the prognostic significance of various factors to understand their impact on clinical outcomes. It aims to optimise the integration of these prognostic factors into prognostic models as well as employ different metrics to quantify their effects.
- **Dynamic prognostic models for spontaneous SAH:** The thesis develops personalised dynamic models for SAH patients, integrating diverse prognostic data such as baseline demographics, dynamic neurological and haematological assessments, intermediate events, and pharmacological impacts. These models generate real-time outcome probabilities predicting complications and clinical outcomes, enhancing predictive accuracy, critical care management, and personalised post-SAH care.
- **Development of a comprehensive prognostic framework:** This thesis introduces an innovative approach in prognostic research that combines both dynamic and static prognostic factors as well as intermediate events to enable real-time, personalised predictions for prognosis research.

This concluding chapter provides an overview of key findings of this thesis and outlines potential directions for future research in this field. Chapter 1 provides a comprehensive overview of physiological and medical background of SAH. It starts with the anatomy and physiology of the brain's cerebral vasculature and meninges, laying the foundational knowledge essential for understanding SAH. This chapter then discusses the epidemiology, risk factors, diagnosis, and complications of spontaneous SAH. Diagnostic techniques like CT, MRI, and DSA are reviewed for their effectiveness in identifying SAH, providing guidance on the optimal use of each method. Furthermore, major complications such as re-bleeding, vasospasm, delayed cerebral ischemia, and hydrocephalus are reviewed with their epidemiology, risks factors, diagnosis and treatments. Lastly, the chapter reviews treatment strategies for spontaneous SAH, including initial stabilisation, neurosurgical interventions, and rehabilitation, to enhance the clinical understanding and management of this condition.

Chapter 2 provides a comprehensive literature review on predicting outcomes for spontaneous SAH, highlighting the significance of prognosis in clinical

decision-making and patient care. The chapter tracks the progression of prognostic approaches, moving from experience-based to evidence-based methods, and from generalised to individualised predictions. Additionally, the chapter discusses the transition from static to dynamic prognostic methods, accounting for changes in patient conditions and disease progression over time. A detailed review of statistical methods for continuous, binary, and time-to-event outcomes in prognosis studies is included, along with an introduction to joint modeling for simultaneous analysis in longitudinal and event outcomes as well as machine learning based techniques. Most importantly, this chapter also includes a comprehensive review of existing prognosis research in spontaneous SAH, with a focus on mortality, poor neurological outcomes, and complications, as well as their associated prognostic factors.

Chapter 3 to Chapter 7 focus on comprehensive and dynamic prognostication for spontaneous SAH from different perspectives. Chapter 3 explores using vital sign indices derived from physiological monitoring of ABP and ECG for dynamic prognostication of survival outcomes for spontaneous SAH. This chapter details methods for extracting and annotating ABP and ECG waveforms to identify key prognostic factors such as SBPV and PPV, which dynamically represent patients' cardiovascular status. Utilising data from the MIMIC-III database, the study incorporates these dynamic predictors alongside baseline covariates, like cerebral oedema, into a joint model for simultaneous analysis of longitudinal data and survival outcomes. The results demonstrate that higher SBPV is significantly associated with increased mortality risk, outperforming static prognostication, particularly in the acute phases of SAH.

Chapter 4 enhances the dynamic prognosis for spontaneous SAH by focusing on ABP management through artefact rejection and synthetic ABP modelling. This chapter introduces dynamic thresholding strategies for artefact detection and rejection, develops a piece-wise parametric model to accurately represent ABP waveforms, and demonstrates its superior performance using MIMIC-II database data. Main applications of the proposed synthetic ABP models as digital twins representing patients' haemodynamics include predicting haemodynamic status of patients, simulation of haemodynamic responses to treatments and, enhancing non-invasive blood pressure monitoring in post-SAH management.

Chapter 5 proposes a neurological intervention transition model for dynamic prediction of good outcomes for spontaneous SAH. This study integrates multiple dynamic covariates for dynamic prognostic modelling, including neurological assessments, haematological biomarkers and vita sign indices, which comprehensively monitor the disease progression of patients. Ultilising a cohort of 701 patients from the MIMIC-IV dataset, this model incorporates dynamic covariates like GCS scores, glucose levels, and WBC counts, significant baseline covariates, and neurological interventions as intermediate events. It is found in this study that the GCS score is the most valuable dynamic covariate for prognostication while WBC

count and glucose levels offer additional prognostic information that complements neurological status. Including neurological interventions (aneurysm clipping and endovascular embolisation) as intermediate events adds granularity to the prognostic model and enhances prediction accuracy,

Chapter 6 primarily discusses pharmacological effects in disease progression and prognostication of SAH. This chapter includes three types of medications for analysis, including those for complication prevention (e.g., nimodipine for vasospasm, levetiracetam for seizures, and heparin for VTE), pain relief (e.g., morphine and acetaminophen), and intracranial and blood pressure control (e.g., mannitol and hydralazine). Through longitudinal analysis of data from 612 SAH patients in the MIMIC-IV dataset, the study evaluates how these medications influence recovery trajectories measured by GCS scores and clinical predictions. The chapter concludes that integrating pharmacological effects into prognostic models enhances prediction accuracy, aiding in personalised treatment strategies and improving SAH patient management.

Chapter 7 develops a comprehensive framework for prognosis in spontaneous SAH by incorporating multiple transient states to reflect the complexity of disease progression. Unlike traditional models that categorise patients into a single "alive" state, this model includes various transient states representing different complications such as vasospasm and hydrocephalus. By utilising longitudinal sub-models, survival sub-models, and state-transition sub-models, the approach dynamically updates a patient's prognostic profile in real-time. This multi-state model aims to improve personalised and comprehensive prognosis, enabling the simultaneous predictions of complications and clinical outcomes jointly, facilitating timely interventions for preventing complications and unfavourable outcomes, and ultimately enhancing patient care in SAH management.

8.2 Future outlook

8.2.1 Potential improvements in chapters

Potential improvements for studies in this thesis have been presented at the conclusion of each main chapter. In Chapter 3, more prognostic valuable factors can be potentially extracted from ABP and ECG waveforms to more comprehensively represent dynamic haemodynamic status. Potential improvements in chapter 4 focus on validating the ability of synthetic ABP models in reconstructing ABP waveforms with non-invasive finger cuff monitoring. In Chapter 5, the focus is on expanding the range of dynamic covariates to provide a more comprehensive representation of disease progression, while Chapter 6 recommends a detailed analysis of the effects of pharmacological agents on various dynamic covariates beyond GCS scores. Finally, Chapter 7 advocates for research on non-linear representations of disease progression, the inclusion of more complications as intermediate events, and the need for external validation.

8.2.2 Future research directions

Despite these potential improvements primarily focusing on further improving the comprehensiveness of SAH prognostication. There are two main future research directions in this field:
(1) **AI integration:** The integration of AI into SAH prognostication primarily faces two challenges. Firstly, high-quality, comprehensive datasets are crucial for training AI-based prognostic models. In many medical research contexts, data may be fragmented and insufficient in volume, making it challenging to develop AI-based models. Another significant challenge in integrating AI into SAH prognostication is the lack of interpretability of AI-based models. As clinicians need to understand how prognostic models make specific predictions, this lack of interpretability hinders the trust and acceptance by clinicians in clinical practice.

To address the first challenge, collaboration among multiple hospitals and research institutes can help integrate a more comprehensive dataset. Secondly, with the advancements of explainable AI (XAI) techniques, developing AI-based models that incorporate explainability features can help improve the transparency of the sequential decision-making process in dynamic prognostication.

(2) Real-time data ultilisation: The datasets used in studies of this thesis are retrospective data, which provide a rich source of clinical data for training prognostic models, allowing for assessment in model performance with known outcomes. While Bayesian optimisation allows for continuously updating model parameters and predictions by sequentially training prognostic models using data up to specific time points, there are still some differences between working with retrospective data and real-time data. A major challenge is that retrospective data are well-organised and convenient for data analysis while real-time data are often unstructured and continuously evolving, posing multiple difficulties.

Firstly, real-time data must be promptly handled to be useful in prognostic modeling, especially when dealing with dynamic covariates extracted from physiological monitoring. Secondly, the time delay between data stream generation and data availability leads to latency issues, which can significantly affect the effectiveness of real-time data ultilisation. Engineering solutions, such as deploying edge computing in medical devices, can pre-process data rapidly and reduce latency. This approach can potentially facilitate the implementation of comprehensive and dynamic prognostication in clinical practice.